UNIVERSIDADE
BEIRA INTERIOR

Radio Resource Management of Heterogeneous Small Cell Networks

Rui Filipe Rosa Paulo

Tese para obtenção do Grau de Doutor em
Engenharia Eletrotécnica e de Computadores
(3º ciclo de estudos)

Orientador: Prof. Doutor Fernando José da Silva Velez

Novembro de 2022

Provas públicas realizadas em 26 de outubro de 2022

Composição do júri

Presidente

Doutor António João Marques Cardoso
Professor Catedrático da Universidade da Beira Interior

Vogais

Doutor Luís Filipe Lourenço Bernardo
Professor Associado da Faculdade de Ciências e Tecnologia da Universidade Nova de Lisboa

Doutor Giuseppe Piro
Professor Associado do Politecnico de Bari, Itália

Doutor Fernando José da Silva Velez
Professor Auxiliar da Universidade da Beira Interior

Doutor Jorge Manuel dos Reis Gama
Professor Auxiliar da Universidade da Beira Interior

Declaração de Integridade

Eu, Rui Filipe Rosa Paulo, que abaixo assino, estudante com o número de inscrição D567 do 3º ciclo de estudos em Engenharia Eletrotécnica e de Computadores da Faculdade de Engenharia, declaro ter desenvolvido o presente trabalho e elaborado o presente texto em total consonância com o **Código de Integridade da Universidade da Beira Interior**.

Mais concretamente afirmo não ter incorrido em qualquer das variedades de Fraude Académica, e que aqui declaro conhecer, que em particular atendi à exigida referenciação de frases, extratos, imagens e outras formas de trabalho intelectual, e assumindo assim na íntegra as responsabilidades da autoria.

Universidade da Beira Interior, Covilhã, 2022/11/15

Assinado por : **RUI FILIPE ROSA PAULO**
Num. de Identificação: 11079491
Data: 2022.11.15 15:01:12 +0000

(assinatura conforme Cartão de Cidadão ou preferencialmente assinatura digital no documento original se naquele mesmo formato)

O segredo é não correr atrás das borboletas...
É cuidar do jardim para que elas venham até si.
(Autor desconhecido)

The secret is not chasing butterflies...
You take care of the garden so that they come to you.
(Unknown author)

Acknowledgements

This work was only possible thanks to the contribution of many institutions and their people. To Instituto de Telecomunições (IT) and to everyone that is or was with us, we are a great team, the best ones. To Universidade da Beira Interior (UBI) and to everyone that is or was with us, we are a family. Once *UBIano*, Forever *UBIano*.
To Professor Fernando J. Velez and everyone that was, is, or will be with WE-Move@Covilhã. Like every team we have some less good days, but it is the blue ones that really count.
To Professor Lajos Hanzo by the easy integration on Communications Group at School of Electronics and Computer Science, University of Southampton.
To Professor Giuseppe Piro, by the development of LTE-Sim and the help to upgrade it. To Professor Jorge Gama, by the support in statistics and by the introduction in the R programming language. To Professor Gastão Bettencourt, by the help in mathematical guidance. To Dr. Daniel Robalo, by the partnership.
This work was performed and financially supported within several projects: National Funding from the FCT-Fundação para a Ciência e a Tecnologia, through the UIDB/50008/2013, CONQUEST (CMU/ECE/0030/2017), NEUF Project, PEst-OE/EEI/LA0008/2011, COST CA15104 IRACON, COST IC1004 Cooperative Radio Communications for Green Smart Environments, ORCIP (22141-01/SAICT/2016) and TeamUp5G. TeamUp5G project has received funding from the European Union's Horizon 2020 research and innovation programme under the Marie Skłodowska-Curie project number 813391. Programa ERASMUS. CREaTION, ECOOP. FANTASTIC-5G project, which receives funding from the European Union's Horizon 2020 research and innovation programme under the grant agreement ICT-671660.
Most part of this work was done with free software, thanks. Software freedom is not a straightforward path, but is possible. It gives a lot of pain at the beginning but looking back it is very gratifying. Fortunately, in some things it seems possible to do science with little.
To my family, family is not about blood. It is about who will hold your hand when need it the most. To friends. We choose our friends based on our preferences and our shared interests and because we feel good when we are with them.

Abstract

While mobile communication users demand new high speed services with enhanced quality, there will always be a need to optimize cellular networks. This work explores the behavior of indoor and outdoor small cells while reducing the cell size to increase system capacity in both links. After justifying evolution of the use of small cells, the concepts of ultra-dense networks and heterogeneous networks toward 5G are then presented.
In the initial part of this work, we have chosen a 3GPP 5x5 grid geometry for indoor scenarios. The average signal-to-interference-plus-noise ratio (SINR) has been studied for reuse pattern two and two types of deployment topologies, one with 25 HeNBs and another with 4 HeNBs. We have also addressed the exponential effective SINR mapping (EESM) by extending the study for topologies with 5 and 6 HeNBs.
Based on an improved version of LTE-Sim, network performance has been evaluated in terms of the goodput, packet loss ratio (PLR), delay, and the maximum number of supported users. We have evaluated the performance by considering 4, 5, 6 and 25 HeNBs. Results complied with the 3GPP recommendations for PLR and delay. One observed that system capacity is higher for topologies with 25 HeNBs, followed by topologies with 6 HeNBs and 4 HeNBS, and then the indoor deployments with 5 HeNBs.
Different packet schedulers have been considered. Results have shown that, with the considered applications and schedulers, it is possible to reduce the transmitter power of HeNBs without compromising the small cell network performance.
In the final part of the work an urban micro line-of-sight cell scenario has been studied by comparing the 2.6 GHz, 3.5 GHz, and 5.62 GHz frequency bands while considering the ITU-R M.2135-1 dual slope path loss model (DS-PLM) in the system level simulations. Results have been obtained for different values of the cell radius. System capacity has been determined by considering the 3GPP quality target of 2% for video applications. For all schedulers and frequency bands, for cell radius shorter than the breakpoint distance, the PLR increases when the cell radius decreases. For cell radius (R) longer than the breakpoint distance and up to the maximum considered cell radius the PLR increase and then decreases. By analyzing the underlying results for the number of supported users, one concludes that the maximum-largest weighted delay first scheduler allows for obtaining the highest goodput, which occurs at 2.6 and 3.5 GHz for $300 \leq R \leq 500$ m, while for the longest Rs the highest goodput occurs at 5.62 GHz.

Keywords

Small cells, femtocells, goodput, delay, HeNBs, LTE-Sim, packet loss ratio, packet scheduler, exponential effective SINR mapping, HeNBs deployment ratio, urban micro-cell, two-slope model, frequency band.

Resumo alargado

A disponibilização de serviços de ritmo de transmissão elevado, com qualidade melhorada, motiva a necessidade de optimização das redes celulares. Este trabalho explora o comportamento de pequenas células em ambientes de interior e exterior. A redução da área de cobertura das células permite aumentar a capacidade de sistema em ambos os sentidos de ligação. A justificação da utilização de células com pequenas áreas de cobertura, é seguida da apresentação do conceito de redes ultra-densas e heterogéneas, um passo rumo à 5G.
Na parte inicial deste trabalho, foi escolhida uma grelha de 5x5 apartamentos para o cenário de interiores definido pelo 3GPP. Estudou-se a relação sinal-interferência-mais-ruído (SINR) média para topologias com padrão de reutilização dois, uma com 25 HeNBs e outra com 4 HeNBs. Também se estudou o mapeamento exponencial efectivo da SINR (EESM), estendendo-o para topologias com 5 e 6 HeNBs.
Com base numa versão melhorada do LTE-SIM, avaliou-se o débito binário, taxa de perda de pacotes (PLR), atraso e o número de utilizadores suportados. O desempenho foi avaliado considerando 4, 5, 6 e 25 HeNBs. Os resultados obtidos cumprem as recomendações do 3GPP para a PLR e o atraso. Observou-se que valores mais elevados da capacidade de sistema são obtidos para a topologia com 25 HeNBs, seguida pelas topologias com 6, 4 e 5 HeNBs.
Consideraram-se várias abordagens para a calendarização de pacotes. Os resultados mostram que, para os escalonadores de pacotes considerados, é possível reduzir a potência de emissão dos HeNBs sem comprometer o desempenho da rede celular.
Na parte final do trabalho, estudou-se um cenário com pequenas células em ambiente urbano e linha de vista. Este estudo foi feito comparando as bandas de frequência de 2.6 GHz, 3.5 GHz e 5.62 GHz, considerando o modelo de atenuação ITU-R M.2135-1 de duplo declive (DS-PLM). Obtiveram-se resultados considerando diferentes valores para o raio das células. Determinou-se a capacidade de sistema para serviços de vídeo, considerando o limiar de 2% para a PLR (do 3GPP). Para todos os escalonadores de pacotes e faixas de frequência, para distâncias de cobertura inferiores à distância de quebra, a PLR aumenta quando o raio de cobertura da célula diminui. Para raios de cobertura (R) superiores à distância de quebra, o valor da PLR, primeiro aumenta, e depois diminui. Conclui-se que o escalonador de atraso máximo-superior ponderado primeiro (M-LWDF) permite obter taxas de débito binário superiores, que ocorrem para as bandas de frequência de 2.6 GHz e 3.5 GHz no intervalo de raios de cobertura $300 \leq R \leq 500$ m, enquanto, para Rs mais longos, valores de débito binário superiores ocorrem para 5.62 GHz.

Palavras-chave

Pequenas células, femtocélulas, débito binário, atraso, HeNBs, LTE-Sim, taxa de perda de pacotes, escalonadores de pacotes, mapeamento exponencial efectivo da SINR, quociente de implantação de HeNBs, micro-célula urbana, modelo de duplo declive, banda de frequência.

Contents

List of Figures

List of Tables

Acronyms

2G	2nd generation mobile networks
3G	3rd generation mobile networks
3GPP	3rd generation partnership project
4G	4th generation mobile networks
5G	5th generation mobile networks
6G	6th generation mobile networks
AWGN	additive white Gaussian noise
BE	best effort
BLER	block error rate
CDF	cumulative distribution function
CQI	channel quality indicator
CR	cognitive radio
CSG	closed subscriber group
CSI	channel state indicator
DL	downlink
DS	dual-slope
eNB	evolved NodeB
EE	energy efficiency
EESM	exponential effective SINR mapping
EH	energy harvesting
eMBB	enhanced mobile broadBand
EPC	evolved packet core
E-UTRAN	evolved UTRAN
EXPRule	exponential rule
FAP	femtocell access point
FDD	frequency division duplex

FFR	fractional frequency reuse
FLS	frame level scheduler
FM	frequency modulation
FMC	fixed mobile convergence
FUE	femtocell user
GERAN	GSM EDGE radio access network
GW	gateway
HetNets	heterogeneous networks
HeNB	home eNodeB
HeNB GW	home eNB gateway
HO	handover
HOL	head of line
HUDN	heterogeneous ultra-dense networks
ICT	Worldwide Information and Communication Technologies
IoT	internet of things
ITBS	index transport block size
ITU	International Telecommunication Union
LoS	line-of-sight
LTE	long-term evolution
LTE-A	LTE-Advanced
M2M	machine-to-machine
MBS	macro base station
MCS	modulation and coding scheme
MIMO	multiple-input multiple-output
MISO	multiple-input single-output
M-LWDF	maximum-largest weighted delay first
MME	mobility management entity
mmW	millimeter waves

MOS	mean opinion score
MUE	macrocell user
NLoS	non-line-of-sight
NOMA	non-orthogonal multiple access
NRT	non-real time
NR	new radio
OFDMA	orthogonal frequency division multiple access
PDN	packet data network
PF	proportional fair
PLM	path loss model
PLR	packet loss ratio
POS	Pareto optimal set
PLMN	public land mobile network
QoS	quality-of-service
RAN	radio access network
RB	resource block
RF	radio frequency
RSSI	received-signal-strength-indicator
RT	real time
SC	single carrier
SE	spectral efficiency
S-GW	serving GW
SINR	signal-to-interference-plus-noise ratio
SS	single-slope
SWIPT	simultaneous wireless information and power transfer
TBS	transport block size
TSG	technical specification group
TDD	time-division duplex

UAV	unmanned aerial vehicle
UDN	ultra-dense networks
UE	user equipment
UMi	urban micro
USRPs	universal software radio peripherals
UTRAN	universal terrestrial radio access network
VID	video
VLC	visible light communications

List of Symbols

A	fitting parameter
A_{Apt}	total affected apartment area
A_{ow}	total integration area
a_i	tunable parameter
B	intercept parameter
BW	bandwidth
b_i	tunable parameter
C	path loss frequency dependence
c	tunable parameter
c_V	velocity of a signal in free space
C/I	carrier-to-interference ratio
$D_{HOL,i}$	head of line packet delay
d	distance between the transmitter and the UE
$d_{BP}^{'}$	breakpoint distance
d_f	physical distance
d_{st}	distance
E	expectation value
F_r	Fraunhofer distance
f_c	frequency
G_{Tx}	transmitter gain
G_{Rx}	receiver gain
h_{BS}	antenna height of the cell
h_{UE}	antenna height of the UE
I_i	cell interference
$\bar{I}$	average level of received interference from a neighboring cell
i^{th}	userth

j^{th}	subchannelth
k^{th}	LTE frame
l	apartment side length
N	number of neighboring cells
NF	noise factor
N_{rt}	value of real-time flows
n_T	number of interfering neighbors
PL	path loss
P_{nh}	average interference power
P_{noise}	thermal noise
$\overline{P_{nh}}$	average interference power
P_{ow}	average power received
P_{Tx}	transmitter power
$q_i(k)$	signal
R	radius
$\bar{R}_i$	average achieved throughput
r_{ij}	achieved throughput
$u_i(k)$	quota of data
w_{ij}	priority metric
X	environment-specific term
x_0	coordinate xx
y_0	coordinate yy
α	orthogonality factor of the codes
α_i	factor computed from QoS
α_0	reference loss at one meter
β	estimated parameter from link-level simulations
δ_i	acceptable PLR
Γ_i^j	spectral efficiency

Γ_x^i	integration region xx
Γ_y^i	integration region yy
γ	path loss exponent
γ_i	vector of the individual values of the SINR for each subcarrier
σ_i	delay threshold
τ_i	packets waiting time

Chapter 1

Introduction

1.1 Motivation and Approach

In his first outdoor experiments, toward the end of September 1895, Guglielmo Marconi conducted the first outdoor radio transmissions. With waves of thirty or forty meters long, he could send Morse code up to a distance of one kilometer. For longer distances, Alfonso, the older brother of Marconi, was equipped with a pole with a white handkerchief at the top to confirm the reception of the transmission. Marconi realized in the same period that his invention only would have importance if it could be possible to cross natural obstacles like hills and mountains. When it was possible to cross the mountains near Villa Grifone, Alfonso needed to use a hunting rifle to confirm the reception of Marconi transmission [1].
In 1901, Marconi made the first transatlantic transmission in Morse code, three dots, the encoding of "S" character (heard by him and his assistant Kemp in their headset), which covered an area of millions of square miles [2]. Using that technology it could accommodate only a single transmission on the Earth's surface [2].
In 2000, Marty Cooper suggested that the number of voice calls has increased one million times since 1950. From this million-times improvement, roughly 15 times resulted from using more spectrum (3 GHz versus 150 MHz), and five times was from frequency division, the ability to divide the radio spectrum into narrower slices (25-kHz channels versus 120-kHz channels). Modulation techniques (such as frequency modulation, FM, single side-band, time-division multiplexing, and various approaches to spread spectrum) can contribute fivefold more. However, Cooper suggested that the most significant improvement, with a factor of about 2700, resulted from confining individual conversations to smaller and smaller areas by spatial division or spectrum reuse, as shown in Figure 1.1, [2]. Shannon's Law also con-

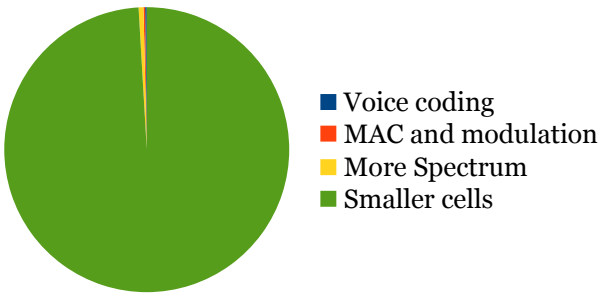

Figure 1.1: Wireless network capacity gains form 1950 until 2001, values suggested by Marty Cooper, [2].

firms that the best way to increase capacity is to shrink cells because short-range improves carrier-to-interference ratio, C/I, while improving capacity and quality.
The prediction of the exponential growth of wireless communications has driven future mobile communication systems research to deal with aspects such as heterogeneous networks

(HetNets), millimeter-wavebands, and multiple-input multiple-output (MIMO) [3]–[6]. To complement the traditional macrocell network to cope with the future services demands, existing networks are being complemented with low power nodes, creating HetNets. With the reduction of the coverage area of cells, today, the cellular network is composed of an amalgamate of different cell types, as show in Figure 1.2. The type and main characteristics of the

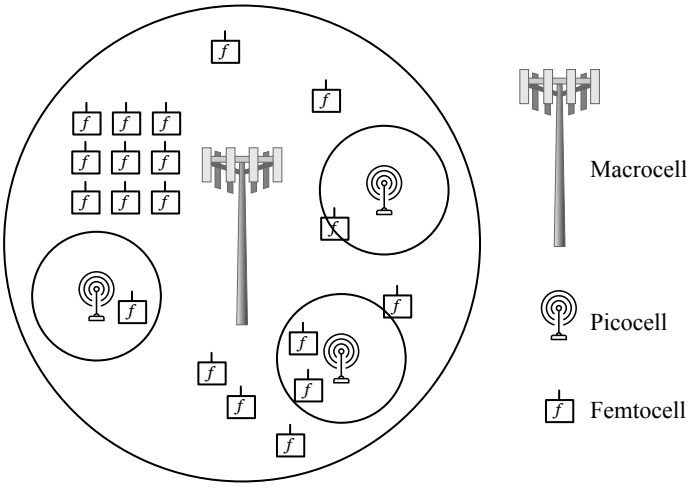

Figure 1.2: Illustration of three types of cellular nodes, from macro to small cells.

different nodes are briefly summarized in Table 1.1.

Table 1.1: Characteristics of different types of cells.

Type	Placement	Radius	Transmitter Power
Macrocell	Outdoor	500 m - tens of km	46 dBm
Microcell	Outdoor	500 m	43 dBm
Picocell	Outdoor or indoor	200 m	23-30 dBm
Femtocell	Indoor	10 m	0-20 dBm

The diversity of cell sizes, network architectures, and the coalition of diverse technologies and frequency bands are characteristics of HetNets that will contribute to the growth of wireless data traffic [7]–[9].

The common characteristic of macrocells, microcells, and picocells is the way how they are installed. These nodes need radio frequency planning, site selection, deployment, and maintenance by the operator. Femtocell networks are unique since end users, themselves, usually deploy them. The deployment of home eNodeBs (HeNBs)[1] differs from traditional transmitter nodes [10] since they are consumer deployed with no planning.

Nowadays, 80% of the traffic occurs indoors, and most cellular networks are composed of evolved NodeBs (eNBs)[2]. Providing in-building coverage with eNBs becomes a challenge. Also, applications require higher throughput [11], [12]. Authors from [3] identify video streaming as one of the applications with the highest throughput requirement. In the future, ultra-high definition videos with virtual reality [4] will require a significant long-term demand for bandwidth. In the longer term forecasts from [4], the consumer segment will have 74% of

[1]HeNB is the hardware that provides radio signal within the femtocell.
[2]eNB is the hardware that provides radio signal within the macrocells.

the total devices connected to the network. Machine-to-machine (M2M) nodes, the fastest growing mobile devices, will be half of the globally connected devices. M2M communications applied to home environments include applications like video surveillance, smart meters, healthcare monitoring, among an infinitude of possibilities. The consumption of video streaming, the increase of M2M devices that include video in their capabilities, and the impact of video devices on mobile network traffic justify the need for studying video performance in mobile networks. Besides, in 4G, mobile broadband and M2M also generate several types of traffic flows with different traffic requirements, from video applications with a maximum delay of 150 ms to applications where the requirements for delay are not very critical (e.g., home environmental monitoring) [13]–[15].

In urban microcell scenarios, indoor users can be served by outdoor eNBs[3]. These urban environments are characterized by high user density and traffic loads focusing on pedestrian and vehicular users. The microcellular test environment defined in [16], [17] includes outdoor and outdoor-to-indoor users. Base stations are located outdoor and users communicate indoors. The channel model for the outdoor urban microcell scenario is known as urban micro (UMi).

When high data rate indoor coverage is provided by outdoor eNBs, if high order modulation and coding schemes are used, e.g., 64/128/256 QAM, the (external) walls from the building make up an obstacle that is difficult to overcome or is impassable, creating indoor areas with weak or none signal coverage. Another approach to increase system capacity is to adopt high frequencies. However, higher frequencies will lead to the same problem of considering high order modulation and coding schemes, as they also imply indoor areas with weak or even no signal coverage at all. Besides, waves at higher frequencies do not go well through walls, especially with windows covered by a metalized coat.

Microcellular solutions do not solve all the identified issues since they do not eliminate the physical barriers between eNBs and the destination nodes (usually known as User Equipment, UE), e.g., walls or urban obstacles. Efforts to achieve cells with small coverage areas lead to developing new cells, such as picocells or femtocells. As mentioned above, HeNBs are one of the smallest cellular nodes and provide radio coverage within these femtocells. HeNBs deal with indoor coverage in areas where traditional eNB networks are ineffective [18]. HeNBs are defined in [10] as small, inexpensive, low-power indoor base stations that are consumer deployed. This possibility of consumers deploying HeNBs, and the variety of previous cell types with irregular sizes, originates chaotic and random coverage shapes [10]. HeNBs are not only deployed in private houses but can also be deployed in offices, shopping centers, and industrial environments [19], [20]. In these cases, we refer to HeNBs as Enterprise HeNBs. The nature of the uncoordinated and disordered deployment of HeNBs differs from the existing network deployments. This deployment may originate new and more complex interference problems in both down and uplinks [21].

This work, apart from addressing the radio resource management problem in 3GPP small cell indoor scenarios, mainly by modeling and simulation approaches, also explores different deployment ratios while seeking optimal deployments. As outdoor deployment in the context

[3]These eNB are the radio equipment that provide coverage within the microcell and picocell.

of heterogeneous small cells are also important toward 5G, urban small cells in the so-called UMi scenarios are also analyzed by comparing different sub-6 GHz frequency bands.

1.2 Growth of the Mobile Communications Sector

The growing use of smartphones and the demand from users to be always connected anywhere, has led to expand physically the network and an exponential increase in traffic. The dimension and complexity of this network that enables smartphones to deliver voice and data services are invisible to the users [22]. Connected devices outpaced the number of people on Earth in 2014, and in 2016, approximately three decades after the invention of the mobile phone, there were 7.6 billion connected devices. From these devices, 3.7 billion were unique subscribers [22]. At the time of writing this thesis, and under [23], there are 10.5 billion connected devices, 5.3 billion unique mobile subscribers. The total world population is 7.8 billion people [24].

Human users are used to be the only player on the mobile network. From years apart and more rapidly in the future, mobile networks are also being invaded by machines [3], [4]. Internet of things (IoT) generates machine-oriented data traffic. This type of traffic not only demands network capacity as well as imposes additional requirements, mainly in end-to-end latency [22].

The trend on the needs and about what we desire leads to have most of the data traffic laid up on the Internet. Currently, the physical location of this data could be very far from the user. The latency is the primary limiting factor to access this data. With fiber optics, the limit is the speed of light. To address this problem, well-planned cloud computing infrastructures, adaptive network management, and congestion control systems need to be implemented. These will help get data traffic closer to the user helping to control latency, opening up the way to a new type and more efficient communications. With this evolution, the future network is becoming our primary interface with the virtual world [25].

Apart from dealing with constant proliferation and more capable mobile devices, the industry also has to deal with the expectation of always providing connections and access to all services anywhere and anytime, which leads to an exponential increase in cellular capacity demand. This capacity demand is not only imposed by humans. It is expected that machines will outnumber human users in the future. Predictions presented in [22] considering the period from 2010 to 2025 expect growth between 61 times to 112 times in the global bearer traffic.

In 2007, the Worldwide Information and Communication Technologies (ICT) carbon footprint was 2%, equal to 830 tons CO_2 and comparable to the global aviation industry, and it was expected to grow to 4% by 2020 [26]. The International Telecommunication Union (ITU) Telecommunication Standardization Bureau releases the objectives of the new ITU standard to reduce greenhouse gas emissions by 45% in 2030 [27]. This reduction constitutes an extra challenge to the industry.

The improvement of network capacity considering the Shannon-Hartley theorem [28] could be made (in a simplified way) by densification, bandwidth, or spectral efficiency [22]. A

macrocell serves multiple users, so the user shares the bandwidth. If the density of users is high, each user is only to have a small portion of that bandwidth. By reducing the cell size, more base stations (BS) have to be deployed to cover the same area. They result from that each BS is going to serve fewer users. Since each BS serves fewer users, the bandwidth per user will increase. If this increase continues until we have one user per cell, the capacity increases linearly. When the number of BSs outpace the number of users, only the signal-to-interference-plus-noise ratio (SINR) is improved, and the capacity increases on a logarithmic scale.

With densification, the transmitter power is reduced, and the total energy consumption becomes less significant. With this reduction, in terms of energy, only the processing power becomes relevant. According to [2], the total costs of deploying and maintaining an operational BS are the significant challenge to densify a network. These BSs are under the total responsibility of the operator. In a different deployment model, users deploy BSs by reusing the existing power and backhaul infrastructure. The BS has to have the ability to perform a fully automatic configuration and a continuous self-optimization during its operational life. However, with this deployment model, it is important to deploy BSs where users are, and 80% of the traffic demand is indoor [29].

To consider more bandwidth to increase capacity presents some challenges. The bandwidth at lower frequency bands is minimal. With the use of higher frequency bands, it is possible to increase bandwidth. However, wireless communications at higher frequency bands present higher path losses. Another drawback when the frequency band is increased is the requirement to increase also the transmitter power due to higher path losses. Besides, more carries need to be allocated. These challenges, on increasing the bandwidth, make the highest frequency bands only usable in small cell networks.

Techniques such as interference mitigation to increase the SINR, multiple antennas, or signal processing through error correction could increase spectral efficiency. Currently, the progress on spectral efficiency has driven to reach the near-saturation in potential gains. The lower number of antennas at the user equipment and issues with the channel state information are the major drawbacks that limit the gains in traditional MIMO systems.

In [22], authors have shown that increasing the number of antennas leads to a slight gain in terms of system capacity. However, densification or increasing bandwidth present higher gains. With multiple antennas, the capacity can increase two times. When increased capacity resorts to the increase in bandwidth, the capacity improvements could be five times. Densifying the network with small cells is one of the best options since it is expected an increase 18 times. This makes small cells the leading solution and a necessary topology evolution, and the following steps to increase system capacity. This growth will be workable until it reaches one user per cell.

1.3 Brief History and Evolution of Small Cells Deployment

In 1895, when Marconi conducted the first radio transmission, although the problem was to increase the transmitter distance, when the need to transmit more wireless data takes off,

the reduction of cell radius happened. The first small cell systems were built in 1984 [30].

These “small cells” were a term used to describe the cell size in a metropolitan area, where a macrocell (on the order of kilometers in diameter) would be split into several smaller cells. With reduced transmit power, known today as metropolitan macrocells or microcells, and having a cell radius of perhaps several hundred meters [10], [30].

In [31], the concern to provide flexible services within buildings leads to the presentation of the precursor of cellular picocells, called low powered micro-cellular systems. These systems had cell sizes ranging from tens of meters to about one hundred meters. The “traditional” small cells were used for capacity and coverage infill, i.e., where macro penetration did not provide a reliable connection or where the macrocell was overloaded. These small cells were essentially a smaller version of the macro BS and required comparable planning, management, and network interfaces [10]. Being a smaller version of the macro BS network, the costs associated with deploying a picocell network outweighed the advantages provided by this topology [22]. A little known industry project presents a concept very similar to the current femtocell concept [32]. In that project, the reuse of the same spectrum as the macrocells was considered and wired backhaul (T1 or PSTN) in that project. The small cell technologies just mentioned were technically a step forward but economically unsuccessful because the cost of deploying and operating many small cells outweighed the advantage they provided.

The adoption of the femtocells represents the last micronization of cellular networks. The major problem in this continued micronization of cellular networks is the fact that the network infrastructure is expensive [33].

The reduced cell sizes (hence increasing numbers of cells), because of the engineering of wireless networks to provide increasingly high data rate applications, with growing traffic densities, and the additional complexity introduced as interoperability among heterogeneous networks becomes commonplace. This led to exacerbated growing costs for the network operator [34]. In the time of [34], the future wireless networks will increasingly use intelligent radio nodes to enhance system performance and profit margins, resulting in a new way of deploying and configuring these types of cellular nodes while enabling the cost-effective deployment of small cells.

Early simulations performed by Bell Laboratories, Alcatel-Lucent for femto and small cells tested techniques like self-optimization, MIMO, energy efficiency, and offloading in that type of network [35]–[37]. It can be stated that these cells, especially femtocells, gave the first step toward a heterogeneous network deployment model [10], [33].

The first residential and commercial deployment of femtocells started in the United States in 2008, followed by Europe and Japan in 2009. In 2011, the deployed 3rd generation mobile networks (3G) small cells (2.3 million), for the first time, exceeded the number of 3G macro base stations (1.6 million) [38]. Although the primary market of femtocells was residential, they extended it to the public spaces to provide coverage or offload to the macrocell network since most of the cellular traffic is generated in these spaces. In 2015, some operators ran small cell networks in enterprises and public buildings [39].

The deployment of small cells is more difficult since their deployment has almost the same problems as the deployment of macro base stations. These problems are the availability of

backhaul, diverse costs, network provisioning as well monitorization. Even with these barriers, small cells proved to be the desired option. These small cells share many hardware and software features from the macrocells, but they are more flexible. They support a high number of simultaneously active users and mainly self-organizing network capabilities. These capabilities allowed to perform self-configuration, self-organization, and relationship management with the neighbor cells.
In July 2021, Small Cell Forum[4] released a market forecast that predicts to have deployed 35.7 million small cell radio units by 2026 [41]. This forecast states that adding a new spectrum and open architectures will facilitate new deployers and business models. As the deployment processes become more simple, scalable, and repeatable, the small cell deployment will speed up, especially by deploying enterprise small cells.

1.4 Ultra-Dense Networks

1.4.1 Toward 5G

The evolution of mobile devices and applications has changed the paradigm of mobile networks [42]. The new paradigm that is coming to arise is the concept of ultra-dense networks (UDN) [43]. It is expected that the 5th generation mobile networks (5G) to be UDN in terms of transmitters and receivers, making the network highly complex [44]. The goal behind UDN is to reduce the distance between access nodes and the users. This is only possible with deploying a massive number of small cells in areas where immense traffic is generated, as shown in Figure 1.3. The radio part of these small cells is hardware operating at lower transmission powers than the well-established macrocells. These nodes are going to have small coverage areas.
When these nodes are deployed indoors, they belong to customers. When they are deployed outdoors, operators deploy them. Optimization of outdoor small cells is addressed in Chapter 5. Typically, outdoor remote radio units are installed in, e.g., lampposts, urban furniture, or building facades. In crowded spaces, usually there are hotspots in train and metro stations, airports, and markets [43]. This densification of cells introduced a new coverage scenario, where a user would be closer to many cells.
Cisco, one of the most recognized industrial players in networking hardware, software, and telecommunications equipment, has been producing successive reports suggesting to a severalfold increase in the mobile world data [3], [4]. It is foreseen that, by 2023, 5.7 billion people will have mobile connectivity (2G, 3G, 4G, or 5G), and 5.3 billion people will be internet users [4]. Since spectrum resources are limited, the long-term solution is to increase the reuse of the existing spectrum. With the reuse of spectrum, the network capacity is improved, and the link to the end-user becomes shorter, resulting in an improvement in the link quality.
The densification of the network has a specific limit, which requires extensive research to get realistic system models to capture the reality of UDNs. The limits of wireless densification

[4]Details about Small Cell Forum could be found in [40].

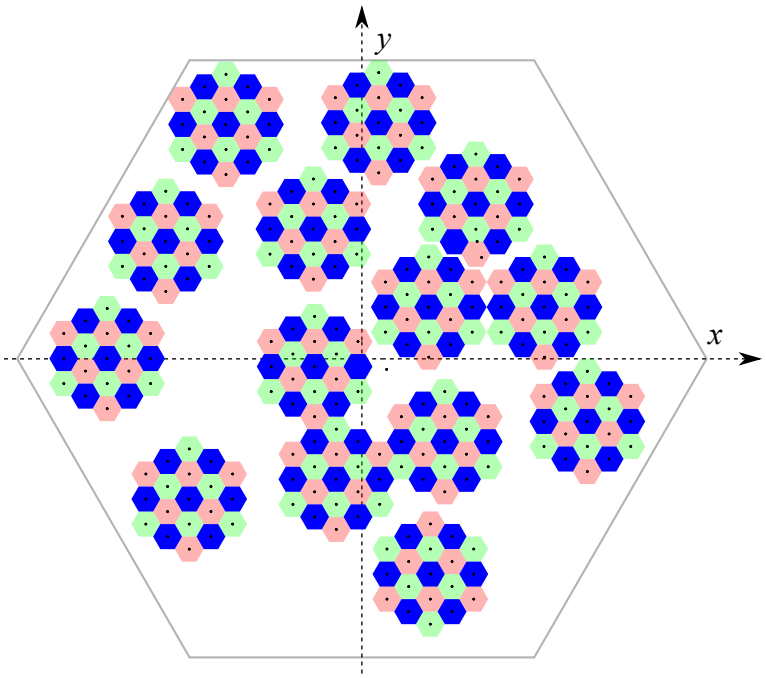

Figure 1.3: Outdoor scenario in UDN.

problems were addressed in [45].

1.4.2 Heterogeneous Networks

It is expected that the macrocells will not continue to be extended in terms of capacity [46]. The capacity extension is being done by adding the new low-power base station to the existing macrocell network. Typically, the scale of these low-power nodes is named from the largest connection capacity as micro, pico, and femto base stations [47]. A network with these low-power nodes and the macrocell node is called a multi-tier network. In each tier, there will be a collection of one type of node. Networks composed of these varieties of nodes are classified as HetNets.

According to [4], M2M connections that support a broad range of IoT applications will represent about 50% (14.7 billion) of total global devices and connections. With the actual and the predicted development of the IoT, the demand for wireless services has been rapidly increasing, and this is also leverage for the importance of HetNets [47], [48]. This mixture of base station types is superior in spectral efficiency to a conventional macro cellular network, relying only on eNBs [49].

1.4.3 Femtocell Concept

A femtocell is a small, low-power access point, inexpensive base station, cellular network access point that connects standard mobile devices to a mobile operator's network using residential DSL, cable broadband connections, or optical fibers [50]–[53]. In 4G, HeNBs are some of the smallest cellular nodes and provide radio coverage within these femtocells. Femtocells provide wireless voice and broadband services to customers in their homes, offices, and other indoor environments. They use fully standardized wireless protocols over the air to

communicate with standard mobile devices, operating in licensed spectrum, generating coverage and capacity over internet-grade backhaul [51]. Some authors could consider or not wireless last-mile technologies as a way to connect a femtocell. Typically, a single femtocell will deliver voice services simultaneously to at least four users within the home [54]. Femtocells are generally consumer deployed and connected to their backhaul connection. From a user perspective, a femtocell appears indistinguishable from a traditional base station [52]. Authors from [10] give a comprehensive overview of the evolution of femtocells. Femtocells are becoming a significant player in cellular networks, mainly for the following reasons:

- It can provide indoor coverage for places where macrocells cannot [55];
- It can offload traffic from the macro cell layer and improve macrocell capacity [56] (while using macrocells to provide indoor coverage, more power from the base station will be needed to compensate for high penetration loss, resulting in a decrease in macrocell capacity);
- One can assume that good isolation (hence the signal leakage from indoor to outdoor will be small) can be achieved. The addition of a femtocell layer will significantly improve the total network capacity by reusing radio spectrum indoors [57];
- There is a growing demand for higher and higher data rates. Because of the high penetration loss, high data rates, services can not be provided indoors apart from those areas near windows facing at a macrocell site. This is because high data rate requires high performance of the radio frequency (RF) links;
- As femtocell access point (FAP) only need to be switched on when the users are at home (for home femtocells) or work (for enterprise femtocells), this makes the use of femtocell "greener" than the use of macrocells [50], [58].

A femtocell differs from traditional small cells in their need to be more autonomous and self-adaptive. The backhaul interface back to the cellular network – which is IP-based and likely supports a lower rate and higher latency than the standard X2 interface connecting macro and picocells – mandates the use of femtocell gateways and other network infrastructure to appropriately route and serve the traffic to and from what will be millions of new base stations [10].
Financial pressures will drive wireless communication network operators to adopt autonomic systems with characteristics of a completely independent, self-healing, self-deploying, and self-optimizing communication network. That will eventually become cognizant, exhibiting some degree of self-awareness. As a step in this direction, in [34], the concept of robotic wireless base stations and discussion of their behavior subject to principles inspired by Asimov's Laws of Robotics was explored. Authors of [34] affirms clearly that the future wireless networks will increasingly use intelligent radio nodes to enhance both system performance and profit margins.
Enabled femtocells to be deployed by the end-user is possible because of their advanced auto-configuration and self-optimization capability. These capabilities enable small cells to be

deployed in a plug-and-play manner, as they can automatically integrate themselves into existing macrocellular networks. This was the critical step in enabling large-scale deployments of small cells [10].

1.4.4 OFDMA Small Cells

The development of fourth generation (4G) cellular standards based on orthogonal frequency division multiple access (OFDMA) and IP-based provide a better platform for femtocell overlays than the 3G. The 3G networks work with code division multiple access (CDMA) networks that are circuit-switched (the femtocell backhaul is inherently IP), and relentless hardware and software integration has made it foreseeable to have a fully functional low power base station [10].
Integrating femtocells in the network brought additional problems. Usually, a 4G network with only a macrocells (1-tier) network is hard to make a mathematical analysis. Considering only a second-tier, composed of femtocells, the mathematical analysis became harder yet. In [59], analysis is made, where it is possible to see the impact of the transition from a carefully planned set of base stations to a complete irregular, unplanned deployment of heterogeneous infrastructures, like femtocells.
Although the deployment of femtocells brings advantages, they also affect the performance of the macrocell layer. In [60], a coverage and interference analysis based on a realistic OFDMA macro/femtocell scenario is provided, and some guidelines on how the spectrum allocation and interference mitigation problems can be approached in these networks. Special attention is paid to the use of self-configuration and self-optimization techniques to avoid interference. Some challenges for OFDMA Femtocells are presented, such as the access method. Femtocells can be configured in three ways [50], [54], [61] to allow or restrict their usage by certain users, as follows:

- Open access - all users may connect;
- Closed access - the femtocell allows only subscribed users to establish connections;
- Hybrid access - non-subscribers use only a limited amount of the femtocell resources.

All three configurations present advantages or disadvantages. Open access is the preferred access control to minimize cross-tier interference and offload traffic from the HeNB layer. The network operators intend to offload traffic. The femtocell owners prefer closed access because of the limited resources of the femtocells. Closed access is also preferred in terms of privacy and security, and in terms of handover efficiency [53].
If closed access is chosen, femtocell users will experience higher throughput, but neighboring cellular users will lower the throughput. The opposite is going to happen in the open access. From the operators' point of view, it is better to provide only open access than a mix of open and closed femto services [62]. The trade-off between open and closed leads to hybrid access, not the ideal option but a compromise between both [50]. Although, as in [63], it was concluded that the open or shared are the preferred methods in most cases in terms of throughput. It is also suggested to opt for hybrid access. For the uplink in OFDMA [61],

the open or closed access option presents a surprising conclusion. It is stated that the best choice highly depends on cellular user density.

1.4.5 Co-layer and Cross-layer Interference in Femtocells

Authors of [50] present an overview of the interference in the presence of femtocells that can be classified as co-layer and cross-layer. Co-layer is the interference between femtocells, and cross-layer is between femto and macrocells.

Co-layer interference is described as the unwanted signal received at a femtocell and sent from other femtocells, decreasing thus the quality of its communication. The name co-layer refers to the fact that all femtocells belong to the same network layer, unlike other elements like base stations, NodeBs, and other types, which belong to the other layers. A diagram summarizing the major problems originating from co-layer interference is presented in Figure 1.4[5].

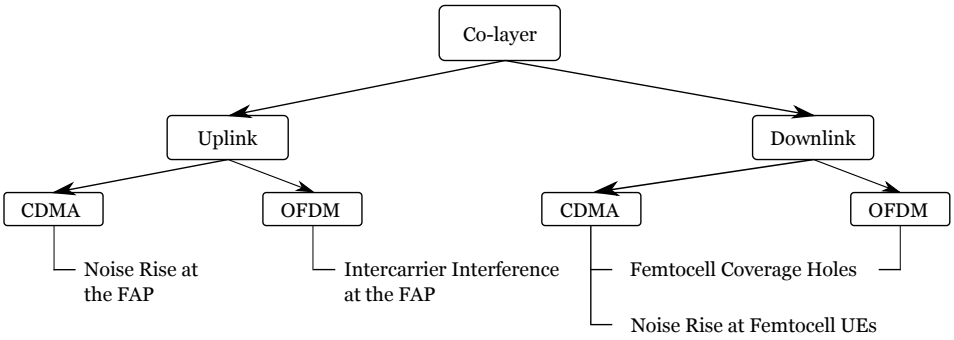

Figure 1.4: Main problems caused by co-layer interference, adapted from [50].

In uplink co-layer interference, femtocell UEs are the aggressors or sources of interference. Neighboring FAPs are the victim systems. In Figure 1.5, a situation is shown in which user two falls within the coverage area of both its femtocell.

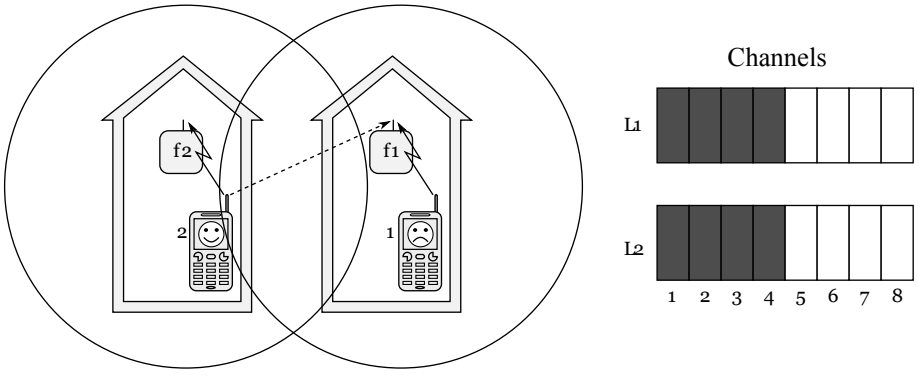

Figure 1.5: Co-layer uplink interference in an OFDMA femtocell network, adapted from [50].

Dead zones in OFDMA femtocells depend on the spectrum occupancy at a particular location. Two femtocell users (FUEs) could be at the same geographic position, and only one of them would suffer interference from surrounding femtocells, i.e., the dead zone would only affect

[5]Although this work only considered OFMDA, CDMA is also presented in some Figures.

some OFDMA subchannels while the other user (i.e., L3 in Figure 1.6) suffers no interference. To illustrate this, Figure 1.6 is presented.

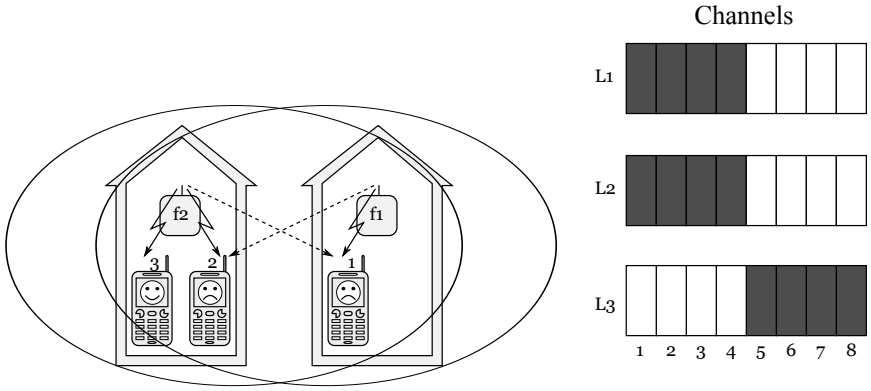

Figure 1.6: Co-layer downlink interference in an OFDMA femtocell network, adapted from [50].

Approaches to overcome co-layer interference are gathered for reference in Figure 1.7.

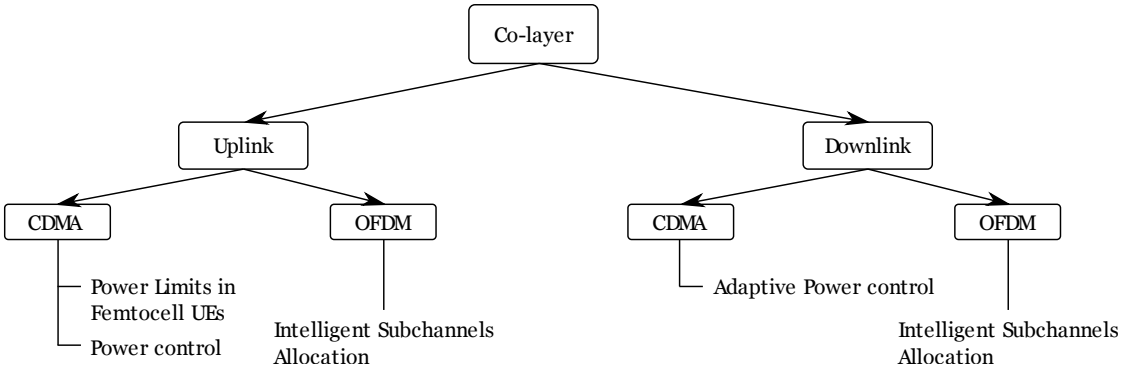

Figure 1.7: Approaches to cope with co-layer interference, adapted from [50].

An interfering signal is assumed to produce **cross-layer interference** in two-layer networks if the aggressor and the victim systems belong to different network layers. For example, the distortion caused by an emitting FAP (member of the femtocell layer) at the downlink (DL) of one or several macrocells (members of the macrocell layer) is an obvious case of cross-layer interference. Likewise, it can also be cross-layer interference if a macrocell user (MUE) at the uplink of a nearby FAP (member of the femtocell layer) causes the distortion. The major problems caused by cross-layer interference are presented in Figure 1.8.

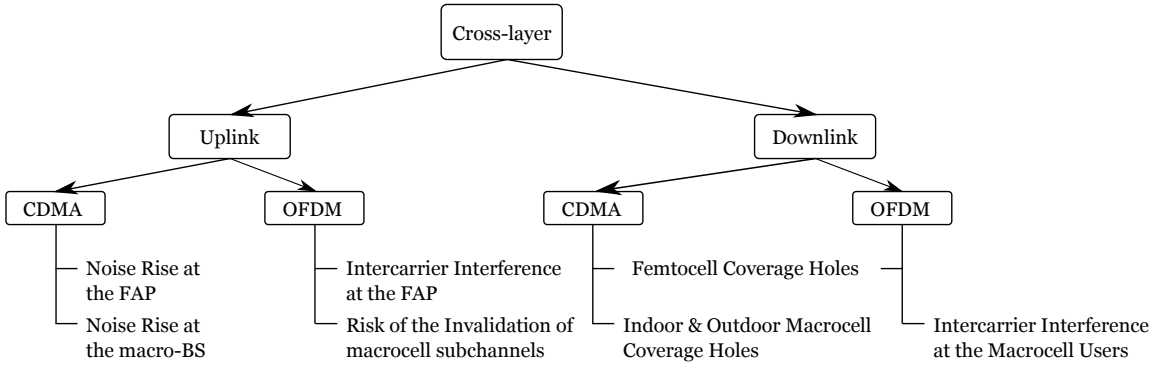

Figure 1.8: Main problems caused by cross-layer interference, adapted from [50].

On the one hand, as illustrated in Figure 1.9, MUE 2 is transmitting with high power in the same subchannels as FUE 1, carrying interference at the FAP. On the other hand, as MUE 4 is transmitting a different channel, the communication between user 3 and receptive FAP is not affected.

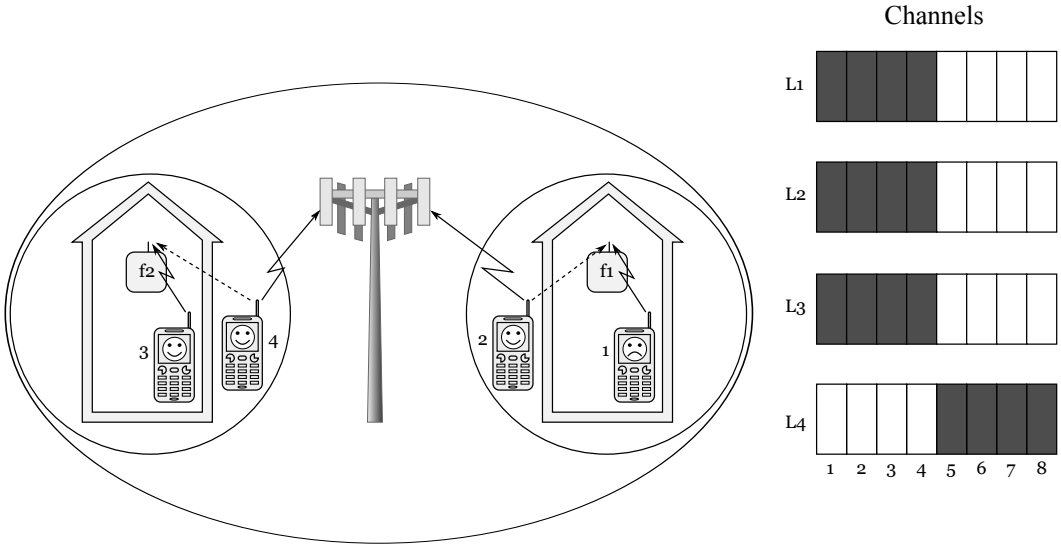

Figure 1.9: Cross-layer uplink interference in an OFDMA co-channel two-layer network, Interference at the femtocell, adapted from [50].

The other type of uplink interference can occur when femtocells are located too close to the macro base station, MBS (interference at the MBS), as shown in Figure 1.10.

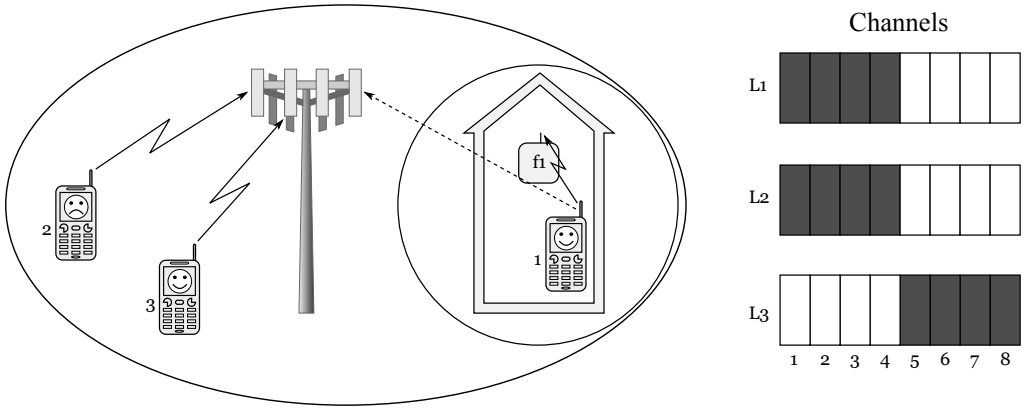

Figure 1.10: Cross-layer uplink interference in an OFDMA co-channel two-layer network, Interference at the macrocell, adapted from [50].

Link and technology-dependent approaches to solve the problem of cross-layer interference are presented. These approaches to coping with cross-layer interference are further summarized in Figure 1.11.

Some works, like [64], present a dynamic interference avoidance scheme that uses inter-cell coordination to prevent excessive inter-cell interference, especially for cell or sector edge users that are most affected by inter-cell interference, with minimal or no impact on the network throughput. The proposed scheme comprises a two-level algorithm, one at the base station level and the other at a central controller to which a group of neighboring base stations

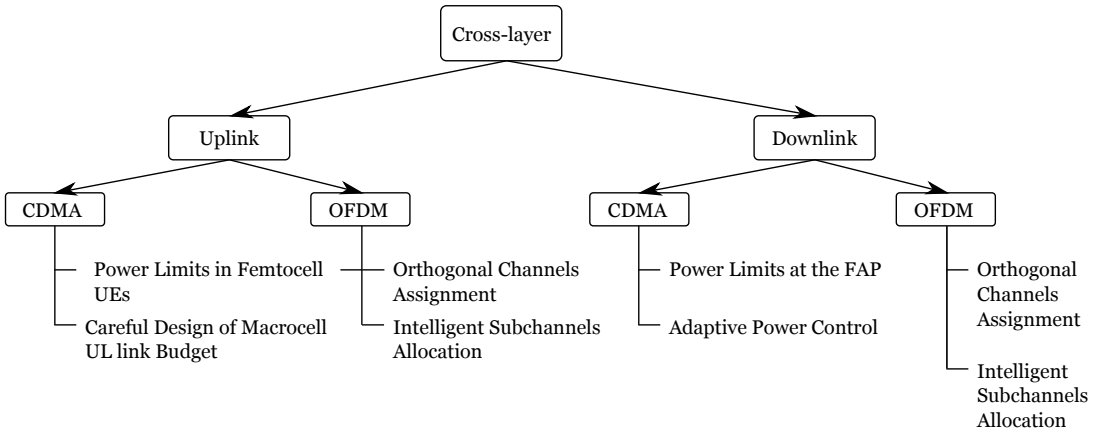

Figure 1.11: Approaches to coping with cross-layer interference, adapted from [50].

is connected. Implementing this type of technique, which requires inter-cell coordination, only becomes possible with the implementation of several network interfaces.

1.4.6 Spectrum Allocation

The different approaches adopted to manage the OFDMA subchannels are shown in Figure 1.12.

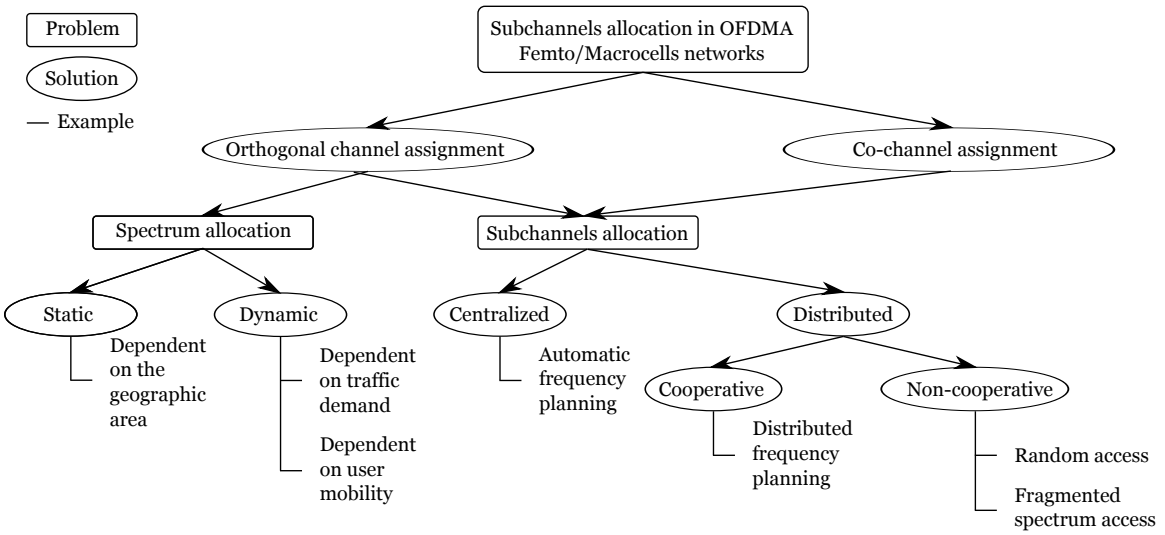

Figure 1.12: Classification and examples of subchannel allocation techniques for OFDMA femtocells, adapted from [50].

An approach that eliminates cross-layer interference is to divide the licensed spectrum into two parts (orthogonal channel assignment). Although it is optimal from a cross-layer interference standpoint, this approach is inefficient in spectrum reuse. Therefore, co-channel assignment of the macrocell and femtocell layers seems more efficient and also profitable for operators, although far more intricate from the technical point of view.
Ideally, to mitigate cross- and co-layer interference, there would be a central entity in charge of intelligently telling each cell which subchannels to use. This entity would need to collect information from the femtocells and their users and find an optimal or a suitable solution

within a short period. However, since the number and position of the femtocells are initially unknown because of the individualistic nature of the FAPs, this approach poses some challenging problems. The presence of hundreds of femtocells makes the optimization problem too complex, and latency issues arise when facilitating the femtocells' communication with the central subchannels broker throughout the backhaul.

A distributed approach to mitigate cross- and co-layer interference, where each cell manages its subchannels, is thus more suitable in this case (i.e., self-organization). In a non-cooperative solution, each femtocell would plan its subchannels to maximize its users' throughput and quality-of-service (QoS).

The adoption of self-configuration and self-optimization is discussed in [60]. Because of the uncertainty in the femtocells' number and positions, FAPs must be self-configurable and self-optimizing units capable of integrating themselves into the existing radio access network, causing the least interference to exist systems. Here, the FAPs must be capable of sensing the air interface and tuning their parameters according to changes in the network or channel.

On a significant number of references, femtocells are treated as one more static element on the network. Base stations are physically static elements working 24 hours a day during their working life. Having this in mind, it is easy to consider the same grid static during a simulation. Although some authors claim the 4G systems have smaller and more irregular cell sizes, they do not consider the possibility of having a grid model constantly changing because of the predicted femtocell behavior.

A decentralized spectrum allocation strategy has been proposed in [65] as an alternative to centralized/coordinated frequency assignment in a two-tier network. The proposed allocation strategy depends on the per-tier throughputs, the loading of users in each tier, and the QoS requirements, accounting for co-channel interference and path losses.

Authors from [66] focus on OFDMA based co-channel femtocells, which share the same spectrum with the macrocell network and aim to use spectrum resources while causing minimum interference macrocell network efficiently. The primary goal of [66] is to introduce an interference avoidance framework between a femtocell and the macrocell-associated mobile stations, which is based on not using the resource blocks[6] (RBs) occupied by closely located macrocell-associated mobile stations.

The fractional frequency reuse (FFR) scheme has attracted the attention of researchers in different standardization bodies and forums. Most proposals on FFR rely on static or semi-static coordination among BSs; it is seen in the literature that FFR schemes that use interference coordination in a static or semi-static manner provide little gain as cell-edge throughput can only be improved with a severe penalty to the system throughput. In addition, such schemes requiring frequency planning cannot be applied to the emerging femtocellular networks, as femtocells will be placed at the end-user locations ad hoc, making any prior frequency planning difficult. Dynamic coordination schemes do not require prior frequency planning and operate based on dynamic interference information from surrounding trans-

[6] A resource block is the smallest unit of resources that can be allocated to a user. The resource block is 180 kHz wide in frequency and 1 slot long in time. In frequency, resource blocks are either 12 x 15 kHz subcarriers or 24 x 7.5 kHz subcarriers wide The number of subcarriers used per resource block for most channels and signals is 12 subcarriers [67].

mitters. The fractional frequency reuse is also studied in [68] with a discussion about optimal power allocation for femtocells with different orthogonal sub-bands, based on analysis of macrocell interferences.

1.4.7 Femtocells Evolution in 3GPP Releases

The 3rd Generation Partnership Project (3GPP)[7] by the Technical Specification Group (TSG) Radio Access Network (RAN)[8] specifies for the first time the architecture to the support of HeNBs in Release 8 [71]. Figure 1.13 presents the overall E-UTRAN architecture, including eNBs and HeNBs.

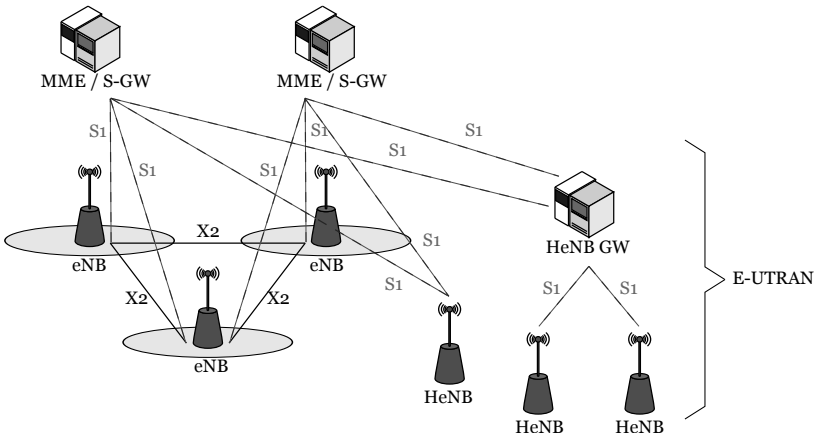

Figure 1.13: Release 8 overall E-UTRAN Architecture with deployed HeNB GW, adapted from [72].

The E-UTRAN architecture may deploy a home eNB (HeNB) gateway (GW) to allow the S1 interface between the HeNB and the evolved packet core (EPC)[9] to scale to support many HeNBs. The deployment of HeNB GW is optional, as this node acts as a concentrator. In Release 8, the specification did not support X2[10] connectivity of HeNBs. The S1 interface is defined as the interface between the HeNB GW and the core network, between the HeNB and the HeNB GW, between the HeNB and the Core Network, and between the eNB and the core network.

Release 10 enhances the support for HeNB with LTE-Advanced (LTE-A). Sometimes, the X2 interface between HeNBs could be used, which provides mobility and interference management between HeNB, and an S5 interface between HeNBs and mobility management entity (MME). Figure 1.14 presents those enhancements.

S5 provides tunnel management between serving GW and packet data network (PDN) GW. It is used for serving GW relocation because of UE mobility and if the serving GW needs to connect to a non-collocated PDN GW for the required PDN connectivity [75].

[7]The 3rd Generation Partnership Project (3GPP) unites seven telecommunications standard development organizations (ARIB, ATIS, CCSA, ETSI, TSDSI, TTA, TTC), known as “Organizational Partner” and provides their members with a stable environment to produce the Reports and Specifications that define 3GPP technologies [69].

[8]The TSG-RAN is responsible for the GERAN, UTRAN and E-UTRAN, including their internal structures and functions, of systems for evolved GERAN, UTRAN, E-UTRAN and beyond [70].

[9]EPC is the core network of the LTE system, details about the EPC are presented in [73], [74].

[10]X2 interface is the signaling interface between eNodeBs

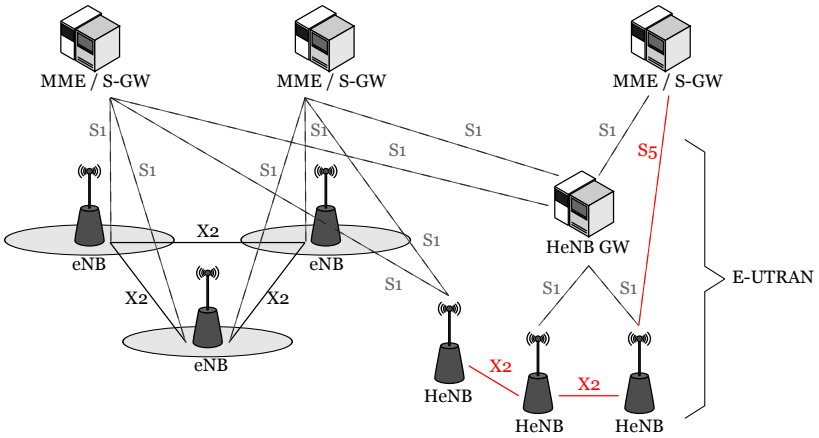

Figure 1.14: Release 10 overall E-UTRAN Architecture with deployed HeNB GW, adapted from [75].

The functions supported by the HeNB are the same as those supported by an eNB and the procedures run between a HeNB and the EPC are the same as those between an eNB and the EPC[11]. X2-based handover (HO) between HeNBs is allowed if no access control at the MME is needed, i.e., when the handover is between closed/hybrid access HeNBs having the same closed subscriber group (CSG) ID or when the target HeNB is an open access HeNB. This specification version supports direct X2-connectivity between HeNBs, independent of whether any of the involved HeNBs is connected to a HeNB GW.

We may have X2 connections between HeNB, especially enabling them to cooperate between them, for example, in the same building or particular location. X2 connections need to be fast. Although these two releases considered the X2 interface, X2-based communications between an eNB and a HeNB are not supported. The difficulty in adopting these connections between eNB and HeNB is its support, network infrastructure (physical interface), and incrementing signaling overhead.

The update presented in Release 11 [76] addresses the supported handovers between transmitter nodes, as shown in Table 1.2.

Table 1.2: X2-based HO support, adapted from [76].

Source node	Target node	Notes
eNB or any HeNB	Open access HeNB	
eNB or any HeNB	Hybrid access HeNB	
Hybrid access HeNB or closed access HeNB	Closed access HeNB	Only applies for same CSG ID and PLMN, and if the UE is a member of the CSG cell.
Any HeNB	eNB	

Release 11 supports direct X2-connectivity between HeNBs, independent of whether any of the involved HeNBs are connected to a HeNB GW. The overall E-UTRAN architecture with deployed HeNB GW is shown in Figure 1.15.

Release 12 [77] adds a new X2 connection and a new X2 GW, as presented in Figure 1.16. This specification version supports X2-connectivity between HeNBs, independent of whether any of the involved HeNBs are connected to a HeNB GW.

[11]The Local IP Access (LIPA) although is considered in [75], in this work is not taken into consideration.

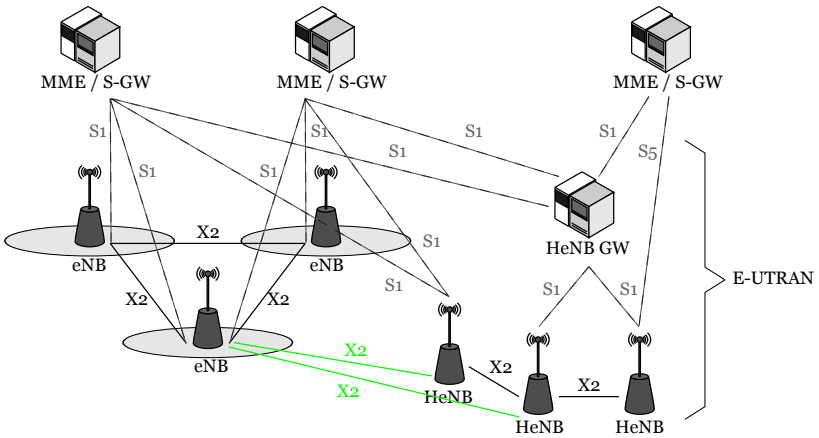

Figure 1.15: Release 11 overall E-UTRAN Architecture with deployed HeNB GW, adapted from [76].

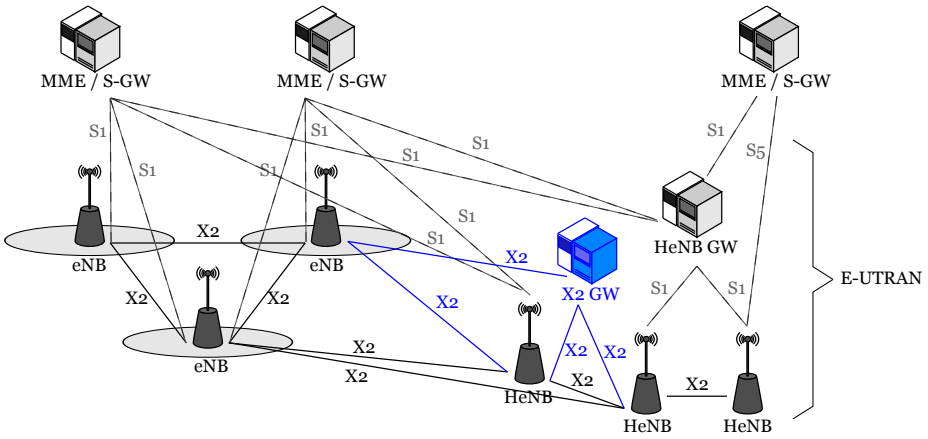

Figure 1.16: Release 12 overall E-UTRAN Architecture with deployed HeNB GW and X2 GW, adapted from [77].

A HeNB only connects to a single X2 GW. Each HeNB has to be pre-configured with information about which X2 GW it connects. There is no limitation on the number of X2 GWs an eNB may connect.
Since Release 12 [77] up to Release 16 [78], 3GPP has not proposed significant updates in the E-UTRAN HeNB logical architecture.

1.5 Main Objectives

The research from this thesis aim to contribute to the study of radio and heterogeneous network optimization and planning in small eNBs deployed in indoor environments and outdoor UMi scenarios. Since most of the traffic occurs indoors, and UEs require more and higher throughputs, this work seeks to understand the indoor environments when HeNBs provide coverage. Besides, the study of a UMi scenario intends to understand the urban space closer to the UE indoor scenarios.
A scenario with a high number of HeNBs to provide coverage to a building floor is studied. In [79], 3GPP determines the number of HeNBs available on a building floor by a probability theory approach. The nature of uncoordinated deployment of HeNBs and the possibility of buying them with no restrictions will originate deployments with high density of HeNBs. This overtakes the recommendations of [79].
Although usually, HeNBs are deployed in an uncoordinated and disordered way, the possibility of deploying HeNBs in a coordinated way cannot be ignored, or at least considering some planning. This statement is applicable in scenarios like offices, shopping centers, and industrial environments [19], [20]. The aim of this work is to present a theoretical study in the considered scenarios. Although this work incorporates some of the knowledge from [80]–[82], the aim is to conduct an autonomous detailed study.
3GPP deployment for indoor scenarios with a geometry of 5x5 apartments considers the total floor area to be fixed. The total floor area is divided into 25 square areas, where each one represents an apartment with an area of 10 m by 10 m. One aim of this work is to extract results when the total floor area varies and extract results for different areas of the floor.
This research addresses the radio resource management problems of small cells deployments. First the 3GPP indoor scenario with 5x5 apartment is considered and different deployment ratios are explored while varying apartment side length. The transmitter power of HeNBs varies between 0 dBm and 20 dBm. This range of values for the transmitter power will be explored in the behavior's study of the HeNBs. Understanding received power versus received interference power trade-off in heterogeneous networks where macrocell are overlaid by this type of femtocells is aim of this part of the work.
Packet scheduling influences the network performance depending on the service mixture [83]–[85]. Knowing that video streaming will be the most important application, packet schedulers are tested while evaluating their performance in different situations.
Outdoor users nearby indoor zones within these blocks of apartments intend to access the same services they use in indoor environments in a seamless way. According to ITU, UMi line-of-sight (LoS) scenario needs to be considered. As cell sizes are of few hundred meters,

a dual-slope path loss model [16], [17] is considered. The aim of this part of the work is to study three sub-6 GHz frequency bands. The optimization goals of this thesis are achieved while preserving the service quality packet loss ratio (PLR) target of 2% for video flows as well as best effort traffic (as well as fulfilling the service quality requirements for best effort traffic).

1.6 Contributions

To achieve above-mentioned goals, existing LTE-Sim [86] and 5G-air-simulator [87] platforms have been upgraded by means of different contributions. The contribution of a freeware extension of the LTE-Sim simulator that implements carrier aggregation functionalities was performed in [88], [89] and upgraded in [90]–[92].
The behavior and performance evaluation of different packet schedulers in a heterogeneous network with HeNBs has been studied in [93] while considering the variation in the transmitter power. This work also leads to the update of the open source LTE-Sim framework used in this work.
Uncoordinated deployment of HeNBs has been widely considered in the research community. However, because of economic or physical constraints, coordinated deployment of HeNBs can also be considered. An initial example of HeNB deployments was investigated in [94], which includes a theoretical study on the average SINR which includes high and middle interference level scenarios, with a maximum of four users per HeNB, were addressed in [95]. These works not only consider system level simulations but also a theoretical study of the SINR, by considering the variation of the transmitter power and the areas of the apartments. One assumed that users in each apartment are served by their own HeNB, i.e., one HeNB serves each apartment in the building. This overrides the 3GPP technical recommendations.
The performance evaluation of small cells whose usage is video streaming while fulfilling the 3GPP PLR target of 2%, was studied in [96]. One HeNB serves each apartment in the building. The number of users in each apartment increased up to the point where PLR for voice services surpassed the recommendations of [97]. In [91], [92], we have updated the 4G outdoor macrocell framework to get uniform distribution of users while enhancing the random numbers generator. The service quality in a UMi LoS cellular scenario in the sub-6 GHz frequency bands while QoS target is not surpassed was presented in [98], [99].
Different contributions resulted from this research work. In [100], the variation of the number of deployed HeNBs within the considered indoor topology is analyzed. The deployment of 4, 5, or 6 HeNBs was compared in the indoor scenario. LTE-Sim was updated to extract values for exponential effective SINR mapping (EESM), PLR, a maximum number of supported users, goodput, and delay in these scenarios. Experimental work to verify the WINNER II indoor propagation model was performed in [101].
The work from [102] studies the performance of HeNBs with varying coverage areas. After a detailed theoretical study of the SINR, performance results are obtained through simulation in small cell indoor scenarios. Goodput, delay, and PLR results are analyzed. Based on

underlying improved version of LTE-Sim, the proportional fair (PF), frame level scheduler (FLS), and exponential rule (EXPRule) are tested in the indoor environment. The scenario was simulated while considering QoS targets. In [91], [92], one has also considered an accurate uniform distribution of users within the cell, while considering the Mersenne Twister pseudo-random generator to obtain near-truly random distributions. In this contribution, optimization of the carrier aggregation by considering multi-band scheduling was addressed in an outdoor macrocellular scenario.
The novel contributions resulting from the research, mentioned above, have already been disseminated in papers published or submitted for possible publication in journals, conferences, and a book chapters, structured as follows:

- Journal Papers:

  [100] R. R. Paulo, F. J. Velez, and B. Khan, "Study of Indoor Small Cell Deployments," in *Journal of Mobile Multimedia*, vol. 17, Iss 1-3, February 2021, pp. 329–344;

  [102] R. R. Paulo, and F. J. Velez, "An Extensive Study on the Performance Evaluation and Scheduling of HeNBs," in *IEEE Access*, vol. 17, March 2021, pp. 1–6;

  [92] B. Khan, A. R. Ramos, R. R. Paulo, and F. J. Velez, "Deployment of Beyond 4G Wireless Communication Networks with Carrier Aggregation," in *International Journal of Electronics and Communication Engineering*, vol. 15, no. 12, March 2021;

  [99] R. R. Paulo, E. B. Teixeira, and F. J. Velez, "Service Quality of the Urban Micro Cellular Scenario in the sub-6 GHz Frequency Bands," submitted for possible publication to *IEEE Transactions on Wireless Communications*, November 2021.

- Conference papers:

  [88] D. Robalo, F. J. Velez, R. R. Paulo, and G. Piro, "Extending the LTE-Sim Simulator with Multi-Band Scheduling Algorithms for Carrier Aggregation in LTE-Advanced Scenarios," in 2015 IEEE 81st Vehicular Technology Conference (VTC Spring), May 2015, pp. 1–6;

  [94] R. R. Paulo, F. J. Velez, and G. Piro, "Design of Coordinated HeNB Deployments," in *2018 IEEE 87th Vehicular Technology Conference (VTC Spring)*, June 2018, pp. 1–6;

  [95] R. R. Paulo, F. J. Velez, and G. Piro, "Performance Evaluation and Packet Scheduling in HeNB Deployments," in *2018 IEEE 88th Vehicular Technology Conference (VTC-Fall)*, August 2018, pp. 1–6;

  [96] R. R. Paulo and F. J. Velez, "A study on system capacity for HeNBs with different schedulers," in *Conf. on Telecommunications - ConfTele*, June 2019, pp. 25–28;

  [91] B. Khan, A. Ramos, R. R. Paulo, F. J. Velez, "Deployment of Beyond 4G Wireless Communication Networks with Carrier Aggregation," in *ICEEE 2020: 14.*

International Conference on Electronics and Electrical Engineering, July 2020 (Best Presentation Award – ICEEE 2020);

[98] R. R. Paulo and F. J. Velez, "System Level Simulation of Urban Micro-cellular 4G Scenarios in the Sub-6 GHz Frequency Bands," in *2021 Telecoms Conference (ConfTELE)*, February 2021, pp. 1–6.

[101] R. M. Andrade, R. R. Paulo, S. M. Francisco, E. B. Teixeira, and F. J. Velez, "Characterization of Indoor Small Cells Propagation," in 2021 *24th International Symposium on Wireless Personal Multimedia Communications (WPMC)*, Dec 2021.

- Book chapter:

  [93] S. Ruiz, H. Ahmadi, G. Gardašević, Y. Haddad, K. Katzis, P. Gracioso, V. Petrini, A. Reichman, M. K. Ozdemir, F. J. Velez, R. R. Paulo, S. Fortes, L. M. Correia, B. Rouzbehani, M. Barahman, M. Deruych, S. Mignardi, K. Nasr, and H. Zhang, *Inclusive Radio Communications for 5G and Beyond*, 1st ed. Academic Press, May 2021, ch. 5G and beyond networks, pp. 141–186.

- Contributions to Book chapters:

  [89] S. Ruiz, M. Garcia-Lozano, D. Gonzalez, M. Lema, J. Papaj, W. Joseph, M. Deruyck, N. Cardona, C. Garcia, F. J. Velez, L. Correia, L. Studer, P. Grazioso, and S. Chatzinotas, *Cooperative Radio Communications for Green Smart Environments* River Publishing, Kent, -1, June 2016, ch. 6 - Green and Efficient RAN Architectures, pp. 195–270.

The work has also been communicated in RTCM Seminars, COST meetings and other meetings:

11th Meeting of the Management Committee of COST IC 1004 - Cooperative Radio Communications for Green Smart Environments, TD(15)12082, Dublin, Ireland, January 2015;

2nd Meeting of the Management Committee of COST CA 15104 - Inclusive Radio Communication Networks for 5G and Beyond,TD(16)01031, Lille, France, June 2016;

4th Meeting of the Management Committee of COST CA 15104 - Inclusive Radio Communication Networks for 5G and Beyond, TD(17)04084, Lund, Sweden, May 2017;

6th Meeting of the Management Committee of COST CA 15104 - Inclusive Radio Communication Networks for 5G and Beyond,TD(18)06018, Nicosia, Cyprus, January 2018;

25th Seminar of the Mobile Communications Thematic Network (RTCM), Porto, Portugal, June 2018;

8th Meeting of the Management Committee of COST CA 15104 - Inclusive Radio Communication Networks for 5G and Beyond, TD(18)08025, Podgorica, Montenegro, October 2018;

10th Meeting of the Management Committee of COST CA 15104 - Inclusive Radio Communication Networks for 5G and Beyond, TD(19)10062, Oulu, Finland, May 2019;

27th Seminar of the Mobile Communications Thematic Network (RTCM), Castelo Branco, Portugal, July 2019;

Ciência 2019 - Encontro com a Ciência e Tecnologia em Portugal, Lisboa, Portugal, July 2019;

29th Seminar of the Mobile Communications Thematic Network (RTCM), Virtual Event, February 2021;

2nd Post-IRACON Meeting of COST CA 15104 - Inclusive Radio Communication Networks for 5G and Beyond, TD(21)14002, Online Meeting, February 2021.

1.7 Structure of the Thesis

This thesis is organized into six chapters and six appendices that support the chapters. This Chapter started by presenting the motivation to study the radio resource management challenges in scenarios with small cells, and the proposed approach. An overview of small cell life cycle (past, present, and future) was provided with more emphasis on femtocells. It discussed how small cells began until our days, passing through themes like ultra-dense and heterogeneous networks as a perspective towards 5G. The concept of how femtocells have been deployed is addressed in detailed. Then, the primary objectives of the research involved in this thesis, and the main contributions are presented.
Chapter 2 introduces a mathematical study in an indoor scenario. We have considered a 3GPP 5x5 grid geometry with twenty-five apartments. In the addressed scenarios, the number of deployed HeNBs varies from 4 HeNBs up to 25 HeNBs. In the mathematical study, frequency reuse pattern two and the WINNER II path loss model for indoor scenarios are assumed. The EESM, channel quality indicator (CQI), and transport block size (TBS), performance metrics are determined by extensive system level simulations.
Chapter 3 introduces improvements to the simulation tool LTE-Sim that facilitates the results for this work. With these improvements, and going beyond 3GPP recommendations, a scenario with 25 HeNBs and reuse patterns one and two has been studied. In a conservative approach, one has considered only four UEs connected to each HeNB. Besides, this chapter considers three different packet schedulers to determine the system's performance, PF, FLS, and EXPRule. The packet scheduler running in the radio nodes distributes the radio resources among the UE. After initial results are analyzed, the maximum supported capacity is determined for frequency reuse pattern two.
An approach more closely related to 3GPP recommendations is considered in Chapter 4. First, a scenario with only 4 HeNBs complements the theoretical approach proposed in Chapter 2. Then results for the maximum capacity with 4, 5, and 6 HeNBs have been extracted. Apart from considering a variation in the number of HeNBs, the impact of independent variations of the transmitter power of HeNBs and the apartment side lengths were studied. In

fact, in this chapter we learn in which extent the orientations appointed by 3GPP to indoor scenarios are the ones that provide the best quality of experience for the UEs.
Chapter 5 studies a UMi LoS scenario considering a dual-slope path loss model. Three different sub-6 GHz frequency bands have been studied, 2.6 GHz, 3.5 GHz, and 5.62 GHz frequency bands. The PF and the maximum-largest weighted delay first schedulers have been considered. The radio performance has been analyzed by considering the EESM and modulation and coding scheme mapping. Simulation results have been obtained while considering the 3GPP QoS targets.
Finally, Chapter 6 presents the conclusions, and recent trends in small cell energy efficient spectrum management research as well suggestions for future research.
The code used in the theoretical study is presented in Appendix A. Appendix B introduces the code that allowed to obtain results for the EESM, CQI, and TBS. Appendix C studies the EESM considering either 25 or 4, 5, and 6 HeNBs and reuse pattern one. Appendix D presents the developed code for the LTE-Sim upgraded version for the 25 HeNBs scenario (and also other scenarios). Appendix E presents the code developed for the scenario that considers 4, 5, or 6 HeNBs. Finally, Appendix F presents simulation results for the variation of the average delay of video flows with 4, 5, or 6 HeNBs.

Chapter 2

SINR and Performance Metrics Analysis in a 3GPP 5x5 Grid Geometry

2.1 Introduction

A user which is receiving data from a node, e.g., eNodeB (eNB) or home eNodeB (HeNB), is not only receiving a signal from the node to which we connect it to but also receiving interfering signals from the co-channel nodes. The studied scenario along this chapter is an indoor scenario, defined in [79], that consist in a building with one floor with a geometry of 5×5 apartment grid with 25 apartments. We can deploy a HeNB in the center of every apartment [79], [103].
In the first part of this chapter, after describing the femtocell network deployment, a detailed mathematical process to get results for the average signal-to-interference-plus-noise ratio (SINR) is presented. The definition of the scenario follows some assumptions of the Technical Specification Group (TSG) Radio Access Network (RAN) from 3GPP [79]. To detail the process to get the equations to determine the average SINR, we consider the deployment of 25 HeNBs with reuse pattern two. After present results for the average SINR for the deployment of 25 HeNBs, we consider the same geometry but with the deployment of 4 HeNBs.
In the second part a study of the exponential effective SINR mapping (EESM) is made for the scenario with 25, 4, 5 and 6 HeNBs. The last three scenarios, is a study around of the maximum value for the deployment ratio appointed by 3GPP [79].
To get the results for the average SINR, the code presented in Appendix A has been developed. Appendix B presents the code developed in LTE-Sim to get EESM results for the considered number of HeNBs, as well as another deployment patterns. Although the core of this chapter considers a reuse pattern two, we present results in terms of EESM for a reuse pattern one in Appendix C.

2.2 Femtocell Network Deployment

The deployment of femtocell requires to mitigate cross-tier interference between the macrocell and femtocells, and intra-tier interference among femtocells, as well as to provide QoS guarantees [104]. In [104] authors express some concerns about this requirement and leverage the cognitive radio technology to propose a new cognitive radio resource management scheme for femtocells to mitigate cross-tier interference.
The addition of small cells, such as femtocells, in the current scenarios, requires an evolution of the traditional cellular model [10]. To predict the impact of the addition of femtocells, there is a need to remodel the cellular networks. There appear to be four high-level approaches to modeling femtocells in cellular networks, although the details can vary from

work to work. And of course, some works may use and even compare several of the below models [105].

The first approach is to keep the familiar grid model for macro base stations (including the special case of a single macro BS (MBS)), and to drop femtocells "on top" of it, either randomly or in a deterministic fashion. One BS (usually the closest and/or strongest) would connect to the mobile user, with all other macrocell and femtocell BSs (downlink) or mobile users (uplink) acting as interference.

A second simpler but less complete model is to focus on a single femtocell (and its associated user) dropped in the cellular network. In the downlink (DL), the interference to the femtocell user (FUE) is assumed to be only from the various macrocells, which is a fairly sparse femtocell deployment, is probably accurate. In the uplink as well, the strong interference is bound to come from nearby mobiles transmitting at high power up to the macro base station, so the model may be reasonable. The main limitation of this model vs. model 1 is that the performance of DL macrocell users (MUEs) – who may experience strong femtocell interference depending on their position – cannot be accurately characterized.

The third model is to allow both the macrocells and femtocells to be randomly placed. An appealing aspect of this approach is that the randomness allows significantly improved tractability and the SINR distribution can be found explicitly. This may allow the fundamental impact of different PHY and MAC designs to be evaluated theoretically.

A fourth model is simply to keep all the channel gains (including interfering channels) and possibly even the various per-user capacities general, without specifying the precise spatial model for the various base stations. This can be used in many higher-level formulations, e.g. for game theory, power control, and resource allocation, although ultimately some distribution of these channel gains must be assumed to do any simulation, and the gains are to a first-order determined by the locations of the various transmitting sources. In [105] it is a state that this fourth model typically will conform to one of the above three models.

For simulators like LTE-Sim [103] and NS-3 [106] it is easier to adopt the first approach, that is to keep the familiar grid model for MBSs, and drop femtocells on top of it. Even using the first approach, it could be possible to adopt some from the fourth model, like to keep all the channel gains.

3GPP defines the simulation assumptions and parameters for FDD HeNB RF requirements in [79]. In this report, 3GPP introduces two modeling deployments for HeNB, suburban modeling and dense deployment modeling.

In the suburban modeling HeNBs are dropped within the macro coverage area with a random uniform distribution, subject to minimum separation to the macro sites. The density of HeNBs per macrocell will be a variable in the simulations. Each of the dropped HeNBs is assumed to be "active", i.e., there is at least one active call. A suburban-type deployment is considered where each HeNB is modeled as a (2 dimensional) rectangular house. Within each house, the HeNB and HeNB user equipments (UEs) are randomly dropped within a specified distance of the center point of the house. All macro UEs are assumed to be indoors. A macro UE maybe within a HeNB house coverage zone [79].

For dense deployment modeling two geometries are proposed: a dual stripe model and a 5x5

grid model. In a dense-urban HeNB modeling, each block represents two stripes of apartments, each stripe has 2 by N apartments, usually, N is 10, as illustrated in the example of Figure 2.1.

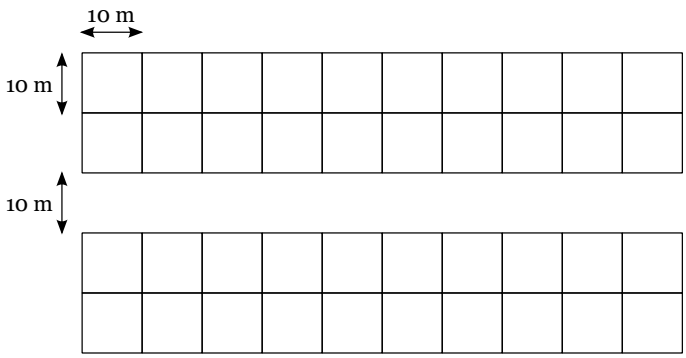

Figure 2.1: A femtocell block in a dual stripe model, adapted from [79], [103].

Each apartment is of size 10 m by 10 m. There is a street between the two stripes of apartments, with a width of 10 m. In each macrocell sector, one or several femtocell blocks are randomly dropped. It is assumed that the femtocell blocks are not overlapping with each other. Each femtocell block has L floors, L is chosen randomly (L could be a number between 1 and 10). If more than one femtocell blocks are dropped, each femtocell block can have a different number of floors.

Another proposed geometry is a 5x5 grid model as an alternative simple HeNB cluster model. It is considered a single-floor building with 25 apartments. The apartments are 10 m by 10 m and are placed next to each other on a 5x5 grid on each floor, Figure 2.2. In addition, it is assumed that, with probability p, there is a HeNB in each apartment. This probability represents the density of HeNB deployment. For the apartments that have a HeNB, the HeNB and UE are dropped randomly and uniformly in the apartment with a minimum separation of 20 cm.

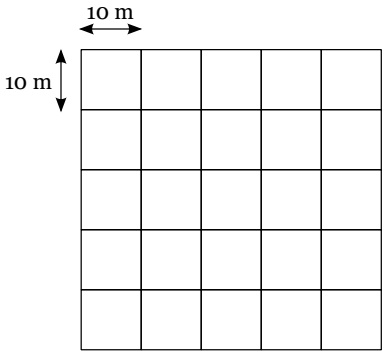

Figure 2.2: A femtocell block in a 5x5 grid model, adapted from [79], [103].

In simulators like LTE-Sim [86], it is possible to create scenarios like the one in Figure 2.3 with high flexibility. This scenario can be extended for integrating real street maps.

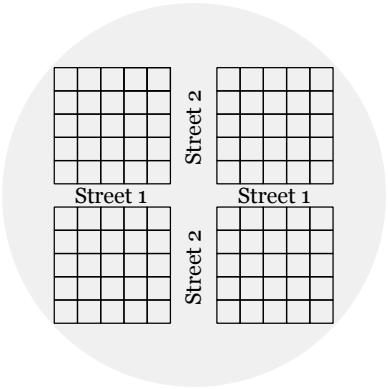

Figure 2.3: Example of a cross composed of two different streets and four 5x5 grid model buildings deployed in a eNB, adapted from [103].

2.3 Study of the Average SINR for Reuse Pattern Two

2.3.1 Definition of the Geometry to a Coverage With 25 HeNBs

To the study of the average SINR, in this research, in practice, a single-floor building with 25 apartments is considered, as shown in Figure 2.4. Apartments are placed next to each other in a 3GPP 5x5 grid geometry [79].

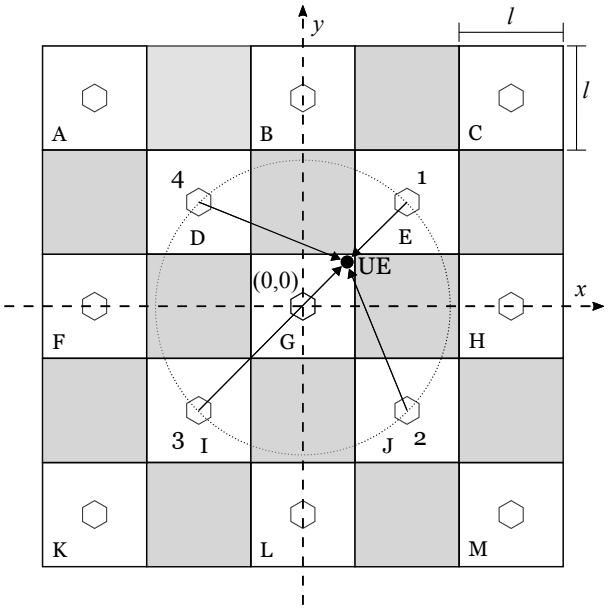

Figure 2.4: Simulation scenario of 25 apartments with 25 HeNBs deployed, reuse pattern 2.

Frequency reuse is the design process of selecting and allocating different channel groups for all cellular base system within a system [107]. Frequency reuse increases both coverage and capacity of the cellular network and reduces the inter-cell interference. For a frequency reuse equal to one, each cell uses all the available subchannels. When the frequency is higher than one, each cell does not use all the available subchannels but only a subset, in such a way that different adjacent cells utilize different subsets of subchannels. A group of cells, using the complete set of available subchannel together, forms a cluster that is regularly replicated in order to cover the whole service area. As described in [108], the number of cells that form the

cluster depends from the evolved universal terrestrial radio access network (E-UTRAN) operative band and on the downlink (uplink) bandwidth. The available bandwidth distributed among clusters in order that all cells belonging to the same cluster have not overlapping channels.

This work considers two different levels of interference, a middle interference scenario when the frequency reuse is equal to one, and a more optimistic low interference scenario with a frequency reuse equal to two at the small cells layer. In the eNBs cell layer the frequency reuse is always equal to one. Although this work also presents results when the frequency reuse is equal to one, due to be more optimistic, the main focus is to obtain a more detailed study with a frequency reuse is equal to two.

Considering a frequency reuse equal to two, as can be seen in Figure 2.4, HeNBs operate with a 10 MHz bandwidth [107], [108], i.e., the total 20 MHz of available bandwidth is divided into two equal parts of 10 MHz. The impact of considering a 20 MHz or 10 MHz bandwidth and the mapping of the SINR into the maximum supported throughput are presented in [80] and [109]. The HeNBs in the apartments, represented by the light gray fill in Figure 2.4, use the 10 MHz bandwidth, while the apartments with white fill use the remaining 10 MHz. In Figure 2.4, the HeNBs are represented by a hexagonal shape. Although there is one HeNB inside each apartment, only HeNBs in the apartments with white fill are represented.

Following the approach implemented in [96], users are truly located inside their own apartments. This means that there are no walls between a user and the corresponding HeNB. When the user is served by a HeNB using a given frequency band, it will suffer interference from the co-channel HeNBs. Since a reuse pattern of two is considered, there will be three different cases of interference for the first tier of interference from the HeNBs to the user terminals. In the first case, the users are inside apartments D, E, G, I, and J, and there are four neighboring interference nodes close to their apartments, as shown in Figure 2.4. In the second case, the users are inside apartments B, F, H, and L, and there are only two neighboring interference nodes HeNBs. In the third case, the users are inside apartments A, C, K, and M, and there is only one neighboring interferer.

2.3.2 SINR at a Given Position

For the sake of simplicity, let us consider the central apartment G and apartment E, which causes interference to users from apartment G, as shown in Figure 2.5. Let us assume a user

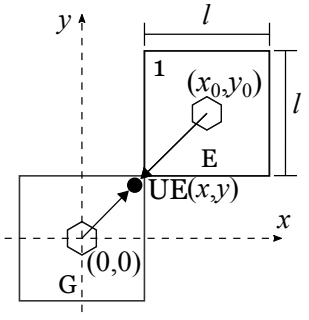

Figure 2.5: Interference received from one of the neighboring HeNBs and the signal from the user's own HeNB.

equipment/terminal, in our case, UE, inside and confined to apartment G.
The center of the apartment is also the origin of the coordinate system (0, 0). To obtain the average SINR, an approach similar to the one described in [94], [110], [111] is applied. In general, the SINR from the considered UE, at a position with the coordinates (x, y), served by a cell with a transmitter power P_{Tx} (in linear terms) can be expressed as

$$\text{SINR}(P_{Tx}, x, y) = \frac{P_{ow}(P_{Tx}, x, y)}{(1-\alpha) \cdot P_{ow}(P_{Tx}, x, y) + P_{nh}(P_{Tx}, x, y) + P_{noise}}, \quad (2.1)$$

where P_{ow} is the average amount of power received from the user's own cell and α is the orthogonality factor of the codes [112]. For the sake of simplicity, and according to [82], α is considered to be equal to one. P_{nh} is the average interference power from the neighboring cells. P_{noise} is the thermal noise power. In (2.1), all these powers are given in linear terms. P_{noise}, in dBW, is defined as follows

$$P_{noise} = -174 + 10 * \log_{10} BW - 30 + NF, \quad (2.2)$$

where the noise figure, NF, is considered to be 8 dB (for LTE, NF is typically 7-9 dB [79]) and the bandwidth BW=10 MHz. The received power from the own cell, P_{ow}, can be expressed as

$$P_{ow}(P_{Tx}, x, y) = P_{Tx} G_{Tx} G_{Rx} 10^{-\frac{PL}{10}} \quad (2.3)$$

where G_{Tx} and G_{Rx} are the transmitter and receiver gains, respectively. PL is the path loss. As stated above the P_{nh} is the interfering power received by a UE from the N neighbor cells, and is given by,

$$P_{nh}(P_{Tx}, x, y) = \sum_{i=1}^{N} I_i(P_{Tx}, x, y) \quad (2.4)$$

where I_i is the i^{th} cell interference and is expressed as

$$I_i(P_{Tx}, x, y) = P_{Tx} G_{Tx} G_{Rx} 10^{-\frac{PL(x,y)_i}{10}} \quad (2.5)$$

i represents the cell from which the interference comes from.
The average interference generated by a neighboring cell can be calculated by integrating each fraction of the interference power over the area of the affected cell. Figure 2.5 shows a cell affected by interference at the origin of the coordinates and one interfering cell at (x_0, y_0). By integrating over the cell area, the average level of the power received from a neighboring cell, $\bar{I}$, may be calculated as

$$\bar{I} = \int_x \int_y f_I(P_{Tx}, x, y) dx dy = \int_x \int_y \frac{P_{Tx} G_{Tx} G_{Rx}}{A_{Apt}} PL(x, y) dx dy, \quad (2.6)$$

A_{Apt} is the total affected apartment area.

3GPP in [79] for the purpose of simulations in dual-stripe model or 5x5 Grid models in urban environments, considers a simplified path loss model (PLM) that does not consider the attenuation of walls, for the link between the UE and HeNB, and stands as follows

$$PL_{HeNB}(x,y) = 127 + 30 * \log_{10}\left(\frac{d}{1000}\right), \quad (2.7)$$

where d is the distance between the transmitter and the UE in meters. The UE is within or outside the building. Since this PLM did not consider the number of walls the WINNER II in building path model [113] is considered in this work. Accounting the number of walls located in between the user and the HeNBs. For an indoor office, the path loss equation of the WINNER II model is as follows

$$PL_{HeNB}(x,y) = A * \log_{10}(d) + B + C * \log_{10}\left(\frac{f_c}{5}\right) + X, \quad (2.8)$$

f_c is the frequency in GHz, and the fitting parameter A includes the path loss exponent. Parameter B is the intercept, parameter C describes the path loss frequency dependence, and X is an environment-specific term (e.g., wall attenuation in the non-line-of-sight (NLoS) scenario [113]). The distance d is determined by the Euclidean distance

$$d = \sqrt{(x - x_0)^2 + (y - y_0)^2}, \quad (2.9)$$

where x_0 and y_0 are the coordinates of the interfering cell and x and y are the coordinates of the UE, as shown in Figure 2.5; in this study, $f_c = 2$ GHz. For line-of-sight (LoS) propagation, A=18.7, B=46.8, and C=20. In the NLoS case, A=20, B = 46.4 and C=20. The environment-specific term X is the sum of the attenuation of the walls between the UE and HeNB. For internal heavy walls, the attenuation is considered 10 dB. An experimental study of the propagation in the indoor scenario is presented in [101].

In the first case, the central HeNB is considered, and there are 4 HeNBs in the first ring of interference (labeled 1, 2, 3 and 4), as shown in Figure 2.4. Considering only the interferer HeNB from Figure 2.5 (identified by number 1), the path loss is given by the following equation

$$PL(x,y)_1 = 20 * \log_{10}\left(\sqrt{(x-l)^2 + (y-l)^2}\right) + 46.4 + 20 * \log_{10}\left(\frac{2}{5}\right) + 2 * 10, \quad (2.10)$$

where l is the apartment side length. For the remaining three HeNBs in the first ring of interference (2, 3 and 4 in Figure 2.4), the coordinates (x_0, y_0) change to $(l, -l)$, $(-l, -l)$ and $(-l, l)$, respectively, as shown in Figure 2.4 and presented in the following equations:

$$\begin{aligned} PL(x,y)_2 &= 20 * \log_{10}\left(\sqrt{(x-l)^2 + (y+l)^2}\right) + 46.4 + 20 * \log_{10}\left(\tfrac{2}{5}\right) + 2 * 10 \\ PL(x,y)_3 &= 20 * \log_{10}\left(\sqrt{(x+l)^2 + (y+l)^2}\right) + 46.4 + 20 * \log_{10}\left(\tfrac{2}{5}\right) + 2 * 10 \\ PL(x,y)_4 &= 20 * \log_{10}\left(\sqrt{(x+l)^2 + (y-l)^2}\right) + 46.4 + 20 * \log_{10}\left(\tfrac{2}{5}\right) + 2 * 10 \end{aligned} \quad . \quad (2.11)$$

In this first case, only four interferes are assumed, as due to the increase in the number of walls and the longest distance between HeNBs from the farthest ring of interference and the user, the underlying share of interference is negligible.

For the second and third cases, in addition to the change in the number of interferer HeNBs, as explained above, the change in coordinates of the user's own cell and of the interferes need to be considered. In the second case, there are only two interference nodes in the first ring of interference, while in the third case, there is only one interferer.

2.3.3 Average SINR for a 3GPP 5x5 Grid Geometry with 25 HeNBs

UEs are uniformly distributed over the apartment area. According to [82], the average SINR experienced by UEs depends on the apartment side length l and on the HeNB transmitter power, P_{Tx}, as follows [114],

$$\overline{\text{SINR}}(l, P_{Tx}) = \frac{\overline{P}_{ow}(l, P_{Tx})}{(1-\alpha)\overline{P}_{ow}(l, P_{Tx}) + \overline{P}_{nh}(l, P_{Tx}) + P_{noise}} \quad (2.12)$$

for simplicity, α is considered equal to one. The $\overline{P_{nh}}(l, P_{Tx})$ is the average interference power from the neighboring HeNBs. The average interference generated by a neighbor cell can be calculated by integrating each fraction of the interfering power over the area of the affected area. The average interference power $\overline{P}_{nh}$ can be defined as

$$\overline{P}_{nh}(l, P_{Tx}) = \sum^{n_T} \bar{I}(l, P_{Tx}), \quad (2.13)$$

which is the total surrounding power received from interfering neighbors at different distances. n_T is the total number of interfering neighbors. The average interference generated by the interfering HeNBs can be calculated by integrating each fraction of the interfering power over the affected area. Since the UE is confined to the apartment area, the average level of received interference from a neighboring cell $\bar{I}$ is integrated over the apartment area

$$\bar{I}_i(l, P_{Tx}) = \sum_{i=1}^{n_T} \int_{\Gamma_x^i} \int_{\Gamma_y^i} f_{I_i}(P_{Tx}, x, y) dy dx = \sum_{i=1}^{n_T} \int_{\Gamma_x^i} \int_{\Gamma_y^i} \frac{P_{Tx} G_{Tx} G_{Rx}}{A_{Apt}} PL(x, y) dx dy. \quad (2.14)$$

Assuming the different distances between the HeNBs and the UE, we may calculate the average interference as,

$$\bar{I}_i(l, P_{Tx}) = \sum_{i=1}^{n_T} \int_{\Gamma_x^i} \int_{\Gamma_y^i} f_{I_i}(P_{Tx}, x, y) dy dx. \quad (2.15)$$

The integration regions for an interfere HeNB are as follows

$$\Gamma_x^i = \{[-l/2, l/2]\} \quad (2.16)$$

and

$$\Gamma_y^i = \{[-l/2, l/2]\}. \quad (2.17)$$

According to [115], the following parameters are considered: G_{Tx}=5 dBi and G_{Rx}=0 dBi. The first tier of HeNBs, $f_I(P_{Tx}, x, y)$ is given by the following equations

$$\begin{aligned} f_{I_1}(P_{Tx}, x, y) &= \frac{P_{Tx}G_{Tx}G_{Rx}}{l^2} 10^{-\frac{20*\log_{10}\left(\sqrt{(x-l)^2+(y-l)^2}\right)+46.4+20*\log_{10}\left(\frac{2}{5}\right)+2*10}{10}} \\ f_{I_2}(P_{Tx}, x, y) &= \frac{P_{Tx}G_{Tx}G_{Rx}}{l^2} 10^{-\frac{20*\log_{10}\left(\sqrt{(x-l)^2+(y+l)^2}\right)+46.4+20*\log_{10}\left(\frac{2}{5}\right)+2*10}{10}} \\ f_{I_3}(P_{Tx}, x, y) &= \frac{P_{Tx}G_{Tx}G_{Rx}}{l^2} 10^{-\frac{20*\log_{10}\left(\sqrt{(x+l)^2+(y+l)^2}\right)+46.4+20*\log_{10}\left(\frac{2}{5}\right)+2*10}{10}} \\ f_{I_4}(P_{Tx}, x, y) &= \frac{P_{Tx}G_{Tx}G_{Rx}}{l^2} 10^{-\frac{20*\log_{10}\left(\sqrt{(x+l)^2+(y-l)^2}\right)+46.4+20*\log_{10}\left(\frac{2}{5}\right)+2*10}{10}} \end{aligned} . \quad (2.18)$$

As l is positive (2.15) is solvable. Accounting only the HeNBs from the first tier

$$\int_{\Gamma_{x,y}^i} (P_{Tx}, x, y) dy dx = P_{Tx}G_{Tx}G_{Rx} 10^{-\frac{\sum_{i=1}^{4} 20*\log\left(\sqrt{x^2+y^2}\right)+46.4+20*\log_{10}\left(\frac{2}{5}\right)+2*10}{10*A_{cell}}}. \quad (2.19)$$

By determining the exponent in (2.19) one gets the total interference. As an example, for the first interfering node in the first tier, the exponent in (2.19) is calculated as follows

$$\int_{-l/2}^{l/2}\int 20 * \log_{10}\left(\sqrt{(x-l)^2+(y-l)^2}\right) + 46.4 + 20 * \log_{10}\left(\frac{2}{5}\right) + 2 * 10 \, \mathrm{d}y \, \mathrm{d}x. \quad (2.20)$$

The average power received from the user's own cell, $\overline{P}_{ow}(P_{Tx,x,y})$, is constant no matter the value of the reuse pattern. It may be obtained by following an approach similar to the one used in the computation of $\overline{P}_{nh}(l, P_{Tx})$ but with a different integrate function

$$\overline{P}_{ow}(l, P_{Tx}) = \int_y \int_x \frac{P_{Tx}G_{Tx}G_{Rx}}{A_{ow}} 10^{-\frac{18.7*\log_{10}\left(\sqrt{(x^2+y^2}\right)+46.8+20*\log_{10}\left(\frac{2}{5}\right)}{10}} dxdy. \quad (2.21)$$

However, the integration area includes the origin of the coordinate system, (x, y)=(0,0). Since the HeNB is at those coordinates [116], equation 2.21 converges to infinity and is unsolvable. Without considering a circular area with a radius equal the Fraunhofer distance, F_r, the circle with the white fill in Figure 2.6, extracted from the total cell area (2.21), becomes solvable. A_{ow} is the total integration area, represented by the grey fill in Figure 2.6,

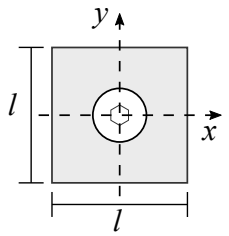

Figure 2.6: Geometry for the own cell with the Fraunhofer distance, adapted from [117].

$$A_{ow} = l^2 - \pi \times F_r^2. \quad (2.22)$$

The integration limits of (2.21) take into consideration subtraction of the circular area with a radius equal the Fraunhofer distance.

2.3.4 Average SINR Results for a Reuse Two With 25 HeNBs

Results presented on Figure 2.7 were obtained with the code presented in Appendix A with Wolfram Mathematica©, [118]. Results for the average SINR are presented in Figure 2.7 as a function of the apartment side length, l, and the transmitter power, P_{Tx}. The apartment side length varies from 5 to 35 m, while the transmitter power varies from -20 to 30 dBm.

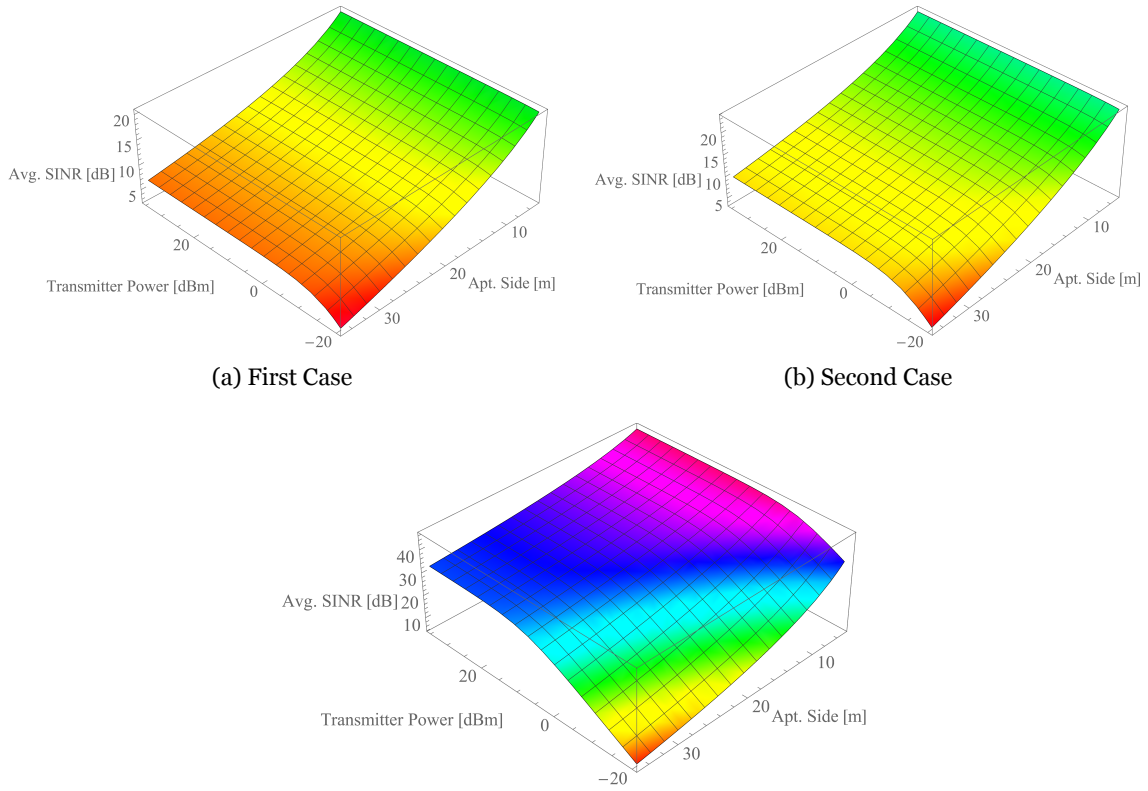

(a) First Case

(b) Second Case

(c) Third Case

Figure 2.7: Average SINR for an apartment side length from 5 to 35 m and a transmitter power from -20 to 30 dBm. The first case has four interferes, the second case has two interferes, and the third case has one interfere.

Figure 2.7a shows that the variation in transmitter power for the same apartment side length does affect the average SINR results for the first case. With the combination of lower values of transmitter power, i.e., $\leq$-15 dBm, and when the apartment side length increases, i.e., $\leq$10 m, the average SINR decays.

For the second case, Figure 2.7b shows that although two interferer nodes are considered (in cells adjacent to apartments B, F, H, and L) the behavior is approximately the same as in the case with four interference nodes. However, the values of the average SINR slightly increase in comparison with the previous case.

Results presented in Figure 2.7c show the case when there are only one interference node

in the adjacent cell of apartments A, C, K, or M. The average SINR increases in some cases more than 20 dBm (while reaching values up to circa 40 dB, for apartment side lengths of 10 m), for example, a transmitter power of 20 dBm and apartment side length of 35 m. The variation of transmitter power has extra impact in the increase in the increase of the average SINR when the of the side length increases.

When the number of interference nodes decreases the average SINR increases. The downside is the impact of varying the transmitter power or the apartment side length present additional impact on the average SINR.

2.4 Average SINR Analysis with Reuse Two and 4 HeNBs

2.4.1 Definition of the Geometry to a Coverage With 4 HeNBs

This scenario with 4 HeNBs to provide coverage is one of the possible ways, when the location and the number of HeNBs is taken into account. HeNBs were deployed as far as possible from the external walls, as well between them. The topology of the building and the apartments are the same as in Section 2.3, a 3GPP 5x5 grid geometry. A reuse two were also considered. The 4 HeNBs are placed in rows two and four and in columns two and four, Figure 2.8[1].

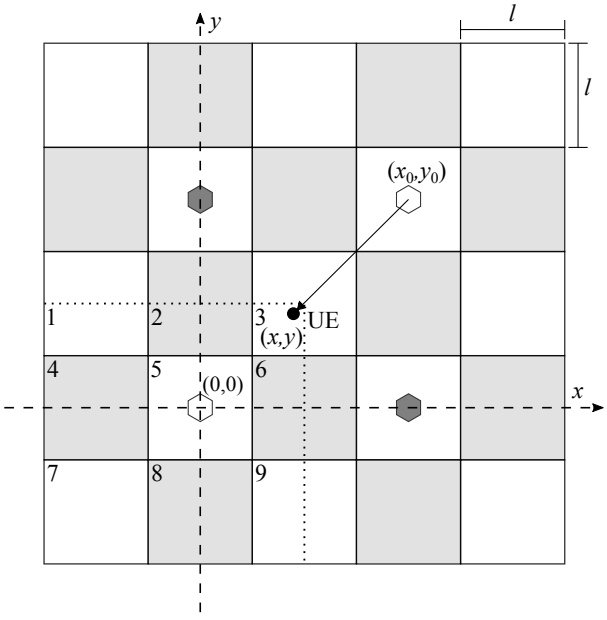

Figure 2.8: Average SINR when the building is with 4 HeNBs.

Each HeNB covers an area represented by the dotted line, meaning that each HeNB serves one-fourth of the total area of the floor, as shown in Figure 2.8. Users are located inside one of such four areas served by the HeNBs.

[1]The apartments in white and gray fields were maintained, but they do not represent the frequency reuse equal two.

2.4.2 Average SINR for a 3GPP 5x5 Grid Geometry With 4 HeNBs

When the user is served by a HeNB using a given frequency bandwidth, it will suffer interference from the co-channel HeNB. Since reuse pattern two is considered, there will be only one interfering HeNB.

The HeNB coverage area is divided by nine smaller areas, numbered from 1 up to 9. For the areas number 1, 3, 7 and 9 the number of walls between the user and the served cell is equal to two. For areas 2, 4, 6 and 8 the number of walls between the cell and the user is one. For the area number 5 there are no walls between the user and the cell.

From the interfering cell when the user is located in area number 3, the number of walls is two. When the user is located in areas 2 and 6, the number of walls is three. For areas 1, 5, and 9, the number of walls between the interfering cell and the user is four. The number of walls between the interfering cell and areas 4 and 8 is five. For area number 7, the number of walls between the user and the interfering cell is six. The own cell is considered being in the position with coordinates (0,0) and the interfering in the position at coordinates $(2*l, 2*l)$. In the area defined by rectangles 1, 2, 6 and 9, and squares 3, 4, 5, 7 and 8, the interference depends on the distance to (x_0, y_0) and the number of walls between the UE and the HeNB placed in (x_0, y_0), as shown in Figure 2.8. In order to compute the receiving interference considering (2.6) and (2.8), the path loss in each one of the squares/rectangles can be expressed as follows

$$\begin{aligned}
PL(x,y)_{1-5-9} =& 20*\log_{10}\left(\sqrt{(x-2*l)^2+(y-2*l)^2}\right)+46.4 \\
&+20*\log_{10}\left(\frac{2}{5}\right)+4*10 \\
PL(x,y)_{2-6} =& 20*\log_{10}\left(\sqrt{(x-2*l)^2+(y-2*l)^2}\right)+46.4 \\
&+20*\log_{10}\left(\frac{2}{5}\right)+3*10 \\
PL(x,y)_{3} =& 20*\log_{10}\left(\sqrt{(x-2*l)^2+(y-2*l)^2}\right)+46.4 \\
&+20*\log_{10}\left(\frac{2}{5}\right)+2*10 \\
PL(x,y)_{4-8} =& 20*\log_{10}\left(\sqrt{(x-2*l)^2+(y-2*l)^2}\right)+46.4 \\
&+20*\log_{10}\left(\frac{2}{5}\right)+5*10 \\
PL(x,y)_{7} =& 20*\log_{10}\left(\sqrt{(x-2*l)^2+(y-2*l)^2}\right)+46.4 \\
&+20*\log_{10}\left(\frac{2}{5}\right)+6*10
\end{aligned} \quad . \tag{2.23}$$

The average SINR measured by the UE follows the same method as Section 2.3.3. The integration limits for the rectangles and squares 1-9 are the ones presented in Table 2.1.

2.4.3 Average SINR Results for a Reuse Two With 4 HeNBs

Results of the average SINR are obtained as a weighted arithmetic mean as function of the apartment side length l and the transmitted power Figure 2.9. The weighted arithmetic mean take in account the weight of the contribution of area, since average SINR in each area is

Table 2.1: Integration limits of the interfering cell when the building is with 4 HeNBs.

	Γ_x^i	Γ_y^i
area 1	$\{[-3\times l/2, -l/2]\}$	$\{[l/2, l]\}$
area 2	$\{[-l/2, l/2]\}$	$\{[l/2, l]\}$
area 3	$\{[l/2, l]\}$	$\{[l/2, l]\}$
area 4	$\{[-3\times l/2, -l/2]\}$	$\{[-l/2, l/2]\}$
area 5	$\{[-l/2, l/2]\}$	$\{[-l/2, l/2]\}$
area 6	$\{[l/2, l]\}$	$\{[-l/2, l/2]\}$
area 7	$\{[-3\times l/2, -l/2]\}$	$\{[-3\times l/2, -l/2]\}$
area 8	$\{[-l/2, l/2]\}$	$\{[-3\times l/2, -l/2]\}$
area 9	$\{[l/2, l]\}$	$\{[-3\times l/2, -l/2]\}$

constrained by the walls. The average SINR was calculated for transmitter powers varying from -10 to 20 dBm, and apartment side length between 5 and 20 m. Results for the average SINR are presented in Figure 2.9.

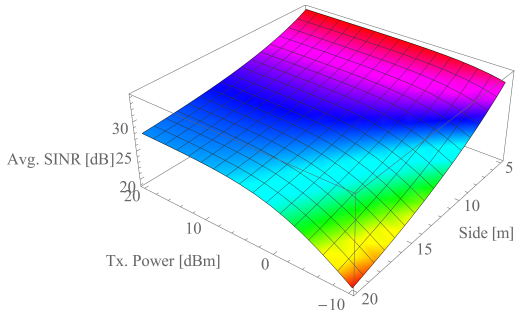

Figure 2.9: Weighted arithmetic mean for the average SINR when the building is with 4 HeNBs.

When the apartment side is longer the transmitter power has more impact. Considering the apartment side length of 20 m for values of transmitter power lower than 8 dBm the average SINR starts to decay. For the shorter apartment side length of 5 m the transmitter power has almost no impact in the average SINR results. The lowest value for the average SINR is obtained for a transmitter power of -10 dBm and apartment side length of 20 m.
The main conclusion is, for longer apartment side lengths the variation on the transmitter power has more impact in the average SINR than in shorter apartment sides. The average SINR study has shown that the smaller the apartment is, the higher the average SINR values are achievable.

2.5 Study of the Exponential Effective SINR Mapping

In its simplified way the SINR measured by the UE in the DL is a ratio between the desired signal and the unwanted sum of noise and interference. The SINR of a subcarrier can be calculated as a function of the subcarrier power [97]. At system level, the exponential effective SINR mapping (EESM) combines multiple SINR values from multiple subcarriers into an effective SINR function [97], [119]–[122]. EESM is mapped to a value of channel quality indicator (CQI), and is a method that maps all subcarries of an user that use the same modulation and coding scheme (MCS). The main overall idea of EESM is to compress the SINR

values from each subcarrier into a single value that represents channel conditions.
In this work, we consider a bandwidth of 20 MHz, yielding the availability of 100 subchannels, resulting in 100 different values of SINR. At the UE a value of SINR is calculated for each subcarrier, for each TTI (= 1ms). To combine N = 100 different values of SINR into a single value that expresses the channel conditions, the following EESM equation is considered [97], [119], [123],

$$EESM(\gamma, \beta) = -\beta \ln \left(\frac{1}{N} \sum_{i=1}^{N} e^{\frac{-\gamma_i}{\beta}} \right), \quad (2.24)$$

where γ_i is the vector of the individual values of the SINR for each subcarrier. The values of β are an estimated parameter that results from link-level simulations, determined, case by case, for different MCSs [124]. These values of β are obtained from curves generated by considering additive white Gaussian noise for each value of MCS [119]. LTE-Sim considers β = 1 and equation 2.24 becomes a exponential weight of all the SINR values.
After the UE equipment determines the EESM, it converts this value to the CQI, Figure 2.10. It transmits the CQI value to the base station. Since the EESM is considered, it will be a

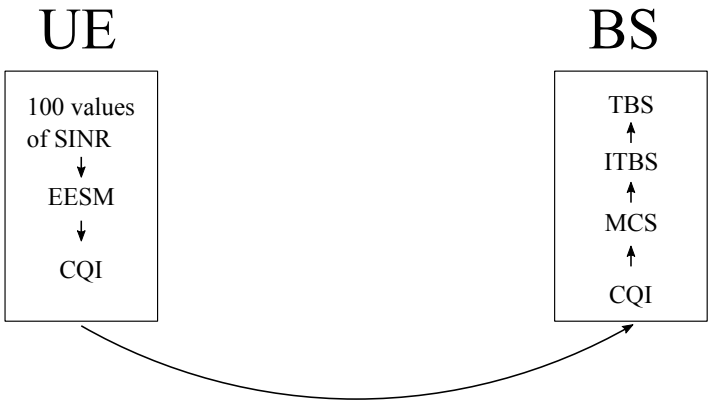

Figure 2.10: Schematics of the process to determine the EESM, CQI and TBS.

reduction of the quantity of CQI values transmitted to the BS, without losing information about the quality of the wireless connection.
At the base station, CQI is mapped to the MCS. Based on the MCS and transport block size (TBS) index (ITBS) value, the TBS is mapped by following the method from 3GPP Technical Specification Group Radio Access Network [72], [125]. The TBS is the number of bits which can be transmitted per TTI. The data from the upper layer (or MAC sublayer) delivered to the physical layer in LTE-Advanced systems is referred as transport block [126], [127]. This study from the EESM up to the TBS facilitates to understand the behavior of the link state.

2.5.1 LTE-Sim and Performance Metrics

Results for the performance metrics were obtained using an improved version of the LTE-Sim [86], [95], [96]. In the last version of the simulator provided by developers, it is not possible to extract EESM results for a building with a 3GPP 5x5 grid geometry. Neither solutions were found in the LTE-Sim community [128]. Another problem of LTE-Sim to extract results for

the performance metrics is the lack of options for the number and position of the HeNBs. In the developers current version, it is only possible to simulate a scenario with 25 active HeNBs.

This section also explores the possibility of deploying HeNBs in a coordinate way. 3GPP defines deployment ratio in [79]. This metric defines if an HeNB is deployed or not on the apartment, and varies from zero to one. If the deployment ratio is zero there are none active HeNBs. On the other hand, if the deployment ratio is one all 25 HeNBs will be active. For an urban-dense HeNB scenario 3GPP appointed 0.2 for the deployment ratio. This corresponds to having 5 HeNBs deployed. The topology with 4 HeNBs has a deployment ratio equal to 0.16. A topology with a deployment ratio is 0.24, corresponds to having 6 active HeNBs.

The improvements made in LTE-Sim to this chapter are presented in Appendix B. An improved version of the simulator, which includes the improvements from this work, is freely available under the GPLv3 license [129]. With these improvements it becomes possible to obtain results for the EESM, MCS and TBS in 3GPP 5x5 building geometries[2].

There is one HeNB at the center of each apartment [79], [103] according to the number of HeNBs to be simulated. The considered values for the transmitter power in the HeNBs are 0 dBm, 10 dBm, and 20 dBm. All HeNBs simultaneously operate at the same power level. In terms of apartment dimensions, in [79], only an apartment side length of 10 m is considered. The side length of the apartments considered are 5 m, 10 m and 20 m. Tab 2.2 presents the least details to extract the performance metrics with LTE-Sim. If a frequency reuse equal to

Table 2.2: Performance metrics simulation parameters.

Parameters	
Frame structure	FDD
CQI	Periodic
Number of HeNBs	4, 5, 6, 25
HeNB cluster	1, 2
HeNB bandwidth	10 MHz/10 MHz + 10 MHz
Access policy	Open
Power of the HeNBs	0, 10, 20 dBm
User speed	0 km/h
Number of buildings	1
Number of floors	1
Geometry of buildings	3GPP 5x5 grid
Apartment side length	5, 10, 20 m
Path loss model	WINNER II

one is considered the frequency bandwidth of 10 MHz is shared by all the HeNBs. Results obtained for frequency reuse equal to one are presented in Appendix C. Results for frequency reuse equal to two are presented and analyzed in the following sections.

[2]LTE-Sim also accounts a scenario with dual stripe model. Since this work only accounts scenarios with 5x5 building geometries, the previous scenario was not taken into account in our work. For our knowledge it is unknown whether it is possible to obtain values for performance metrics in a dual stripe model scenario.

2.5.1.1 Twenty-five HeNBs

Figure 2.11 presents results when 25 active HeNBs are considered, with reuse pattern two and apartment side length equal to 20 m. Figure 2.11a presents the case for a transmitter power

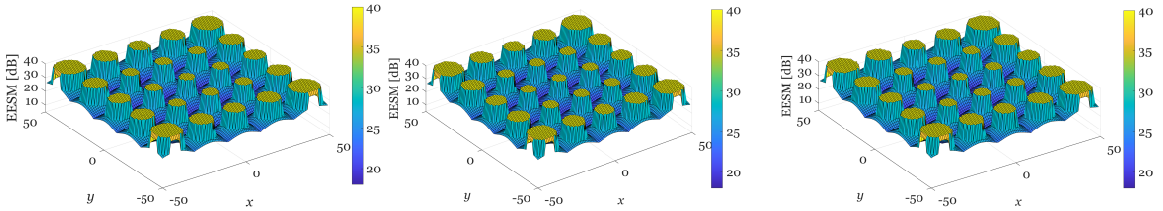

(a) 0 dBm (b) 10 dBm (c) 20 dBm

Figure 2.11: ESSM in a 5x5 geometry, 25 HeNB, reuse pattern two, apartment side length 20 m, transmitter power 0 dBm, 10 dBm and 20 dBm.

of 0 dBm, Figure 2.11b presents the case for a transmitter power of 10 dBm and Figure 2.11c when the transmitter power is 20 dBm. In the three cases, the variation of transmitter power did not show any impact on results of EESM. Apartments on the corners of the buildings sustain the EESM for a wider area than the other apartments. Has presented in Section 2.3.2, as the number of interferes in the first ring of interference decrease, the coverage area where the EESM is the maximum increases. Resulting that the apartments closer to the middle of the building present the worst EESM results.

When the apartment side length is 10 m Figure 2.12 results are identical to the previous one. For all the transmitter powers, 0 dBm Figure 2.12a, 10 dBm Figure 2.12b and 20 dBm. There

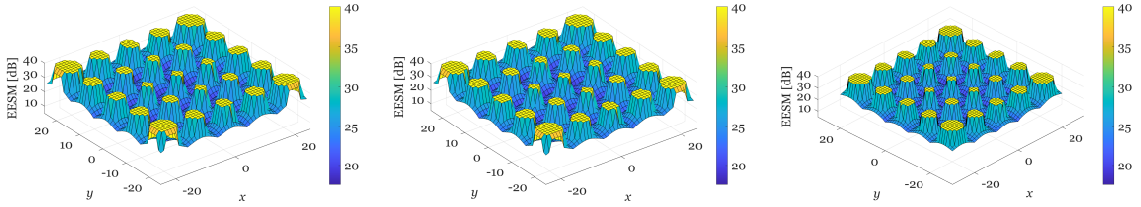

(a) 0 dBm (b) 10 dBm (c) 20 dBm

Figure 2.12: ESSM in a 5x5 geometry, 25 HeNB, reuse pattern two, apartment side length 10 m, transmitter power 0 dBm, 10 dBm and 20 dBm.

is not any noticeable variation on the obtained EESM results[3].

When the apartment side length is 5 m Figure 2.13, and for the same values of transmitter power is possible to observe the same behavior of the previous cases Figure 2.11 and 2.12. Also with an apartment side length of 5 m, it is easy to conclude that variations on the transmitter power did not present any impact on EESM for the same apartment areas. However the shorter distance between HeNBs increases the interference, resulting in narrower areas where the ESSM is the maximum. These results confirm the conclusions on the theoretical study in Section 2.3.4, variations on the transmitter power for the same apartment side

[3]Since the grid that serves as a base to collect EESM are the same in the scenario with apartment side length of 20 m or 10 m, and Figure 2.11 and Figure 2.13 did not reflect the scale of the buildings, some misinterpretations could arise during analysis.

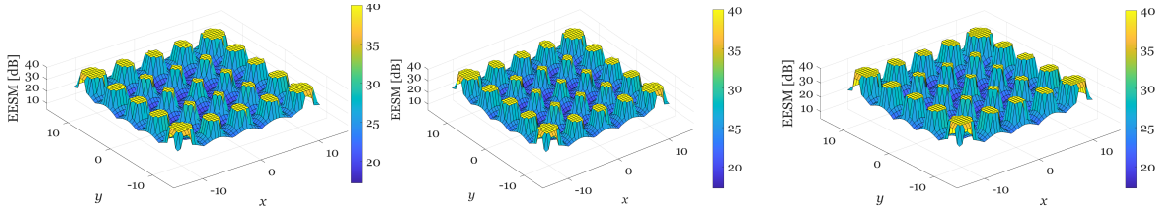

(a) 0 dBm (b) 10 dBm (c) 20 dBm

Figure 2.13: EESM in a 5x5 geometry, 25 HeNB, reuse pattern two, apartment side length 5 m, transmitter power 0 dBm, 10 dBm and 20 dBm.

length does not affect the EESM. Contrary to the variation on the apartment side length that has impact on the EESM results.

2.5.1.2 Four HeNBs

Results for the EESM for a 3GPP 5x5 grid geometry with 4 HeNBs and apartment side length 20 m are presented in Figure 2.14. With the option of consider only 4 HNBs and a trans-

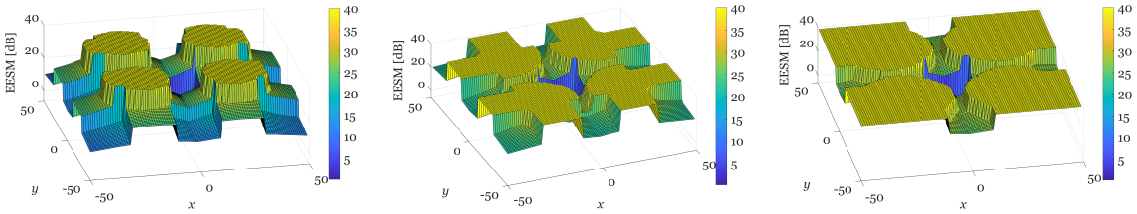

(a) 0 dBm (b) 10 dBm (c) 20 dBm

Figure 2.14: EESM in a 5x5 geometry, 4 HeNB, reuse pattern two, apartment side length 20 m, transmitter power 0 dBm, 10 dBm and 20 dBm.

mitter power of 0 dBm is possible to observe the effect of the attenuation imposed by walls Figure 2.14a. Since a reuse pattern of two is considered and nodes in the same channels are operating at a longer distance between them, this allows to observe the impact of the attenuation of walls[4].

With the increase of the transmitter power to 10 dBm Figure 2.14b is possible to observe that the area where the ESSM is the maximum increases. The increase in the EESM is specially significant at the apartments on the edges of the building. When the transmitter power is 20 dBm Figure 2.14c the area where the EESM is the maximum increases again. This effect is more evident on the apartments at the corners. In some areas, the increase of the transmitter power compensate the effect of attenuation from the walls. Nevertheless, the central area of the building floor keeps to be a problematic area. In the remaining area, the EESM is always higher than 25 dB.

The central area (that matches with the central area of the building) presents the lowest EESM. In the edge of this area, the EESM drops from 40 dB (in yellow) to 8 dB (in blue). This area, with lower EESM, corresponds to 5.76% of the total area of the building floor. One

[4]The attenuation of walls is expressed in Equation 2.8 by the environment-specific term X.

way to overcome the effect of walls to avoid areas with lower EESM values is to consider higher transmitter powers.
Figure 2.15 presents results for an apartment side length of ten meters. With this apartment

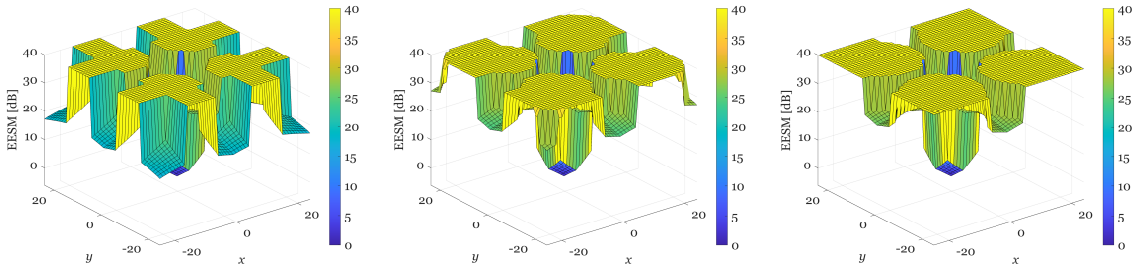

(a) 0 dBm (b) 10 dBm (c) 20 dBm

Figure 2.15: EESM in a 5x5 geometry, 4 HeNB, reuse pattern two, apartment side length 10 m, transmitter power 0 dBm, 10 dBm and 20 dBm.

side length is possible to observe that in areas where the EESM were the lower, know these values are higher, excluding the central area of the building. In Figure 2.14a at the apartments at the corners the EESM was lower than 10 dBm, in Figure 2.15a at the same apartments the EESM higher than 15 dBm. Them same happens from the case in Figure 2.14b and Figure 2.15b, the ESSM increases from approximately 20 dB to around 27 dB. In Figure 2.15c is considered the maximum transmitter power, the consequence is to obtain a wider area where the EESM is the maximum.
Figure 2.16 presents results for an apartment side length of 5 m. With a transmitter power

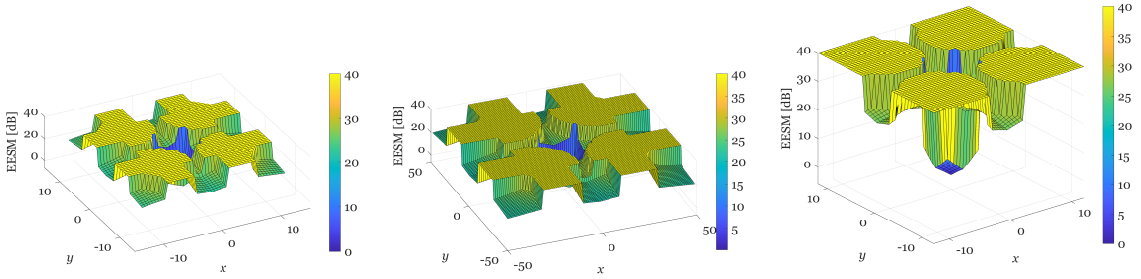

(a) 0 dBm (b) 10 dBm (c) 20 dBm

Figure 2.16: EESM in a 5x5 geometry, 4 HeNB, reuse pattern two, apartment side length 5 m, transmitter power 0 dBm, 10 dBm and 20 dBm.

of 0 dBm Figure 2.16a, and contrary to the case with 25 HeNBs in Section 2.5.1.1, with only 4 HeNBs and a narrower apartment side length the EESM increases. At the apartments with higher attenuation imposed by walls the EESM increases up to ≈25 dBm.
With a transmitter power of 20 dBm Figure 2.16c the total are where the EESM is 40 dBm increases. With the shorter apartment side length and with the increase of transmitter power the attenuation imposed by walls almost disappear. The decrease on the EESM is almost an effect of the interference imposed by the interfere nodes. Here this area also corresponds to 5.76% of the total area of the building floor.

With 4 HeNBs and for the studied combinations of apartment side lengths and transmitter powers the central area of the building floor is always a problematic area. These area, with the lowest EESM values, always corresponds to 5.76% of the total area of the building floor.

2.5.1.3 Five HeNBs

With 4 HeNBs it was possible to observe that the central area of the building is a problematic point. To overcome this problem, the approach was to add one HeNB to the floor. Like presented in Figure 2.17. With 5 HeNBs the deployment ratio is equal to 0.2. HeNBs 1, 2, 4

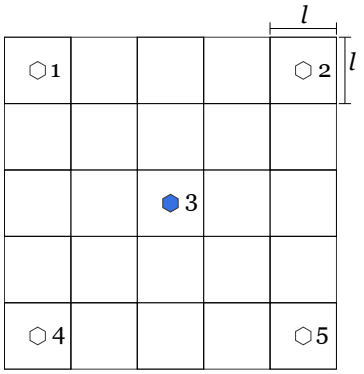

Figure 2.17: 5 HeNB deployment geometry.

and 5 operate in the same 10 MHz of bandwidth, the central HeNB, 3, operate in a different 10 MHz of bandwidth. The HeNB in the center eliminates the area that presents lower EESM in the 4 HeNB scenario. The deployment of HeNBs in the corners intends to maintain the EESM on the maximum values possible in the areas near the exterior walls.
Figure 2.18 presents results for an apartment side length of 20 m. In Figure 2.18a is possible

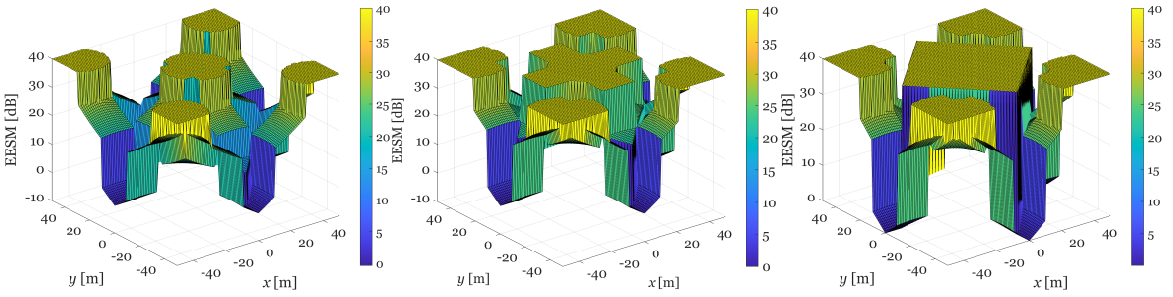

(a) 0 dBm (b) 10 dBm (c) 20 dBm

Figure 2.18: EESM in a 5x5 geometry, 5 HeNB, reuse pattern two, apartment side length 20 m, transmitter power 0 dBm, 10 dBm and 20 dBm.

to observe when the transmitter power is 0 dBm the attenuation of walls and the distance imposes a faster decay on the achieved EESM. With the increase of the transmitter power to 10 dBm Figure 2.18b, is possible to increase the area where the EESM is the maximum. In the HeNB in the center is possible to observe that the signal strength could transpose two walls. Results with a transmitter power of 20 dBm, shows a center cell with the higher coverage area. The limits of the coverage are not imposed by the attenuation of walls or by the distance, but by the distance between the neighboring nodes. At the cells on the corners

the decay on the coverage area is mainly imposed by the neighbor cells that are operating in the same subchannels.

The introduction of one HeNB (compared to the 4 HeNBs scenario) to eliminate the central area with lower EESM values was successfully achieved. However, in areas near the middle of the building side walls, the EESM drops to values lower or closer than 0 dB (the areas in dark blue fill in the Figures). These areas are around 7.2% of the total area of the building.

For an apartment side length of 10 m results are presented in Figure 2.19. With the reduction on the apartment side length, and when the transmitter power is 0 dBm Figure 2.19a the central node could provide a coverage at the maximum EESM in five apartments. But this is

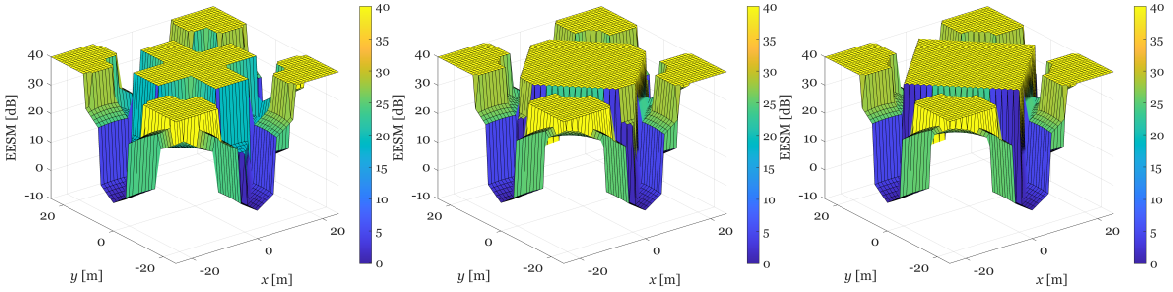

(a) 0 dBm (b) 10 dBm (c) 20 dBm

Figure 2.19: EESM in a 5x5 geometry, 5 HeNB, reuse pattern two, apartment side length 10 m, transmitter power 0 dBm, 10 dBm and 20 dBm.

possible because is the only node in the same subchannels. Since the HeNBs at the corners are operating in the same channels the decay on the EESM is imposed by the interference.

This effect at the HeNBs on the corners are maintained for a transmitter power of 10 dBm Figure 2.19b and a 20 dBm Figure 2.19c. With these increases on transmitter power the area where the central cells provides the maximum EESM increases and is the maximum when the transmitter power is 20 dBm.

Figure 2.20 presents results for an apartment side length of 5 m. When the transmitter power

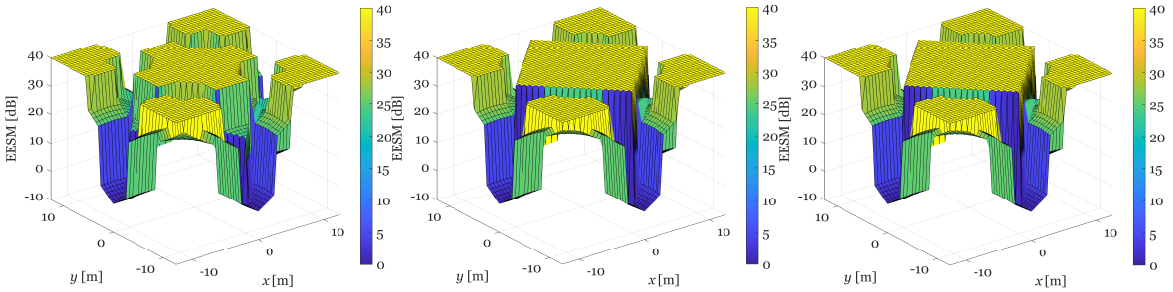

(a) 0 dBm (b) 10 dBm (c) 20 dBm

Figure 2.20: EESM in a 5x5 geometry, 5 HeNB, reuse pattern two, apartment side length 5 m, transmitter power 0 dBm, 10 dBm and 20 dBm.

is 0 dBm Figure 2.20a, is possible to observe a slight increase of the total area where the ESSM is the maximum. However with the decrease on the inter-cell distance the interference increases and so the gains are not more visible. For a transmitter power is 20 dBm Figure 2.20c

the behavior is the same, and the area with lower values for the ESSM corresponds to around 7.2% of the total area of the building.

2.5.1.4 Six HeNBs

The geometry considered a deployment of 6 HeNBs has is presented in Figure 2.21. This

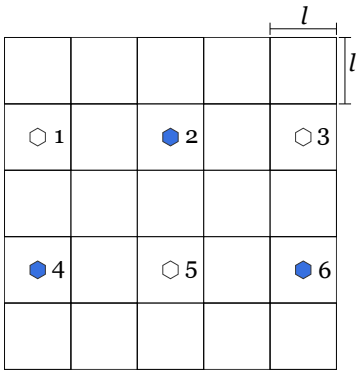

Figure 2.21: 6 HeNB deployment geometry.

geometry corresponds to a deployment ratio of 0.24. In this deployment, the space between the nearest HeNBs is one apartment. But since a reuse equal to two is considered in the first ring of interference the distance between HeNBs in the same subchannels is equal to $\sqrt{8} \times l$. Which is the same distance in the scenario with 4 HeNBs. But with more two HeNBs, that means more resources, is expected to obtain a wider area were the EESM is at the maximum value.

Results for the EESM are presented in Figure 2.22 for apartment sides lengths of 20 m. Fig-

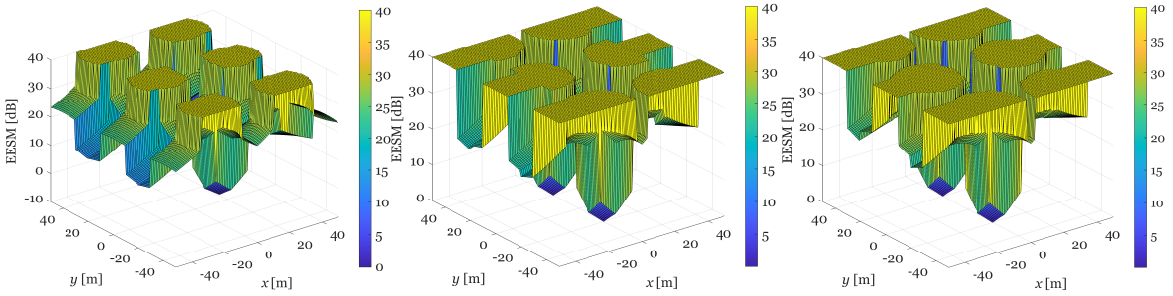

(a) 0 dBm (b) 10 dBm (c) 20 dBm

Figure 2.22: EESM in a 5x5 geometry, 6 HeNB, reuse pattern two, apartment side length 20 m, transmitter power 0 dBm, 10 dBm and 20 dBm.

ure 2.22a presents results when the transmitter power of 0 dBm is considered, and shows that HeNBs can not provide higher values of EESM for apartments in the side of y axis. This values mainly result of attenuation of walls but also of interference. When the transmitter power is 20 dBm Figure 2.22c the ESSM of these apartments increases. But in two apartments that are in the row in the middle the EESM keep very low, to values near 1 dB (in blue). This two areas correspond to 10.4% of the total area of the building floor. Comparing with the previous geometries, with 4 HeNBs or 5 HeNBs, the area with lowest values for the ESSM increases.

The effects on reducing the apartment side length to 10 m Figure 2.23 are the same of the previous cases. This is specially seen for a transmitter power of 0 dBm Figure 2.23a. In

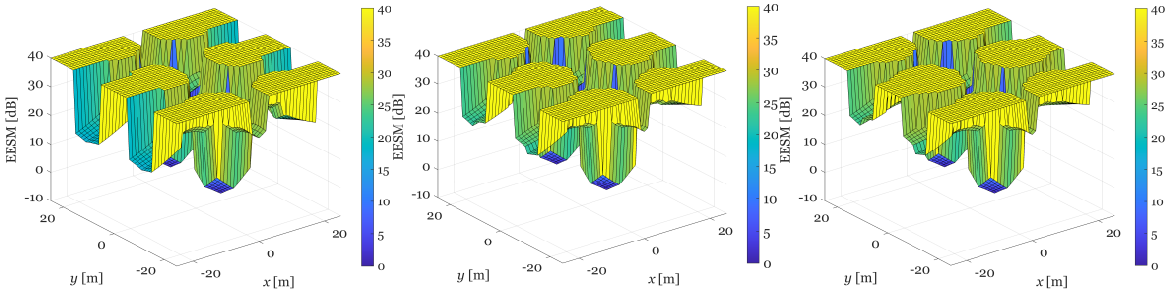

(a) 0 dBm (b) 10 dBm (c) 20 dBm

Figure 2.23: EESM in a 5x5 geometry, 6 HeNB, reuse pattern two, apartment side length 10 m, transmitter power 0 dBm, 10 dBm and 20 dBm.

areas where the interference is smaller the HeNB could provide coverage with a EESM at the maximum in the neighbor apartments.

When the transmitter power increases to 10 dBm Figure 2.23b and to 20 dBm Figure 2.23b is observed that the area with the higher EESM increases. This increases is when the attenuation imposed by the higher number of walls is overpassed. After this limitation is transposed the signal decays with the distance and interference imposed by the interferer HeNBs.

Considering smaller apartments side lengths of 5 m, results are presented in Figure 2.24. For a transmitter power of 0 dBm, the apartments with lower ESSM in the side of y axis the

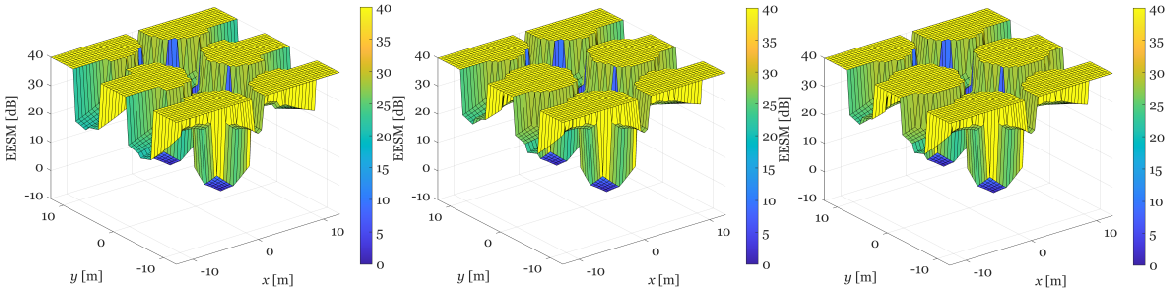

(a) 0 dBm (b) 10 dBm (c) 20 dBm

Figure 2.24: EESM in a 5x5 geometry, 6 HeNB, reuse pattern two, apartment side length 5 m, transmitter power 0 dBm, 10 dBm and 20 dBm.

EESM increase near 10 dBm Figure 2.24a. For a transmitter power of 20 dBm Figure 2.24c the effects of consider a smaller area are not so visible. The areas where the ESSM drops to the lower values continue to be around 10.4% of the cell.

2.5.1.5 Lessons Learned from the EESM Study

This section has studied the ESSM considering a different number of HeNBs 25, 4, 5 and 6 HeNBs to provide resources to a building with a 3GPP 5x5 grid geometry. 25 HeNBs were considered, with reuse pattern two that corresponds to a deployment ratio equal to one. For an urban-dense scenario HeNB, 3GPP appointed 0.2 for the deployment ratio. This corre-

sponds to having 5 HeNBs deployed, with 4 HeNBs the deployment ratio is equal to 0.16 and a deployment ratio equal to 0.24 corresponds to have 6 active. These presented ways of deploying HeNBs are some of the ways that could be adopted. Due to the large number of HeNBs when 25 HeNBs are considered the maximum value of 40 dBm for the EESM is visible for the areas near the several HeNBs. The interference areas are the zones where typically the EESM drops near the walls.

Results for other values of deployment ratio show that a scenario with 4 HeNBs can provide more coverage area with higher EESM than the topologie with 5 HeNBs. The scenario with 6 HeNBs the scenario achieved the worst results for the EESM. With 6 HeNBs, although the number of resources available to users is higher than with 5 HeNBs and 4 HeNBs, fewer resources are made available.

When the transmitter power is 20 dBm, it is possible to have wider areas where the EESM achieves its maximum value. With 4 HeNBs, the area with the lowest EESM is the same, for any combination of apartment side length and transmitter power. When more HeNBs are added to the floor, the total area with low values of EESM increases, from 5.76% with 4 HeNBs, to 7.2% with 5 HeNBs, and to 10.4%, with 6 HeNBs. With this area occupation, we expect better results for the number of supported users and system capacity for 4 HeNBs, followed by the topology with 5 HeNBs.

2.6 Summary and Conclusions

This chapter has studied the average SINR and the EESM in an indoor scenario with a 3GPP 5x5 grid geometry for a single floor. A detailed mathematical process to obtain the average SINR has been presented. When 25 HeNBs are considered, i.e., there is one HeNB inside of each apartment. In the first tier of interference the variation in transmitter power for the same apartment side length does affect the average SINR results. In the second and third tier, as the number of interferers decreases, the average SINR increases. However, when the apartment side length increases and the transmitter power decreases, the signal strength is not enough to provide an increase in the average SINR. This effect is clearer for longer apartment side length and lower transmitter power.

When only 4 HeNBs are covering the same geometry and areas, in terms of the average SINR when the apartment side is longer, the transmitter power has more impact. For the shorter apartment side length of 5 m, the transmitter power has almost no impact on the average SINR results.

At the downlink, the SINR measured by the UE, in its simplified way, is a ratio between the desired signal and the unwanted noise-plus-interference. In system simulations, e.g., by considering a bandwidth of 20 MHz, 100 resource blocks (RB) are needed, (N.B: a different value of SINR corresponds to each RB). One way to combine the values of SINR of multiple RBs into an effective SINR (and the most commonly used) is the EESM. For the study of the EESM, an indoor scenario with a 3GPP 5x5 grid geometry for a single floor has been considered. 25 HeNBs has also been considered. With reuse pattern two, results show only that in areas closer to the HeNBs the EESM achieves its maximum. Closer to the walls, the

EESM drops because of the interference imposed by the interfering HeNBs.
For an urban-dense scenario, 3GPP appointed 0.2 for the deployment ratio. This corresponds to having 5 HeNBs deployed. With 4 HeNBs, the deployment ratio is equal to 0.16 while a deployment ratio equal to 0.24 corresponds to have 6 active HeNBs. In the topology with 4 HeNBs, the area covered by the highest EESM is larger than in the case with 5 HeNBs. Although the number of resources available with 6 HeNBs is higher than with 5 and 4 HeNBs, this scenario presents the lowest area covered when the EESM achieves its maximum. By analyzing different topologies, we have concluded that, increased values of the transmitter power correspond to wider areas where the EESM achieves the maximum value of 40 dBm. With 4 HeNBs, for any combination of apartment side lengths and transmitter powers, the area with the lowest EESM is the same. This area corresponds to 5.76% of the total area. With 5 HeNBs, this area is 7.2% while with 6 HeNBs it becomes 10.4% of the total covered area.

Chapter 3

Performance Evaluation With 25 HeNBs Deployment

3.1 Introduction

Chapter 2 provided results for the study of the average signal-to-interference-plus-noise ratio (SINR), and exponential effective SINR mapping. Such study could indicate the performance of the considered home eNodeBs (HeNBs) deployments. In this chapter LTE-Sim is also used to evaluate the network performance in terms of the goodput, packet loss ratio (PLR), delay and maximum number of supported users. Goodput is the sum of bits correctly received by the users. PLR is the ratio between the total packets that cannot reach their destination and the total transmitted packets. Delay is the time interval within which each packet must be received.

The LTE-Sim, in its stable release R5 [86], is considered to investigate the overall performance of the system. The system performance has been studied for the downlink (DL), considering the parameters and assumptions discussed below as also updates.

For the considered application mixture (video and best effort), the proportional fair (PF) scheduler, frame level scheduler (FLS) and exponential rule (EXPRule) scheduler are considered in the simulations while seeking system saturation. It is worth studying these schedulers since for 5G, there is still freedom in the choice to be considered [130]. In [130], some minor revisions in some schedulers (such as the PF considered in this work) that allow them to support packet scheduling in the downlink OFDMA-based 5G networks are also presented. A comparison of the different schedulers facilitates the identification of their limitations and advantages in typical indoor deployment scenarios [84], [85].

This work is in some way complementary to other simulation works, such as [131]–[133], since it presents a higher number of deployed HeNBs and a path loss model that considers and counts the number of walls between users and HeNBs. Appendix D presents the upgrades in LTE-Sim to support this chapter.

3.2 Improvements in LTE-Sim

3.2.1 Generation of Uniform Random Positions

Early LTE-Sim simulation results showed that it would not be possible to consider the simulator in its original form. Further analysis of results produced by the simulator, shows most of the buildings and also users over a circular-shaped macrocell were close to the center. Hence, they were not truly uniformly distributed over the macro-cellular area. This limitation required improvement. Results presented in the Figure 3.1, show this identified prob-

lems. Figure 3.1 is a representation of the deployment of 100 000 different buildings in the

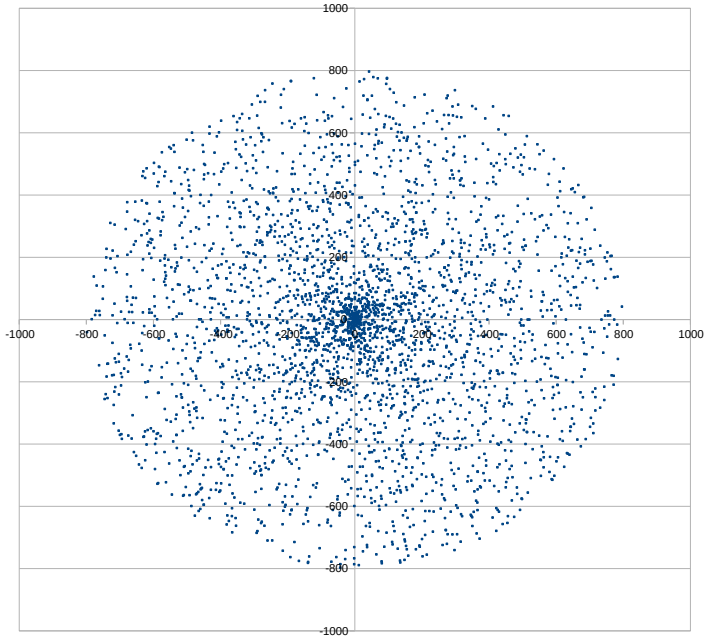

Figure 3.1: Results for a random function in ISO/IEC 14882:1998.

evolved NodeB (eNB) coverage area. Considering the eNB is located in the origin of the system with coordinates (0,0), it is easy to conclude that, the simulator in authors version tends to generate most part of values closer to zero.
The code provided by the developers to generate Figure 3.1 is presented in Listing 3.1.

```
GetUniformBuildingDistribution (int idCell, int nbBuilding)
{
  NetworkManager * networkManager = NetworkManager::Init();
  vector<CartesianCoordinates*> *vectorOfCoordinates = new vector<
      CartesianCoordinates*>;

  Cell *cell = networkManager->GetCellByID(idCell);

  double radius = (cell->GetRadius()*1000)*0.8;

  CartesianCoordinates *cellCoordinates = cell->GetCellCenterPosition();
  double r; double angle;

  for (int i = 0; i < nbBuilding; i++)
    {
    r = (double)(rand() %(int)radius);
    angle = (double)(rand() %360) * ((2*3.14)/360);

    double x = r * cos (angle);
    double y = r * sin (angle);

    CartesianCoordinates *newCoordinates = new CartesianCoordinates(
        cellCoordinates->GetCoordinateX () + x, cellCoordinates->
```

```
        GetCoordinateY () + y);

    vectorOfCoordinates->push_back(newCoordinates);
    }

  return vectorOfCoordinates;
}
```

Listing 3.1: Original code used in the simulator to generate random positions of buildings.

The simulator considers Cartesian coordinates generated from polar coordinates. To overcome the identified limitations and achieve a uniform random distribution of the users or buildings within the circular area that represents the macrocell, the simulator obtains the radial distance by multiplying the radius by the square root of a uniform random number between zero and one. To ensures that buildings do not cross the macrocell edge this radius is 80% of the cell radius, in the case of buildings. The radius of the eNB is multiplied by 0.8 that corresponds to deploy buildings in 80% radius of the macrocell. Moreover, the angular coordinate is uniformly distributed between zero and 360 degrees. The results presented in this work already benefit from these improvements made to the simulator. In its stable release R5, it is compiled with an ISO/IEC 14882:1998 compiler. With this compiler, the underlying random number generator may not be uniformly distributed.
In this work and in [94], the authors solved this by taking advantage of the Mersenne Twister pseudorandom generator [134]. The Mersenne Twister is the most widely used general-purpose pseudorandom number generator and was made available in ISO/IEC 9899:2011 [135], [136]. To correctly start the Mersenne Twister pseudorandom number generator, the seeds consider the time library Chrono. This library is also available in ISO/IEC 9899:2011 [136]. The final adopted code is presented in Listing 3.2.

```
GetUniformBuildingDistribution (int idCell, int nbBuilding)
{
  NetworkManager * networkManager = NetworkManager::Init();
  vector<CartesianCoordinates*> *vectorOfCoordinates = new vector<
      CartesianCoordinates*>;

  Cell *cell = networkManager->GetCellByID(idCell);

  double radii = (cell->GetRadius()*1000)*0.8;

  CartesianCoordinates *cellCoordinates = cell->GetCellCenterPosition();
  double r; double angle;


  for (int i = 0; i < nbBuilding; i++)
    {

   unsigned seed = std::chrono::system_clock::now().time_since_epoch().
       count();
```

```
    std::mt19937 rng_mt(seed);
    std::uniform_real_distribution<double> dist_double(0.0, 1.0);
    std::uniform_real_distribution<double> theta_double(0.0, 360.0);

    double r=dist_double(rng_mt);
    double th=theta_double(rng_mt);

    double theta = 2*M_PI*th/360;
    double r1 = sqrt(r);
    double radius = radii*r1;
    double x = radius*cos(theta);
    double y = radius*sin(theta);

    CartesianCoordinates *newCoordinates = new CartesianCoordinates(
        cellCoordinates->GetCoordinateX () + x, cellCoordinates->
        GetCoordinateY () + y);

    vectorOfCoordinates->push_back(newCoordinates);
     }

  return vectorOfCoordinates;
}
```

Listing 3.2: Updated code used in the simulator to generate random positions of buildings.

Figure 3.2 present the results of the improvements in the simulator with the code presented in Listing 3.2. This simulation also presents a hundred thousand points. Comparing Figure 3.2

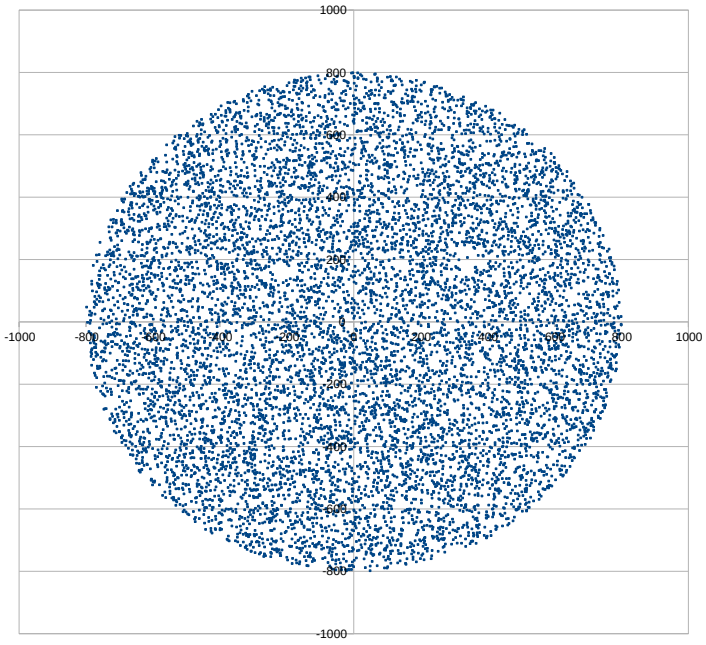

Figure 3.2: Results for a random function in ISO/IEC 9899:2011.

with Figure 3.1 it is easy to conclude with the previous improvements, new points are now distributed uniformly in a circular area. Figure 3.3 present three random cases extracted

from simulations. It presents the location of the uniform random deployment of 50 buildings extracted from simulations. The dashed line represents the radius of 80% of the maximum

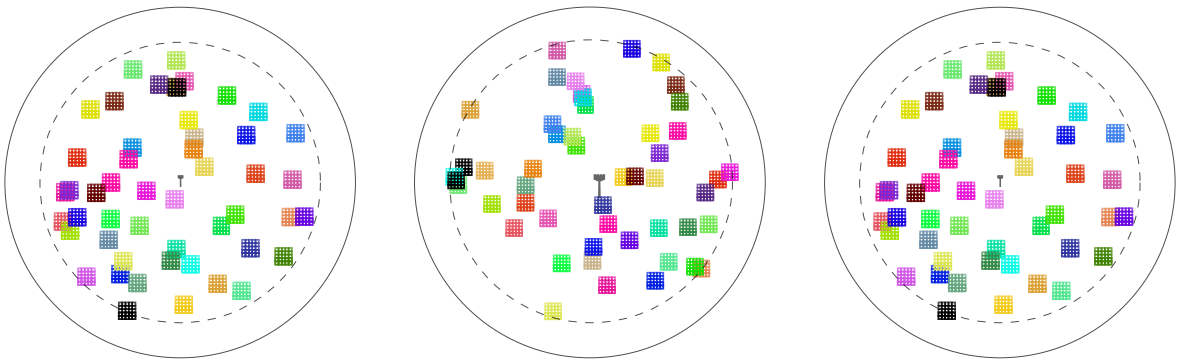

(a) First Case (b) Second Case (c) Third Case

Figure 3.3: Three simulation results of 50 buildings distribution in a eNB coverage.

cell radius.

3.2.2 Users Distribution in a Circular Area

The code for the distribution of the users in a cell, eNB or HeNB, is presented in Listing 3.3.

```
GetUniformUsersDistribution (int idCell, int nbUE)
{
  NetworkManager * networkManager = NetworkManager::Init();
  vector<CartesianCoordinates*> *vectorOfCoordinates = new vector<
      CartesianCoordinates*>;

  Cell *cell = networkManager->GetCellByID(idCell);

  double radius = (cell->GetRadius()*1000)*0.8;

  CartesianCoordinates *cellCoordinates = cell->GetCellCenterPosition();
  double r; double angle;

  for (int i = 0; i < nbUE; i++)
    {
    r = (double)(rand() %(int)radius);
    angle = (double)(rand() %360) * ((2*3.14)/360);

    CartesianCoordinatefs *newCoordinates =
        GetCartesianCoordinatesFromPolar (r, angle);

    //Compute absoluteCoordinates
    newCoordinates->SetCoordinateX (cellCoordinates->GetCoordinateX () +
        newCoordinates->GetCoordinateX ());
    newCoordinates->SetCoordinateY (cellCoordinates->GetCoordinateY () +
        newCoordinates->GetCoordinateY ());
```

```
    vectorOfCoordinates->push_back(newCoordinates);
    }

  return vectorOfCoordinates;
}
```

Listing 3.3: Original code used in the simulator to generate random positions for users.

Comparing this code with the code for the distribution of the buildings presented in Listing 3.1 it is easy to conclude that the same effect observed in the distribution of the building occur in the distribution of the users. So, this code was also update. These updates follow the same beginnings. The new code is present in Listing 3.4.

```
GetUniformUsersDistribution (int idCell, int nbUE)
{
  NetworkManager * networkManager = NetworkManager::Init();
  vector<CartesianCoordinates*> *vectorOfCoordinates = new vector<
      CartesianCoordinates*>;

  Cell *cell = networkManager->GetCellByID(idCell);

  double radii = (cell->GetRadius()*1000)*0.8;

  CartesianCoordinates *cellCoordinates = cell->GetCellCenterPosition();
  double r; double angle;

  for (int i = 0; i < nbUE; i++)
    {

      unsigned seed = std::chrono::system_clock::now().time_since_epoch
          ().count();
      std::mt19937 rngf_mt(seed);
      std::uniform_real_distribution<double> dist_double(0.0, 1.0);
      std::uniform_real_distribution<double> theta_double(0.0, 360.0);

      double radius=dist_double(rng_mt);
      double th=theta_double(rng_mt);

      double angle = 2*M_PI*th/360;
      double r1 = sqrt(radius);
      double r = radii*r1;


    CartesianCoordinates *newCoordinates =
        GetCartesianCoordinatesFromPolar (r, angle);

    //Compute absoluteCoordinates
    newCoordinates->SetCoordinateX (cellCoordinates->GetCoordinateX () +
        newCoordinates->GetCoordinateX ());
```

```
    newCoordinates->SetCoordinateY (cellCoordinates->GetCoordinateY () +
        newCoordinates->GetCoordinateY ());

    vectorOfCoordinates->push_back(newCoordinates);
    }

  return vectorOfCoordinates;
}
```

Listing 3.4: Modified code used in the simulator to generate random positions for users.

3.2.3 Users Distribution in a Square Area

According to 3GPP the HeNB are deployed in square areas, and the users are deployed inside that areas [79]. The code presented in the Listing 3.5 is the code provided by the simulator developers.

```
GetUniformUsersDistributionInFemtoCell (int idCell, int nbUE)
{
  NetworkManager * networkManager = NetworkManager::Init();
  vector<CartesianCoordinates*> *vectorOfCoordinates = new vector<
      CartesianCoordinates*>;

  Femtocell *cell = networkManager->GetFemtoCellByID(idCell);

  double side = cell->GetSide();

  CartesianCoordinates *cellCoordinates = cell->GetCellCenterPosition();
  double r; double angle;

  for (int i = 0; i < nbUE; i++)
    {
    r = (double)(rand() %(int)side);
    angle = (double)(rand() %360) * ((2*3.14)/360);

    CartesianCoordinates *newCoordinates =
        GetCartesianCoordinatesFromPolar (r, angle);

    //Compute absoluteCoordinates
    newCoordinates->SetCoordinateX (cellCoordinates->GetCoordinateX () +
        newCoordinates->GetCoordinateX ());
    newCoordinates->SetCoordinateY (cellCoordinates->GetCoordinateY () +
        newCoordinates->GetCoordinateY ());

    vectorOfCoordinates->push_back(newCoordinates);
    }

  return vectorOfCoordinates;
```

```
}
```

Listing 3.5: Original code used in the simulator to generate random positions for users in the HeNB.

With the release of the simulator available, the positions of the femtocell users are generated for a circular area Figure 3.4a. Were the radius is equal to the side length of the area (apartment). With this, some users are deployed out of the square area of the apartment, and they are not uniformly deployed. Users could undesirably be deployed outdoor.

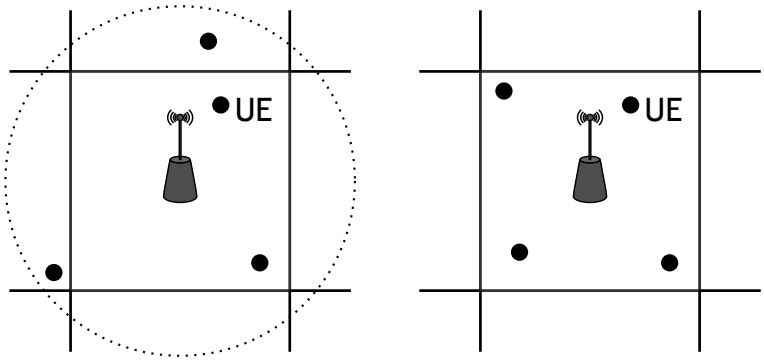

(a) Original version (b) Updated version

Figure 3.4: Users distribution in a HeNB.

To ensure that each user are inside of the square area of apartment served by the HeNB the code was modified, Listing 3.6.

```
GetUniformUsersDistributionInFemtoCell (int idCell, int nbUE)
{
  NetworkManager * networkManager = NetworkManager::Init();
  vector<CartesianCoordinates*> *vectorOfCoordinates = new vector<
      CartesianCoordinates*>;

  Femtocell *cell = networkManager->GetFemtoCellByID(idCell);

  double sidehome = cell->GetSide();

  CartesianCoordinates *cellCoordinates = cell->GetCellCenterPosition();
  double r; double angle;

  for (int i = 0; i < nbUE; i++)
    {

      unsigned seed = std::chrono::system_clock::now().time_since_epoch
          ().count();
      std::mt19937 rng_mt(seed);
      std::uniform_real_distribution<double> distx_double(0.0, 1);
      std::uniform_real_distribution<double> disty_double(0.0, 1);

      double xa=distx_double(rng_mt);
      double ya=disty_double(rng_mt);
```

```
        double x = sidehome*xa-(sidehome/2);
        double y = sidehome*ya-(sidehome/2);

       CartesianCoordinates *newCoordinates = new CartesianCoordinates ();
       newCoordinates->SetCoordinates(x,y);

    newCoordinates->SetCoordinateX (cellCoordinates->GetCoordinateX () +
        newCoordinates->GetCoordinateX ());
    newCoordinates->SetCoordinateY (cellCoordinates->GetCoordinateY () +
        newCoordinates->GetCoordinateY ());

    vectorOfCoordinates->push_back(newCoordinates);
    }

  return vectorOfCoordinates;
}
```

Listing 3.6: Modified code used in the simulator to generate random positions for users in the HeNB and inside of the apartments and buildings.

With the changes it is assured that a user is located in the square area of the served area of its HeNB Figure 3.4b. With this improvement is possible to ensure that a user belong to a HeNB and is for sure indoor.

3.2.4 Reuse Pattern Two in HeNBs

Frequency reuse is also considered in many works as a way to deal with co-channel interference and to extend the system performance. This work considers frequency reuse one and two. Frequency reuse is the design process of selecting and allocating different channel groups for all cellular base system within a cellular system [107], [108]. Although frequency reuse is available in LTE-Sim, in some simulation scenarios it was not developed by simulator team. Particularly when is considered a scenario with eNBs and HeNBs. For this work the simulator was also update to accommodate scenarios with eNBs and HeNBs with different frequency reuse patterns between layers. In some scenarios in this work, eNB could operate with a bandwidth of 20 MHz, and the 20 MHz of bandwidth is divided into two equal parts of 10 MHz for the HeNBs. The code updates is presented in Appendix D.

3.3 Packet Schedulers

In LTE-Advanced, packet scheduling occurs at base station (BS), (HeNBs, eNBs or small cell nodes), as shown in Figure 3.5. User traffic is supported by the BS, which continuously exchange data with them.
In its simple form, the scheduler receives the information about the desired quality-of-service (QoS) and system configuration, as well as the channel quality indicator (CQI), determined by the UE. After gathering this information, the BS responsible to distribute the available

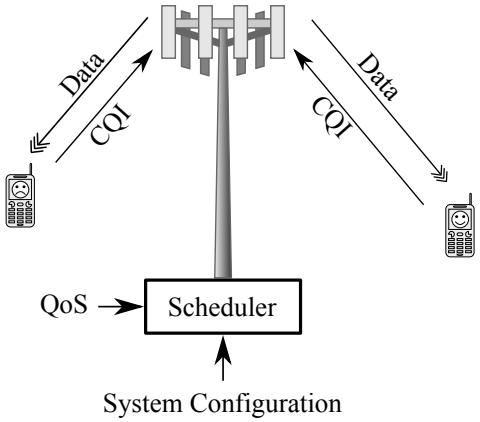

Figure 3.5: Simplified view of the scheduler operation.

radio resources among UEs, decides on the assignment of resource blocks (RBs) to UEs, and how much RBs should be assigned to transport data [108]. The packet scheduler in the BS distributes the available radio resources among the UE. The details on the scheduling algorithms are left to the HeNB implementation. Figure 3.6 shows a generic function of the downlink scheduler.

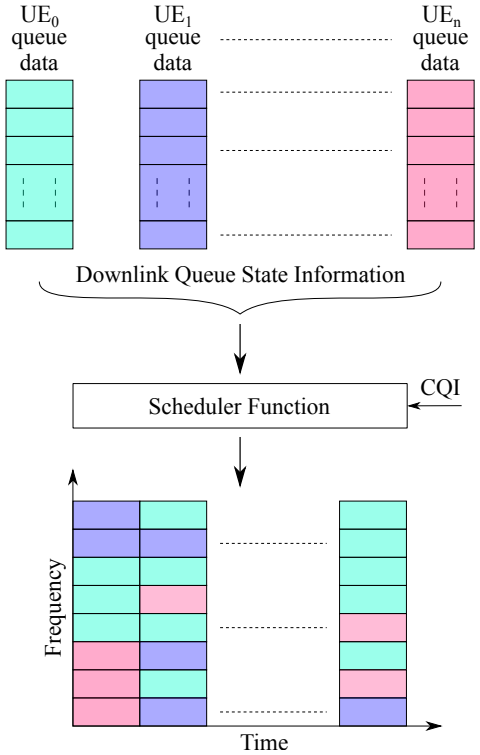

Figure 3.6: Simplified generic view of a wideband resource scheduler. Adapted from [108].

Data are scheduled to a number of users on a shared set of physical resources. Packet schedulers can make scheduling decisions based on the CQI. The CQI is determined at the user equipment (UE) and then transmitted to the BS via feedback signaling channels Figure 3.5. Feedback is an important measurement since this information helps to maximize the data rate [108]. With this information, the scheduler at the BS must manage the data requirements of the UE under its control. These requirements exist to ensure that transmissions

meet the desired service quality. In recent years, DL packet schedulers have being studied aiming at maximizing the end-user QoS [132]. As mentioned before, QoS considers a network centric approach and evaluates several performance parameters of broadband cellular networks, such as PLR, goodput and delay. The choice of the most efficient packet scheduling algorithm has been studied in [130], [132].

The considered applications in this work are video and best effort. Different from [137], [138], where a new scheduling algorithm was developed and/or a new bandwidth aggregation scheme was implemented to minimize the energy consumption, in this Section 3.3, we explore the possibility of reducing the transmitter power of HeNBs without compromising the overall system performance. To analyse the overall performance of the system, three schedulers available in LTE-Sim, in its stable release R5, are considered for the downlink (DL), [86], as follows: PF, FLS and EXPRule. According to [84] and [85], these schedulers are channel sensitive, i.e., the UEs intermittently forward a CQI report to the eNB. This CQI report presents the channel quality experienced by each UE, and estimated by the scheduler.

3.3.1 Proportional Fair

Proportional fair (PF) schedules a user when its instantaneous channel quality is high relative to its own average channel condition over time [108]. PF scheduler is used as a typical way to find a trade-off between requirements on fairness and spectral efficiency scheme [139]. It is effective in reducing variations in user bit rates with little average bit rate degradation, as long as user average values of SINR are fairly uniform [140]. The limitation of PF is low spectral efficiency [84].

PF does not consider any QoS parameter, it only schedules a user when its instantaneous channel quality is high relatively to its own average channel condition over time. The priority metric is defined by the following expression

$$w_{ij} = \frac{r_{ij}}{\bar{R}_i}, \quad (3.1)$$

where w_{ij} is the priority metric for the i^{th} user on j^{th} subchannel. r_{ij} is the achieved throughput, $\bar{R}_i$ is the average achieved throughput [83].

3.3.2 Frame Level Scheduler

Frame level scheduler (FLS) is presented in [85]. Authors develop a two level framework that guarantees bounded delays to real-time flows. In this approach, the time is seen as an endless sequence of frames, which are further split in time intervals. The two levels of the resource allocation procedure work on different time granularity. At the highest level, an innovative low complexity resource allocation algorithm was designed using discrete time linear control theory, which is referred as a FLS. At the beginning of each frame, FLS computes the amount of data that each real-time source should transmit within the frame, to satisfy its delay constraint.

To evaluate the quota of data $u_i(k)$ assigned to the i^{th} flow, it is used the control law

$$u_i(k) = h_i(k) * q_i(k), \quad (3.2)$$

where "$*$" operator is the discrete time convolution [141]. As in [85], equation 3.2 means that the amount of data to be transmitted by the i^{th} flow during the k^{th} LTE frame is obtained by filtering the $q_i(k)$ signal (i.e., the queue level) through a time-invariant linear filter with pulse response $h_i(k)$.
Then, to ensure a good level of fairness among multimedia flows, the lowest level scheduler assigns radio resources according to the PF algorithm [142] subject to the constraint imposed by FLS. The PF priority metric was defined in equation 3.1.

3.3.3 Exponential Rule

In [143], the exponential rule (EXPRule) was studied as a scheduling algorithm which explicitly uses information on the state of the channel and queues. Authors mention as main result that the EXPRule throughput is optimal, i.e., it renders queues stable in any system for which stability is feasible at all, with any other rule. Although the complexity of these schedulers is high [84], the EXPRule and Logarithmic Rule have been presented as the most promising approaches for DL scheduling in LTE systems with delay-sensitive applications, [144].
The scheduling computation metrics is defined by the following equation,

$$w_{ij} = b_i exp\left(\frac{a_i D_{HOL,i}}{c + \sqrt{\frac{1}{N_{rt}}\sum_{i=1}^{N_{rt}} D_{HOL,i}}}\right)\Gamma_i^j, \quad (3.3)$$

where $D_{HOL,i}$ the head of line (HOL) packet delay for the i_{th} user, a_i, b_i and c are tunable parameters. N_{rt} is the value of real-time flows which are active in the downlink. Γ_i^j is the spectral efficiency for the user on the j^{th} subchannel [83], [145], [146].
According to [85], [146] and [147] the optimal parameter set for the tunable parameters are

$$a_i \in \left[\frac{5}{0.99\tau_i}, \frac{10}{0.99\tau_i}\right], \quad (3.4)$$

τ_i symbolizes the packets waiting times threshold values;

$$b_i = \frac{1}{\mathrm{E}[\Gamma^i]}, \quad (3.5)$$

E, means the expectation value of the variable, and c=1.

3.4 Scenario Simulation Parameters for Frequency Reuse One

As state above in Section 2.3.1, when the frequency reuse is higher than one, there are an increase in both coverage and capacity of the cellular network. However, and although it has not been taken into consideration the frequency reuse equal to one in the Chapter 2,

here it is taken into consideration. In order to perform simulations it is needed to define the parameters presented in Table 3.1.

The simulation duration is the time interval associated to the whole simulation. The flow duration is the time interval during which a single flow is active. All flows do not start at the same time. Cluster is the frequency reuse and is the design process of selecting and allocating different channel groups for all cellular base system within a cellular system [107], [108]. In this case since cluster is equal to one means that the available bandwidth is share by all nodes. The considered frame structure is the frequency division duplex (FDD). Deployment density is considered dense, four users per HeNB appointed by 3GPP is considered [79]. Since the deployment density is dense, all HeNB are considered active. There are one HeNB for each apartment the total number of HeNBs is the same of the total number of apartments. HeNBs can operate with a closed policy where only authorized equipments could connect to the them, for this scenario these closed policy was considered.

In [79] the transmitter power variation of HeNBs is between zero and 20 dBm. Since results of the theoretical study of the average SINR in Chapter 2 for the same deployment scenario, shows that is possible to operate the HeNBs for values of transmitter power lower than zero dBm. For the simulations the transmitter power is decreased to a value of -10 dBm. So the transmitter power of HeNBs varies from -10 dBm up to 20 dBm, in steps of 5 dBm. The user speed is zero kilometers per hour which means users are in the same position during the all simulation.

Table 3.1: Considered simulation parameters with 10 MHz of bandwidth in the eNB and HeNBs.

Parameter	Value
Simulation duration	30 s
Flow duration	20 s
eNBs and HeNBs cluster	1
Bandwidth	10 MHz
Number of eNBs	1
eNB radius	1 km
Power of the eNB	43 dBm
Number of HeNBs	25
Power of the HeNBs	[-10; -5; 0; 5 ; 10; 15; 20] dBm
Access policy	Closed
Deployment density	Dense
Number of users per HeNB	4
User speed	0 km/h
User equipment position	Random
Number of buildings	1
Number of floors	1
Geometry of buildings	5x5
Apartment side length	[5, 10, 15, 20] m
Building position	Random
Application type	Video and best effort
Video bit rates	440 kb/s
Maximum delay	0.1 s
Frame structure	FDD
Number of simulations for each combination	50
CQI	Periodic
Path loss model	WINNER II

As discussed in Section 3.2.2 the distribution of users and building follow an improved random distribution compared to the original provided by the LTE-Sim simulator. As considered in Chapter 2 the building has a 3GPP 5x5 grid geometry with only one floor. The number of buildings per simulation is one. Also square apartments are considered in this building topology, the apartments side lengths also varies. In [79] an apartment side length of ten meters is appointed for simulations. Since, apartment side length could be smaller or large, in simulations also variation of the apartment side lengths is considered, from the smaller side of five meters to the larger of twenty meters, in steps of five meters.
The video application, is a video trace that is compressed using the H.264 standard compression at the average coding rate of 440 kb/s, which is available in [148]. The best effort (BE) application models an ideal greedy source that always has packets to send. The BE application only transmit packets when the are enough resources to send it.
A maximum of 100 ms for the maximum delay is considered. Maximum delay is the maximum tolerable time interval within which the packet must be received. When this maximum delay is suppressed the package is dropped. The considered channel quality indicator (CQI) feedback is considered periodic. For CQI reporting feature, the UE estimates the channel quality and converts it into a set of CQI feedbacks reported periodically to the eNB.
3GPP path loss model presented in [79] is an alternative simplified model based on LTE-A evaluation methodology which avoids modeling any walls to perform simulations. The other path loss model available and considered for the simulations, is the WINNER II path loss model. This model considered the effect of the walls, distinguish between internal and external walls and also the number of walls between nodes.
For each possible combination of the parameters presented in Table 3.1 with possible options, in this case the transmitter power of the HeNBs and the apartment side length, simulations run fifty times.

3.4.1 Simulations Results With Reuse Pattern One

In this scenario eNB operate with a bandwidth of 10 MHz and frequency reuse one. HeNBs also operate in frequency reuse with the same 10 MHz bandwidth. In this case, this scenario is considered a scenario with a middle interference, since all nodes are in the same bandwidth. Fitting surfaces were made using a polynomial surface with a confidence interval of 95% [149].

3.4.1.1 PF Scheduler

Figure 3.7a presents the average goodput with the use of the PF scheduler for video application.
The maximum values for the average goodput have been obtained when the apartment side length is 20 m and the transmitter power is between 0 and 10 dBm. The lowest values have been obtained when the apartment side length is also 20 m but the transmitter power is -10 dBm. For BE flows, in Figure 3.7b the maximum values for the goodput have been obtained for a transmitted power of 20 dBm and for an apartment side length of 20 m.

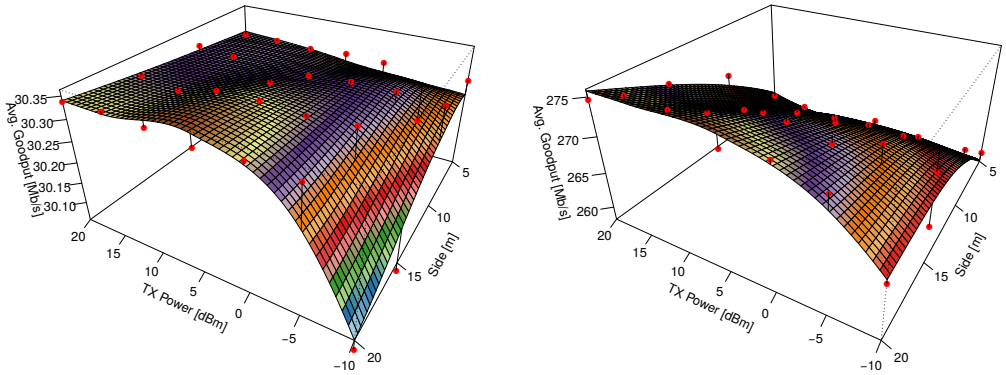

(a) Video flows with a bit rate of 440 kb/s.

(b) Best effort flows.

Figure 3.7: Variation of the average goodput for all users in the building for PF scheduler and different values of transmitter power and room side with WINNER II.

The maximum average PLR for the video flows with the PF scheduler Figure 3.8a, is in the maximum 1.2%, which is lower than the PLR target of 2% appointed by 3GPP for a real-time video [97]. The maximum PLR for BE is very low as expected Figure 3.8b, since the few

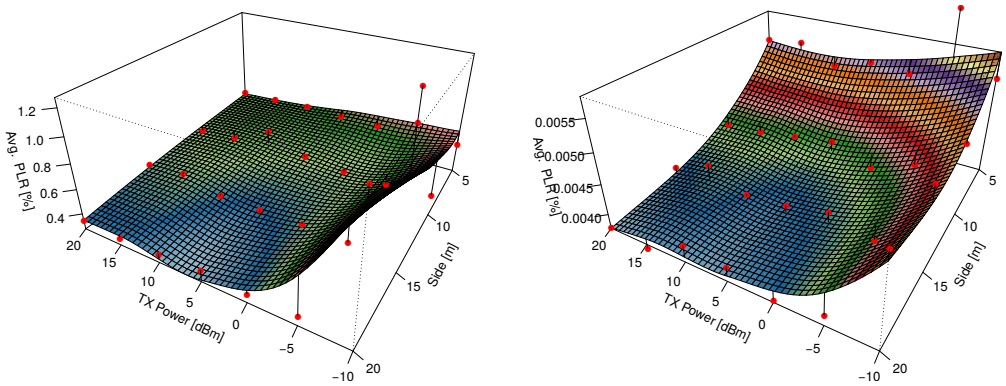

(a) Video flows with a bit rate of 440 kb/s.

(b) Best effort flows.

Figure 3.8: Variation of the average PLR for all users in the building for PF scheduler and different values of transmitter power and room side with WINNER II.

packets that do not reach their destination are lost because of the errors in the physical layer.

3.4.1.2 FLS Scheduler

With the FLS scheduler the average goodput of video flows Figure 3.9a, the maximum value was obtained for values of a transmitter power around -5 dB and apartment side length around 10 m.

This maximum average goodput is near the minimum average goodput, the minimum average goodput has obtained for a transmitter power of -10 dBm and and apartment side length of 5 m. Comparing the obtained results for the PF and FLS schedulers, the variation of the average is lower when the FLS scheduler is considered. For the average goodput for BE flows Figure 3.9b the average goodput is steadier with FLS instead of the PF, for the same value of apartment side length.

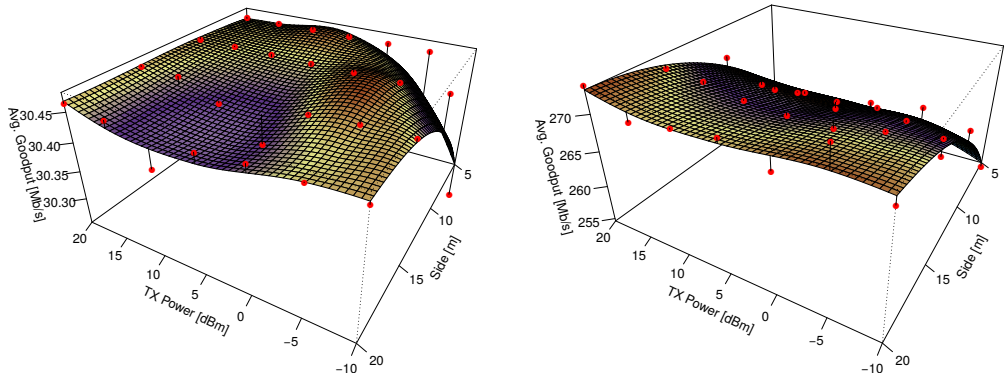

(a) Video flows with a bit rate of 440 kb/s.

(b) Best effort flows.

Figure 3.9: Variation of the average goodput for all users in the building for FLS scheduler and different values of transmitter power and room side with WINNER II.

The average PLR for both flows, Figure 3.10 continue to be very small and can be considered almost imperceptible for the UE.

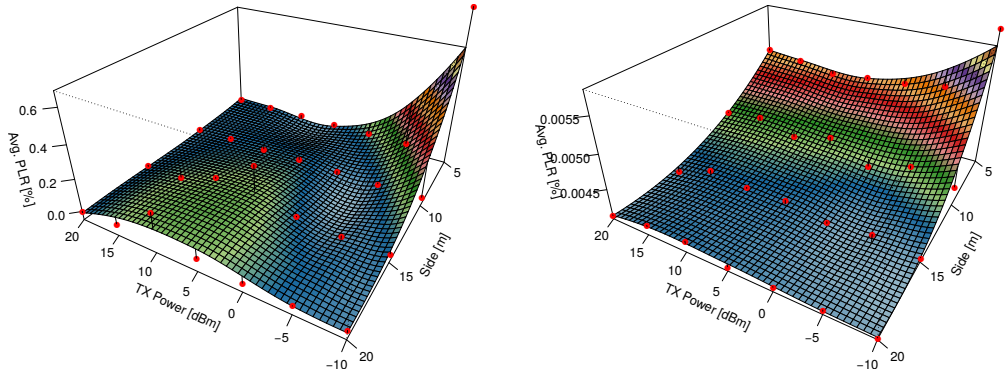

(a) Video flows with a bit rate of 440 kb/s.

(b) Best effort flows.

Figure 3.10: Variation of the average PLR for all users in the building for FLS scheduler and different values of transmitter power and room side with WINNER II.

The average PLR for video flows is in the maximum 0.6% Figure 3.10a. For BE the PLR is very low as seen in Figure 3.10b.

3.4.1.3 EXPRule Scheduler

Figure 3.11a, presents approximately the same maximum values when compared with the other schedulers. But the great advantage to use this EXPRule scheduler is that, the difference between the maximum and the minimum values for the average goodput is the smallest among the three considered schedulers. The behaviour of the average goodput for the BE flows Figure 3.11b are between the values obtained in the other two schedulers. Between the three schedulers the lowest average path loss ratio is also obtained with the use of the EXPRule and for video, Figure 3.12a.

The maximum average PLR for video is 0.14%, but minimum average PLR never reaches 0%. The average PLR for BE flows is low as it has to be Figure 3.12b.

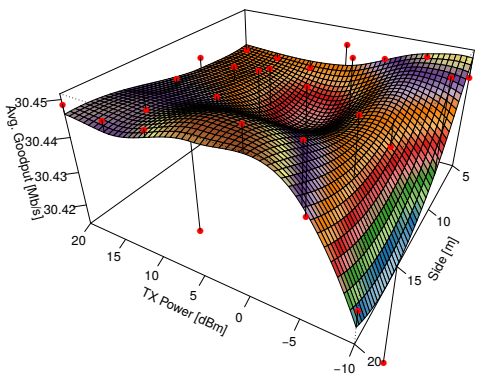

(a) Video flows with a bit rate of 440 kb/s.

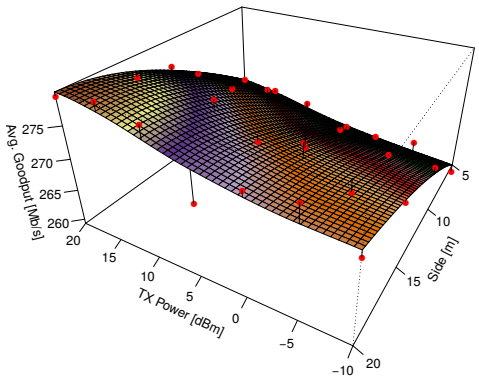

(b) Best effort flows.

Figure 3.11: Variation of the average goodput for all users in the building for EXPRule scheduler and different values of transmitter power and room side with WINNER II.

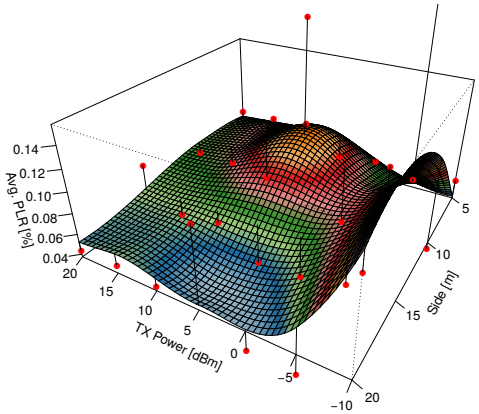

(a) Video flows with a bit rate of 440 kb/s.

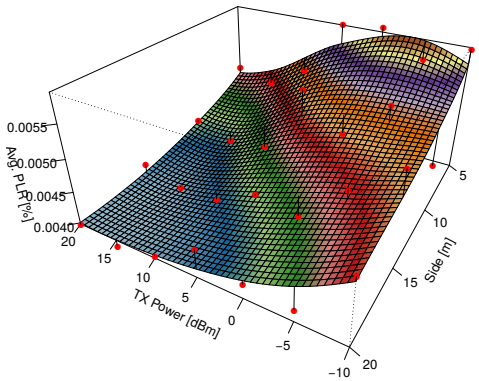

(b) Best effort flows.

Figure 3.12: Variation of the average PLR for all users in the building for EXPRule scheduler and different values of transmitter power and room side with WINNER II.

3.4.2 Lessons Learned for Frequency Reuse One

This Section presented results for a simulation study in a scenario 3GPP 5x5 grid geometry for a single floor with the deployment of 25 HeNBs. The eNB and the HeNBs share the same 10 MHz of bandwidth, i.e., the frequency reuse is one.
When the PF scheduler is considered the average goodput for the video flow, the maximum is obtained for an apartment side length of 20 m and for a transmitter power between 10 dBm and 5 dBm. When the apartment side length is short the average goodput for the video flow and BE decays. The maximum average PLR for the video flows with the PF scheduler is in the maximum 1.2%.
With the FLS scheduler the maximum average goodput for video is near the minimum average goodput. The maximum has been obtained for an apartment side length of 10 m and a transmitter power between 0 dBm and -5 dBm. We have got the lower average goodput for video for an apartment side length of 5 m and a transmitter of -10 dBm. BE shows the same behavior as in the PF scheduler. The average PLR for video flows is in the maximum of 0.6%.
The great advantage to use the EXPRule scheduler is that the difference between the maximum and the minimum values for the average goodput is the smallest among the three considered schedulers. But is also that ones that present the most irregular behavior. BE shows a closer behavior as in the previous schedulers. The maximum average PLR for video is 0.14%, the lowest one compared with the other scheduler.

3.5 Simulation Parameters for Frequency Reuse Two

As introduced in Section 3.2.4, with the introduction of the frequency reuse two it is expected to improve the system capacity. The assumptions for this scenario are introduced in Table 3.2. The eNB operate with a bandwidth of 20 MHz and frequency reuse one. The HeNBs operate with 10 MHz bandwidth and frequency reuse two. The 20 MHz used by the eNB were split in to equal parts each one with 10 MHz each one. Table 3.2 updates the parameters for simulation.

3.5.1 Simulations Results with Reuse Pattern Two

In this scenario eNB operate with a bandwidth of 20 MHz and frequency reuse two. HeNBs operate in frequency reuse two with 10 MHz bandwidth for 12 HeNBs and the other 10 MHz for the remaining HeNBs. In this case, this scenario is considered a scenario with low interference. Fitting surfaces were made using a polynomial surface with a confidence interval of 95% [149].

3.5.1.1 PF Scheduler

The adoption of frequency reuse allowed the system to have better values for the average goodput for the video flows for shorter apartments side length, Figure 3.13 when compared with Figure 3.7. For the video flows, Figure 3.13a, the gains are not very highs, but for the best effort flows, Figure 3.13b the goodput is four times fold comparing the case without the

Table 3.2: Considered simulation parameters with 20 MHz of bandwidth in the eNB and 10+10 MHz bandwidth in the HeNBs.

Parameter	Value
Simulation duration	30 s
Flow duration	20 s
eNBs cluster	1
Bandwidth eNB	20 MHz
Number of eNBs	1
eNB Radius	1 km
Power of the eNB	43 dBm
HeNBs cluster	2
Bandwidth HeNBs	10 MHz + 10 MHz
Number of HeNBs	25
Power of the HeNBs	[-10; -5; 0; 5 ; 10; 15; 20] dBm
Access Policy	Open
Deployment density	Dense
Number of users per HeNB	4
User speed	0 km/h
User equipment position	Random
Number of buildings	1
Number of floors	1
Geometry of buildings	5x5
Apartment side length	[5, 10, 15, 20] m
Building position	Random
Application type	Video and best effort
Video bit rates	440 kb/s
Maximum delay	0.1 s
Frame structure	FDD
Number of simulations for each combination	50
CQI	Periodic
Path loss model	WINNER II

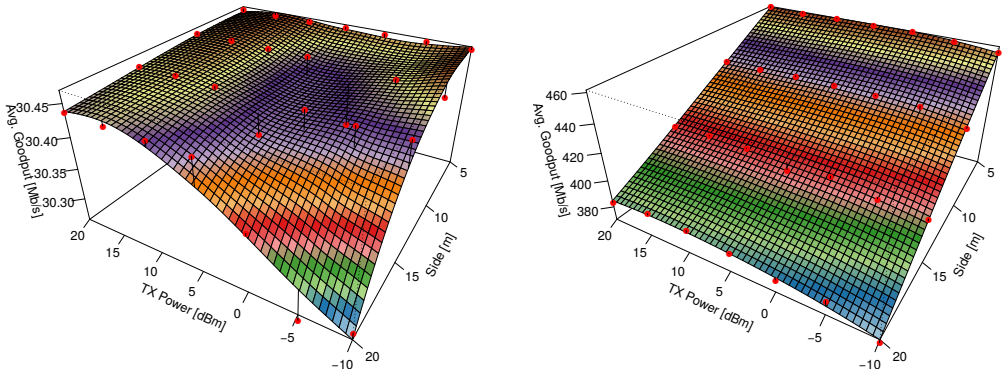

(a) Video flows with a bit rate of 440 kb/s.

(b) Best effort flows.

Figure 3.13: Variation of the average goodput for all users in the building for PF scheduler and different values of transmitter power and room side with WINNER II, with 20 MHz of bandwidth in the eNB and 10+10 MHz of bandwidth in the HeNBs.

use of frequency reuse, Figure 3.7b. In this case the adoption of the frequency reuse allowed the increase of the average goodput specially for shorter apartment side lengths.
The maximum average PLR for the video flows Figure 3.14a decrease for half of the case without frequency reuse, Figure 3.8. For the BE flow the PLR is negligible Figure 3.14b.

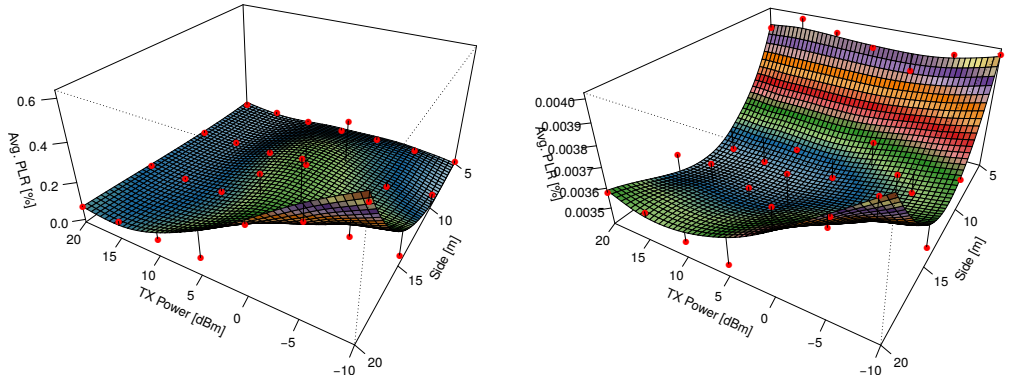

(a) Video flows with a bit rate of 440 kb/s.

(b) Best effort flows.

Figure 3.14: Variation of the average PLR for all users in the building for PF scheduler and different values of transmitter power and room side with WINNER II, with 20 MHz of bandwidth in the eNB and 10+10 MHz of bandwidth in the HeNBs.

3.5.1.2 FLS Scheduler

For the FLS scheduler the value for the average goodput for the video flows, Figure 3.15a, results are almost the same comparing with case without frequency reuse, Figure 3.9a.

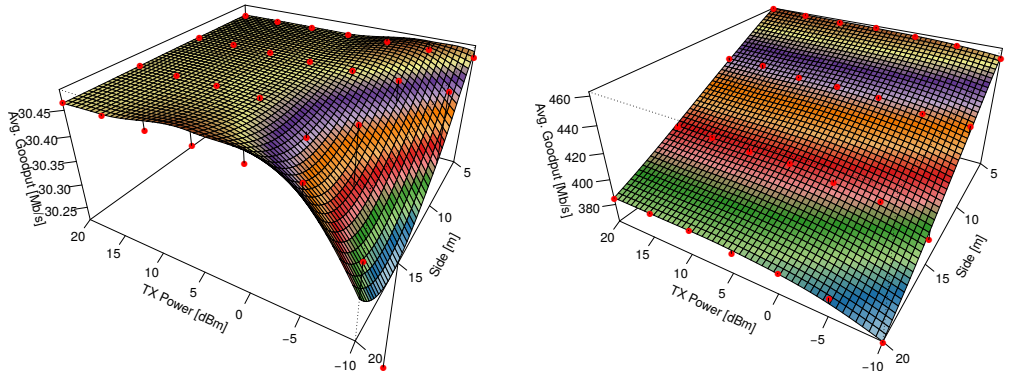

(a) Video flows with a bit rate of 440 kb/s.

(b) Best effort flows.

Figure 3.15: Variation of the average goodput for all users in the building for FLS scheduler and different values of transmitter power and room side with WINNER II, with 20 MHz of bandwidth in the eNB and 10+10 MHz of bandwidth in the HeNBs.

A more accurate analysis reveals that for a transmitter power of -10 dBm and for and apartment side length of 15 m the average goodput for video is lower comparing to the case without frequency reuse Figure 3.9a. Apart of this combination in all the other combinations of transmitter power and apartment side length the FLS sustain the maximum average goodput in most of the combinations. The average goodput for the BE flows with the FLS scheduler

Figure 3.15b are also obtained for lower apartment side lengths and present the a similar behaviour when the PF scheduler is considered Figure 3.9b.
The average PLR obtained for the of video flows, Figure 3.16a, at most of the combinations is or near 0% in most of the simulated situations Figure 3.16a. Since the average PLR is the

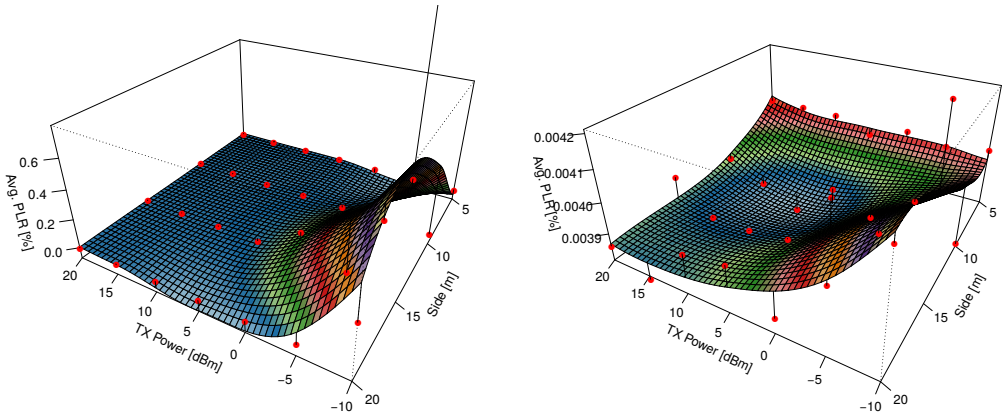

(a) Video flows with a bit rate of 440 kb/s.

(b) Best effort flows.

Figure 3.16: Variation of the average PLR for all users in the building for FLS scheduler and different values of transmitter power and room side with WINNER II, with 20 MHz of bandwidth in the eNB and 10+10 MHz of bandwidth in the HeNBs.

complement of the average goodput the highest value for the average PLR for the video flows was obtained when the transmitter power of -10 dBm and for and apartment side length of 15 m Figure 3.16a. The maximum average PLR is 0.6%. The average PLR for best effort flows is almost zero Figure 3.16b.

3.5.1.3 EXPRule Scheduler

The average goodput of the video flows for the EXPRule scheduler and frequency reuse two is shown in Figure 3.17, and kept the same behavior when frequency reuse is not considered Figure 3.11. Presenting the highest values of average goodput of the video flows among the three considered scenarios. The average goodput for the BE flows with the EXPRule sched-

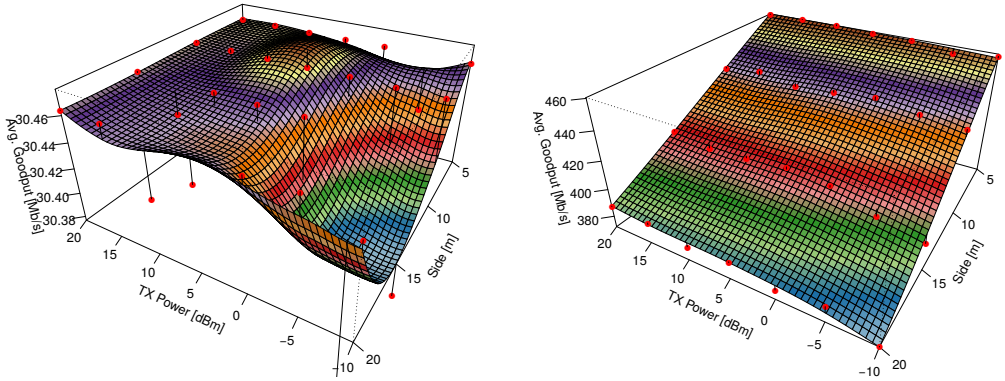

(a) Video flows with a bit rate of 440 kb/s.

(b) Best effort flows.

Figure 3.17: Variation of the average goodput for all users in the building for EXPRule scheduler and different values of transmitter power and room side with WINNER II, with 20 MHz of bandwidth in the eNB and 10+10 MHz of bandwidth in the HeNBs.

uler Figure 3.17b presents the same values and behavior of the other considered schedulers. An unwary analysis of the average PLR between the case with frequency reuse Figure 3.18 and without frequency reuse Figure 3.12 could lead to misunderstand interpretation. Although

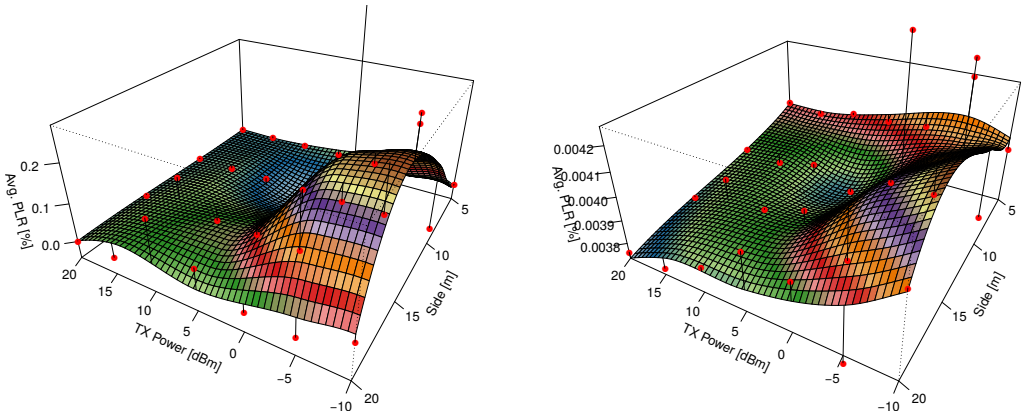

(a) Video flows with a bit rate of 440 kb/s.

(b) Best effort flows.

Figure 3.18: Variation of the average PLR for all users in the building for EXPRule scheduler and different values of transmitter power and room side with WINNER II, with 20 MHz of bandwidth in the eNB and 10+10 MHz of bandwidth in the HeNBs.

the maximum average PLR with frequency reuse is higher, 0.2% this value is only 10% of the maximum appointed by the 3GPP. And is most of the cases the average PLR is 0%.

3.5.2 Lessons Learned

This Section presented results for a simulation study in a scenario 3GPP 5x5 grid geometry for a single floor with the deployment of 25 HeNBs. The eNB operates with a 20 MHz bandwidth and HeNBs operate with a 10+10 MHz of bandwidth.

For the PF scheduler, the adoption of frequency reuse allowed the system to have better values for the average goodput for the video flows for shorter apartments side length. The maximum average PLR for the video flows decrease to half of the case without frequency reuse. For the BE flows, the goodput is four times fold comparing the case without the use of frequency reuse.

For the FLS scheduler the value for the average goodput for the video flows, results are almost the same as compared with the case without frequency reuse. The maximum average PLR for the video flows is 0.6%. The average goodput for the BE flows with the FLS scheduler is also obtained for lower apartment side lengths and present a similar behavior of the PF scheduler.

The average goodput of the video flows for the EXPRule scheduler kept the same behavior when frequency reuse is one. Presenting the highest values of average goodput of the video flows among the three considered scenarios. The average goodput for the BE flows with the EXPRule scheduler presents the same values and behavior of the other considered schedulers. The maximum average PLR with frequency reuse two is 0.2%, the highest among the three schedulers.

The interpretation of these results may be two-fold. First, frequency reuse two did not bring any advantage, in terms of average goodput for video flows. The second interpretation needs

a broader analysis. When the frequency reuse pattern increases the average goodput for the BE flow considerably increases. This means that there are more available resources to transport more data. Since the average goodput with both reuse patterns is the same, we can conclude that it is possible to support more users in each HeNB. Values obtained for the PLR also show that, in fact, that we are not closer to the 2% PLR target.

3.6 Maximum Supported Capacity for 25 HeNBs With Reuse Pattern Two

Results in the previous Sections show that, with the maximum number of four users per HeNB appointed by 3 GPP in [79] the system is not reaching system saturation. The system is saturated when the PLR $\geq$ 2% for video.
In this Section, the system is driven into saturation by gradually increasing the number of users in each HeNB in an equitable way. Contrary to the simulation works from [11], [150]–[152], our study considers a higher number of users per HeNB, which implies a very large density of users within a building.
For simulation purposes, although fewer schedulers are considered for the simulation than in [132] and changes to existing schedulers are not considered as in [133], in this work, an in-depth determination of the variation in the number of supported users for a PLR target of 2%, as a function of the apartment side length and the transmitter power is carried out with narrower confidence intervals.
Simulations have been performed to obtain the variation in not only the PLR, goodput and delay for a video application but also the goodput for the best BE application. We have also performed a detailed comparison of the performance of the considered packet schedulers.

3.6.1 PLR for Video

In this Section, the video application is considered. Figure 3.19 presents the results for the average PLR as a function of the number of users for all the considered scenarios. The values of the transmitter power are 0, 10 and 20 dBm. The considered apartment side lengths are 20, 15, 10 and 5 m.
In the simulations, for all combinations of the apartment side length, transmitter power and scheduler, the number of users spans between 6 users per HeNB and the number of users that corresponds to surpassing the PLR target of 2%. According to [97], the PLR target for video is 2%, i.e., PLR$<$2%. The results are presented in [131], [133], where the users determine their quality of experience by analyzing video transmissions expressed by the mean opinion score (MOS). A literature review indicates that for values of the PLR higher than 2%, the MOS decays, resulting in an uncomfortable video user experience and yielding a PLR target of 2%.
For the three schedulers, the average PLR increases with the number of users. Furthermore, it is a worth comparing the results by distinguishing two cases:

- apartment side lengths of 20, 15 and 10 m (Figures 3.19a, 3.19b and 3.19c, respectively);

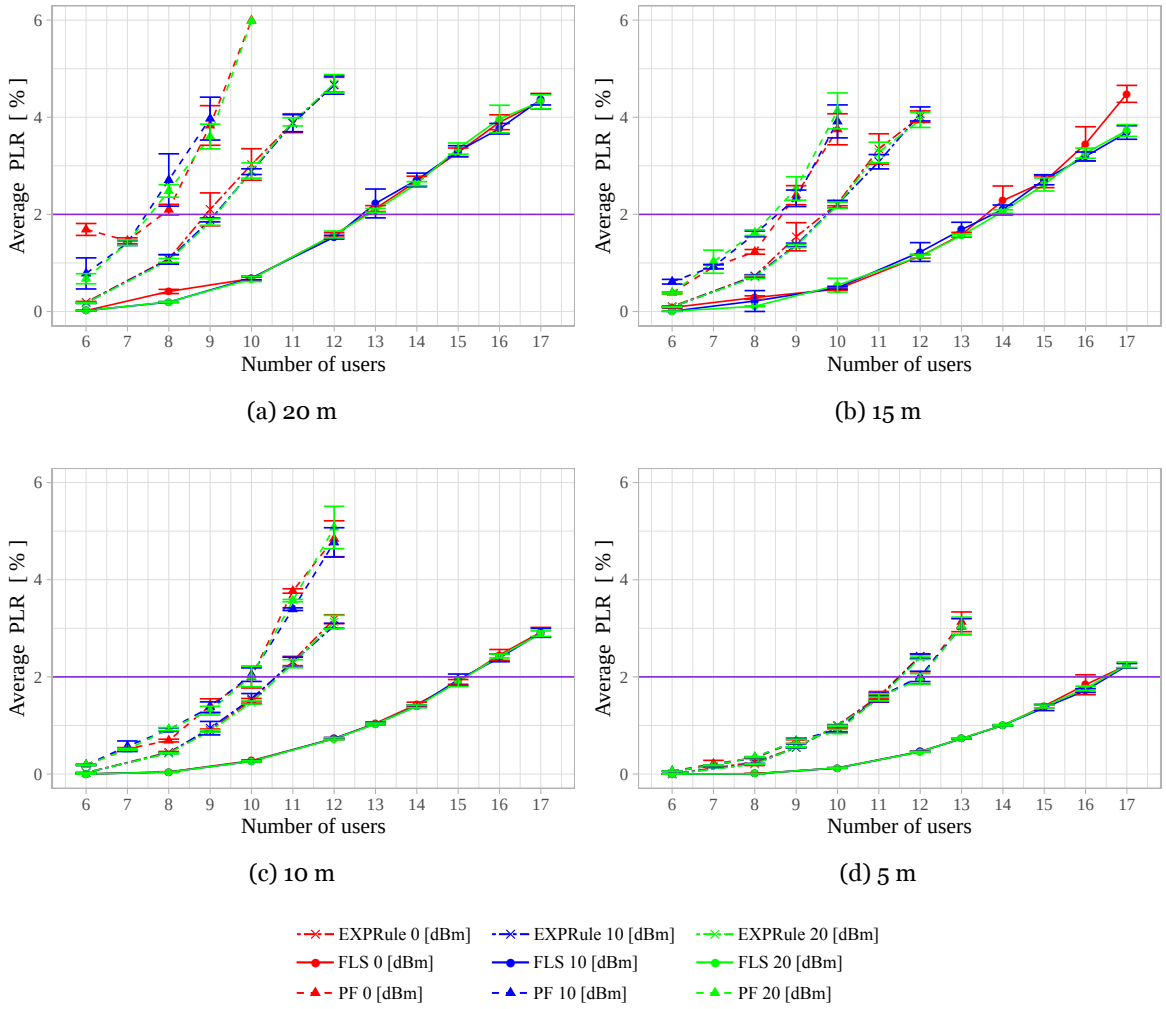

(a) 20 m

(b) 15 m

(c) 10 m

(d) 5 m

Figure 3.19: Average PLR for Video, for different apartment side lengths.

- apartment side length of 5 m (Figure 3.19d).

For the first case, when the target is 2%, the PF (dashed line) scheduler supports fewer users than the EXPRule (double-dashed line) scheduler. The EXPRule also supports fewer users than the FLS (solid line).
For the second case, the EXPRule presents a higher average PLR than that of the PF. However, both schedulers continue to have worse results than those of the FLS. One can conclude that with this increase in apartment side length, all schedulers present a higher average PLR for video. Overall, the FLS performs better than the PF and EXPRule schedulers.

3.6.2 Maximum Number of Supported Users

Table 3.3 summarizes the number of supported users for different side lengths of the apartments, values of the transmitter power and schedulers. We obtain these values for a PLR $<$ 2%.

Table 3.3: Maximum number of users served by each scheduler for a PLR $<$ 2%.

Max. number of users		Transmitter power [dBm]								
		0			10			20		
		PF	EXPRule	FLS	PF	EXPRule	FLS	PF	EXPRule	FLS
Side length [m]	5	12	11	16	11	11	16	12	11	16
	10	10	10	15	9	10	15	9	10	15
	15	8	9	13	8	9	13	8	9	13
	20	7	8	12	7	9	12	7	9	12

For the FLS, i.e., the scheduler with the best performance, for an apartment side length of 5 m, the maximum number of supported users is 16 for all values of the transmitter power. For an apartment side length of 20 m, the FLS supports only 12 users.
For the EXPRule scheduler, for an apartment side length of 5 m, the maximum number of supported users is 11, while an apartment of 20 m supports 9 users (for a transmitter power of 10 and 20 dBm) or 8 users (for a transmitter power of 0 dBm).
For an apartment side length of 5 m, with the PF scheduler, the maximum number of supported users is 12 (for a transmitter power of 0 and 20 dBm) or 11 (for a transmitter power of 10 dBm), while for an apartment of 20 m, the PF scheduler supports only 7 users.

3.6.3 Maximum Average Goodput for Video

Considering an average PLR target of 2%, it is worthwhile to determine the maximum average goodput. We also compare the behavior of the maximum average goodput with the trend of the average SINR, as shown in Figure 2.7.
When the apartment side length is 20 m or 15 m, the maximum average goodput is determined for video for the PF scheduler and all values of the transmitter power, as shown in Figure 3.20a. For other apartment side lengths, the average goodput is higher for a transmitter power of 0 dBm. For a side length of 5 m and a transmitter power of 20 dBm, the maximum values of the average goodput are the same as for a transmitter power of 0 dBm.

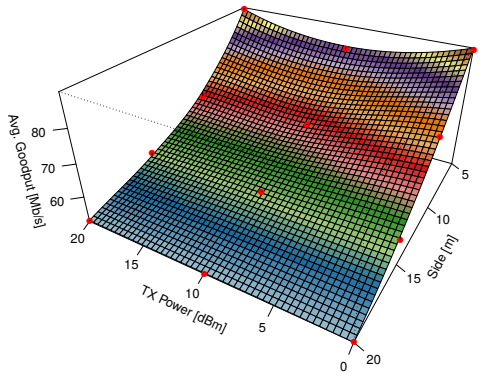

(a) PF scheduler.

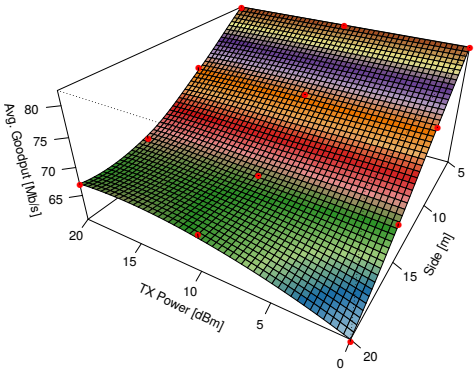

(b) EXPRule scheduler.

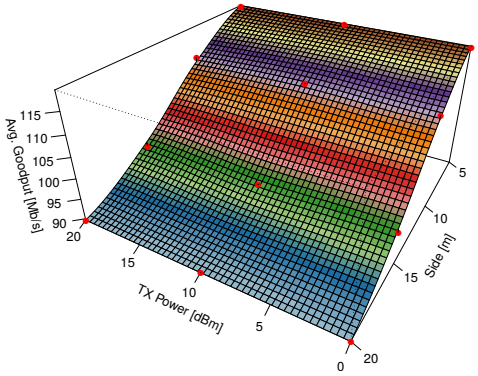

(c) FLS scheduler.

Figure 3.20: Maximum Average Goodput for Video.

The maximum average goodput for EXPRule, from Figure 3.20b, has the same variations as those of the chart corresponding to the average SINR. In general, along the same apartment side, the variation in the transmitter power does not affect the maximum average goodput. The exception occurs when combining an apartment side length of 20 m and a transmitter power of 0 dBm. Under these conditions, the EXPRule cannot sustain system performance. This behavior in the study of the average SINR occurs for the lowest values of the transmitter power and the longest apartment side lengths.

The FLS is the scheduler that supports more users. Varying the transmitter power along the same apartment sides has no impact, as shown in Figure 3.20c. The goodput for the FLS follows the same behavior as that of the average SINR.

For all schedulers, we observed a significant variation in the maximum average goodput along the apartment side. We obtained higher values for lower apartment side lengths, which agrees with the values and the lessons learned in Chapter 2. Table 3.4 presents a summary of the maximum average goodput for each scheduler for video and BE applications.

Table 3.4: Average goodput of video and BE applications for PLR $< 2\%$.

Avg. goodput [Mb/s]	PF		EXPRule		FLS	
	Min.	Max.	Min.	Max.	Min.	Max.
Video	45.5	89	45.5	82	89	119
BE	310	390	315	400	285	361

3.6.4 Maximum Average Delay for Video

We observe that the delay also increases when the number of users increases. The maximum delay for the PF scheduler was 55 ms, for EXPRule was 25 ms and for the FLS was 28 ms. In none of the simulations did we exceed the maximum 3GPP limit of 150 ms for the maximum video delay.

3.6.5 Maximum Average Goodput for Best Effort

The best effort (BE) application makes use of the remaining resources left by the video application. Since the BE application sends packets only when there are enough resources to send them, the PLR is zero or near-zero. The few packets that do not reach their destination are lost because of the errors in the physical layer.
The maximum average goodput for BE is presented in Figures 3.21a, 3.21b and 3.21c, respectively, for the PF, EXPRule and FLS. The EXPRule scheduler achieves the highest average

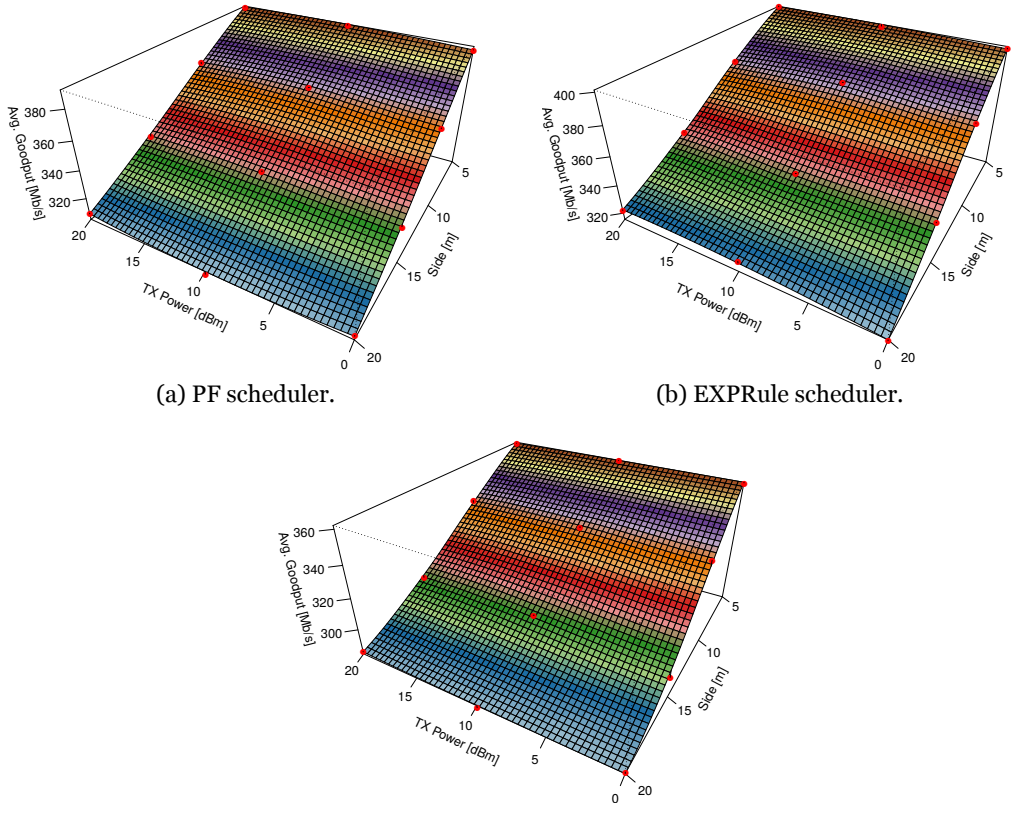

(a) PF scheduler.

(b) EXPRule scheduler.

(c) FLS scheduler.

Figure 3.21: Maximum Average Goodput for BE.

goodput (400 Mb/s) among the three schedulers. The scheduler with the lowest maximum average goodput (285 Mb/s) is the FLS. More results for the maximum average goodput from BE are given in Table 3.4.
The results are in line with the results from Chapter 2. As opposed to the results obtained for the video application, the EXPRule scheduler presents the best performance for the BE application. The opposite occurs for the FLS.

It is straightforward to conclude that the behavior of all the packet schedulers when users are considering the BE application is identical. The goodput varies only when the apartment side length also varies. The maximum average goodput for BE retains the same behavior as that of the theoretical average SINR. The results show that the higher the maximum goodput for video is, the lower the maximum goodput for BE.

3.6.6 Comparison Between Packet Schedulers

To determine which packet scheduler has the best performance, we compare the results of the difference in the values of the goodput between each pair of schedulers. Figure 3.22a presents the difference in the goodput between PF and EXPRule. For apartments with a 5

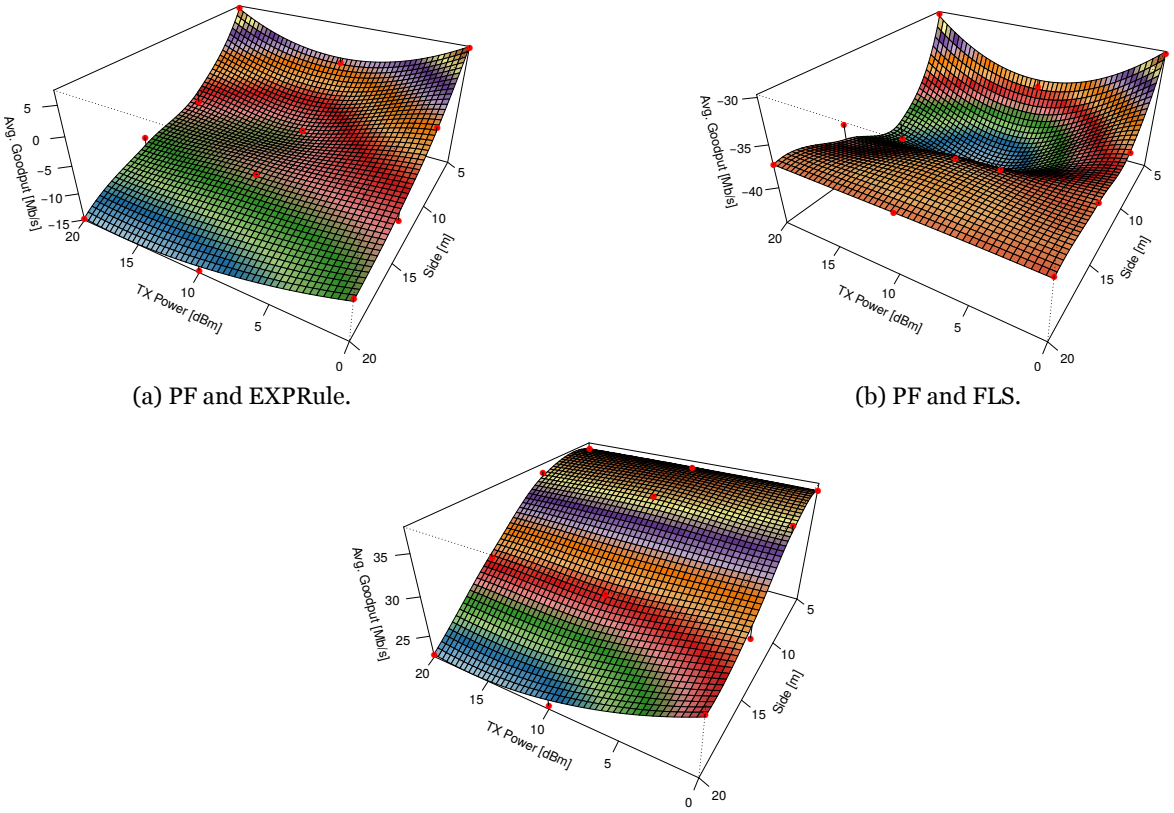

(a) PF and EXPRule.

(b) PF and FLS.

(c) FLS and EXPRule.

Figure 3.22: Maximum Average Goodput for Video: comparison between schedulers.

m side length, the PF scheduler has the best performance. For other apartment side lengths, the EXPRule scheduler has the best performance.

Figure 3.22b compares the goodput between the PF scheduler and FLS. The FLS has the best performance for any pair of values of the transmitter power and apartment side length. The FLS could, in the best case, operate with a goodput higher than 44 Mb/s compared to the PF scheduler.

In comparison to the EXPRule scheduler, the FLS shows once more its superior behavior, as shown in Figure 3.22c. The overall analysis shows that for the considered applications, the FLS performs better than the other two packet schedulers. In some combinations, the FLS performance is approximately 44 Mb/s higher than that of PF.

For small apartment sizes, PF is a better option than the EXPRule scheduler. For larger apartment sizes, the opposite is observed, and the EXPRule option prevails.

3.7 Summary and Conclusions

As most mobile communication traffic is shifting from outdoor to indoor environments, this work studied HeNBs (a particular case in the family of small cells) to offer indoor coverage. We considered a building with a 5x5 apartment topology. This work goes further than the assumptions of 3GPP by considering a higher-density deployment of HeNBs and users. This work also explored variations in the transmitter power of HeNBs and variation in the geometrical dimensions.

An updated version of LTE-Sim was adopted to study the indoor 4G system for a PLR target of 2%. The number of users served by each HeNB increased until the PLR surpassed the target value of 2% for video. For all considered combinations of the transmitter power and apartment side length, the maximum number of users appointed by 3GPP (i.e., 4) was largely surpassed by all schedulers.

The comparison between the PF and EXPRule schedulers shows that, for apartments with a 5 m side length, the PF scheduler has the best performance. For longer apartment side lengths, the EXPRule scheduler has the best performance. In comparison with PF, the FLS has the best performance for any value of transmitter powers and apartment side length. The FLS also performs better than the EXPRule scheduler. For the considered video flow, FLS presents the best overall performance. It enables service for up to sixteen users. For the video application, the results also show that it is possible to consider a reduction in the transmitter power without compromising the video performance.

The results for BE applications show that it is possible to consider, in most of the cases, a reduction in the transmitter power. This reduction does not have a negative impact on system performance and can provide a reduction in energy consumption for both video and BE flows.

Chapter 4

Performance Study for Different Deployment Ratios in Indoor Scenarios

4.1 Introduction

This chapter explores the possibility of deploying home eNodeBs (HeNBs) with different patterns, as shown in Figure 4.1, to provide coverage to a 3GPP 5x5 apartment grid geometry. 3GPP defines deployment ratio in [79]. The deployment ratio determines whether HeNBs are deployed or not in all apartments, and varies from zero to one. For an urban-dense scenario, 3GPP suggest a value of 0.2 for the deployment ratio. This corresponds to having 5 HeNBs deployed within 25 apartments, as presented in Figure 4.1b.

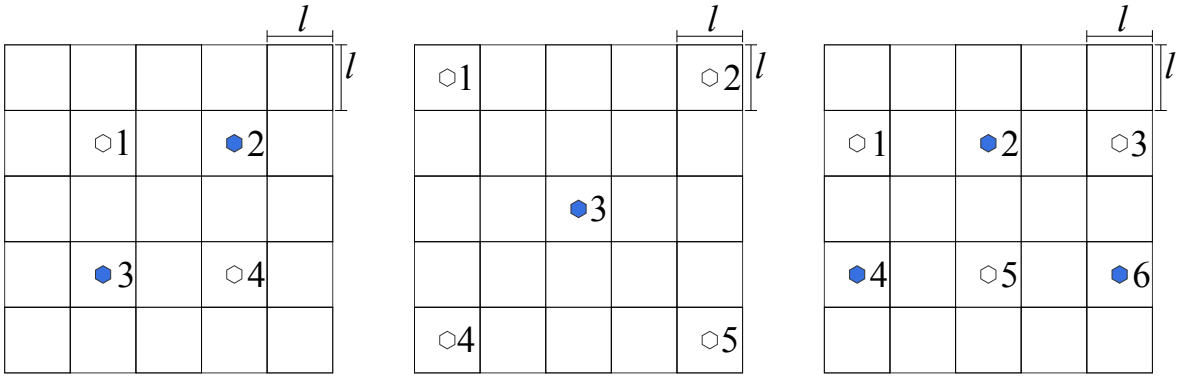

(a) 4 HeNBs (b) 5 HeNBs (c) 6 HeNBs

Figure 4.1: Considered pattern for the deployment of HeNBs to cover the same floor area.

Figure 4.1a with 4 HeNBs shows a deployment ratio of 0.16 and in Figure 4.1c the deployment ratio is 0.24 that correspond to have 6 active HeNBs. As an example Figure 4.1 presents three of the many deployments that can be adopted.
An updated version of LTE-Sim is presented in Appendix E, and is considered to extract values for packet loss ratio (PLR), maximum number of supported users, goodput and delay.
In the first part of this Chapter we study in detail the case with 4 HeNBs to cover the whole building area. With this deployment pattern, there are at least one apartment between HeNBs, and are also one apartment between the exterior walls and the HeNBs. The idea behind the choice for not to deploy HeNBs in apartments with exterior walls, is to avoid (or at least reduce) interference from the evolved NodeB (eNB). In this case we follow the approach of 3GPP for industrial femtocells and consider eight simultaneous users per HeNB.
In the second part we studied the saturation conditions for different values of deployment ratio. With 5 and 6 HeNBs, as show in Figure 4.1, it was considered not to deploy HeNBs in contiguous apartments. As a result there are HeNBs deployed in apartments that have a

exterior wall. These HeNBs are going to experience higher interference from the eNB. We determine the maximum number of supported users as well the supported goodput, considering a PLR target of 2% for video.

4.2 Performance Evaluation with Eight Users per HeNB

4.2.1 Deployment Scenario and System Settings

Section 2.4 described a scenario with only 4 HeNBs to provide coverage to a 3GPP 5x5 grid geometry building, as shown in Figure 4.2. To evaluate the network performance considering

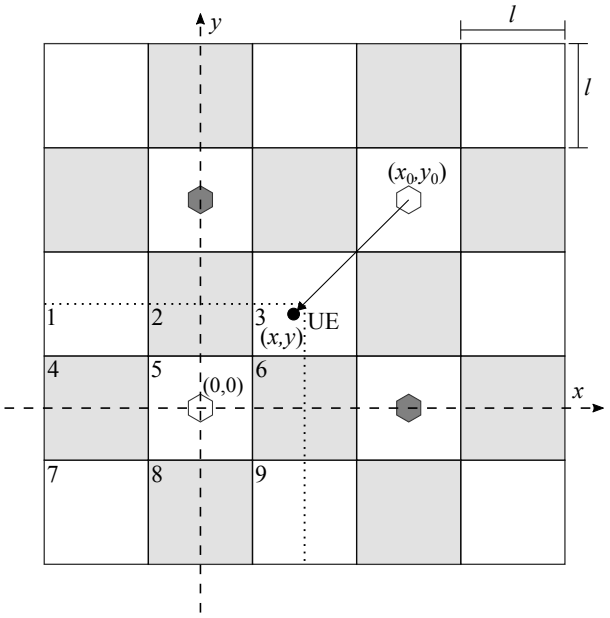

Figure 4.2: Topology with 4 HeNBs deployed.

this scenario, reuse pattern two is considered. The 4 HeNBs (represented by a hexagonal shape) are placed on rows two and four and on columns two and four. Nodes operating with one part of the bandwidth are represented with a white fill while the other HeNBs are represented with dark grey fill.

To analyze the overall performance of the system, three schedulers are considered for the downlink (DL), as follows: proportional fair (PF) [108], [139], frame level scheduler (FLS) [85], [142] and exponential rule (EXPRule) [143], [144].

In order to address the behavior of the heterogeneous network considering a real deployment scenario, a macrocell with one kilometer radius was considered to the simulation scenario. As introduced in Section 3.2, the building is created in a circular area with 80% of the macro cell radius. There are 4 HeNBs in a pre-determined apartment [79], [103]. This geometry represents actual deployment scenarios, like offices and shopping centers. Each cell serves eight users. In HeNBs, transmitter power varies from -10 dBm to 20 dBm, in steps of 5 dBm, and all cells simultaneously operate at the same power. The apartment side lengths vary from 5 to 20 m, in steps of 5 m.

For each scheduler and for each combination of the values of HeNB transmitter power and

apartment side lengths, fifty simulations have been performed. In each simulation, the position of the building is randomly chosen considering a Mersenne Twister pseudo-random generator along the cell topology (eNB coverage zone). The determination of the position of the users also considers a Mersenne Twister pseudo-random generator but only along the coverage area of the HeNB that includes rectangles/squares 1-9 (marked with a dotted line in Figure 4.2). An HeNB only serves the users inside the served area. The goal of accounting for different positions of user equipments (UEs) is to acquire the general behavior that integrates the contribution of the effect of having the building and consequently the HeNBs and the served users at different cell distances from the HeNBs topology. All details for the simulation parameters are presented in Table 4.1.

Table 4.1: Considered simulation parameters with 20 MHz of bandwidth in the eNB and 10+10 MHz bandwidth in the 4 HeNBs.

Parameter	Value
Simulation duration	30 s
Flow duration	20 s
eNBs cluster	1
Bandwidth eNB	20 MHz
Number of eNBs	1
eNB Radius	1 km
Power of the eNB	43 dBm
HeNBs cluster	2
Bandwidth HeNBs	10 MHz + 10 MHz
Number of HeNBs	4
Power of the HeNBs	[-10; -5; 0; 5 ; 10; 15; 20] dBm
Access Policy	Open
Deployment density	Dense
Number of users per HeNB	8
User speed	0 km/h
User equipment position	Random
Number of buildings	1
Number of floors	1
Geometry of buildings	5x5
Apartment side length	[5, 10, 15, 20] m
Building position	Random
Application type	Video and best effort
Video bit rates	440 kB/s
Maximum delay	0.1 s
Frame structure	FDD
Number of simulations for each combination	50
CQI	Periodic
Path loss model	WINNER II

The applications considered are the same presented on Chapter 3. One is the video application, a video trace that is compressed using the H.264 standard compression at the average coding rate of 440 kb/s. The adoption of this video application accounts for the trend of users to watch high quality videos. The other application is BE. These BE flows are modeled through infinite buffer sources which model an ideal source where there are always packets to be sent. We evaluate the network performance by considering these video and BE flows [103]. Fitting surfaces were made using a polynomial surface with a confidence inter-

val of 95% [149].
In the simulations, we assume that the eNB 20 MHz bandwidth is split into two equal parts to be made available to the HeNBs, each portion with 10 MHz bandwidth. The 4 HeNBs are placed as shown in Figure 4.2. The network performance has been evaluated with reference to the goodput achieved by BE flows and the goodput, PLR and delay of video.
With any of the considered schedulers, the 3GPP limit of 150 ms for the maximum delay has not been overcame [97], Appendix F.

4.2.2 Average Goodput and Packet Loss Ratio with 4 HeNBs

4.2.2.1 Results with PF

Although 3GPP suggests a deployment ratio of 0.2, which correspond to 5 HeNBs per floor (with 25 apartments) in this section we consider a deployment ratio of 0.16. Figure 4.3a presents the average goodput with the use of the PF scheduler for video application.

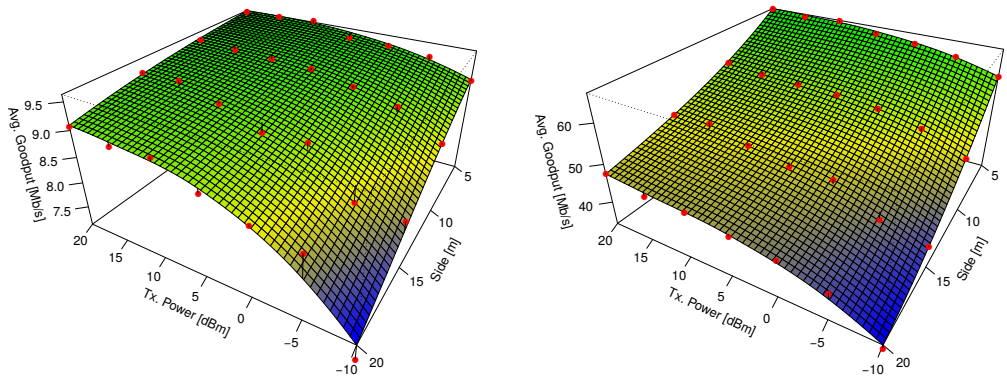

(a) Video flows with a bit rate of 440 kb/s.

(b) Best effort flows.

Figure 4.3: Variation of the average goodput of video and BE flows with 4 HeNBs scenario, with PF scheduler and for different values of transmitter power and apartment side length.

The maximum values for the average goodput have been obtained when the apartment side length is 5 m and the transmitter power is 20 dBm. The lowest values have been achieved when the apartment side length is 20 m and the transmitter power is -10 dBm. For BE flows, in Figure 4.3b the maximum and minimum values for the goodput have been obtained in the same points as for the video flows in Figure 4.3a. For both flows, the obtained results are in line with the results obtained for the average signal-to-interference-plus-noise ratio (SINR). The average packet loss ratio (PLR) for video flows, shown in Figure 4.4, presents values that go beyond the target of 2% indicated by the 3GPP. However, it is possible to obtain results for the PLR lower than or closer to 2%, namely when the apartment side length is 5 m. For transmitter power of 10 dBm and apartment side length of 5 m, the PLR is lower than 2%. For larger apartment side lengths the PLR is higher than 2%.

4.2.2.2 Results with FLS

Comparing the average goodput of video flows with the use of the FLS scheduler, as shown in Figure 4.5a, with the previous case (PF scheduler), shown in Figure 4.3a, with the FLS

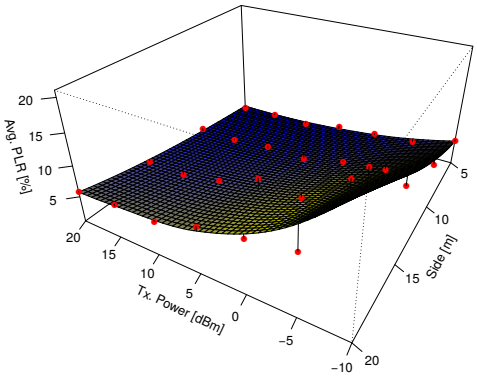

Figure 4.4: Variation of the average PLR of video flows, with PF scheduler and for different values of transmitter power and apartment side length.

scheduler, the average goodupt increases, although both schedulers have identical behavior.

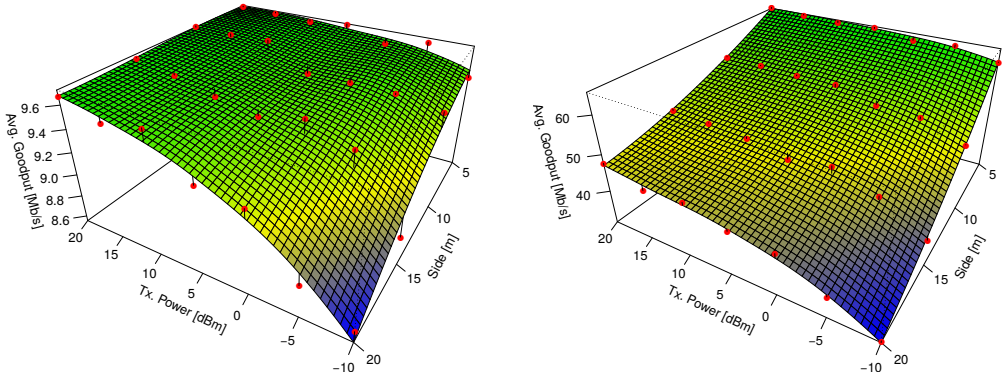

(a) Video flows with a bit rate of 440 kb/s.

(b) Best effort flows.

Figure 4.5: Variation of the average goodput of video and BE flows with 4 HeNBs scenario, with FLS scheduler and for different values of transmitter power and apartment side length.

When the transmitter power is 20 dBm and the apartment side length is 20 m, the average goodput clearly increases by a value near 0.59 Mb/s, from 9.8 Mb/s to 9.67 Mb/s. Even in the worst case, for a transmitter power of -10 dBm and apartment side length of 20 m, the average goodput increases more than 1.8 Mb/s, from 6.83 Mb/s to 8.65 Mb/s. Since video takes advantage form the FLS scheduler, the BE application is penalized. The average goodput for the BE application, as shown in Figure 4.5b, is in average, circa 1 Mb/s lower than the previous case Figure 4.3b.

The adoption of the FLS scheduler also brings advantages in the results obtained for the PLR for the video application, as shown in Figure 4.6.

By comparing these results with the values obtained for the PF scheduler, as shown in Figure 4.4, the average PLR with the FLS decays, and it is possible to keep the PLR lower than 2% for more combinations of the transmitter power and apartment side length. Even the worst values obtained decay from a maximum of 28% to a maximum of 10.8%. Both values were obtained for the same transmitter power of -10 dBm and apartment side length of 20 m.

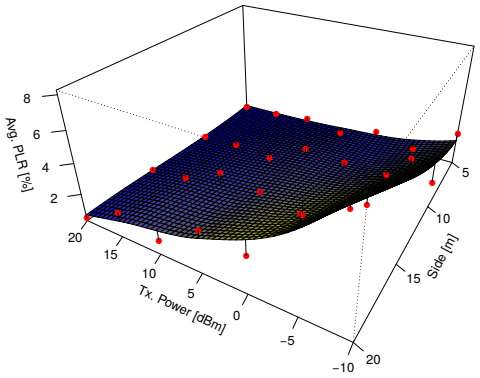

Figure 4.6: Variation of the average PLR of video flows, with FLS scheduler and for different values of transmitter power and apartment side length.

4.2.2.3 Results with EXPRule

Contrary to the previous cases, Figure 4.3a and Figure 4.5a, the behavior of the average goodput of video flows with the use of the EXPRule scheduler is more irregular, as shown in Figure 4.7a, and has a clear local maximum.

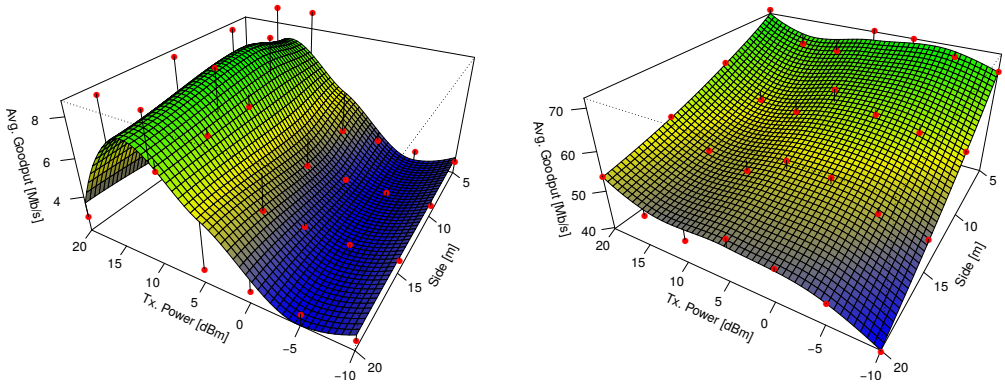

(a) Video flows with a bit rate of 440 kb/s.

(b) Best effort flows.

Figure 4.7: Variation of the average goodput of video and BE flows with 4 HeNBs scenario, with EXPRule scheduler and for different values of transmitter power and apartment side length.

The maximum average values of the goodput for the video application occurs for transmitter powers between 10 and 15 dBm. By considering a constant transmitter power, the variation of the side of the apartment length does not impact the average goodput. Although the maximum average goodput is identical in the three schedulers, the EXPRule scheduler present the worst average goodput for the video application. Since the video flows were impaired by the use of the BE flows, the average goodput for the BE flows increases, as shown in Figure 4.7b. As an example, the average goodput with the EXPRule scheduler is 7.68 Mb/s higher than the average goodput for BE flows, as shown in Figure 4.5b. Although the EXPRule scheduler is not itself the best choice in terms of goodput, the average PLR for video flows, for values of transmitter power equal or higher than 0 dBm, is in most of the cases lower than 2%, as shown in Figure 4.8. In fact, the maximum PLR is the lowest from the three studied schedulers, with a value of 6.4%.

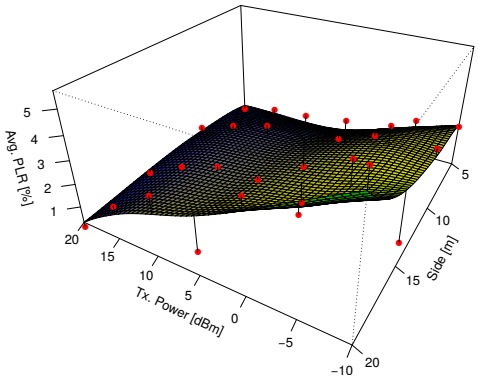

Figure 4.8: Variation of the average PLR of video flows, with EXPRule scheduler and for different values of transmitter power and apartment side length.

4.2.3 Lessons learned

The performance evaluation of deploying 4 HeNBs that serves each one eight users, considered an upgraded version of the LTE-Sim. The PF and FLS schedulers perform very identically in terms of average goodput, with a slight advantage for the FLS. However, in terms of the average PLR, the FLS presents better performance, since it achieves values lower than 2% more often. This performance enhancement occurs when the transmitter power is between 10 and 20 dBm for all the apartment side lengths.

In this comparison between the PF scheduler and the FLS, the PF scheduler also presents better results for the average goodput for BE flows. These two schedulers confirm the expected results for average SINR that were analytically derived.

Contrary to the PF scheduler and FLS, the best performance of EXPRule scheduler was obtained for transmitter powers between 10 and 15 dBm. It is important to note that the values of average goodput for video flows are identical for a transmitter power of either 20 dBm or 0 dBm. For the average PLR, values lower than 2% were achieved for transmitter power lower than 15 dBm when the apartment side length is 15 m. But when the apartment side length is 5 m, values of average PLR lower than 2% were obtained for values of the transmitter power higher than 0 dBm.

With EXPRule scheduler, the variation of the average goodput of BE flows with 4 HeNBs and 8 UEs scenario shows a behavior approximated to the one from other studied schedulers.

It is important to highlight that is possible to operate the system without the need to set the HeNBs transmitter power to the maximum value without compromising the overall system performance. If the transmitter power is set to lower values, this can be a step to achieve greener mobile communication systems.

4.3 Saturation Conditions in Scenarios with a Variable Deployment Ratio

This Section explores the possibility of deploy HeNBs with deployment ratios 0.16, 0.20 and 0.24 as shown in Figure 4.1. Results for the maximum number of users supported in each

deployment scenario and goodput are presented in saturation conditions. They were determined taking into account a target of 2% for the PLR [97], when users are using a video application and BE application. In terms of delay, with any of the considered schedulers, the 3GPP limit of 150 ms for the maximum delay has not been overcame, Appendix F.
This Section also presents a different approach to deploy users. Usually users are deployed either inside the femtocells or, as in Chapter 3, [96], users are deployed inside of the HeNB own apartment. To deploy users without considering wall boundaries of the apartment creates a unbalanced scenario in terms of users per cell. In this part of the work, we follow this approach and users are deployed on the building floor, which creates an unbalanced behavior in terms of users per cell. At the start of the each simulation users are deployed on the floor building. According to the received signal strength, users are going to connect to a HeNB.

4.3.1 Scenario Parameters

The assumptions for these scenarios to study the maximum capacity are introduced in Table 4.2. Buildings are deployed in an area with a radius of 80% of the macrocell radius. The

Table 4.2: Considered simulation parameters for operation of 4, 5 and 6 HeNBs.

Parameter	Value
Simulation duration	30 s
Flow duration	20 s
eNB cluster	1
eNB bandwidth	20 MHz
Number of eNBs	1
eNB radius	1 km
Power of the eNB	43 dBm
HeNBs cluster	2
HeNBs bandwidth	10+10 MHz
Number of HeNBs	[4 ; 5; 6]
Power of the HeNBs	[5 ; 10; 20] dBm
Access policy	Open
Deployment density	Dense
User speed	0 km/h
User equipment position	Random
Number of buildings	1
Number of floors	1
Geometry of buildings	5x5
Apartment side length	[5, 10, 15, 20] m
Building position	Random
Application type	Video and best effort
Video bit rate	440 kb/s
Maximum delay	0.1 s
Frame structure	FDD
Number of simulations for each combination	50
CQI	Periodic
Path loss model	WINNER II
Packet scheduler	Frame level scheduler

eNB operates with a 20 MHz bandwidth and HeNBs operates with a reuse pattern two. It divides the 20 MHz bandwidth into two equal parts of 10 MHz [94], [95], and uses one part

by HeNBs represented in Figure 4.1 with a white fill, and another by the remaining HeNBs, represented with light-blue fill.
To compare the new options adopted to the simulator, the applications adopted are the same presented in Chapter 3, [95] and [94]. A video trace with an average coding rate of 440 kb/s [148] and a BE application [103].
The primary approach of simulators such as LTE-Sim is to allocate a predetermined number of users per HeNB. This means that every HeNB in a simulation has the same number of femtocell users, leading to a balanced system. Since this work seeks to extract the maximum number of supported users by a number of femtocells on a building floor, the former approach was abandoned. The newly implemented approach consist of assigning a determined number of users to the floor. Users are deployed on the building floor. Each user connects to the HeNB that serves it with the highest received transmitter power. Although the building could be deployed near the eNB and, in this case, users could receive the highest transmitter power from the eNB, it does not allow them to connect to the eNB. Users only are able to connect to the HeNBs. Users are uniformly distributed around HeNBs. As their distribution is random there will no be the same number of users per HeNB.

4.3.2 Packet Loss Ratio

4.3.2.1 Deployment with 4 HeNBs

Aiming to extract the maximum capacity for the considered scenarios, the first step is to determine the packet loss ratio (PLR) as a function of the number of users. In [97], 3GPP defines for video the 2% target for PLR. Results has been extracted for all combinations of transmitter power of HeNBs (0, 10 and 20 dBm) and apartment side lengths (5, 10, 15 and 20 m). Figure 4.9 presents results for the scenario with 4 HeNBs by considering all combinations of the parameters.
For an apartment side length of 5 m, for all values of transmitter power, results of PLR are almost identical, as shown in Figure 4.9a. For an apartment side length of 20 m, the PLR increases, as shown in Figure 4.9d. The same behavior is observed for apartment side lengths of 10 m and 15 m, as shown in Figure 4.9b and Figure 4.9c, respectively.
When the transmitter power is 0 dBm the increase in the apartment side length results in an increase of the PLR. The PLR is almost identical between the curves for transmitter powers of 10 dBm and 20 dBm up to 84 users. The PLR is the lowest for a transmitter power of 20 dBm.

4.3.2.2 Deployment with 5 HeNBs

With 5 HeNBs, the deployment ratio correspond to the value suggested by 3GPP, i.e., 0.20. Figure 4.10 presents results for this deployment ratio. For apartment side lengths of 5 m, the PLR results are similar for the considered values of the transmitter power, as shown in Figure 4.10a.
However, for a transmitter power of 0 dBm, the 2% target for PLR is surpassed for less users than for other transmitter power values. The same behavior occurs for apartment side

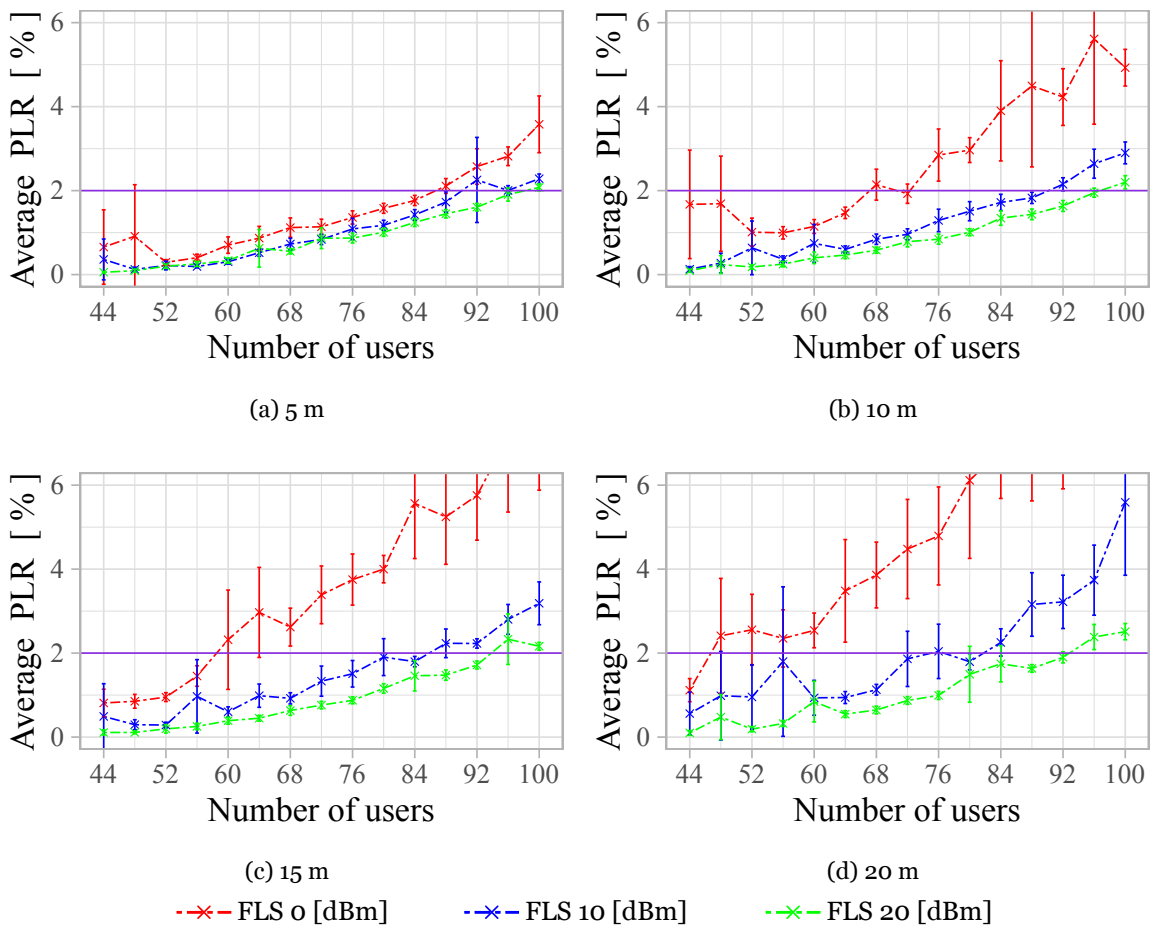

Figure 4.9: Maximum Average goodput for Video with 4 HeNBs.

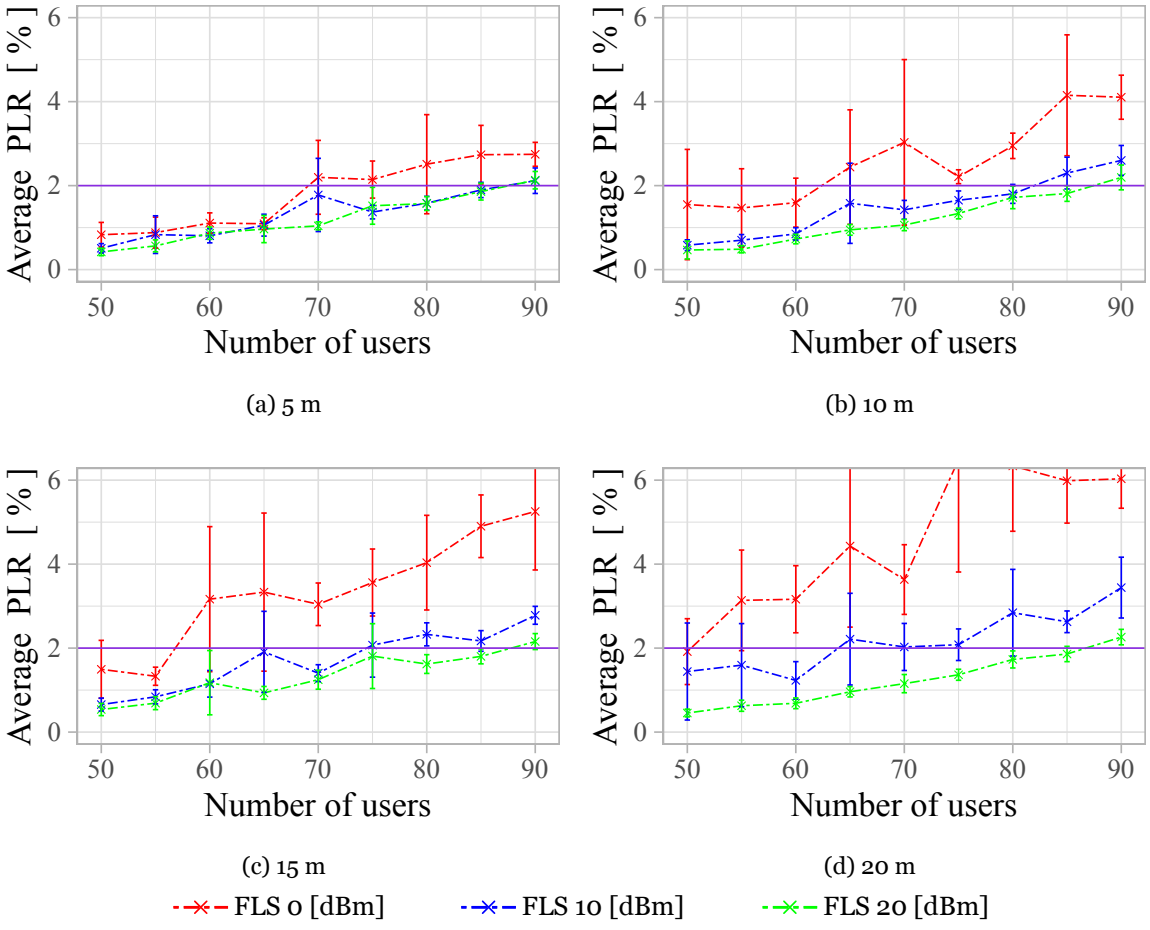

Figure 4.10: Maximum Average goodput for Video with 5 HeNBs.

lengths of 10 m, as shown in Figure 4.10b, and 15 m, as shown in Figure 4.10c. For an apartment side length of 20 m, results presented in Figure 4.10d also shows that, for a transmitter power of 0 dBm, the target value of 2% is surpassed less users than for other transmitter powers. PLR results for transmitter powers of 10 dBm and 20 dBm are similar, specially for apartment side lengths from 5 m up to 15 m. However, for a transmitter power of 10 dBm, the PLR target of 2% is surpassed for lesser users than for transmitter power of 20 dBm.

4.3.2.3 Deployment with 6 HeNBs

Figure 4.11 presents results for the 6 HeNBs deployment. For apartment side lengths of 5 m

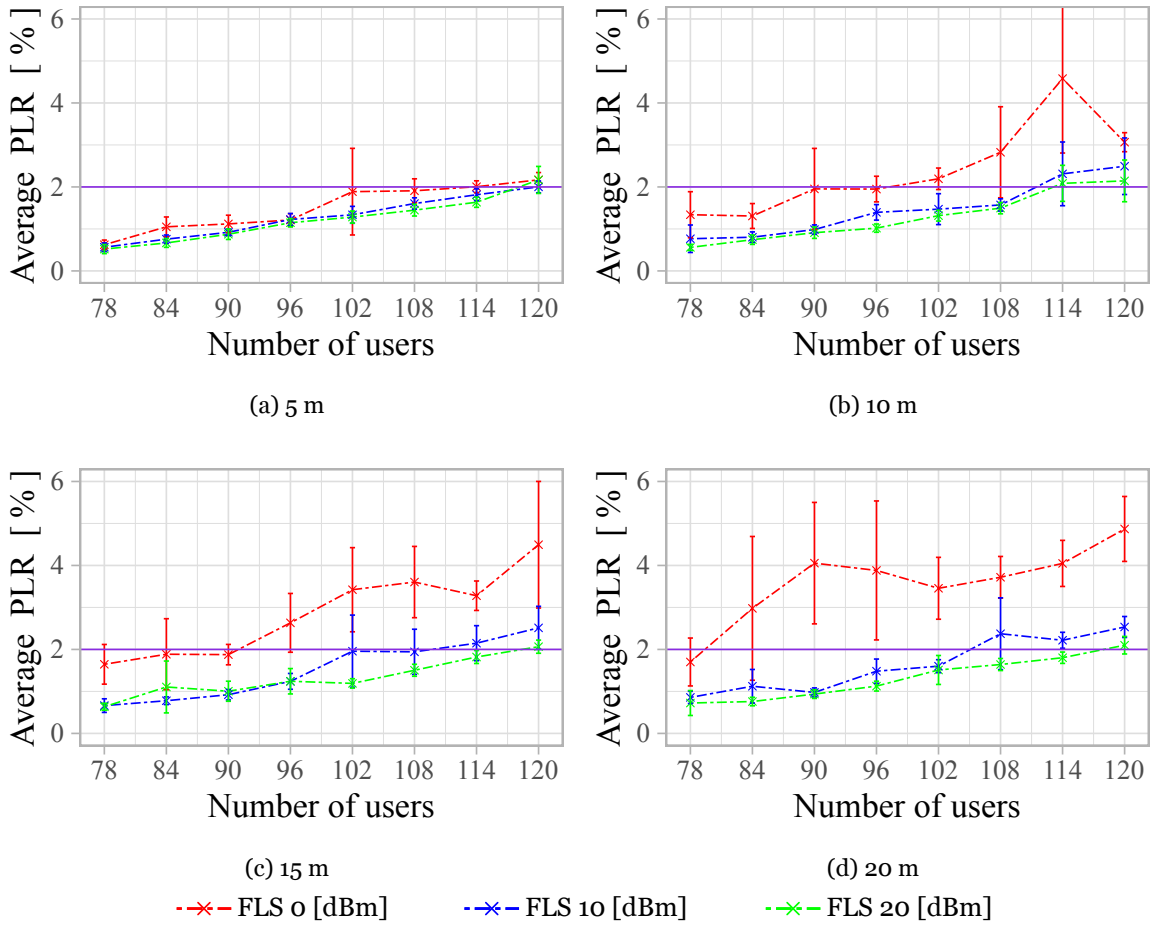

Figure 4.11: Maximum Average goodput for Video with 6 HeNBs.

Figure 4.11a for any values of transmitter the values of PLR are almost identical. There are only a slight disadvantage for 0 dBm. For an apartment side lengths of 10 m Figure 4.11b, and for values of transmitter power of 10 dBm and 20 dBm the behavior is closer to previous one. For 0 dBm the target value of 2% for the PLR is surpassed sooner than the other transmitter powers.

When the apartment side length increases to 20 m a transmitter power of 0 dBm, the PLR surpassed the 2% sooner than the other values Figure 4.11d. Although more users are supported for a transmitter power of 20 dBm, with a transmitter power of the 10 dBm values

of PLR are similar. When the apartment side length is 15 m Figure 4.11c the behavior of the PLR is closer to the behavior as when the apartment side length is 20 m.

4.3.2.4 Analysis of PLR

Results for an apartment side length of 5 m for all values of transmitter power shows in all cases the variation of the PLR is closer no matter the values of the transmitter power. When 20 m apartment side length is considered and the transmitter power is 0 dBm the PLR increases faster than the other transmitter powers. With 5 HeNBs Figure 4.10d with a transmitter power of 10 dBm the target of 2% is achieved sooner than the other two scenarios.

Some confidence intervals presented from the point of view of statistics mean that more simulations need to be performed [153]. Another away is identify outliers [154] analyze and treat data [153]. In this work none of these solutions are needed. The confidence intervals means in the cases with apartment side lengths of 20 m and transmitter power of 0 dBm that HeNBs could not offer enough resources to that users. It reduces this effect increasing the transmitter to 10 dBm and almost vanish when the transmitter power is 20 dBm.

Another cause of this problem it could be the probability of deploying a larger share of users in the areas with lower EESM identified in Chapter. 2. Furthermore adopting to deploy a determined number of users to the floor and not per HeNB creates in most of the simulations an unbalanced number of users per HeNB. This means that in some cases most of the users are concentrated in a few HeNBs. Leaving the remaining HeNBs with fewer users. Both cases could be misunderstand as outliers during the statistical analysis.

4.3.3 Maximum Supported Users

Table 4.3 presents the maximum number of users supported for a PLR $< 2\%$.

Table 4.3: Maximum number of users served by each configuration for a PLR $< 2\%$.

		Transmitter Power [dBm]								
		0			10			20		
Number of HeNBs		4	5	6	4	5	6	4	5	6
Side [m]	5	84	65	108	88	85	114	96	85	114
	10	72	60	96	88	80	108	96	85	108
	15	56	55	90	84	70	108	92	85	114
	20	44	50	78	80	60	102	92	85	114

This analysis shows the number of users that could be supported with the considered applications. Taking into account the results in Chapter 2, it is expected to support more users with 4 HeNBs than the other options. Although the deploy of 6 HeNBs get a lower EESM, the number of available HeNBs as more resources to support more traffic data. Although 5 HeNBs as more available resources than 4 HeNBs, this one could support more users. The only exception is when the transmitter power is 0 dBm and the apartment side length is 20 m.

4.3.4 Supported Goodput for Video

Goodput is the sum of bits correctly received by users divided by flow time. The supported goodput for the video application when 4 HeNBs are considered is presented in Figure 4.12a.

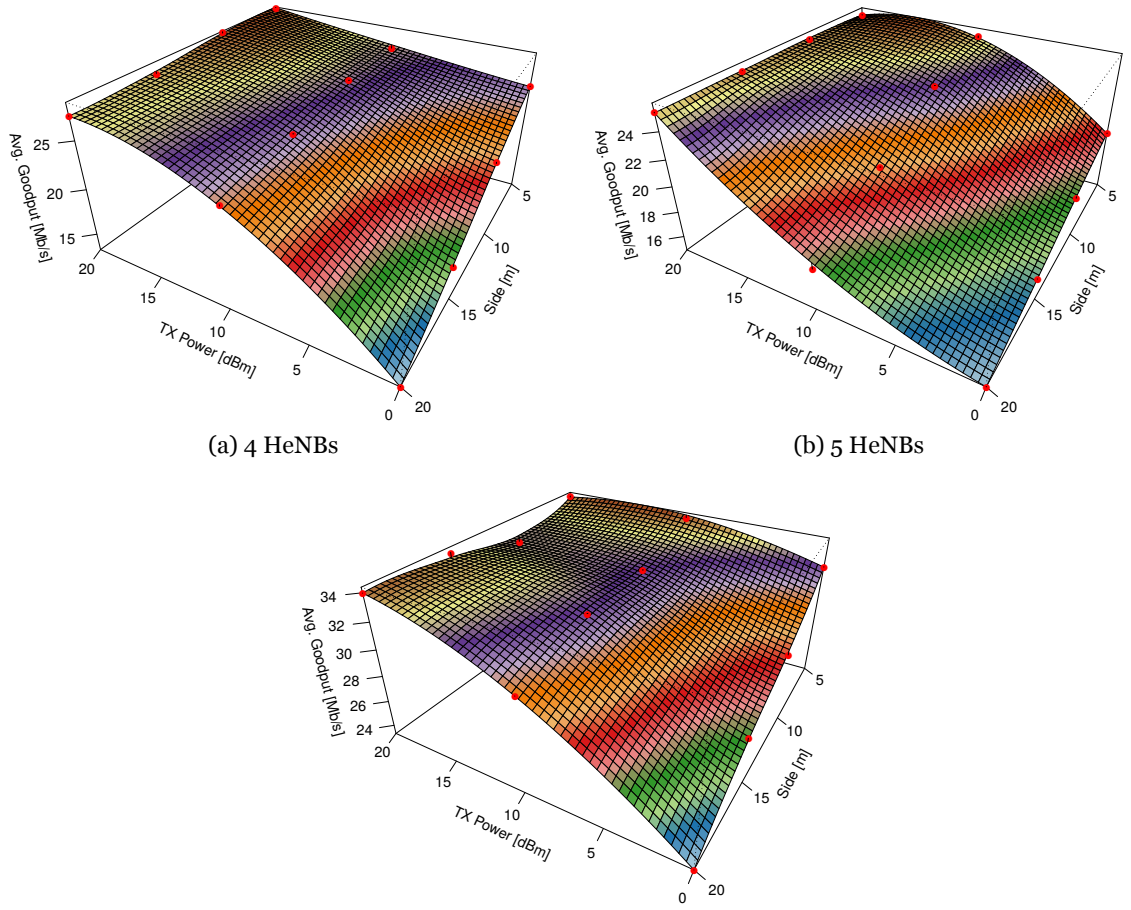

(a) 4 HeNBs

(b) 5 HeNBs

(c) 6 HeNBs

Figure 4.12: Maximum Average goodput for Video with 4, 5 and 6 HeNBs.

The maximum goodput is 28.5 Mb/s and is got when the transmitter power is 20 dBm and the apartment side length of 5 up to 10 m. Out of this combination the goodput decrease more when the combination converges to a transmitter power of 0 dBm and apartment side length of 20 m to 13.2 Mb/s.

Figure 4.12b presents the results for 5 HeNBs. With this number of HeNBs, worst results are got than the previous case. The maximum goodput of 25.3 Mb/s where get with a transmitter power between 20 and 10 dBm and the apartment side length of 5 m. The lowest value of 14.9 Mb/s was also got for a transmitter power of 0 dBm and an apartment side length of 20 m. When 6 HeNBs are considered the goodput Figure 4.12c is higher than the other two options.

The maximum goodput is 34 Mb/s for a transmitter power of 20 dBm when the apartment side length is 5 m. Also for a 5 m side and the transmitter power of 10 dBm the goodput is near the maximum. 6 HeNBs also could not deal with the larger apartment side length of 20

m and the lower transmitter power of 0 dBm. Here the average goodput is 23.3 Mb/s, but higher than the other two options of 4 and 5 HeNB.

4.3.4.1 Supported Goodput for BE

The maximum goodput for BE application increase with the availability of resources Figure 4.13.

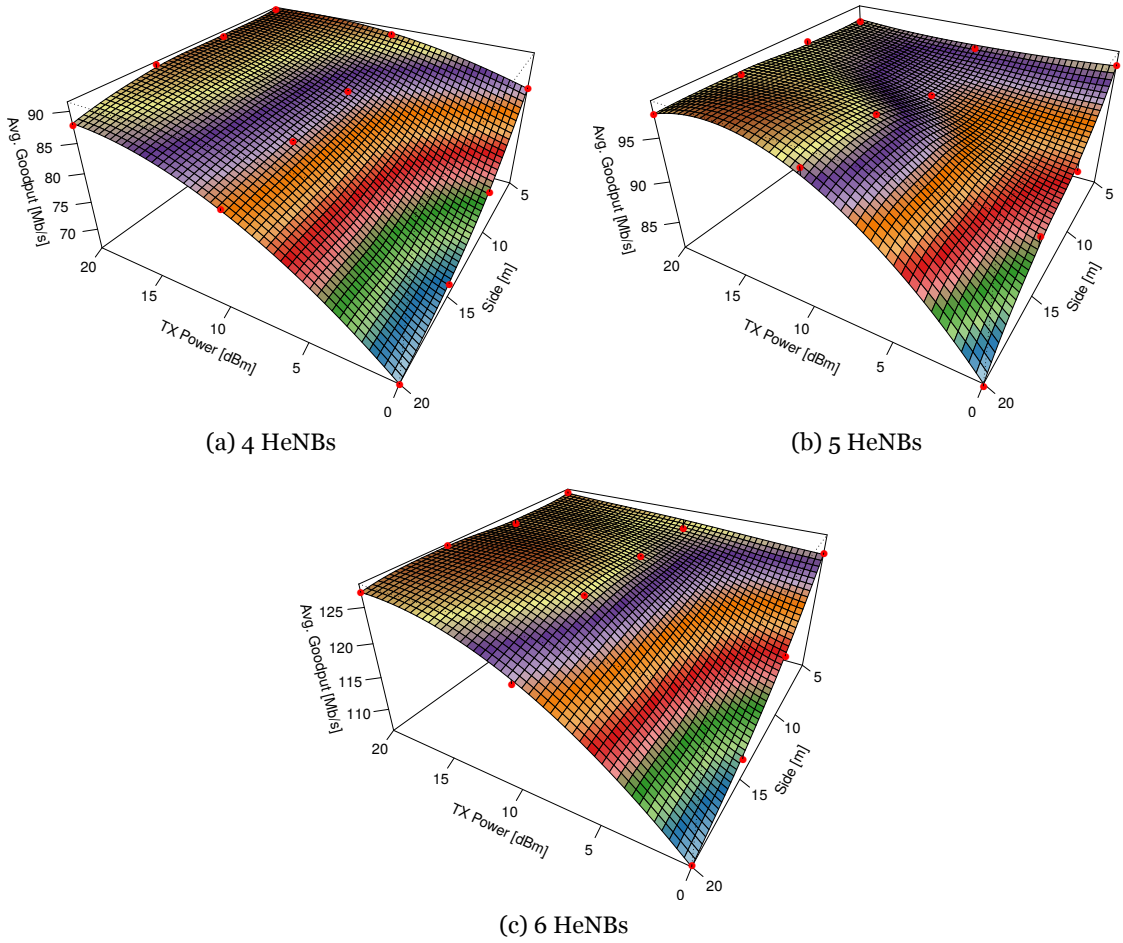

(a) 4 HeNBs

(b) 5 HeNBs

(c) 6 HeNBs

Figure 4.13: Maximum Average goodput for BE with 4, 5 and 6 HeNBs.

With 4 HeNBs, Figure 4.13a the maximum goodput is obtained for a transmitter power of 20 dBm and an apartment side length of 5 m. For 5 HeNBs, Figure 4.13b the maximum goodput occurs for transmitter power between 20 and 10 dBm and an apartment side length between 20 and 15 m. In the scenario with 6 HeNBs, Figure 4.13c the scenario with the higher goodput, the maximum was obtained for a transmitter power between 20 and 10 dBm and an apartment side length of 15 m.

There are a convergence in all scenarios to present the lowest average goodput when the transmitter power is 0 dBm and the apartment side length is longer, 20 m. For 0 dBm when the apartment side length decrease the average goodput increases around 20 Mb/s. For 5 m apartment side length, the variation of transmitter power as a lower impact on the average goodput.When the transmitter power is 20 dBm the variation of apartment side length as

little impact.

4.3.5 Different Deployment Ratio Lessons Learned

In this Section the impact of considering a different number of HeNBs from 4 to 6 HeNBs to provide resources to a building with a 3GPP 5x5 grid geometry has been tested. The impact of independent variations of the transmitter power of HeNBs from 0 to 20 dBm and the apartment side lengths from 5 to 20 m was contributed to the test system.
This Section also takes advantage of the improvements presented in Appendix E. The major update is to permit using any deployment ratio for the HeNBs, from zero up to one. Simulations were perform to extract values for the PLR for the video application. Considering a PLR target of 2% values for the maximum number of supported users and goodput of video and BE were got. The scenario with 6 HeNBs gets the best results. The best for video goodput was 34 Mb/s. Followed by the 4 HeNBs with 28.5 Mb/s and by the scenario with 5 HeNBs with 25.3 Mb/s.
The valuable conclusion in the case of video flows, is if the concern is to guarantee the higher goodput or support, for the maximum number of users, the best option is to consider the scenario with 6 HeNBs. Followed by the scenario 4 HeNBs, and the worst was the scenario with 5 HeNBs.
For BE the behavior for all scenarios is the same. Since the scenario with 5 HeNBs for the video application for 5 m is penalized for lower transmitter powers the BE is near constant for an apartment side length of 5 m for any value of transmitter power.
3GPP suggested a maximum of 5 HeNBs that corresponds to a deployment ratio of 0.2. However, this deployment shows the worst performance compared to the topology with 4 HeNBs. The geometry with 6 HeNBs is the one with the best overall performance results for the 5x5 grid of apartments.

4.4 Summary and Conclusions

The first approach of this chapter is to consider only 4 HeNBs to provide coverage in a building with a 3GPP 5x5 apartment topology. Each one of the HeNBs was serving 8 users. In this case, we know HeNBs as Enterprise HeNBs.
In the performance evaluation study the PF and FLS schedulers perform identically in terms of average goodput, with a slight advantage for the FLS. However, in terms of the average PLR, the FLS presents better performance, since it achieves values lower than 2% more often. This performance enhancement occurs when the transmitter power is between 10 and 20 dBm for all the apartment side lengths. In this comparison between the PF scheduler and the FLS, the PF scheduler also presents better results for the average goodput for BE flows.
Contrary to the PF scheduler and FLS, the best performance of EXPRule scheduler was obtained for transmitter powers between 10 and 15 dBm. It is important to note that the values of average goodput for video flows are identical for a transmitter power of either 20 dBm or 0 dBm. For the average PLR, values lower than 2% were achieved for transmitter power lower than 15 dBm when the apartment side is 20 m. But when the apartment side is 5 m, values of

average PLR lower than 2% were got for values of the transmitter power higher than 5 dBm. With EXPRule scheduler, the variation of the average goodput of BE flows shows a behavior approximated to the one from other studied schedulers.
This Chapter considers a study on the impact of considering the deployment of 4, 5 and 6 HeNBs in the same scenario. These deployment scenarios were analyzed in terms of saturation conditions. By considering a PLR target of 2%, results for variation of the maximum number of supported users and goodput have been obtained for the video and BE applications. As the number is higher, the scenario with 6 HeNBs enables to achieve enhanced performance (34 Mb/s against 28.5 Mb/s with 4 HeNBs and 25.3 Mb/s with 5 HeNBs). While with 6 HeNBs provide higher capacity, a scenario with 4 HeNBs enables better coverage.
With the considered scenario and simulation parameters, this work shows to future practitioners looking at deployment scenarios that the 3GPP appointed deployment ratio is not the optimal choice. Other deployment geometries probably could present a similar behavior of the topologies considered in this work. We have also concluded that the maximum number of HeNBs suggested by 3GPP is not the best choice for HeNB deployment.

Chapter 5

Service Quality of the Urban Micro Cellular Scenario in the sub-6 GHz Frequency Bands

5.1 Introduction

This Chapter studies the urban micro cellular outdoor scenario by comparing the impact of the ITU-R M.2135-1 dual slope path loss model in the service quality among the 2.6, 3.5 and 5.62 GHz frequency bands. An updated version of LTE-Sim is considered to obtain results for the exponential effective signal-to-interference-plus-noise ratio whilst determining the modulation and coding scheme. Considered cell radii vary from values shorter than the breakpoint distance, $d_{BP}^{'}$, up to 1000 m. System capacity is determined by considering a video application at 3.1 Mb/s while comparing the proportional fair (PF) and the modified largest weighted delay first (M-LWDF) schedulers through system level simulations. We have learned that the packet loss ratio (PLR) is higher for cell radius, R, shorter than the $d_{BP}^{'}$. For cell radii longer than the $d_{BP}^{'}$ and up to R = 1000 m, the PLR first decreases and then increases. The number of supported users has then been determined, for a PLR target of 2%. For both schedulers, the M-LWDF scheduler allows for obtaining the highest goodput, which occurs at 2.6 and 3.5 GHz for $300 \leq R \leq 500$ m, while for the longest Rs the highest goodput occurs at 5.62 GHz.

5.2 Urban Micro Cellular Scenario

The exponential growth of the wireless communications sector has driven the research community to investigate future systems such as heterogeneous networks (HetNets), millimeter-wave and multi-input multi-output [4]–[6]. To complement the traditional macrocell network to answer to the future service demands and the growth of wireless data traffic [7]–[9], lower power nodes are being added to the existing networks, creating what is known as HetNets. The effectiveness of the answer to HetNets business opportunities is determined by the diversity of cell sizes and network architectures, together with the coalition of diverse technologies and availability of licensed/unlicensed frequency bands.

Studies on performance analysis of cellular networks usually resort on single-slope (SS) path loss models (PLMs). SS are simple PLMs that fail on capturing the short distance path loss behavior [155]. This happens since a SS-PLM considers a homogeneous path loss along the cell coverage range, as shown in Figure 5.1a.

In urban scenarios, where there are a plethora of non homogeneous obstacles, like vehicles and urban obstructions/elements, attenuation increases when the distance between the transmitter and receiver nodes increases. This may lead to inaccurate results in performance

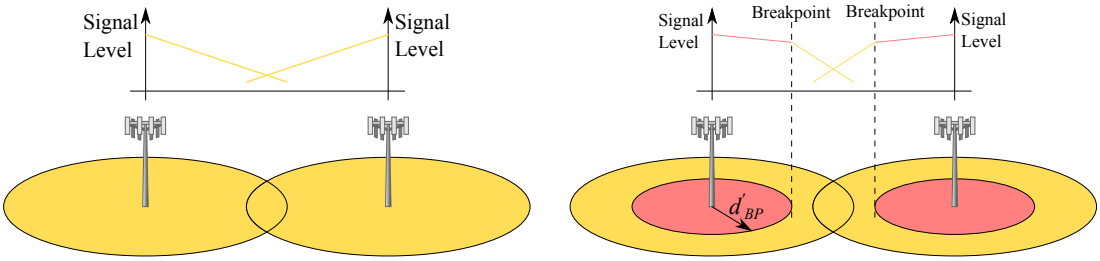

(a) Single-Slope PLM (b) Dual-Slope PLM

Figure 5.1: Different slope behaviors in the path loss models of cellular system.

evaluation of dense networks. Dual-slope (DS) PLMs can be a solution to overcome limitations of SS-PLMs, since these models more accurately represent the outdoor small cell link variations along the distance (represented by the change of the propagation exponent beyond the breakpoint distance), mainly due to the combination of a direct ray plus a ray reflected on the ground (e.g., asphalt).

DS-PLMs represent the dependence of the path loss over distance, and this implies a DS behavior [156]. Authors from [157] have shown that, compared the SS-PLMs, DS-PLMs more closely match empirical data, while capturing the relationship between the path loss and the distance between the transmitter and the receiver. While path loss exponent slope is around 2-2.2 for distances in the range close by the cell center, a value around 4 is identified for the longest distances, as shown in Figure 5.1b. According to [158], the breakpoint distance can be obtained either by regression analysis or by considering the geometry when the Fresnel zone just touches the ground. The breakpoint distance can also define the turning point between the line-of-sight (LoS) and non-line-of-sight (NLoS) situation, as explained in [156], [158]. Furthermore, PLMs can be generalized for any number of slopes, as in [159].

DS-PLMs have captured the attention of the research community and are being studied in a multitude of areas of implementation. One of these areas is vehicular technology, in applications as intra-vehicular [160], [161], vehicle-to-vehicle [162], [163], vehicle-to-cyclist [164], vehicle-to-infrastructure [165] or pedestrian-to-vehicle [166] communications. Another area of application is unmanned aerial vehicles (commonly known as UAVs) operating at low-altitude [167]. Some deployment scenarios are also being considered for rural [6], [163], highway [163], suburban [6] or urban [168] environments, where detailed analysis has conducted to consider a street canyon environments [169], or indoor scenarios [170], [171]. Coverage in these scenarios is provided by cells with longer cell radius, R, known as macrocells. On the other hand, the cell radius of indoor and urban small cells is shorter [159], [172], [173].

Furthermore, the millimeter wavebands are being considered to answer to enormous quantity of information demand in small cell networks [174]. However, despite DS-PLMs have been considered, only SS-PLMs are applied, as the breakpoint distance is far beyond the size of small cells. Literature review contains research works on frequency bands from 800 MHz up to 82.5 GHz [175], [176].

Although several propagation scenarios have been considered and developed for 5G [177], so far, the underlying impact of different packet scheduling algorithms is still being investigated [130]. For successive generations of broadband cellular networks, packet scheduling has

played an important role in the management of radio resources. In particular, aiming at providing a user quality of service (QoS) that guarantees a sufficient grade of service, the choice of the packet scheduler is of particular interest.

QoS metrics are network centric performance variables that do not directly consider the user experience. Usually, QoS metrics may be based on four key quantitative parameters: packet loss ratio (PLR), throughput (or goodput), packet delay and jitter [83]. Indirectly, these QoS metrics may be mapped into quality of experience [102].

Packet schedulers have been developed to support real time (RT) services, like videoconferencing, or non-real time (NRT) services, as internet browsing [84], [178]. In 4G, there are two key strategies for the downlink (DL) packet scheduling, QoS-aware and QoS-unaware strategy [132]. Prior to this classification, DL scheduling strategies have also been divided into channel dependent or channel sensitive ones [84].

Authors from [173], [179] evaluated the impact of different path loss models on the capacity of 4G networks composed by small cells considering a carrier frequency of 2.6 GHz. They compared four urban path loss models, two SS-PLMs, one DS-PLM in LoS, and another DS-PLM, for NLoS. They concluded that, for values of R longer than the breakpoint, the supported cell physical throughput is steady or decreases with the R when using the traditional single-slope propagation models. Besides, for values of R shorter than the breakpoint, the two-slope propagation model leads to values of the throughput lower than the ones obtained with the SS-PLMs.

The 2.6 GHz, 3.5 GHz and 5.62 GHz sub-6 GHz frequency bands were studied in [180]. By mathematical modeling, authors from [180] concluded that, in terms of supported throughput, for R shorter than $\approx$ 550 m, the 2.6 GHz frequency band presents the highest throughput. For cell radii 550 $\lesssim R \lesssim$ 650 m, the 3.5 GHz frequency band presents the highest throughput. For coverage distances (d) longer than $\approx$ 650 m, the 5.62 GHz frequency band is the best one.

This research is inspired in the mathematical modeling presented in [173], [179], combined with the theoretical studies and simulations from [100], [102]. It extends the knowledge about the DS-PLM performance in urban micro cellular (UMi) outdoor LoS scenarios for the sub-6 GHz frequency bands by studying the impact of considering different packet scheduling strategies for small cell sizes.

In this study, an improved version of LTE-Sim [86] has been considered. LTE-Sim is an open source framework to simulate LTE-Advanced networks that was earlier improved to produce the results presented in [98], [102]. None of the previous works considers the M-LWDF scheduler. In this work, the UMi scenario for LoS, defined by ITU in [16], and a given reuse pattern, has been included in the simulator. Differently from [98] where the bit rate is 440 kb/s, this work assumes a video of 3.1 Mb/s. Besides, it also analytically studies the supported throughput based in the average signal-to-interference-plus-noise ratio (SINR), while comparing analytical and simulation results for the system capacity achieved when PLR $<$ 2% in deployments either with video application only, or video plus best effort usage. Figure 5.2 presents the frequency reuse for the considered small cell deployment.

Nineteen small cells are deployed with frequency reuse pattern three. The impact of varying

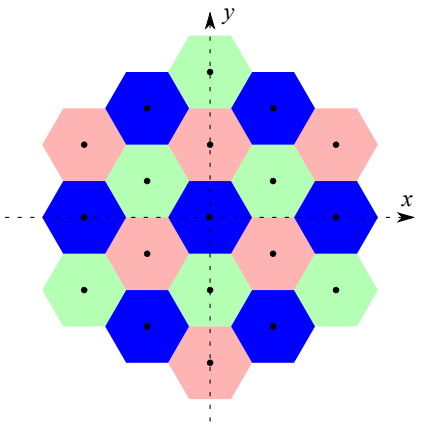

Figure 5.2: Simulation scenario for the UMi LoS small cell network with reuse pattern three.

the cell radius is taken into account. An outdoor environment is considered where antennas of the 4G base stations (BS) and user equipments (UEs) are well below the tops of surrounding buildings. This deployment scenario is presented in [16], with focus on pedestrian and slow vehicular users, and is known as an UMi cell scenario. We have considered that the radio link between the cell nodes and UEs is in LoS. The DS-PLM is considered to determine coverage and co-channel interference.

First, as a contribution beyond [98], the radio conditions are studied by extracting results for the exponential effective SINR mapping (EESM) for different values of the cell radius and its cumulative distribution function (CDF) at the UE. Results for the modulation and coding schemes (MCSs) used to communicate with different users within the cell are expressed in terms of its CDF. Secondly, the LTE-Advanced radio performance is studied through system level simulations.

By considering an implicit function formulation for the dependence of the physical throughput with the distance between UEs and BS [181], we have analyzed the dependence of the supported throughput, in average terms, with R for each frequency band (in the sub-6 GHz range). As the behavior of the average SINR (and average EESM) is similar to the trend of the curve of the supported throughput, we have sought optimum values for R when they are simultaneously maximized.

While evaluating the performance of the radio network, one considers the 3GPP technical specification (TS) 22.105 that establishes the performance target for the PLR of video streams [97]. The impact of considering the PF and the M-LWDF schedulers is compared when users are continuously communicating video streams in the downlink. PF is a scheduler that is not only unaware of the service type but also QoS-unaware. M-LWDF, in turn, is a QoS-aware scheduler that is aware of the service type [84], [133], [178]. Results are presented in terms of PLR, goodput, and delay, in average terms, as well the number of supported users. To determine maximum average goodput in the air interface, a best effort (BE) application is also considered. It has packets to send whose transmission only occurs when there are enough resources [102].

The remaining of the Chapter is organized as follows. Section 5.3 presents the single and dual slope path loss models. In Section 5.4, the considered schedulers are addressed. Section 5.5

describes the simulation scenario. The cellular planning trade-off is presented in Section 5.6, where results for the EESM, achieved MCS and supported cell throughput are presented. Achievable system performance for PLR $<$ 2% (and maximum delay less than the 150 ms target) is studied in Section 5.7. From the results for the PLR, goodput, delay as a function of the maximum number of users, the system capacity is determined in terms of supported goodput. Additionally, Section 5.8 presents results beyond the saturation level, i.e., PLR $\geq$ 2%. Finally conclusions are drawn in Section 5.9, where suggestions for the further research are also presented.

5.3 Path Loss Models

Signal transmission is subject to propagation loss or path loss. The diversity and type of obstacles between the transmitter and receiver (like, buildings, trees, vehicles, lampposts and so on) have a substantial contribution on the accounting of the total propagation losses. Cellular optimization trade-offs result from the co-channel interference imposed by nodes in the same heterogeneous network layer or by nodes in other sublayers operating with the same subchannels.
The cellular planning process allows predicting the cell range, cell coverage and throughput trade-offs [155], [168], [182], [183]. In the cellular optimization and planning process propagation losses are expressed through SS-PLMs and DS-PLMs.

5.3.1 Single Slope Modeling

For the sake of simplicity, lets consider the PLMs presented in [5], [156], [184], a generalization of other SS-PLMs studied in [173], [176]. Apart from the constant parameters, The path loss, PL, only depends on the physical distance along the path, d_f, and is defined as follows

$$PL_1(x) = \alpha_0 d_f^{\gamma}, \quad (5.1)$$

where α_0 is the reference loss, at one meter, γ is the path loss exponent (which, in this case, is constant for any value of d), while d takes any value between one meter and R. The path loss exponent could be determined experimentally by using an interpolation procedure [170].
SS-PLMs are the simplest way to model propagation losses since they have simple mathematical expressions and may lead to a large error between the PLM and the local path loss values [155]. Because of their "single" mathematical expression, SS-PLMs do not capture the impact of different topographic environments, or the difference in the behavior after the distance that separates the zone where the first Fresnel zone just touches the ground, or even the impact of irregular cell patterns [155]. In HetNets, SS-PLMs also fails at estimating losses, since the laws of physics applied to urban environments, where there is a reflection on the ground, show that a dual slope (DS) behavior is observed. This behavior is more evident in small cells networks for the sub-6 GHz bands [185]. To overcome the above limitations of the SS-PLM, DS-PLM can be used, since they can appropriately describe the channel propagation behavior in the UMi scenario.

5.3.2 Dual Slope Modeling

We can express a DS-PLM as follows

$$PL_2(x) = \begin{cases} \alpha_0 d_f^{\gamma_1} & \text{if } 1 < x < d_{BP}^{'} \\ \alpha_0 d_f^{\gamma_2} / d_{BP}^{'\gamma_2-\gamma_1} & \text{if } x \geq d_{BP}^{'} \end{cases}, \quad (5.2)$$

where $d_{BP}^{'}$ is the breakpoint distance, either determined when the first Fresnel zone just touches the ground or by the turning point between the LoS and NLoS zones [7], [158]. γ_1 and γ_2 are the path loss exponents, where $\gamma_1 \leq \gamma_2$. γ_1 represents the path loss exponent for distances shorter than $d_{BP}^{'}$ while γ_2 stands for distances longer than $d_{BP}^{'}$.

Authors from [173], [181], [185], [186] compare mathematical modeling approaches between SS-PLMs and DS-PLMs. They show that the use of DS-PLMs imply higher supported throughput for the longest cell radii in small cell outdoor environments. Authors from [7], [159], [185] highlight that DS-PLMs present more accurate performance results for coverage probability and user association than SS-PLMs. In fact, DS-PLMs are gaining importance in the characterization of propagation environments of the successive generations of mobile communications systems, not only in earlier 3GPP releases [177] but also in the ones from [187], [188], for 5G New Radio (NR) scenarios [130].

5.4 Packet Scheduling

As a QoS-unware scheduler, PF does not consider any QoS parameter [84], [108], [189]. It only schedules the traffic from a user when its instantaneous channel quality is high compared to its own average channel conditions over time. The priority metric is defined above in Section 3.3.1 by equation 3.1.

As a QoS-aware scheduler [84], [108], M-LWDF extends the the metric considered in PF by taking into consideration factors as delay and PLR, as follows

$$w_{ij} = \alpha_i D_{HOL,i} \frac{r_{ij}}{\bar{R}_i}, \quad (5.3)$$

where α_i is a factor computed from QoS and $D_{HOL,i}$ is the head of line (HOL) delay for the i_{th} user. The factor α_i is determined as follows

$$\alpha_i = -\frac{\log(\delta_i)}{\sigma_i}, \quad (5.4)$$

where δ_i is the acceptable PLR for the i_{th} user and σ_i is the delay threshold for the i_{th} user [83].

The weakness of the PF scheduler is its low spectral efficiency. In turn, the strength of the PF is the good trade-off between the system throughput and data rate fairness among users. M-LDWF is an inefficient scheduler at overloaded considerations but supports considerable system throughput and enables an acceptable level of fairness [84].

5.5 Scenario

5.5.1 Physical Scenario

The UMi test scenario is composed by nineteen small cells with frequency reuse pattern three (k = 3), as presented in Figure 5.2. This scenario deployment is an outdoor environment with high density of users and traffic loads, where the antennas of the BSs and UEs are well below the rooftops.
Results have been extracted at the central hexagonal-shaped cell, while interference is imposed by the remaining six cells, as shown in Figure 5.3. When users move to another cell,

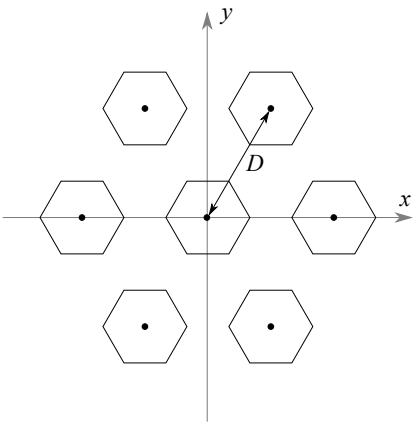

Figure 5.3: Simplified view of the UMi test scenario, where there is a tier of interference with the same subchannels in each node.

they suffer handover, and start using the subchannels from the frequency band available in the new cell. The inter-site distance, D, is the distance between two cells (one is the central one and others are in the first tier of interference) operating with the same set of subchannels, is equal to $D = \sqrt{3k}R$, where R is the cell radius [179].

5.5.2 Urban Micro line-of-sight

We have considered the UMi scenario in LoS, and the deterministic DS-PLM from [16]. Equation 5.5 presents the path loss, PL, between the BS, at the cell center, and UEs located up to the breakpoint distance, as shown in Figure 5.1b

$$PL_a(x) = 22.0\log_{10}(d) + 28.0 + 20\log_{10}(f_c), \quad (5.5)$$

where d is the distance between the BS and the receiver, in meters, and f_c is the frequency, given in GHz. For distances longer than the breakpoint distance, the PL is calculated by equation 5.6

$$\begin{aligned} PL_b(x) = {} & 40.0\log_{10}(d) + 7.8 - 18\log_{10}(h_{BS} - 1.0) \\ & - 18\log_{10}(h_{UE} - 1.0) + 2\log_{10}(f_c), \end{aligned} \quad (5.6)$$

where h_{BS} and h_{UE} are the antenna heights for the BSs and UEs, respectively. The BS and UE antennas are outdoor and located below the rooftops of the surrounding buildings. The

breakpoint distance, d'_{BP}, is computed as follows

$$d'_{BP} = \frac{4(h_{BS} - 1.0)(h_{UE} - 1.0)f_c}{c_v}, \quad (5.7)$$

where c_v is the velocity of the radio frequency signal in free space (equal to the speed of light), generally accepted to be approximately 3×10^8 m/s.

5.5.3 Radio and Simulation Parameters

This work compares the 4G radio coverage and frequency reuse trade-off of the 2.6 GHz, 3.5 GHz, and 5.62 GHz frequency bands. The bandwidth available per tier is 20 MHz, i.e., 60 MHz bandwidth in total, as reuse pattern three is considered. Figure 5.3 presents the cell of interest and six cells from first tier of interference. Different frequencies are represented by different colors in Figure 5.2. The height of small cell BS is 10 meters while the height of UEs is 1.5 meters. R varies from 20 m up to 1000 m. The top part of Table 5.1 presents the values of the radio parameters.

Table 5.1: Radio and Simulation Parameters.

Parameters	Frequency Bands		
	2.6 GHz	3.5 GHz	5.62 GHz
Transmitter power [dBm]	40	42.2478	46.6953
Number of BSs	19		
Reuse pattern	3		
Bandwidth per tier [MHz]	20		
Effective BS height [m]	10		
Effective UE height [m]	1.5		
R [m]	[20, 1000]		
Application	Video		
Bit rate [Mb/s]	3.1		
Simulation duration [s]	46		
Flows duration [s]	40		
Number of simulations	100		

More simulation parameters need to be considered to evaluate radio network performance, as presented at the bottom part of Table 5.1. The considered application is video with a bit rate of 3.1 Mb/s [88]. The simulated time is 46 seconds and video flows have a duration of 40 seconds. In order to obtain statistical significance for the results, each combination of the parameters was simulated one hundred times.

Improvements in LTE-Sim were made to account for the UMi scenario. The version of the simulator considered in this work includes not only the improvements specifically implemented for this work but also previous improvements, which are freely available under the GPLv3 license in [190].

The improvements involved to upgrade the bandwidth manager class in the code of the simulator (to accommodate the 3.5 GHz and 5.62 GHz frequency bands for the DL and uplink).

The class that defines the location of the cells has also been updated to consider frequency reuse three, as shown in Figure 5.2.

5.6 Cellular Planning Trade-Off

The carrier-to-interference ratio (C/I) and SINR are considered in the cellular planning in the DL while assuming orthogonal frequency division multiplexing with static allocation scheme. The adoption of dynamic MCSs involves that each MCS entails a minimum SINR. Coverage and frequency reuse optimization is required to optimize the radio and network planning trade-off.

5.6.1 Carrier-to-interference Ratio Formulation

C/I comprises a formulation with exact values of the interference from the BS of the first, second and third tiers of co-channel cells (interfering nodes) into the UEs, that can be expressed as shown equations 5.8, 5.9, 5.10. In these equations, the exact position of each interferer is considered in each tier of interference. In the DL, the C/I is given by the following equations, for the 1st, 2nd and 3rd rings of interference of the small cell network, respectively, for K = 3 [181],

$$\frac{C}{I}_{1\text{st}} = \frac{R^{-\gamma}}{2(D+0.66394R)^{-\gamma} + 2(D-0.31395R)^{-\gamma} + (D+R)^{-\gamma} + (D-R)^{-\gamma}}, \quad (5.8)$$

$$\frac{C}{I}_{2\text{nd}} = \frac{R^{-\gamma}}{2\left(\sqrt{3}D+0.88915R\right)^{-\gamma} + 2\left(\sqrt{3}D+0.8591R\right)^{-\gamma} + 2\left(\sqrt{3}D-0.84799R\right)^{-\gamma}}, \quad (5.9)$$

$$\frac{C}{I}_{3\text{rd}} = \frac{R^{-\gamma}}{2(2D+0.55802R)^{-\gamma} + 2(2D+0.47727R)^{-\gamma} + (2D+R)^{-\gamma} + (2D-R)^{-\gamma}}. \quad (5.10)$$

To consider the first tier of interference nodes is a valid approximation, since the interference obtained from the second and third tiers, is minimal compared to the preceding tiers. N.B.: in equations 5.8, 5.9, 5.10, one is not representing different propagation exponents, although different distances are considered for R and D, and different exponents may then be applied in the real computations.

5.6.2 Exponential Effective SINR Mapping

Figure 5.4 presents high resolution results for the EESM considering the cell radii of 100 m and 500 m. Figures 5.4a, 5.4b, 5.4c present results for the cell radius of 100 m, for the three frequency bands. Short cell radius implies low values for the EESM, specially near the cell edge. These happens since the interference imposed by the interfering neighboring cells is too high.

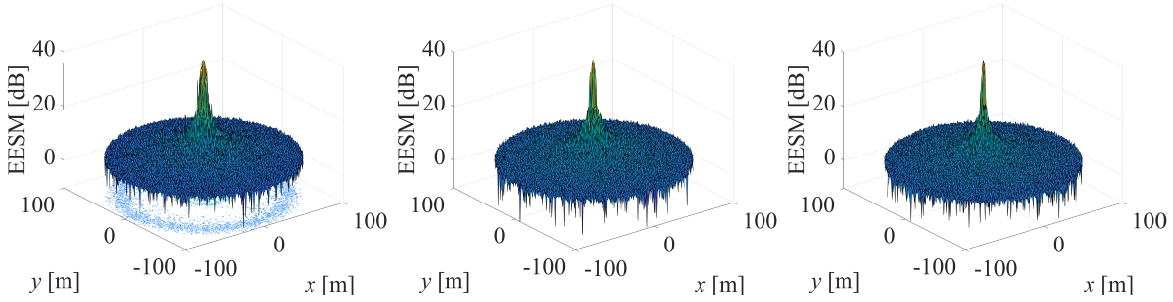

(a) 2.6 GHz, R = 100 m (b) 3.5 GHz, R = 100 m (c) 5.62 GHz, R = 100 m

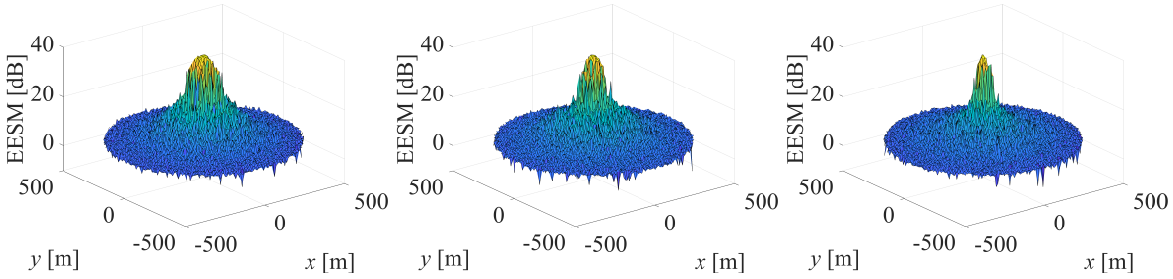

(d) 2.6 GHz, R = 500 m (e) 3.5 GHz, R = 500 m (f) 5.62 GHz, R = 500 m

Figure 5.4: EESM for cell radii of 100 m and 500 m.

Figure 5.4a presents results for the lowest considered frequency, i.e., 2.6 GHz, where there is a slight advantage compared to the other two frequency bands. In the 2.6 GHz band, the highest values of EESM occur for a broader zone of the total area of the cell, compared to the other two bands, and then in the 3.5 GHz frequency band, compared to the 5.62 GHz band, as shown in Figure 5.4b. When the cell radius varies from 100 m to 500 m Figures 5.4d, 5.4e, 5.4f, there is a clear enhancement EESM, which achieves the highest values in a broader central zone of the cell. The increase in frequency leads to a similar behavior in comparison with cells of 100 m.

Figure 5.5 presents results for the cumulative distribution function (CDF) of EESM for radii of 100 m and 500 m. For R = 100 m and an EESM up 8 dB the 2.6 GHz frequency band

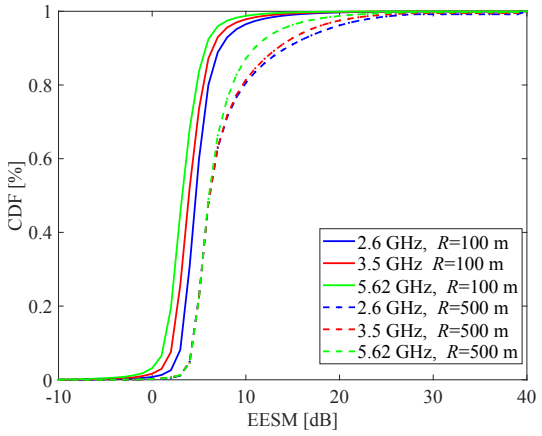

Figure 5.5: Comparison of CDF of the EESM between different frequency bands, for cell radii of 100 m and 500 m.

achieves 93%, for 3.5 GHz 95% and for 5.62 GHz 97%. By considering R = 500 m, EESM

equal to 8 dB is used in 72% of the cell area for the 2.6 GHz and 3.5 GHz frequency bands, while the corresponding area is 76% for cells operating at the 5.62 GHz band.

5.6.3 Achievable Modulation and Coding Scheme

UEs determine the CQI from the value of EESM from the received transmission. After the determination of the CQI, the UE sends its value to the cell node via a feedback channel with the adjustable delay. With this received channel quality information, the cell node can determine the MCS, and translate it to the transport block size (TBS), with the adequate procedure [108]. The MAC sublayer determines the payload for the physical layer. This payload is the TBS and quantifies the number of bits to be transferred in the ongoing TTI (1 ms). The TBS table available from [191] provides the size of data to be transmitted to the UE. Figure 5.6 presents the results of the CDF for the MCS for R = 100 m and 500 m. At 2.6 GHz

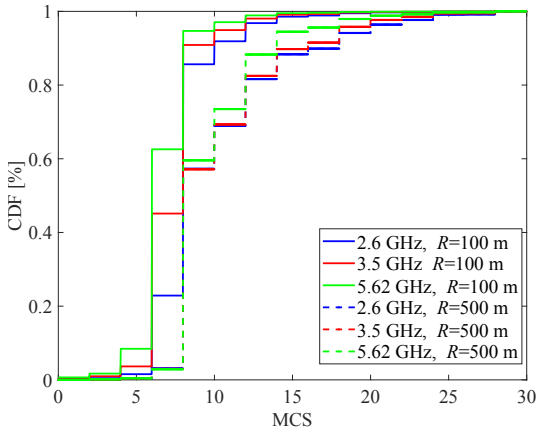

Figure 5.6: Comparison of the CDF of the MCSs among different frequency bands, for cell radii of 100 m and 500 m.

for R = 100 m, a MCSs lower than 10 is achieved in 86% of the cells, while in the 3.5 GHz and 5.62 GHz frequency bands it is achieved for 90% and 95%, respectively.
When R = 500 m, the values of the MCSs are identical for the 2.6 GHz and 3.5 GHz frequency bands. In these bands, 69% of the cell uses a MCS lower than 12, whereas, for the 5.62 GHz frequency band, 73% of the cell users achieve a MCS lower than 12.

5.6.4 Frequency Reuse Trade-off

Figures 5.7a and 5.7b present the variation of the SINR along with the distance d [181], from the cell center to the UE, for cell coverage radius of R = 100 m and R = 500 m, where distances follows $0 \leq d \leq R$.
The behavior of the SINR curve is similar for all curve frequency bands. A minor inflection point is observed at the breakpoint distance. The breakpoint distance is calculated by considering equation 5.7. Values of the breakpoint distance are presented in Table 5.2.
The 2.6 GHz frequency band shows the highest SINR. Due to the highest path loss between the small evolved NodeB (eNB) and UEs when C/I is lower, the resulting SINR is lower. In practice, this effect is more evident near the cell edge, because, overall, the chance of having

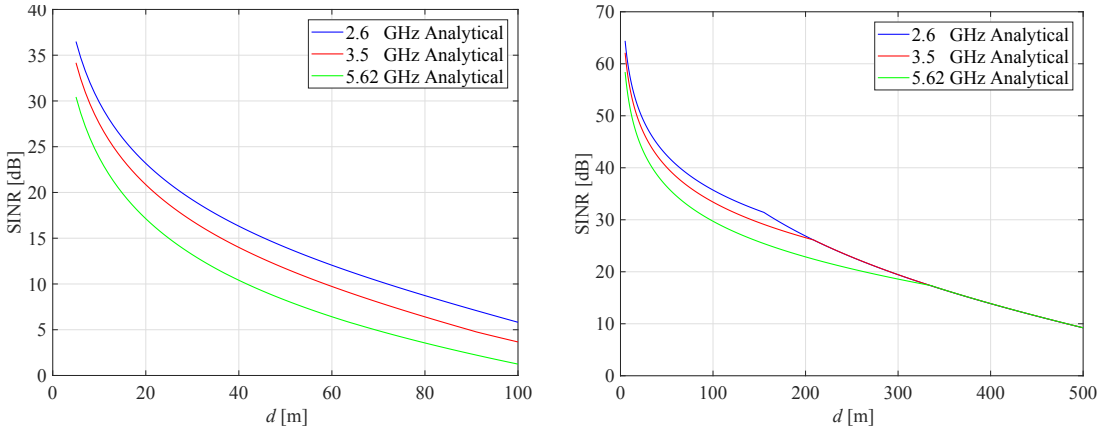

(a) d = 100 m (b) d = 500 m

Figure 5.7: Comparison of the SINR among 2.6, 3.5 and 5.62 GHz frequency bands.

Table 5.2: Values of the breakpoint distance for different frequency bands.

	Frequency Bands		
	2.6 GHz	3.5 GHz	5.62 GHz
$d_{BP}^{'}$	156 m	210 m	337.2 m

NLoS at long distances is higher. The propagation exponent is γ = 2.2 for the shortest d, corresponding to a considerably lower SINR, as shown in Figure 5.7a and Figure 5.7b.

5.6.5 Supported Cell Throughput

The supported cell throughput can be used as measure to predict the system capacity [181]. By considering the implicit function formulation from [181], the supported cell throughput is computed by weighting the physical throughput at each coverage ring by the size of the crown, as follows

$$R_{b\_sup} = \sum_{i=1}^{n} \frac{R_{b_i}(d_i^2 - d_{i-1}^2)}{R^2}, \quad (5.11)$$

where R_{b_i} is the physical throughput for the MCS that corresponds to the i^{th} ring. Results are presented in Figure 5.8, where the mapping with the average SINR [181] is also presented. Results for the supported throughput as a function of R are presented in Figure 5.8, where the mapping with the average SINR [180] is also presented.
For the considered frequency bands and cell radii shorter than 1000 m, values of the supported throughput per cell, R_{b_sup}, are similar among the bands for R_s up to circa $d_{BP}^{'}/r_{cc}$, where r_{cc} is the reuse factor (for example at 2.6 GHz, $d_{BP}^{'}$ = 156 m, then R = 52 m for k = 3, and $r_{cc} = \sqrt{3k} = 3$). For Rs shorter than this value the propagation exponent for interference is γ = 2.2. Only for $D = r_{cc} \times R$ beyond $d_{BP}^{'}$ the propagation exponent becomes γ = 4, and system capacity benefits from the highest power decay. Then, it increases faster for the lowest frequency bands but achieves a similar maximum value. For Rs up to circa 850 m, even though lower values of the supported throughput occur at 5.62 GHz, one can perceive

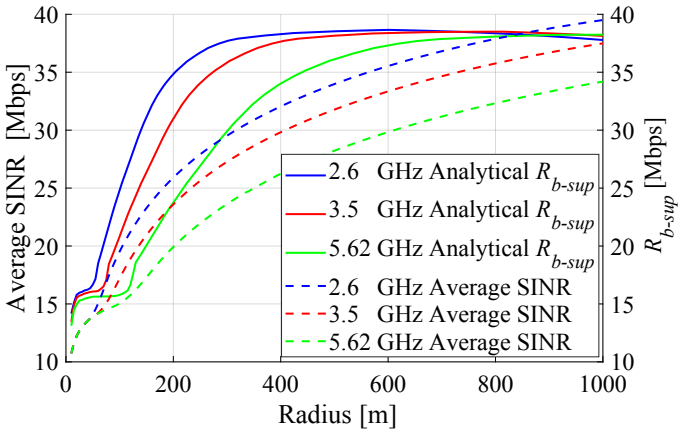

Figure 5.8: Mapping between the average SINR and equivalent supported throughput for the 2.6, 3.5 and 5.62 GHz frequency bands, for values of cell radius up to 1000 m.

that, when the system turns to be noise limited (not interference limited anymore) the supported throughput at 5.62 GHz becomes higher than the ones at 2.6 GHz and 3.5 GHz (for Rs of circa 840 m and 880 m, respectively). After achieving its maximum value, the supported throughput decreases at 600 m, 820 m or 1040 m (although the latter results is not shown in the view graph), for 2.6 GHz, 3.5 GHz and 5.62 GHz, respectively.

5.7 Simulation Results at the Saturation Level

Results for system capacity are determined at a saturation level, corresponding to PLR $< 2\%$ (and maximum delay less than the 150 ms target), according to 3GPP TS 22.105 [97]. The packet loss ratio (PLR) is the ratio between the total number of packets that do not reach their destination and the total transmitted packets. Above this 2% target, the user's service quality (mapped into the quality of experience) decays. The network topology considered in this work and presented in Figure 5.2 comprises a set of small cell nodes and UEs. UEs are uniformly assumed to be distributed in the central cell, according to the assumptions from [102].

5.7.1 Simulation Method

The bit rate of the considered video trace is 3.1 Mb/s. By considering the mathematical modeling available in the literature, and results for the EESM and MCS from Figure 5.5 and Figure 5.6, we have adopted the following approach in the simulations. Simulations have been run for different values of R and frequency band, by initially considering only one user. Simulations runs have been performed 100 times. First, we have extracted values for the average PLR. If the average PLR did not surpass the 2% target, we would add one more user and perform new 100 simulation runs for each R, and frequency band. Then, users kept being added up to the PLR surpassed the 2% target. A 95% confidence interval has been considered.

5.7.2 Packet Loss Ratio

Figures 5.9, 5.10, 5.11 present results for the average PLR as a function of R, with the number of users as a parameter by considering the above mentioned simulation method. Fig-

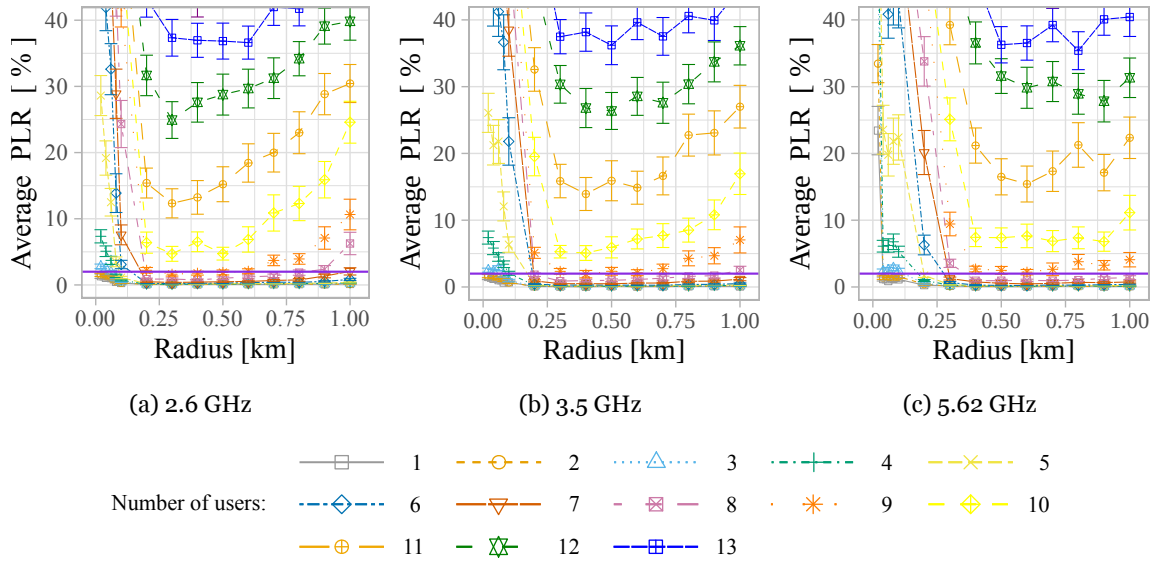

(a) 2.6 GHz (b) 3.5 GHz (c) 5.62 GHz

Figure 5.9: Results for the average PLR as a function of the cell radius with the number of users as a parameter, for the different frequency bands for the PF scheduler and 3.1 Mb/s video trace.

ures 5.9a, 5.9b, 5.9c show the impact of the breakpoint distance for all frequency bands, the number of users varied from one up to fifteen users. For values of R, shorter than the breakpoint distance, the PLR presents the worst results. In fact, the PLR is considerably high when short values of R are considered.

Results are presented in Figure 5.10 for the M-LWDF scheduler. With the M-LWDF, the

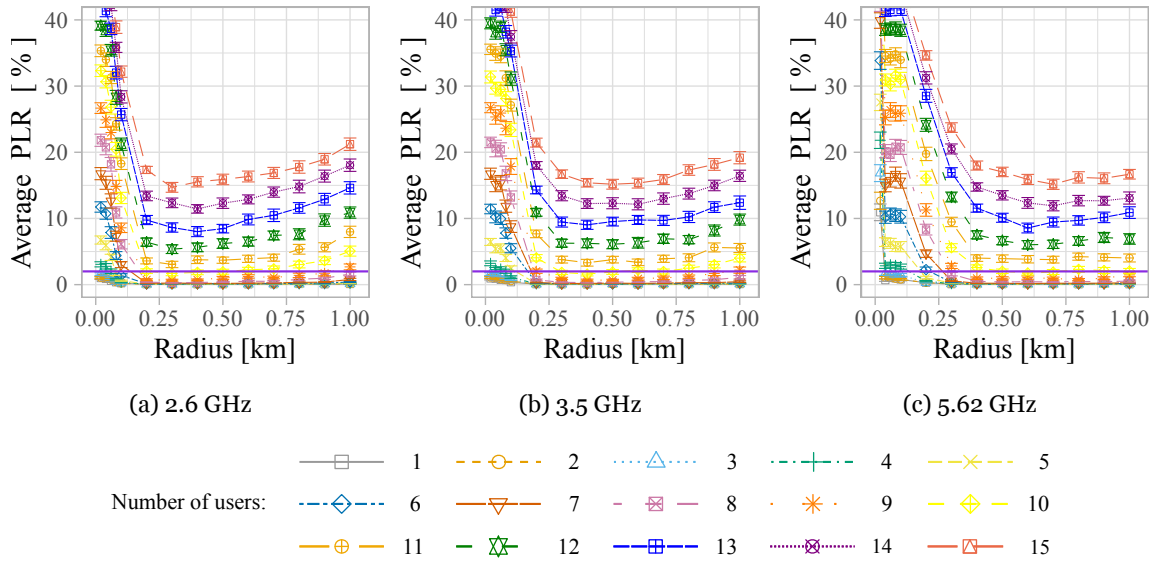

(a) 2.6 GHz (b) 3.5 GHz (c) 5.62 GHz

Figure 5.10: Results for the average PLR as a function of the cell radius with the number of users as a parameter, for the different frequency bands for the M-LWDF scheduler and 3.1 Mb/s video trace.

breakpoint distance has the same impact. For Rs shorter than d'_{BP}/rcc (rcc = 3) in the

present study, the average PLR is considerably higher than for Rs longer than the breakpoint distance. It is worthwhile to note that for the same number of supported users, the M-LWDF clearly presents lower values for the average PLR. As introduced in Section 5.3, the behavior of having much larger values of the PLR for $R \leqq d'_{BP}/rcc$ was expected, since somehow the two-slope behavior penalizes the shortest cell radius.
Another way to analyze the behavior of the average PLR is to present results as a function of the number of users, with the cell radius as a parameter, as shown in Figure 5.11. As such

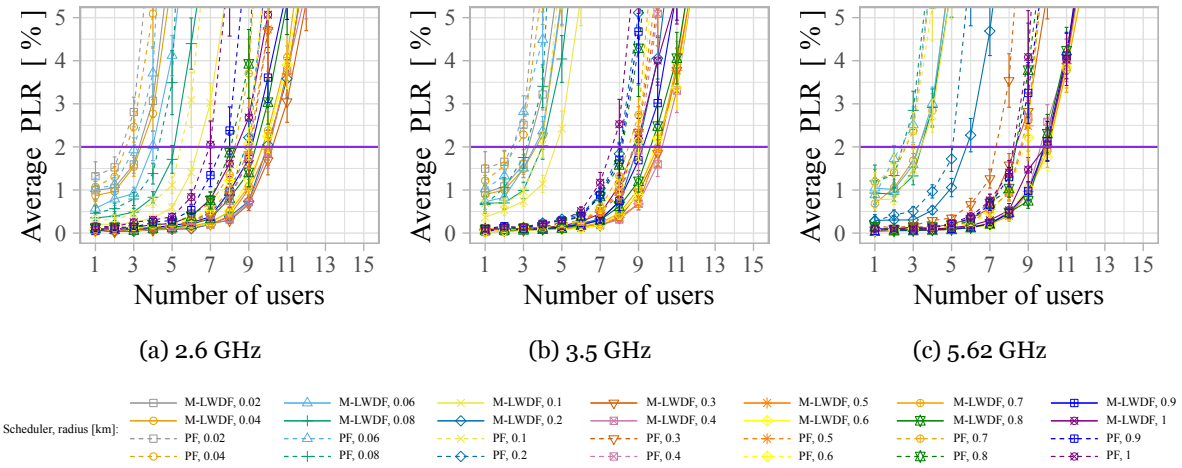

Figure 5.11: Results for the average PLR as a function of the number of users with the cell radius as a parameter, for the different frequency bands for the PF and M-LWDF schedulers and 3.1 Mb/s video trace.

the impact of considering more users is better visualized, as shown in Figures 5.11a, 5.11b, 5.11c. For longer values of the cell radius (corresponding to more supported users), when the number of users increases beyond a giver number of users (typically for more than six users), the PLR starts to increase exponentially. For the shortest Rs, the PLR starts increasing exponentially for few users.

5.7.3 Maximum Number of Supported Users

We have obtained the number of supported users for a PLR $< 2\%$, as presented in Figure 5.12. For both schedulers, the maximum number of supported users was obtained for values of R longer than the breakpoint distance. From Rs equal 20 m up to 80 m, the 2.6 GHz and 3.5 GHz frequency bands support the same number of users. For $80 \leq R \leq 250$ m, the best performance occurs for the 2.6 GHz frequency band. Between $250 \leq R \leq 500$ m, the 2.6 GHz and 3.5 GHz frequency bands support the same number of users. For the remaining, Rs the 5.62 GHz band presents the best performance. In some cases, the maximum number of users is supported for more values of R. For 3.5 GHz, this behavior occurred for four values of R, and three/two times for the 2.6 and 5.62 GHz frequency bands, respectively.

5.7.4 Maximum Average Goodput

After determining the maximum number of supported users considering the PLR target of 2%, it is possible to extract the maximum average goodput for all the considered frequency

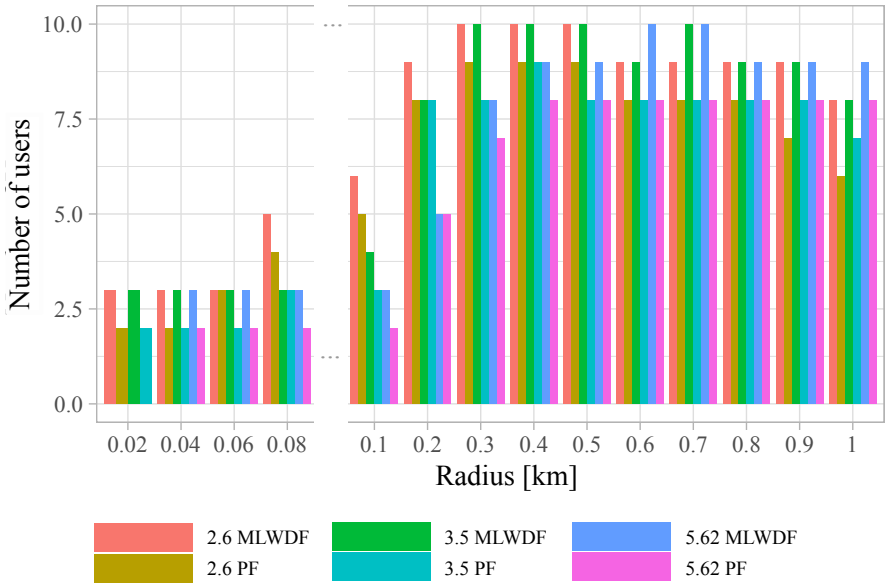

Figure 5.12: Maximum number of supported users as a function of the cells radius for different frequency bands.

bands, as shown in Figure 5.13 (example for the M-LWDF scheduler). For the considered

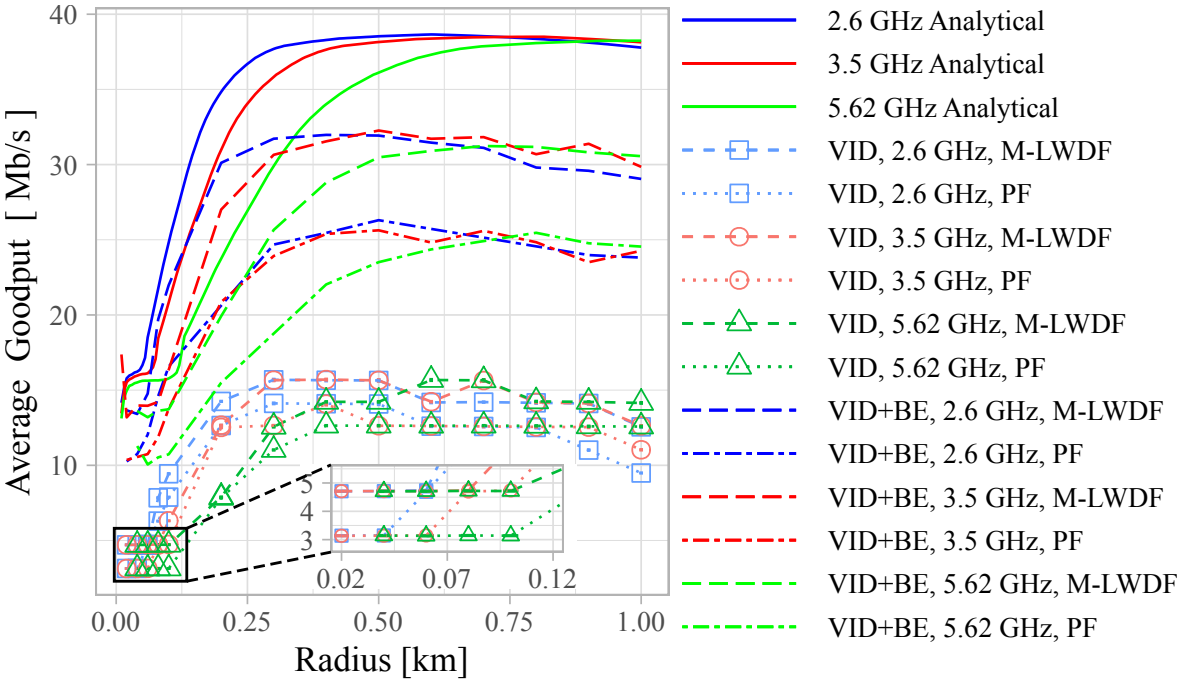

Figure 5.13: Schedulers, Maximum Average Goodput, with a video (VID) trace 3.1 Mb/s and BE.

video (VID) application, the maximum obtained average goodput was $\approx$ 15.7 Mb/s. The maximum average goodput for the 2.6 GHz frequency band occurs for cell radii in the range from 300 m up to 500 m. At 3.5 GHz, the same behavior is observed but the approximate maximum is obtained between 300 and 700 m. At 5.62 GHz, the maximum for the average goodput occurs for Rs between 600 m and 700 m.

Average goodput results for the PF scheduler from Figure 5.13 are slightly lower than the ones obtained with the M-LWDF scheduler. The maximum average goodput for the frequency

band of 2.6 GHz also occurs for 300 $\leq R \leq$ 500 m. However, for the 3.5 GHz frequency band, the maximum average goodput only occurs at R = 400 m. On the other hand, the maximum average goodput in the 5.62 GHz frequency band becomes constant for values of the cell radius longer than 300 m. Because the system becomes noise limited for the longest cell radii, a common behavior for both schedulers and frequency bands (the only exception is for the M-LWDF scheduler and the 5.62 GHz frequency band) is the decrease of the average goodput after its maximum is achieved. This occurs for $R >$ 900 m (longest Rs for higher frequencies). The highest maximum average goodput is achieved for a broader range of Rs in the 3.5 GHz frequency band. In this simulation results the 95% confidence interval does not exceed 0.2% of the represented value.
The maximum analytical supported throughput presented in Section 5.6.5 is also presented in Figure 5.13 for comparison purposes. By only considering the video application with an average bit rate of 3.1 Mb/s one achieves values much lower than the supported throughput. However, it is a worth noting that the overall behavior of the curves is similar. The rational behind this behavior is the inability of this video application to use all the resources for the PLR $<$ 2% service quality goal.
To make use of the resources that may be still available, one has considered that, apart from watching video, users also consume BE applications. The BE application is modeled as an ideal greedy source that always has packets to send, it only transmits packets when there are available resources to send them [102].
The lines identified with "VOI+BE" in the view chart from Figure 5.13 present the sum of the goodput of the video flows plus the goodput of the BE flows. The condition PLR $<$ 2% is verified by observing the curves, one can conclude that the above trend for the curves along the cell size is similar. Furthermore, M-LWDF scheduler presents better performance than the PF scheduler. With the addition of the BE flows, results closer to the analytical supported throughput are achieved. The difference is justified by the use of SINR instead of EESM in the analytical modeling.

5.7.5 Delay

Figure 5.14 and Figure 5.15 present the achieved maximum delays for the PF and M-LWDF schedulers, respectively, while considering 2.6, 3.5 and 5.62 GHz frequency bands, and PLR $<$ 2%. The ITU-T limit of 150 ms for the maximum delay was never achieved [192], [193]. The maximum average delay of 32 ms occurs for the 3.5 GHz frequency band for R = 300 m and ten supported users.

5.8 Behavior Beyond the Saturation Level

In [131], [133], the user quality of experience was determined by considering the mean opinion score (MOS). To better understand the system behavior, results for the average goodput beyond the PLR target of 2%, i.e., saturation level, are also presented in this work. Figure 5.16 presents results when the PF scheduler is considered. It is possible to observe that the average goodput does not increase linearly after the saturation level. After the turning point for

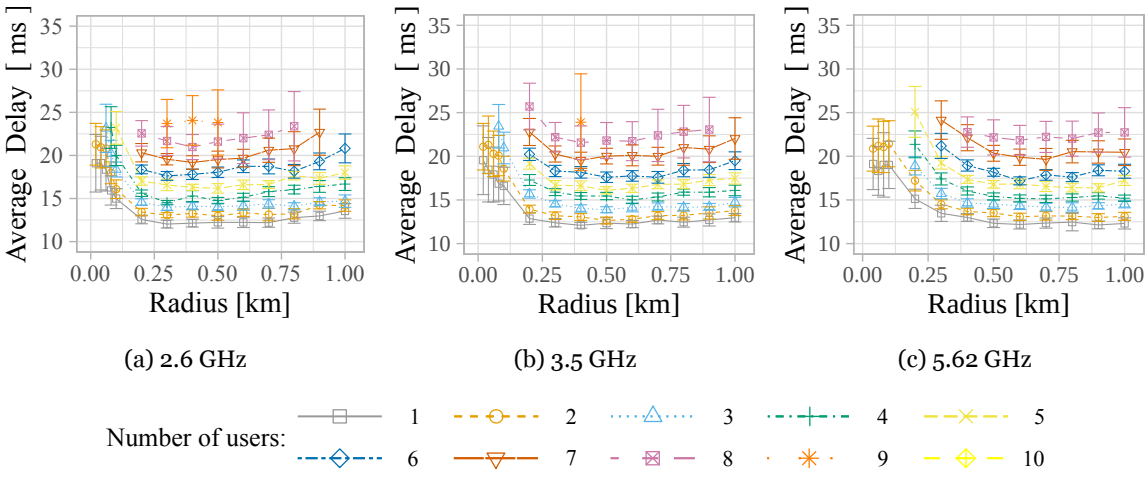

Figure 5.14: PF scheduler Maximum Average Delay, with a video trace of 3.1 Mb/s.

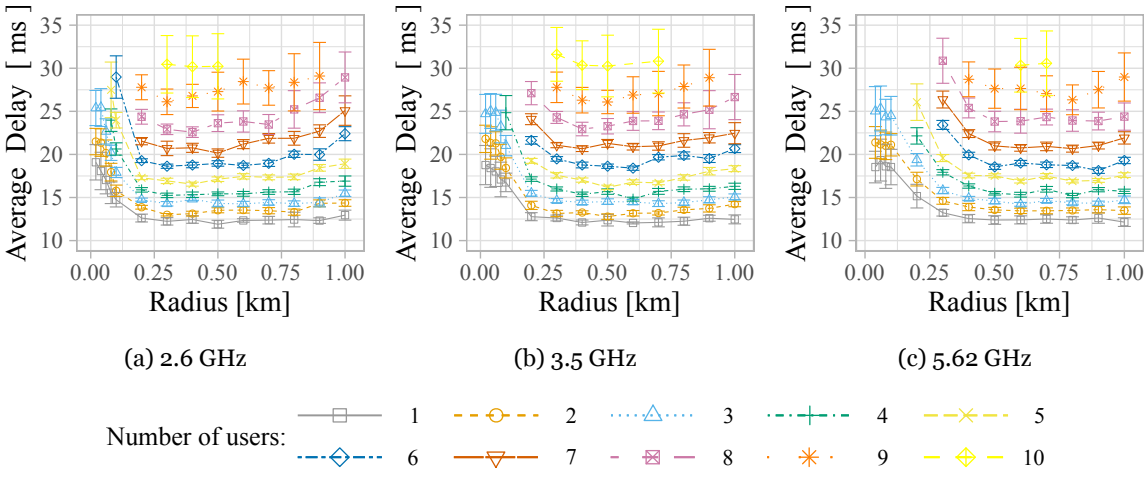

Figure 5.15: M-LWDF scheduler Maximum Average Delay, with a video trace of 3.1 Mb/s.

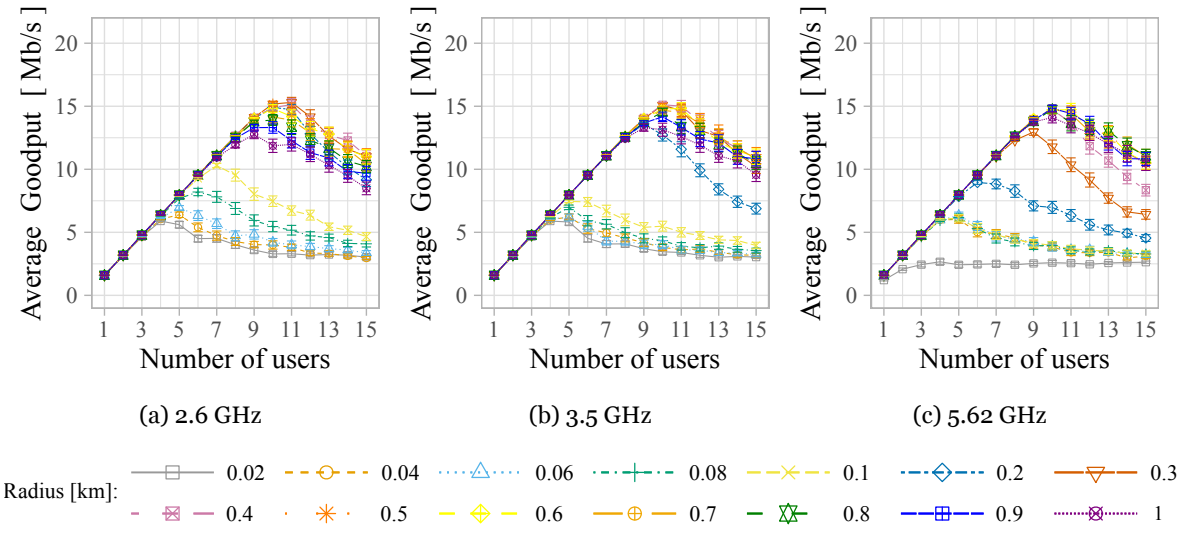

Figure 5.16: PF scheduler Average Goodput, with a video trace of 3.1 Mb/s.

the number of users, the slope of the average goodput decays, as shown in Figure 5.16. The same behavior occurs for all the considered frequency bands, and achieves a maximum of ≈ 15 Mb/s (≈ 15.7 Mb/s the 5.62 GHz frequency band).
Figure 5.17 presents results for the average goodput for the M-LWDF scheduler. It is ob-

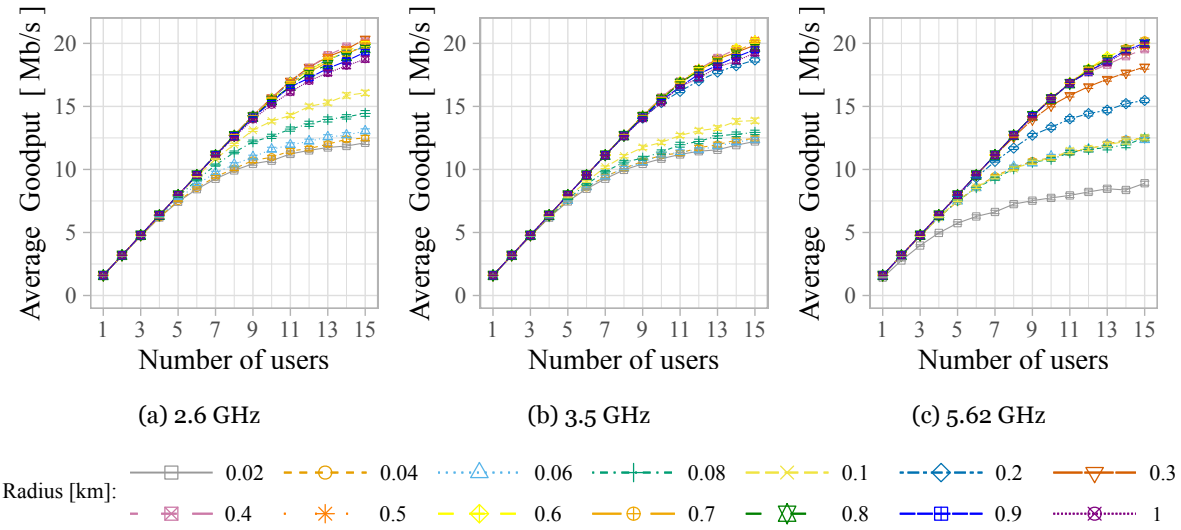

Figure 5.17: M-LWDF scheduler Average Goodput, with a video trace of 3.1 Mb/s.

served that as shown in Figures 5.17a, 5.17b, 5.17c, while the the average goodput increases with a constant slope up to the maximum achievable capacity (corresponding to the PLR target of 2%). After this turning point, it presents a decreasing slope for the three frequency bands (and up to 15 users). In this case, the maximum goodput is ≈ 20 Mb/s. Although results for the average delay are not presented here, overall, in the simulations, with the PF scheduler, we have obtained maximum values of around 230 ms for the delay. On the other hand, the maximum delay is around 53 ms for the M-LWDF scheduler.

5.9 Summary and Conclusions

This Chapter investigated the sub-6 GHz urban micro cellular (UMi) outdoor scenario by considering a dual-slope path loss model (DS-PLM). The benefits of considering the DS-PLMs to better capture the behavior of the propagation losses along the distance over the single-slope path loss models (SS-PLM) are discussed.
From the analytical study, we have concluded that, even though lower values of the supported throughput occur at 5.62 GHz for cell radius up to circa 850 m, one can perceive that, when the system turns to be noise limited (not interference limited anymore), the supported throughput in theoretical terms at 5.62 GHz becomes higher than the ones at 2.6 GHz and 3.5 GHz (for Rs of circa 840 m and 880 m, respectively). Results for the exponential effective SINR mapping (EESM) at the 2.6 GHz are better for a wider cell area than results for the other frequency bands for the same values of Rs. By considering system level simulations, values for the packet loss ratio (PLR), goodput, and average delay as a function of the number of users were obtained. To determine the maximum performance of the radio network for PLR $<$ 2%, we have considered video flows with a bit rate of 3.1 Mb/s. The number of supported

users was determined for the video application. The proportional fair, PF, and the modified largest weighted delay first, M-LWDF, were assumed.
Values obtained for the PLR adhere to the lessons learned in the analytical study. First, for R shorter than the breakpoint distance, when R decreases the PLR increases exponentially. Second, for Rs longer than the breakpoint distance and up to 1000 m, the PLR first increases and then decreases. For both schedulers, the M-LWDF scheduler allows for obtaining the highest goodput, which occurs at 2.6 and 3.5 GHz for $300 \leq R \leq 500$ m, while for the longest Rs the highest goodput occurs at 5.62 GHz. N.B.: Although M-LWDF scheduler presents the best performance than the PF in few cases the PF scheduler matches the M-LWDF performance.
The maximum number of supported users is 10 for $300 \leq R\text{s} \leq 700$ m and all frequency bands. The maximum average goodput obtained was $\approx$ 15.7 Mb/s (at 5.62 GHz).
As the achieved values for the goodput (with video only) are much lower than the analytical supported throughput, in a new set of simulations, one has considered that simultaneous usage of video and best effort (BE) applications, while using resources that are still available. It is observed that, with the addition of BE flows, results closer to the analytical supported throughput are achieved when the M-LWDF scheduler is considered. It is also a worth noting that, for PLR $< 2\%$ and $R \geq d'_{BP}$, delay first decreases and then increases. The maximum obtained average delay is 32 ms (at 3.5 GHz, R = 300 m and 10 UEs).
Results for the average goodput and delay for values of the number of users with PLR $\geq 2\%$ were also presented. It is possible to observe that although the average goodput increases with a constant slope up to turning point that corresponds to the saturation level, after this point, the slope of the the goodput curves decreases. While for the PF scheduler, we have obtained a maximum value for the delay around 230 ms, for the M-LWDF scheduler, the maximum delay is $\approx$ 53 ms. N.B.: No restriction on the values of the PLR is considered while extracting these values.
Suggestions for future work are two-fold: i) consider the EESM (and not only SINR) in the analysis of the supported throughput, and ii) consider 5G New Radio and the 5G-air-simulator [87] in the analysis.

Chapter 6

Conclusions and Topics for Future Research

6.1 Conclusions

If one truth is that Marconi's first transatlantic transmission in 1901 was a significant step toward advancing wireless telecommunications, the other most significant improvement has been to confine base station coverage to successively smaller areas. Martin Cooper suggested that the most significant improvement from 1950 to 2000 resulted from effectively confining individual conversations to smaller and smaller areas by spatial division of spectrum reuse. Shannon's Law also confirms that the best way to increase capacity is to shrink cells because short-range may improves the carrier-to-interference ratio while improving capacity and quality.

Connected devices outpaced the number of people on Earth in 2014. In 2016, approximately three decades after the invention of the mobile phone as we see it today, there were 7.6 billion connected devices. From these devices, 3.7 billion were unique subscribers. In December 2021 while the total world population was 7.8 billion people, there were 10.5 billion connected devices. From these, 5.3 were billion unique mobile subscribers.

Beyond our desire, we also need to have most of the data traffic laid on the Internet. Applications are also requiring higher and higher throughputs, and Cisco identifies video streaming as the application with the highest throughput requirement. In the future, ultra-high definition videos with virtual reality will require a significant long-term demand for bandwidth. In the longer-term forecast the consumer segment will have 74% of the total devices connected to the network. Machine-to-machine (M2M) nodes, the fastest-growing type of mobile device, will be half of the globally connected devices.

Network capacity improvements considering the Shannon-Hartley theorem can be made (in a simplified way) by densification, bandwidth, or spectral efficiency. A base station (BS) serves multiple users, so users share the bandwidth. If the density of users is high, each user is only to have a small portion of that bandwidth. Reducing the cell size, more BSs have to be deployed to cover the same area. Each BS is going to serve fewer users. Since each BS serves a few users, the bandwidth per user will increase. If this increase continues until we have one user per cell, the capacity increases linearly. With densification, the transmitter power is reduced, and the total energy consumption becomes insignificant. With this reduction, in terms of energy, only the processing power becomes relevant.

With the densification of the network, a new paradigm arises, the concept of ultra-dense networks (UDN). The goal behind UDN is to reduce the distance between access nodes and the users, which is only possible with the deployment of a massive number of small cells in areas where immense traffic is generated. As a consequence, it is expected that the macrocells will not continue to be extended in terms of capacity. Capacity extension is being done

by adding new low-power base stations in small cells overlaying to the existing macrocell network. These low-power nodes are named (from the largest connection capacity) as micro, pico, and femto base stations. A network with these low-power nodes and the macrocell nodes is called a multi-tier network or heterogeneous networks (HetNets). As, in each tier, there will be a collection of one type of node.

Macrocells, microcells, and picocells form outdoor mobile networks that need radio frequency planning, site selection, deployment, and maintenance (mainly by the operator). Nowadays, 80% of the traffic occurs indoors, and most cellular networks are composed of evolved NodeBs (eNBs). When high data rate indoor coverage is provided by outdoor eNBs, if high order modulation and coding schemes, e.g., 64/128/256 QAM, are used, the (external) walls from the buildings constitute an obstacle that is difficult to overcome, or is impassable, and create indoor areas with weak or none signal coverage. Another approach to increase system capacity is to adopt high frequencies. However, higher frequencies will lead to the same problem of considering high order modulation and encoding schemes as signal coverage will also be poor indoors. However, the microcellular solution does not solve all the identified issues since it does not eliminate the physical barriers between eNBs and destination nodes (usually known as user equipment, UE).

Efforts to achieve cells with small coverage areas lead to developing new type of cells, such as picocells or femtocells. Femtocell networks are unique since end-users usually deploy them indoors, with no planning. A home eNB (HeNB) is the hardware that provides radio signals within the femtocell, a small, inexpensive, and low-power indoor base station. The nature of the uncoordinated and disordered deployment of HeNBs is diverse from the existing network deployments. This kind of deployment may originate new and more complex interference problems in both down and uplinks.

In this thesis, Chapter 2 discussed femtocell deployments for a 3GPP dense indoor deployments. A modeling approach was followed where two types of topology were purposed, a dual stripe model and a 5x5 grid model. This work adopted the 3GPP 5x5 grid model. The studied indoor scenario comprises a building with one floor with a geometry of 5×5 apartment grid, with 25 apartments. A HeNB can be deployed in the center of every apartment.

A mathematical modeling approach was presented to get results for the average signal-to-interference-plus-noise ratio (SINR). In the UEs, the signal of interest is degraded by interfering signals from the co-channel nodes. In the analysis of the SINR we considered the deployment of 25 HeNBs with reuse pattern two. We obtained the average SINR as a function of the apartment side length and of the transmitter power. The apartment side length varied from 5 to 35 m, while the transmitter power varied from -20 to 30 dBm.

Since reuse pattern two has been considered, we identified three different cases for the first tier of interference as discussed in Section 2.3.1 and picketed in Figure 2.4. In the so-called first case, there are four neighboring interferes just touching the vertices of the cell, there are four adjacent co-channel cells causing interference (i.e., apartments just touching the vertices in the square that define the considered cell) as shown in Figure 2.4 close to their apartments. In the second case, there are only two neighboring interferes just touching the vertices of the cell. In the third case, there is only one apartment neighboring interfere. Results show that

for a grow apartment side length the increase of the transmitter power has impact in the average SINR. From the second to the third cases, as the number of interferes decreases, the average SINR considerably increases. However, while the apartment side length increases and the transmitter power decreases, the average SINR considerably degrades.

After determining the average SINR for deployments with 25 HeNBs, we considered the same topology but now with 4 HeNBs. For deployments with 4 HeNBs, the study of the average SINR has shown that, for longer apartment sides, the variation on the transmitter power has more impact on the average SINR than for shorter apartment side lengths. The study of the average SINR has shown that the smaller the radius is the higher the average SINR values are.

At the system level, the exponential effective SINR mapping (EESM) combines multiple SINR values from multiple subcarriers into an effective SINR function that represents channel conditions. Chapter 2 also presented a study of the EESM for the scenario with 25, 4, 5, and 6 HeNBs. For deployment ratio one, all 25 HeNBs will be active. For an urban-dense HeNB scenario, 3GPP suggests 0.2 for the deployment ratio. This corresponds to having 5 HeNBs deployed in 5x5 apartment floor. The topology with 4 HeNBs has a deployment ratio equal to 0.16 while the topology with 6 HeNBs has deployment ratio of 0.24. Aiming at obtaining results for the EESM, one adopted the use of LTE-Sim. LTE-Sim is an open-source framework used to simulate LTE-Advanced networks, whose reproducibility of the results is high. LTE-Sim was updated by us along the successive stages of this work and is freely available as open source code [129], [190].

For a 25 HeNBs deployment, results show that only in the areas closer to the HeNBs the EESM achieves the maximum value. Closer to the walls, the EESM drops because of the interference imposed by the neighbor interfering HeNBs. In the scenario with 4 HeNBs, the area covered by the higher EESM is more extensive than is the case with 5 HeNBs. Although the number of resources available with 6 HeNBs is higher than with 5 or 4 HeNBs, this scenario presents lower areas/zones where the EESM reaches the maximum value. By analyzing different scenarios, one concludes that increased transmitter power values correspond to expanded areas where the EESM achieves the maximum value of 40 dBm. With 4 HeNBs, the area with the lowest EESM is the same for any combination of apartment side length and transmitter power. This area corresponds to 5.76% of the total area. With 5 HeNBs, this area is 7.2%, while with 6 HeNBs the area with the lowest EESM is 10.4% of the total covered area.

By considering system level simulations with LTE-Sim, values for the packet loss ratio (PLR), goodput, and average delay as a function of the number of users were obtained. The considered applications is video (at 440 kb/s) and best effort (BE). We considered the proportional fair (PF), frame level scheduler (FLS), and exponential rule (EXPRule). These schedulers are channel sensitive, i.e., the UEs intermittently forward a channel quality indicator (CQI) report to the eNB. This CQI report presents the channel quality experienced by each UE and estimated by the scheduler. The packet scheduler in the BS assigns the radio resources to the UEs.

In this part of the work, first we considered a simulation scenario with four UEs per HeNB,

frequency reuse one, and 10 MHz bandwidth for the eNB and HeNBs. From the simulated results, we observe that the FLS presents better performance than the PF and EXPRule schedulers. The best performance occurs when the transmitter power is between 10 and 20 dBm for all the apartment sides.

Simulations were also performed for the same topology with frequency reuse two. In this case the eNB operates with a bandwidth of 20 MHz and frequency reuse one. HeNBs operate with 10 MHz bandwidth and frequency reuse two, and are the same frequency band for the eNB. One observed that the performance of the FLS is nearly identical when the frequency reuse is equal to one. When the frequency reuse pattern increases the average goodput for the BE flow considerably increases. This means that there are more available resources to transport more data. Since the average goodput with both reuse patterns is the same, we can conclude that it is possible to support more users in each HeNB. Values obtained for the PLR also show that, in fact, we are not closer to the 2% PLR target.

With reuse pattern two, we consider the 2% PLR target for video to obtain the maximum supported capacity for 25 HeNBs. The system was taken into saturation by equitably escalating the number of users (consuming video applications) in each HeNB. For apartment side lengths of 20, 15, and 10 m, the PF scheduler supports between seven and twelve users. EXPRule supports between eight and eleven users, while allows for FLS supporting between twelve and sixteen users for the PLR target 2%. For small apartment sizes, PF is a better option than the EXPRule scheduler. When larger apartment sizes are analyzed, the opposite is observed, and the EXPRule option prevails. The overall analysis shows that the FLS performs better than the other two packet schedulers for the considered applications. For the BE flow, it is straightforward to conclude that the behavior of all the packet schedulers is identical. The goodput varies only when the apartment side length also varies. The maximum average goodput for BE keeps the same behavior as that of the theoretical average SINR. Results show that the higher the maximum goodput for video is the lower the maximum goodput for BE is.

Chapter 4 addresses the possibility of deploying 4, 5, or 6 HeNBs to provide coverage to a 3GPP 5x5 apartment grid geometry. First, we analyzed a performance evaluation in a scenario with 4 HeNBs and each one of the HeNBs serving eight users. The three schedulers, PF, FLS, and EXPRule, obtain the same maximum average goodput. All present schedulers combinations of transmitter power and apartment side length were the average PLR is lower than 2%. This means that the system is possible to add more users and explore saturation conditions.

We have analyzed the system, when the 2% PLR target is achieved for the video application in the scenarios with a variable deployment ratio, i.e., with 4, 5, and 6 HeNBs while considering the FLS scheduler (N.B.: The 3GPP target for delay was never achieved in our simulations). By considering results from Chapter 2, we expect to support more users in 5x5 apartment floor with 4 HeNBs than with the other options. As the number is higher, the scenario with 6 HeNBs enables to achieve more supported users (114 UEs against 96 UEs with 4 HeNBs and 85 UEs with 5 HeNBs). Although 6 HeNBs get a lower EESM, the available HeNBs have more resources to support more traffic data. While with 6 HeNBs provide higher capacity, a

scenario with 4 HeNBs enables better coverage. For BE, the behavior for all scenarios is the same. 3GPP suggested a maximum of 5 HeNBs corresponding to a deployment ratio of 0.2. However, this deployment shows the worst performance compared to the other topologies.

The research at the indoor scenario goes further than the assumptions of 3GPP by considering an high-density deployment of HeNBs and users. This work also explored variations in the transmitter power of HeNBs and variation in the apartment floor topology dimensions. For indoor scenarios and video flows, it is essential to highlight that it is possible to operate the system without setting the HeNBs transmitter power to the maximum value. With this action, we will not compromise the overall system performance. If the transmitter power is set for lower values, this can be a step toward achieving greener mobile communication systems. The results for BE applications also show that it is possible to consider, in most cases, a reduction in the transmitter power. This reduction does not have a negative impact on system performance and can provide a reduction in energy consumption for both videos and BE flows.

Simulation results confirm the lessons learned from the theoretical and performance studies. With the considered indoor scenarios and simulation parameters, this work shows to future practitioners looking at deployment scenarios that the 3GPP appointed deployment ratio is not the optimal choice. In terms of coverage area with higher SINR or even in terms of capacity. Other deployment geometries probably could present a similar behavior to the considered in this work, where the maximum number of HeNBs suggested by 3GPP is not the best choice.

Although mobile communications traffic is shifting from outdoor to indoor environments, we must also address service quality in outdoor scenarios. Chapter 5 investigated the sub-6 GHz urban micro cellular (UMi) outdoor scenario by considering a dual-slope path loss model (DS-PLM). The benefits of considering the DS-PLMs to better capture the behavior of the propagation losses along the distances (over the single-slope path loss models, SS-PLM) is discussed.

From the analytical study, we have concluded that, even though lower values of the supported throughput occur at 5.62 GHz for cell radius up to circa 850 m, one can perceive that, when the system turns to be noise limited (not interference limited anymore), the supported throughput in theoretical terms at 5.62 GHz becomes higher than the ones at 2.6 GHz and 3.5 GHz (for cell radius, Rs, of circa 840 m and 880 m, respectively). Results for the EESM (obtained by simulation with LTE-Sim) at the 2.6 GHz are better for a wider cell area than results for the other frequency bands for the same values of cell radius, Rs.

To determine the maximum performance of the radio network for PLR $< 2\%$, we have considered video flows at a bit rate of 3.1 Mb/s. The number of supported users was determined for the video application. The proportional fair, PF, and the modified largest weighted delay first, M-LWDF, were assumed. The 3GPP target for delay was never overcame in these simulations.

Values obtained for the PLR adhere to the lessons learned from the analytical study. First, for R shorter than the breakpoint distance, when R decreases, the PLR increases exponentially. Second, for Rs longer than the breakpoint distance and up to 1000 m, the PLR first increases

and then decreases. For both schedulers, the M-LWDF scheduler allows obtaining the highest goodput, which occurs at 2.6 and 3.5 GHz for 300 $\leq R \leq$ 500 m, while for the longest Rs, the highest goodput occurs at 5.62 GHz. The maximum number of supported users is 10 for 300 $\leq R$s $\leq$ 700 m and for all frequency bands. In this 4G outdoor deployment, the maximum cell average goodput obtained was $\approx$ 15.7 Mb/s (at 5.62 GHz).

6.2 Recent Research Trends in Literature

Beyond the research from this thesis, the research community is studying femtocells in the last years, publishing works in topics such as power control, interference, energy and spectral efficiency, beamforming, resource allocation on resource sharing, network configuration, techniques to reduce delay, mmWave, UAVs scenarios and visible light communications (VLC). The evolution that leads us to the 5G cellular networks leverages the importance of small cells as small cells are gaining critical importance in fulfilling the requirements of 5G networks [20] and their evolution.

6.2.1 Power Control, Resource Allocation and Energy Efficiency

The non-orthogonal multiple access (NOMA) is a power-based multiple access technique in which multiple users combine at different power levels but at the same time or frequency or code [194]. This technique is being used for 5G networks to enhance the spectral efficiency of all networks. As in [194] the new power allocation scheme for downlink (DL) takes advantage of multiplexing cognitive radio (CR) with NOMA. For two femtocell users (FUEs) that are using the same channel, the stronger user is interfering with the weak user. An CR-NOMA is required to control the NOMA interference among the FUEs. The CR applied to NOMA provides a channel assignment at the femtocell networks to mitigate the co and cross-tier interference. This will result in an enhancement in the data rates of FUEs and also in the macrocell users (MUEs). They integrate also a joint channel allocation and power control with CR-NOMA at the femtocell layer.
The resource allocation for a single carrier (SC) is studied in [195]. It is considered that the macrocell shares spectrum with some femtocells, to protect the data rate of MUEs. To limit the interference over the assigned subcarriers, authors consider two different criteria. In the first criteria, the interference for each FUE to the macro base station is restricted. This applies to distributed network femtocells without a central processing unit. In the second, they confined the total interference for all FUEs at the macro base station. They required here a central processing unit with global channel information to perform the subcarrier and power allocation. These central units could not be desirable and different femtocells could implement a semi-distributed algorithm based. Authors obtained the optimal power and subcarrier allocation in the scenario with the first criteria. In a scenario with the second criteria, authors also get optimal power and subcarrier allocation.
Based on a theoretical analysis, authors from [196] proposed two distributed algorithms, which are suitable to the decentralized blockchain-based femtocell networks. Their aim is to guarantee the QoS requirements for the macro and FUEs based supported in power control.

The proposed power control scheme improved data transmission and guarantees the relay requirements, thus enhancing the QoS of the mobile communication based on the blockchain.

The hybrid access mode for femtocells is not ideal, but a compromise between the open or closed modes is studied in [11] to seek rate maximization. Based on a Stackelberg game, the authors proposed a mechanism to incentivize femtocells to adopt the hybrid mode. They proposed the incentive mechanism in order to solve the robust DL power control problem, formulated in a two-tier femtocell network. They base this on an economic return from the macro BS, the femto base stations decide whether is worth opening their resources. With the proposed mechanism the throughout the networks improved and well the outage probability of users was reduced.

In line with the previous work [11], a power control scheme in a two-tier femtocell is also proposed in [197]. They proposed a fuzzy logic system to infer and estimate the channel gain. Since the fuzzy logic system requires small computation, the channel state indicator (CSI) can be obtained on the communication, including transmitting, power and received-signal-strength-indicator (RSSI). The authors proposed an effective power control scheme to guarantee the performance of a two-tier network. When the communication environment change, using fuzzy inference the proposed fuzzy logic system, the power allocation can timely adjust according to the instantaneous CSI. The proposed scheme not only minimizes the power but also guarantees the QoS of each user.

In [198] is assumed that femtocells have cognitive radio capacity and that capacity are used to seek unused resource blocks (RB). In this work, they divided the optimization problem of resource allocation in RB allocation and power allocation, either focus on the power control. A proportional-integral controller for femtocell is proposed. The presented numerical results illustrate the convergence of the algorithm, as well as verify the advantages of the proposed scheme.

The trade-off between spectral efficiency (SE) and energy efficiency (EE) metrics of OFDMA based macro and femtocell networks was studied in [199]. When optimizing, either EE or SE does not signify that both are becoming optimized. As matter of fact, the optimum EE response may result in bad SE and also vice-versa. They express mathematically it an EE-SE trade-off multi empirical case, with the establishment of transmit power Pareto optimal set (POS) for constant BS density and the BS density POS for constant transmit power. By analytical and simulation results, they showed the significant rule for optimal transmit power and SINR threshold in the response of EE as a function of SE.

Authors from [200] proposed an energy-efficient resource allocation scheme for simultaneous wireless information and power transfer (SWIPT)-NOMA, based in FUEs. Authors considered FUEs present imperfect channel state information. They integrated the SWIPT and NOMA at the femto base station in the quest to improve energy efficiency and spectral efficiency of femtocells. They integrate SWIPT since it enhances the transmission power of Femto users. Integrating NOMA is made to improve the spectral efficiency. To increase the EE the NOMA and energy harvesting (EH) were integrated into the femtocell network, in order to increase the EE. The optimal value of power was determined using a Lagrangian dual decomposition. Mathematical analysis and simulations showed results of the effectiveness

of the proposed scheme showed it.
The question of what operation mode should a small cell use is discussed in [201]. The four addressed modes are the active, standby, sleep and off ones. The authors aim is to enhance the EE for hyper-dense small cell networks by designing a low-complexity sleep strategy for the BSs. In this work it is specified that the active standby and sleep modes are for serving the delay-intolerant, delay-sensitive, and rate-sensitive demands. They proposed it a low-complexity algorithm that serves to boost the EE of small cell networks by switching properly, the BSs into lower-energy operation modes. In one case, authors could boost the EE by 72% and 51%, while according to [201], 2.66 and 1.2 BS could be turned off. Also 2.7 BSs could operate in the sleeping mode, and 3.2 BSs could operate on standby.

6.2.2 Interference Mitigation and Hardware Implementation

To mitigate the interference in a two-tier femtocell in [202] is proposed, a power control scheme. They discussed how to allocate powers efficiently, this means guaranteeing the QoS requirements of MUEs while admitting as many FUEs as possible. To solve it, authors use a non-cooperative game theory, where they plan the interactions among MUEs and FUEs. After that a distributive iterative power update strategy to allocate the transmission power was developed. By simulation, authors showed that with the proposed scheme is possible to guarantee the UES required SINR while allowing as many FUEs as possible to share network resources.
Authors from [203], identify the interferer HeNB as a rogue-HeNB. These rogue HeNBs are a consequence of the ad hoc deployment of HeNBs since they are deployed uncoordinated or as an illegitimate HeNB. In [203] it is tried to locate these rogue-HeNBs by a two-dimensional map of the received SINR. They derive mathematical proof to justify that the existence of any femtocell interference. Then the method proposed was tested in two real-world experiments. These experiential results show with the proposed method that the estimation of the position is below one meter in the studied indoor environment.
The method proposed in [204] takes advantage of the availability of multiple subchannels to identify inter-femtocell interference. In an experimental scenario, authors make use of universal software radio peripherals (USRPs) that emulate 4G networks [205]. In conjunction with USRPs, the GNU radio software development toolkit that provides signal processing blocks to implement software radios is also used [206]. The implemented setup is a proposed and efficient method to identify inter-femtocell interference by analyzing the received patterns observed by mobile stations. With the setup and the proposed method, it was to show that the proposed interference identification method can successfully identify real interferes while excluding non-interfering femtocells from suspect femtocells. Results show an error probability of less than 0.2. The proposed method successfully identifies all real interferes and at least 94% of the non-interfering femtocells.
Authors from [207] proposed a scheme to jointly suppress the interference on the macrocell users, and preserve the high data rates required by femtocell users under a centralized radio access network. The contribution given is is to jointly mitigate cross-tier interference on the macrocell UE, and to ensure high data rates for the femtocell UE under the same allocated

power, time, and frequency resources. This results in a perspective of the femto base station and the macro base station are treated as joint transmitters serving macrocell UE. Results showed the superiority of the proposed scheme in achieving higher throughput compared to more conventional schemes.
Research in the interference for 5G is also being conducted as in [208], where it is proposed a joint resource allocation, interference minimization, user-level, and cell-level fairness. The proposed joint aims to get the maximum resource reuse in 5G heterogeneous small cell networks. The scenario considers macro, femto and pico base stations. To solve the planned resource allocation problem while minimizing interference, maximizing fairness, and resource reuse, they proposed three algorithms, a centralized, a distributed, and a randomized distributed. Results obtained by simulation show that the proposed algorithms show an increase in performance of 26% and 16% compared to the existing distributed random access and interfering model, respectively.
In 5G HetNets, the overall network needs to be improved to gain robustness and also reduce harmful interference. In [209], to improve the robustness of resource allocation and maximize the total interference efficiency is proposed a joint optimization of the transmitter power of the femto base station and a subcarrier allocation factor. Obtained simulation results show the effectiveness and superiority of the proposed scheme in terms of interference efficiency and with a reduction in the interference at the macro users.
The power optimization and interference management in 5G UDN are still critical issues [210]. In a two-tier micro-femtocell scenario, is proposed an allocation of femtocells that takes place inside the microcell based on user density. This means femtocells form groups according to the adjacency and the leader selection of each group. The aim of [210] is to purpose a game theory to provide a frequency allocation method, which will provide better SINR, spectral efficiency and effective resource utilization. The authors show through simulation, that in the proposed network and game theory, the power transmission decreases by 23%-41%, the SINR improves by 12%-39% and spectral efficiency by 10%-37% than the compared cellular network systems.
Authors from [211] studied the beamforming design problem for maximizing the minimum sum rate of all the FUEs in a multi-cell multiple-input single-output HetNet. The aim is to overcome the negative impact of hardware impairments on system performance. The optimization of the system is made taking into accounting the constraints of the maximum transmit power of each femto base station and the QoS of UE. Through simulation, authors verify that the purposed algorithm by them achieves a good trade-off between the transmission rate of the femtocells and the ability to overcome the hardware impairments.

6.2.3 Reduction of Delay, Scheduling, Adaptive Cell Selecting, UAVs and VLC

Caching content in femtocell networks is an attractive method for alleviating network congestion in 5G wireless networks [212]. In [212] are presented caching policies that can be deployed at femtocell networks with limited storage capacity to pursue the reduction of delay. Authors used real-world data-sets the NS-3 simulator, to show how the proposed caching policies reduce the delay as also retrieving content in femtocell networks reduce the delay in

femtocell networks. Results show that a 6% percent reduction in the average delay is obtained in the worst case.

A new algorithm based on radius reduction and a scheduling strategy is proposed in [213]. This algorithm aims to achieve a reduction in power consumption and interference while increasing fairness. In the first phase, a radius reduction of the femtocells is performed. The densely deployed femtocells cooperate in finding the most suitable power setting for the environment that surrounded it. In the second phase, the scheduling algorithm provides a resource block scheduling scheme that uses vacancy requests to improve resource sharing and service to users to meet their performance requirements. Authors have tested their algorithm by prototyping experiments and simulations, where they could confirm the benefits of their approach. They showed that the percentage of users who cannot meet their throughput requirements decrease, operating with lower transmission power and resulting in less interference to macrocell users.

Within 5G, the heterogeneous ultra-dense networks (HUDN) are an enabling technology comprising several types of small cells to enhance the performance of the network [214]. Authors in [214] propose a novel adaptive cell selection that adapts to various characteristics of HUDNs and vehicle movements. This adaptive cell selection shows up derived from the traditional technique for cell selection is inapplicable in HUDN. The proposed cell selection enhances the average achievable downlink data rates and spectral efficiency per vehicle by 3.98% and 2.79% compared with the traditional and the relevant recent schemes.

Unmanned Aerial Vehicle (UAV) is one interesting platform that is being equipped with femtocells as in [215]. They presented it as joint use of UAVs and femtocells to perform intelligent data sensing and geo-localization to identify off missing persons in natural disasters. The search for people dispersed in a post-earthquake scenario is made through an innovative algorithm for coupling mobile terminals. During the work, authors consider typical conditions of a real application scenario, the accuracy obtained was greater than 60% with an average error in estimating the position of about one meter.

The next step onto shrink BS is probably to adapt them to work with optical communications, as proposed in [216], [217]. The growing demand for increased transmission capacity and bandwidth together with 5G wireless systems has been opening up new opportunities for non-radio frequency (RF)-based wireless technologies. VLC technology is a potential candidate for access networking in 5G, which offers higher spectral efficiency than RF-based femtocell networks of three orders of magnitude [216]. The experimental results with VLC presented in [216] show data rates of 1 Gbps and 2 Gbps in the proposed scenarios. The study in [217] presents a high sensitivity optical receiver that does not require light concentrating optical devices and can tolerate angular variations up to 27°. This is a sign that the requirement of direct light between the access point and the terminal is in study to give up to be an issue.

6.3 Topics for Future Research Towards 5G Evolution

As discussed before, ITU releases the objectives of the new ITU standard to reduce greenhouse gas emissions 45% by 2030. To achieve this important goal for the world, new research works have to seek the reduction of energy consumption as one of the main priorities. Future works on the 5G are being made in the power control, interference, energy and spectral efficiency that is step forward. This research line can give a contribution toward more and better services while reducing energy consumption.

One key part of the 5G NR air interface is the frame format, clearly impacted by the numerology. Numerology varies form zero up to four, and is an indication of the subcarrier spacing. Higher numerology only can be applied to smaller cell sizes, as well as when the frequency increases. The research from this thesis, may be transposed to new simulators that consider 5G new radio, like the 5g-air-simulator, where the numerology can effectively be explored, an open opportunity to immediate research.

3GPP started work on 5G-Advanced in Release 18, which will certainly be a challenge for future research and development. By the end of June and early July of 2021, TSG radio access network started to define what will Release 18 be. The high-level objective was to gather company proposals in three areas: enhanced mobile broadBand (eMBB) driven work; non-eMBB driven functionality, and cross-functionality for both.

As suggested by 5G Infrastructure Public Private Partnership, PPP, in the coming decade, 6th generation mobile networks (6G) will bring a new era in which billions of things, humans, and connected vehicles, robots and drones will generate zettabytes of digital information. 6G will be dealing with more challenging applications, e.g., holographic together with 5G evolution framework, tele-presence and immersive communications, and meet far more stringent requirements. These use cases in future communication systems will certainly be a challenge for future research and development.

References

[1] D. Marconi, *My Father, Marconi*, 1st ed. McGraw-Hill Book Comapny, Inc., 1962. 1

[2] W. Webb, *Wireless communications: The future*. Wiley, 2007. 1, 5

[3] C. W. Paper, "Cisco Visual Networking Index: Global Mobile Data Traffic Forecast Update 2014–2019 White Paper," Cisco Systems, Inc., Tech. Rep., February 2015. [Online]. Available: http://www.cisco.com/c/en/us/solutions/collateral/service-provider/visual-networking-index-vni/white_paper_c11-520862.pdf 2, 4, 7

[4] Cisco, "Cisco Annual Internet Report (2018–2023) White Paper," Cisco Systems, Inc., Tech. Rep., March 2020. [Online]. Available: https://www.cisco.com/c/en/us/solutions/collateral/executive-perspectives/annual-internet-report/white-paper-c11-741490.pdf 2, 4, 7, 8, 97

[5] Y. Xu and S. Zhou, "On the Coverage and Capacity of Ultra-Dense Networks With Directional Transmissions," *IEEE Wireless Communications Letters*, vol. 9, no. 3, pp. 271–275, March 2020. 2, 97, 101

[6] I. Vilà, J. Pérez-Romero, O. Sallent, and A. Umbert, "Characterization of Radio Access Network Slicing Scenarios With 5G QoS Provisioning," *IEEE Access*, vol. 8, pp. 51 414–51 430, 2020. 2, 97, 98

[7] H. Munir, S. A. Hassan, H. Pervaiz, Q. Ni, and L. Musavian, "Resource Optimization in Multi-Tier HetNets Exploiting Multi-Slope Path Loss Model," *IEEE Access*, vol. 5, pp. 8714–8726, 2017. 2, 97, 102

[8] A. Ghosh, N. Mangalvedhe, R. Ratasuk, B. Mondal, M. Cudak, E. Visotsky, T. A. Thomas, J. G. Andrews, P. Xia, H. S. Jo, H. S. Dhillon, and T. D. Novlan, "Heterogeneous cellular networks: From theory to practice," *IEEE Communications Magazine*, vol. 50, no. 6, pp. 54–64, June 2012. 2, 97

[9] A. Damnjanovic, J. Montojo, Y. Wei, T. Ji, T. Luo, M. Vajapeyam, T. Yoo, O. Song, and D. Malladi, "A survey on 3GPP heterogeneous networks," *IEEE Wireless Communications*, vol. 18, no. 3, pp. 10–21, June 2011. 2, 97

[10] J. G. Andrews, H. Claussen, M. Dohler, S. Rangan, and M. C. Reed, "Femtocells: Past, Present, and Future," *IEEE Journal on Selected Areas in Communications*, vol. 30, no. 3, pp. 497–508, April 2012. 2, 3, 6, 9, 10, 25

[11] Z. Liu, W. Wang, K. Y. Chan, K. Ma, and X. Guan, "Rate Maximization for Hybrid Access Femtocell Networks With Outage Constraints Based on Pricing Incentive Mechanism," *IEEE Transactions on Vehicular Technology*, vol. 69, no. 6, pp. 6699–6708, June 2020. 2, 71, 123

[12] R. Baines, “The Need for WiMAX picocell Femtocells,” in *WiMax London 2007*, April 2007, pp. 1–36. 2

[13] ETSI, “Machine-to-Machine communications (M2M); Definitions,” ETSI, TR 102 725 V1.1.1, 7 2013. 3

[14] ——, “Machine-to-Machine communications (M2M); M2M service requirements,” ETSI, TS 102 689 V2.1.1, 7 2013. 3

[15] ——, “Machine-to-Machine communications (M2M); Functional architecture,” ETSI, TS 102 690 V2.1.1, 10 2013. 3

[16] ITU, “Guidelines for evaluation of radio interface technologies for IMT-Advanced,” ITU, Tech. Rep. Rep. ITU-R M.2135-1, Dec 2009. [Online]. Available: https://www.itu.int/pub/R-REP-M.2135-1-2009 3, 20, 99, 100, 103

[17] ——, “Guidelines for evaluation of radio interface technologies for IMT-2020,” ITU, Tech. Rep. Rep. ITU-R M.2412-0, Nov 2017. [Online]. Available: https://www.itu.int/dms_pub/itu-r/opb/rep/R-REP-M.2412-2017-PDF-E.pdf 3, 20

[18] M. R. K. Sial, H. F. Usman, and S. Hamid, “Green Cognitive Femtocells Deployment House Modelling for Interference Mitigation,” in *2018 15th International Conference on Electrical Engineering/Electronics, Computer, Telecommunications and Information Technology (ECTI-CON)*, July 2018, pp. 376–379. 3

[19] I. Ashraf, H. Claussen, and L. T. W. Ho, “Distributed Radio Coverage Optimization in Enterprise Femtocell Networks,” in *2010 IEEE International Conference on Communications*, May 2010, pp. 1–6. 3, 19

[20] S. R. Valizadeh and J. Abouei, “An adaptive distributed coverage optimization scheme in LTE enterprise femtocells,” in *2014 22nd Iranian Conference on Electrical Engineering (ICEE)*, May 2014, pp. 1723–1728. 3, 19, 122

[21] H. Zhang, C. Jiang, N. C. Beaulieu, X. Chu, X. Wen, and M. Tao, “Resource Allocation in Spectrum-Sharing OFDMA Femtocells With Heterogeneous Services,” *IEEE Transactions on Communications*, vol. 62, no. 7, pp. 2366–2377, July 2014. 3

[22] H. Claussen, D. López-Pérez, L. Ho, R. Razavi, and S. Kucera, *Small Cells—The Future of Cellular Networks*. John Wiley & Sons, Ltd, 2017, ch. 1, pp. 1–21. [Online]. Available: https://onlinelibrary.wiley.com/doi/abs/10.1002/9781119307600.ch1 4, 5, 6

[23] G. Intelligence. (2021) GSMA Intelligence, Data. [Online]. Available: https://www.gsmaintelligence.com/data/ 4

[24] U. S. C. Bureau. (2021) U.S. and World Population Clock. [Online]. Available: https://www.census.gov/popclock/ 4

[25] M. K. Weldon, *The Future X Network: A Bell Labs Perspective*. USA: CRC Press, Inc., 2015. 4

[26] G. Clemo, G. Maile, C. Forster, C. Forster, and I. Dickie, "Understanding the Environmental Impact of Communication Systems," Ofcom, eftec, Plextek, Tech. Rep. Version 03, April 2009. [Online]. Available: https://webarchive.nationalarchives.gov.uk/20100507155336/http:/www.ofcom.org.uk/research/technology/research/sectorstudies/environment/environ.pdf 4

[27] ITU. (2020) ICT industry to reduce greenhouse gas emissions by 45 per cent by 2030. [Online]. Available: https://www.itu.int/en/mediacentre/Pages/PR04-2020-ICT-industry-to-reduce-greenhouse-gas-emissions-by-45-percent-by-2030.aspx 4

[28] C. Shannon, "Communication in the presence of noise," *Proceedings of the IRE*, vol. 37, no. 1, pp. 10–21, Jan 1949. 4

[29] Nokia, "Indoor deploymnet strategies, White Paper," Nokia, Tech. Rep., June 2014. 5

[30] A. Stocker, "Small-cell mobile phone systems," *IEEE Transactions on Vehicular Technology*, vol. 33, no. 4, pp. 269–275, Nov 1984. 6

[31] R. Iyer, J. Parker, and P. Sood, "Intelligent networking for digital cellular systems and the wireless world," in *Global Telecommunications Conference, 1990, and Exhibition. 'Communications: Connecting the Future', GLOBECOM '90., IEEE*, Dec 1990, pp. 475–479 vol.1. 6

[32] R. Brickhouse and T. Rappaport, "Urban in-building cellular frequency reuse," in *Global Telecommunications Conference, 1996. GLOBECOM '96. 'Communications: The Key to Global Prosperity*, vol. 2, Nov 1996, pp. 1192–1196 vol.2. 6

[33] V. Chandrasekhar, J. Andrews, and A. Gatherer, "Femtocell networks: a survey," *Communications Magazine, IEEE*, vol. 46, no. 9, pp. 59–67, September 2008. 6

[34] H. Claussen, L. Ho, H. Karimi, F. Mullany, and L. Samuel, "I, base station: Cognisant robots and future wireless access networks," in *Consumer Communications and Networking Conference, 2006. CCNC 2006. 3rd IEEE*, vol. 1, Jan 2006, pp. 595–599. 6, 9

[35] H. Claussen, L. T. W. Ho, and L. G. Samuel, "Financial Analysis of a Pico-Cellular Home Network Deployment," in *2007 IEEE International Conference on Communications*, June 2007, pp. 5604–5609. 6

[36] H. Claussen, "Performance of macro- and co-channel femtocells in a hierarchical cell structure," in *2007 IEEE 18th International Symposium on Personal, Indoor and Mobile Radio Communications*, Sep 2007, pp. 1–5. 6

[37] L. T. W. Ho and H. Claussen, "Effects of user-deployed, co-channel femtocells on the call drop probability in a residential scenario," in *2007 IEEE 18th International Symposium on Personal, Indoor and Mobile Radio Communications*, Sep 2007, pp. 1–5. 6

[38] S. C. Forum. (2011, June) 3G femtocells now outnumber conventional 3G basestations globally. [Online]. Available: https://www.smallcellforum.org/press-releases/3g-femtocells-now-outnumber-conventional-3g-basestations-globally/ 6

[39] ——, "Market status statistics June 2015," Small Cell Forum, Tech. Rep., June 2015. [Online]. Available: https://scf.io/en/documents/050_-_Market_status_report_June_2015_-_Mobile_Experts.php 6

[40] ——. (2021, June) SCF, About us, Who we are. [Online]. Available: https://www.smallcellforum.org/about-us/ 7

[41] ——, "Market Forecast Report 2021," Small Cell Forum, Tech. Rep. 050.0.1, June 2021. [Online]. Available: https://scf.io/en/download.php?doc=050 7

[42] P. Pirinen, "A brief overview of 5G research activities," in *1st International Conference on 5G for Ubiquitous Connectivity*, Nov 2014, pp. 17–22. 7

[43] M. Kamel, W. Hamouda, and A. Youssef, "Ultra-Dense Networks: A Survey," *IEEE Communications Surveys Tutorials*, vol. 18, no. 4, pp. 2522–2545, Fourthquarter 2016. 7

[44] S. Samarakoon, M. Bennis, W. Saad, M. Debbah, and M. Latva-aho, "Ultra Dense Small Cell Networks: Turning Density Into Energy Efficiency," *IEEE Journal on Selected Areas in Communications*, vol. 34, no. 5, pp. 1267–1280, May 2016. 7

[45] J. G. Andrews, X. Zhang, G. D. Durgin, and A. K. Gupta, "Are we approaching the fundamental limits of wireless network densification?" *IEEE Communications Magazine*, vol. 54, no. 10, pp. 184–190, October 2016. 8

[46] R. Ahmad, E. A. Sundararajan, and A. Khalifeh, "A survey on femtocell handover management in dense heterogeneous 5G networks," *Telecommunication Systems*, vol. 75, no. 4, pp. 481–507, Dec 2020. [Online]. Available: https://doi.org/10.1007/s11235-020-00718-1 8

[47] O. Sevim, H. Y. Öksüz, and M. Akar, "Joint Frequency and Power Control for Self–Organizing OFDMA Femtocell Networks," *IEEE Transactions on Vehicular Technology*, vol. 69, no. 5, pp. 5089–5101, May 2020. 8

[48] Z. Gao, L. Dai, S. Han, C.-L. I, Z. Wang, and L. Hanzo, "Compressive Sensing Techniques for Next-Generation Wireless Communications," *IEEE Wireless Communications*, vol. 25, no. 3, pp. 144–153, JUNE 2018. 8

[49] R. Bendlin, V. Chandrasekhar, R. Chen, A. Ekpenyong, and E. Onggosanusi, "From homogeneous to heterogeneous networks: A 3GPP Long Term Evolution rel. 8/9 case study," in *2011 45th Annual Conference on Information Sciences and Systems*, March 2011, pp. 1–5. 8

[50] J. Zhang and G. de la Roche, *Femtocells: Technologies and Deployment*. Wiley Publishing, 2010. 8, 9, 10, 11, 12, 13, 14

[51] S. C. Forum, "Small Cell Forum, Release 7.0," Small Cell Forum, Tech. Rep. 101.07.03, June 2014. [Online]. Available: https://scf.io/en/documents/101_Release_One_Home_overview.php 8, 9

[52] J. Andrews, H. Claussen, M. Dohler, S. Rangan, and M. Reed, "Femtocells: Past, Present, and Future," *Selected Areas in Communications, IEEE Journal on*, vol. 30, no. 3, pp. 497–508, April 2012. 8, 9

[53] T. Q. S. Quek, G. de la Roche, I. Gven, and M. Kountouris, *Small Cell Networks: Deployment, PHY Techniques, and Resource Management*. USA: Cambridge University Press, 2013. 8, 10

[54] S. Saunders, S. Carlaw, A. Giustina, R. Bhat, V. Rao, and R. Siegberg, *Femtocells: Opportunities and Challenges for Business and Technology*, ser. Telecoms Explained. John Wiley & Sons, 2009. [Online]. Available: http://books.google.pt/books?id=PXHcif36qaEC 9, 10

[55] L. F. Ibrahim, H. A. Salman, Z. F. Taha, N. Akkari, G. Aldabbagh, and O. Bamasak, "A survey on heterogeneous mobile networks planning in indoor dense areas," *Personal and Ubiquitous Computing*, vol. 24, no. 4, pp. 487–498, Aug 2020. [Online]. Available: https://doi.org/10.1007/s00779-019-01243-y 9

[56] M. M. S. Maswood, U. K. Dey, S. Akter, M. A. Uddin, M. M. I. Mamun, S. S. Sonia, and A. G. Alharbi, "Improving System Performance in Indoor Environment by Designing Femtocell Considering Interference and Mobility Management," in *2021 IEEE 11th Annual Computing and Communication Workshop and Conference (CCWC)*, Jan 2021, pp. 1204–1209. 9

[57] S. Mahmud, G. Khan, H. Zafar, K. Ahmad, and N. Behttani, "A Survey on Femtocells: Benefits Deployment Models and Proposed Solutions," *Journal of Applied Research and Technology*, vol. 11, no. 5, pp. 733–754, 2013. [Online]. Available: https://www.sciencedirect.com/science/article/pii/S1665642313715827 9

[58] H. Claussen, D. López-Pérez, L. Ho, R. Razavi, and S. Kucera, *Dormant Cells and Idle Modes*. John Wiley & Sons, Ltd, 2017, ch. 13, pp. 393–418. [Online]. Available: https://onlinelibrary.wiley.com/doi/abs/10.1002/9781119307600.ch13 9

[59] H. Dhillon, R. Ganti, F. Baccelli, and J. Andrews, "Modeling and Analysis of K-Tier Downlink Heterogeneous Cellular Networks," *Selected Areas in Communications, IEEE Journal on*, vol. 30, no. 3, pp. 550–560, April 2012. 10

[60] D. Lopez-Perez, A. Valcarce, G. de la Roche, and J. Zhang, "OFDMA femtocells: A roadmap on interference avoidance," *Communications Magazine, IEEE*, vol. 47, no. 9, pp. 41–48, September 2009. 10, 15

[61] P. Xia, V. Chandrasekhar, and J. Andrews, "Open vs. Closed Access Femtocells in the Uplink," *Wireless Communications, IEEE Transactions on*, vol. 9, no. 12, pp. 3798–3809, December 2010. 10

[62] S. Yun, Y. Yi, D.-H. Cho, and J. Mo, "Open or close: On the sharing of femtocells," in *2011 Proceedings IEEE INFOCOM*, April 2011, pp. 116–120. 10

[63] H. Jo, P. Xia, and J. G. Andrews, "Open, closed, and shared access femtocells in the downlink," *EURASIP Journal on Wireless Communications and Networking*, vol. 2012, no. 1, p. 363, Dec 2012. [Online]. Available: https://doi.org/10.1186/1687-1499-2012-363 10

[64] M. Rahman and H. Yanikomeroglu, "Enhancing cell-edge performance: a downlink dynamic interference avoidance scheme with inter-cell coordination," *Wireless Communications, IEEE Transactions on*, vol. 9, no. 4, pp. 1414–1425, April 2010. 13

[65] V. Chandrasekhar and J. Andrews, "Spectrum allocation in tiered cellular networks," *Communications, IEEE Transactions on*, vol. 57, no. 10, pp. 3059–3068, October 2009. 15

[66] M. E. Sahin, I. Guvenc, M.-R. Jeong, and H. Arslan, "Handling cci and ici in ofdma femtocell networks through frequency scheduling," *IEEE Transactions on Consumer Electronics*, vol. 55, no. 4, pp. 1936–1944, November 2009. 15

[67] A. Technologies, "3GPP Long Term Evolution: System Overview, Product Development,and Test Challenges," Agilent Technologies, Inc., Tech. Rep., June 2009. [Online]. Available: http://literature.cdn.keysight.com/litweb/pdf/5989-8139EN.pdf 15

[68] J. Y. Lee, S. J. Bae, Y. M. Kwon, and M. Y. Chung, "Interference Analysis for Femtocell Deployment in OFDMA Systems Based on Fractional Frequency Reuse," *Communications Letters, IEEE*, vol. 15, no. 4, pp. 425–427, April 2011. 16

[69] 3GPP. (2021) About 3GPP Home. [Online]. Available: https://www.3gpp.org/about-3gpp/about-3gpp 16

[70] ——. (2021) TSG RAN. [Online]. Available: https://www.3gpp.org/specifications-groups/ran-plenary 16

[71] ——, "TS 36.300 Evolved Universal Terrestrial Radio Access (E-UTRA) and Evolved Universal Terrestrial Radio Access (Release 8)," 3rd Generation Partnership Project,

Tech. Rep. V8.7.0, Dec 2008. [Online]. Available: https://www.3gpp.org/ftp/Specs/archive/36_series/36.300/36300-870.zip 16

[72] ——, "TS 36.213 Services and service capabilities (Release 16)," 3rd Generation Partnership Project, Tech. Rep. V16.3.0, Oct 2020. [Online]. Available: https://www.3gpp.org/ftp//Specs/archive/36_series/36.213/36213-g30.zip 16, 38

[73] ——, "TS 23.002 Network architecture," 3rd Generation Partnership Project, Tech. Rep., 2021. [Online]. Available: https://portal.3gpp.org/desktopmodules/Specifications/SpecificationDetails.aspx?specificationId=728 16

[74] ——, "TS 23.401 General Packet Radio Service (GPRS) enhancements for Evolved Universal Terrestrial Radio Access Network (E-UTRAN) access," 3rd Generation Partnership Project, Tech. Rep., 2021. [Online]. Available: https://portal.3gpp.org/desktopmodules/Specifications/SpecificationDetails.aspx?specificationId=849 16

[75] ——, "TS 36.300 Evolved Universal Terrestrial Radio Access (E-UTRA) and Evolved Universal Terrestrial Radio Access (Release 10)," 3rd Generation Partnership Project, Tech. Rep. V10.2.0, Dec 2010. [Online]. Available: https://www.3gpp.org/ftp/Specs/archive/36_series/36.300/36300-a20.zip 16, 17

[76] ——, "TS 36.300 Evolved Universal Terrestrial Radio Access (E-UTRA) and Evolved Universal Terrestrial Radio Access (Release 11)," 3rd Generation Partnership Project, Tech. Rep. V11.4.0, Dec 2012. [Online]. Available: https://www.3gpp.org/ftp/Specs/archive/36_series/36.300/36300-b40.zip 17, 18

[77] ——, "TS 36.300 Evolved Universal Terrestrial Radio Access (E-UTRA) and Evolved Universal Terrestrial Radio Access (Release 12)," 3rd Generation Partnership Project, Tech. Rep. V12.2.0, June 2014. [Online]. Available: https://www.3gpp.org/ftp/Specs/archive/36_series/36.300/36300-c20.zip 17, 18, 19

[78] ——, "TS 36.300 Evolved Universal Terrestrial Radio Access (E-UTRA) and Evolved Universal Terrestrial Radio Access (Release 12)," 3rd Generation Partnership Project, Tech. Rep. V16.5.0, March 2021. [Online]. Available: https://www.3gpp.org/ftp/Specs/archive/36_series/36.300/36300-g50.zip 19

[79] ——, "R4-092042 Simulation assumptions and parameters for FDD HeNB RF requirements," 3rd Generation Partnership Project, Tech. Rep. Meeting #51, May 2009. [Online]. Available: https://www.3gpp.org/ftp7tsg_ran/WG4_Radio/TSGR4_51/Documents/\R4_092042.zip 19, 25, 26, 27, 28, 30, 31, 39, 55, 61, 62, 71, 79, 80, 181

[80] D. Robalo, "Planning and dynamic spectrum management in heterogeneous mobile networks with QoE optimization," Ph.D. dissertation, Universidade da Beira Interior, August 2014. [Online]. Available: https://ubibliorum.ubi.pt/handle/10400.6/4033 19, 29

[81] O. Cabral, “Optimization of the interoperability and dynamic spectrum management in mobile communications systems beyond 3G,” Ph.D. dissertation, Universidade da Beira Interior, August 2010. [Online]. Available: https://ubibliorum.ubi.pt/handle/10400.6/680 19

[82] K. Chen and J. de Marca, *Mobile WiMAX*, ser. Wiley - IEEE. Wiley, 2008. [Online]. Available: https://books.google.es/books?id=7TWzvbZkLMgC 19, 30, 32

[83] P. Uthansakul, P. Anchuen, M. Uthansakul, and A. A. Khan, “QoE-Aware Self-Tuning of Service Priority Factor for Resource Allocation Optimization in LTE Networks,” *IEEE Transactions on Vehicular Technology*, vol. 69, no. 1, pp. 887–900, Jan 2020. 19, 59, 60, 99, 102

[84] B. Abdelmula, H. S. Ali, M. Warip, M. N. Bin, O. Bi, and Y. Naimah, “Technical review of RRM for carrier aggregation in LTE-Advanced,” *Journal of Theoretical and Applied Information Technology*, vol. 91, no. 2, pp. 397–410, 09 2016. 19, 49, 59, 60, 99, 100, 102

[85] G. Piro, L. A. Grieco, G. Boggia, R. Fortuna, and P. Camarda, “Two-Level Downlink Scheduling for Real-Time Multimedia Services in LTE Networks,” *IEEE Transactions on Multimedia*, vol. 13, no. 5, pp. 1052–1065, Oct 2011. 19, 49, 59, 60, 80

[86] G. Piro, L. A. Grieco, G. Boggia, F. Capozzi, and P. Camarda, “Simulating LTE Cellular Systems: An Open-Source Framework,” *IEEE Transactions on Vehicular Technology*, vol. 60, no. 2, pp. 498–513, Feb 2011. 20, 27, 38, 49, 59, 99

[87] S. Martiradonna, A. Grassi, G. Piro, and G. Boggia, “5G-air-simulator: An open-source tool modeling the 5G air interface,” *Computer Networks*, vol. 173, p. 107151, 2020. [Online]. Available: https://www.sciencedirect.com/science/article/pii/S1389128619317359 20, 116

[88] D. Robalo, F. J. Velez, R. R. Paulo, and G. Piro, “Extending the LTE-Sim Simulator with Multi-Band Scheduling Algorithms for Carrier Aggregation in LTE-Advanced Scenarios,” in *2015 IEEE 81st Vehicular Technology Conference (VTC Spring)*, May 2015, pp. 1–6. 20, 21, 104

[89] S. Ruiz, M. Garcia-Lozano, D. Gonzalez, M. Lema, J. Papaj, W. Joseph, M. Deruyck, N. Cardona, C. Garcia, F. J. Velez, L. Correia, L. Studer, P. Grazioso, and S. Chatzinotas, *Chapter 6 - Green and Efficient RAN Architectures*. River Publishing, Kent, -1, June 2016, ch. 6, pp. 195–270. [Online]. Available: https://www.riverpublishers.com/downloadchapter.php?file=RP_9788793379145C6.pdf 20, 22

[90] A. R. Ramos, “Cellular Planning and Optimization for 4G and 5G Mobile Networks,” Master’s thesis, Universidade da Beira Interior, July 2019. [Online]. Available: https://ubibliorum.ubi.pt/bitstream/10400.6/10065/1/7124_15081.pdf 20

[91] B. Khan, A. R. Ramos, R. R. Paulo, and F. J. Velez, “Deployment of Beyond 4G Wireless Communication Networks with Carrier Aggregation,” in *Proc. of ICEEE*

2020: 14. International Conference on Electronics and Electrical Engineering. World Academy of Science, Engineering and Technology, Jul 2020. [Online]. Available: https://waset.org/electronics-and-electrical-engineering-conference-in-july-2020-in-toronto 20, 21

[92] B. Khan, A. R. Ramos, R. R. Paulo, and F. J. Velez, "Deployment of Beyond 4G Wireless Communication Networks with Carrier Aggregation," *International Journal of Electronics and Communication Engineering*, vol. 15, no. 2, Mar. 2021. [Online]. Available: https://doi.org/10.5281/zenodo.4569341 20, 21

[93] S. Ruiz, H. Ahmadi, G. Gardašević, Y. Haddad, K. Katzis, P. Grazioso, V. Petrini, A. Reichman, M. K. Ozdemir, F. Velez, R. Paulo, S. Fortes, L. M. Correia, B. Rouzbehani, M. Barahman, M. Deruyck, S. Mignardi, K. Nasr, and H. Zhang, "Chapter 6 - 5G and beyond networks," in *Inclusive Radio Communications for 5G and Beyond*, C. Oestges and F. Quitin, Eds. Academic Press, 2021, pp. 141–186. [Online]. Available: https://www.sciencedirect.com/science/article/pii/B9780128205815000122 20, 22

[94] R. R. Paulo, F. J. Velez, and G. Piro, "Design of Coordinated HeNB Deployments," in *2018 IEEE 87th Vehicular Technology Conference (VTC Spring)*, June 2018, pp. 1–6. 20, 21, 30, 51, 86, 87, 165

[95] ——, "Performance Evaluation and Packet Scheduling in HeNB Deployments," in *2018 IEEE 88th Vehicular Technology Conference (VTC-Fall)*, Aug 2018, pp. 1–6. 20, 21, 38, 86, 87

[96] R. R. Paulo and F. J. Velez, "A study on system capacity for HeNBs with different schedulers," in *Conf. on Telecommunications - ConfTele*, June 2019, pp. 25–28. 20, 21, 29, 38, 86

[97] 3GPP, "TS 22.105 Services and service capabilities (Release 15)," 3rd Generation Partnership Project, Tech. Rep. V15.0.0, July 2018. [Online]. Available: https://www.3gpp.org/ftp/Specs/archive/25_series/25.892/25892-600.zip 20, 37, 38, 63, 71, 82, 86, 87, 100, 109, 208

[98] R. R. Paulo and F. J. Velez, "System Level Simulation of Urban Micro-cellular 4G Scenarios in the Sub-6 GHz Frequency Bands," in *2021 Telecoms Conference (ConfTELE)*, Feb 2021, pp. 1–6. 20, 22, 99, 100

[99] R. R. Paulo, E. B. Teixeira, and F. J. Velez, "Service Quality of the Urban Micro Cellular Scenario in the sub-6 GHz Frequency Bands," November 2021, submitted. 20, 21

[100] R. R. Paulo and F. J. Velez, "Study of Indoor Small Cell Deployments," *Journal of Mobile Multimedia*, vol. 17, no. 1-3, p. 329–344, Feb 2021. 20, 21, 99, 165

[101] R. M. Andrade, R. R. Paulo, S. M. Francisco, E. B. Teixeira, and F. J. Velez, "Characterization of Indoor Small Cells Propagation," in *2021 24th International Symposium on Wireless Personal Multimedia Communications (WPMC)*, Dec 2021. 20, 22, 31

[102] R. R. Paulo and F. J. Velez, "An Extensive Study on the Performance Evaluation and Scheduling of HeNBs," *IEEE Access*, pp. 1–1, 2021. 20, 21, 99, 100, 109, 113, 165

[103] F. Capozzi, G. Piro, L. Grieco, G. Boggia, and P. Camarda, "On accurate simulations of LTE femtocells using an open source simulator," *EURASIP Journal on Wireless Communications and Networking*, vol. 2012, no. 1, p. 328, 2012. [Online]. Available: http://jwcn.eurasipjournals.com/content/2012/1/328 25, 26, 27, 28, 39, 80, 81, 87

[104] S.-Y. Lien, Y.-Y. Lin, and K.-C. Chen, "Cognitive and Game-Theoretical Radio Resource Management for Autonomous Femtocells with QoS Guarantees," *Wireless Communications, IEEE Transactions on*, vol. 10, no. 7, pp. 2196–2206, July 2011. 25

[105] D. Hu and S. Mao, "On Medium Grain Scalable Video Streaming over Femtocell Cognitive Radio Networks," *Selected Areas in Communications, IEEE Journal on*, vol. 30, no. 3, pp. 641–651, April 2012. 26

[106] C. Project. (2021) ns-3. [Online]. Available: https://www.nsnam.org/ 26

[107] T. S. Rappaport, *Wireless Communications: Principles and Practice*, 2nd ed. Upper Saddle River, NJ: Prentice Hall PTR, 2002. 28, 29, 57, 61

[108] S. Sesia, I. Toufik, and M. Baker, *LTE, The UMTS Long Term Evolution: From Theory to Practice, 2nd Edition*. Wiley Publishing, 2011. 28, 29, 57, 58, 59, 61, 80, 102, 107

[109] 3GPP, "TS 36.213 Evolved Universal Terrestrial Radio Access (E-UTRA); Physical layer procedures (Release 15)," 3rd Generation Partnership Project, Tech. Rep. V15.0.0, June 2014. [Online]. Available: http://www.3gpp.org/ftp/Specs/archive/36series/36.213/36213-f00.zip 29

[110] J. Habetha and J. Wiegert, "Network capacity optimisation, part 1: Cellular radio networks," in *Proceedings of 10th Symposium on Signal Theory*, Sep 2001, pp. 125–132. 30

[111] ——, "Network capacity optimisation, part 2: Multihop ad hoc radio networks," in *Proceedings of 10th Symposium on Signal Theory*, Sep 2001, pp. 133–140. 30

[112] H. Holma and A. Toskala, *WCDMA for UMTS - HSPA evolution and LTE*, 1st ed. West Sussex, England: JohnWiley & Sons, Ltd., 2007. 30

[113] P. Kyösti, J. Meinilä, L. Hentilä, X. Zhao, T. Jämsä, C. Schneider, M. Narandzić, M. Milojević, A. Hong, J. Ylitalo, V. Holappa, M. Alatossava, R. Bultitude, Y. de Jong, and T. Rautiainen, "IST-4-027756 WINNER II D1.1.2 V1.2 WINNER II Channel Models," Information Society Technologies, Germany, Tech. Rep. D1.1.2 V1.2, February 2008. [Online]. Available: http://www.cept.org/files/1050/documents/winner2-finalreport.pdf 31, 165

[114] K. Chen and J. de Marca, *Mobile WiMAX*, ser. Wiley - IEEE. John Wiley & Sons, Ltd, 2008, ch. Dimensioning Cellular Multi-Hop WiMAX Networks, pp. 203–234. [Online]. Available: https://books.google.es/books?id=7TWzvbZkLMgC 32

[115] X. Xu, G. Kutrolli, and R. Mathar, "Energy efficient power management for 4G heterogeneous cellular networks," in *2013 IEEE 9th International Conference on Wireless and Mobile Computing, Networking and Communications (WiMob)*, Oct 2013, pp. 231–238. 33

[116] O. Cabral, F. Meucci, A. Mihovska, F. J. Velez, N. R. Prasad, and R. Prasad, "Integrated Common Radio Resource Management with Spectrum Aggregation Over Non-Contiguous Frequency Bands," *Wireless Personal Communications*, vol. 59, no. 3, pp. 499–523, 2011. [Online]. Available: http://dx.doi.org/10.1007/s11277-011-0242-6 33

[117] M. J. Wester, Y. Yaacob, and S. Steinberg, "Computing integrals over polynomially defined regions and their boundaries in 2 and 3 dimensions," *Mathematics and Computers in Simulation*, vol. 82, no. 1, pp. 79 – 101, 2011, {ACA} 2008 - 2009 + {MASCOT} 2008. [Online]. Available: http://www.sciencedirect.com/science/article/pii/S0378475411001522 33

[118] W. R. Inc., "Mathematica, Version 12.2," champaign, IL, 2020. [Online]. Available: https://www.wolfram.com/mathematica 34, 149

[119] S. Mumtaz and A. Gameiro, "Enhanced Algorithm for Link to System Interface Mapping," in *(IJCSIS) International Journal of Computer Science and Information Security*, vol. 3, no. 3, Jul 2009, pp. 1–3. 37, 38

[120] K. Brueninghaus, D. Astely, T. Salzer, S. Visuri, A. Alexiou, S. Karger, and G. Seraji, "Link performance models for system level simulations of broadband radio access systems," in *2005 IEEE 16th International Symposium on Personal, Indoor and Mobile Radio Communications*, vol. 4, Sep 2005, pp. 2306–2311 Vol. 4. 37

[121] S. Ahmadi, *LTE-Advanced: A Practical Systems Approach to Understanding 3GPP LTE Releases 10 and 11 Radio Access Technologies*, 1st ed. USA: Academic Press, Inc., 2013. 37

[122] Z. Hanzaz and H. D. Schotten, "Analysis of effective SINR mapping models for MIMO OFDM in LTE system," in *2013 9th International Wireless Communications and Mobile Computing Conference (IWCMC)*, July 2013, pp. 1509–1515. 37

[123] S. Mumtaz, A. Gameiro, and R. Sadeghi, "Enhanced Algorithm for Link to System level Interface Mapping," *CoRR*, vol. abs/0908.1116, 2009. [Online]. Available: http://arxiv.org/abs/0908.1116 38

[124] 3GPP, "TR 25.892 Feasibility Study for OFDM for UTRAN enhancement (Release 6)," 3rd Generation Partnership Project, Tech. Rep. V1.1.0, March. 2004, technical

Specification Group Radio Access Network. [Online]. Available: https://www.3gpp.org/ftp/Specs/archive/25_series/25.892/25892-110.zip 38

[125] ——, "TS 36.213 Services and service capabilities (Release 16)," 3rd Generation Partnership Project, Tech. Rep. V16.4.0, Dec 2020. [Online]. Available: https://www.3gpp.org/ftp/Specs/archive/36_series/36.213/36213-g40.zip 38

[126] S. Ahmadi, *A Practical Systems Approach to Understanding 3GPP LTE Releases 10 and 11 Radio Access Technologies*. Academic Press, 2014, p. 1152. [Online]. Available: http://www.sciencedirect.com/science/article/pii/B9780124051621000O\34 38

[127] S. Sesia, I. Toufik, and M. Baker, *LTE-the UMTS long term evolution: from theory to practice, 2nd Edition*. John Wiley & Sons, 2011. 38

[128] LTE Simulator. LTE-Sim Forum. [Online]. Available: https://groups.google.com/forum/#!forum/lte-sim 38

[129] R. R. Paulo and F. J. Velez, "LTE-SIM-RP," https://github.com/RRP-IT/LTE-Sim-RP.git, 2020. 39, 119, 165

[130] H. A. M. Ramli, "A Study on Packet Scheduling Algorithms for Healthcare Contents over Fifth Generation (5G) Mobile Cellular Network," *International Journal of Electronics and Telecommunications*, vol. vol. 66, no. No 4, pp. 729–735, 2020. 49, 59, 98, 102

[131] I. U. Rehman, M. M. Nasralla, and N. Y. Philip, "Multilayer Perceptron Neural Network-Based QoS-Aware, Content-Aware and Device-Aware QoE Prediction Model: A Proposed Prediction Model for Medical Ultrasound Streaming Over Small Cell Networks," *Electronics*, vol. 8, no. 2, 2019. [Online]. Available: https://www.mdpi.com/2079-9292/8/2/194 49, 71, 113

[132] M. M. Nasralla, "A Hybrid Downlink Scheduling Approach for Multi-Traffic Classes in LTE Wireless Systems," *IEEE Access*, vol. 8, pp. 82 173–82 186, 2020. 49, 59, 71, 99

[133] M. M. Nasralla, N. Khan, and M. G. Martini, "Content-aware downlink scheduling for LTE wireless systems: A survey and performance comparison of key approaches," *Computer Communications*, vol. 130, pp. 78 – 100, 2018. [Online]. Available: http://www.sciencedirect.com/science/article/pii/S0140366418302020 49, 71, 100, 113

[134] M. Matsumoto and T. Nishimura, "Mersenne Twister: A 623-dimensionally Equidistributed Uniform Pseudo-random Number Generator," *ACM Trans. Model. Comput. Simul.*, vol. 8, no. 1, pp. 3–30, jan 1998. [Online]. Available: http://doi.acm.org/10.1145/272991.272995 51

[135] S. Marsland, *Machine Learning: An Algorithmic Perspective, Second Edition*, 2nd ed. Chapman & Hall/CRC, 2014. 51

[136] International Standards Organization and International Electrotechnical Commission, *ISO/IEC 9899:2011, Programming Languages – C*, 1st ed. 11 West 42nd Street, New York, New York 1O036: American National Standards Institute (ANSI), Dec 2011. [Online]. Available: http://www.open-std.org/jtc1/sc22/wg14/ 51

[137] J. Wu, B. Cheng, M. Wang, and J. Chen, "Energy-Efficient Bandwidth Aggregation for Delay-Constrained Video Over Heterogeneous Wireless Networks," *IEEE Journal on Selected Areas in Communications*, vol. 35, no. 1, pp. 30–49, Jan 2017. 59

[138] J. Wu, C. Yuen, B. Cheng, M. Wang, and J. Chen, "Energy-Minimized Multipath Video Transport to Mobile Devices in Heterogeneous Wireless Networks," *IEEE Journal on Selected Areas in Communications*, vol. 34, no. 5, pp. 1160–1178, May 2016. 59

[139] R. Basukala, H. A. M. Ramli, and K. Sandrasegaran, "Performance analysis of EXP/PF and M-LWDF in downlink 3GPP LTE system," in *2009 First Asian Himalayas International Conference on Internet*, Nov 2009, pp. 1–5. 59, 80

[140] R. Kwan, C. Leung, and J. Zhang, "Proportional Fair Multiuser Scheduling in LTE," *IEEE Signal Processing Letters*, vol. 16, no. 6, pp. 461–464, June 2009. 59

[141] K. J. Åström and B. Wittenmark, *Computer-Controlled Systems*, 3rd ed. USA: Prentice-Hall, Inc., 1997. 60

[142] E. Dahlman, S. Parkvall, J. Skold, and P. Beming, *3G Evolution, Second Edition: HSPA and LTE for Mobile Broadband*, 2nd ed. Academic Press, 2008. 60, 80

[143] S. Shakkottai and A. L. Stolyar, *Scheduling for multiple flows sharing a time-varying channel: The exponential rule*. 201 Charles Street Providence, Rhode Island: American Mathematical Society Translations, Series, Nov 2002, pp. 185–201. 60, 80

[144] B. Sadiq, S. J. Baek, and G. de Veciana, "Delay-Optimal Opportunistic Scheduling and Approximations: The Log Rule," *IEEE/ACM Transactions on Networking*, vol. 19, no. 2, pp. 405–418, April 2011. 60, 80

[145] E. M. Ang, K. Wee, Y. H. Pang, and K. K. Phang, "A performance analysis on packet scheduling schemes based on an exponential rule for real-time traffic in LTE," *EURASIP Journal on Wireless Communications and Networking*, vol. 2015, no. 1, p. 201, Aug 2015. [Online]. Available: https://doi.org/10.1186/s13638-015-0429-8 60

[146] F. Capozzi, G. Piro, L. Grieco, G. Boggia, and P. Camarda, "Downlink Packet Scheduling in LTE Cellular Networks: Key Design Issues and a Survey," *IEEE Communications Surveys Tutorials*, vol. 15, no. 2, pp. 678–700, Second 2013. 60

[147] B. Sadiq, R. Madan, and A. Sampath, "Downlink Scheduling for Multiclass Traffic in LTE," *EURASIP J. Wirel. Commun. Netw.*, vol. 2009, Mar. 2009. [Online]. Available: https://doi.org/10.1155/2009/510617 60

[148] V. T. Library. (2019) http://trace.eas.asu.edu/tracemain.html. [Online]. Available: http://trace.eas.asu.edu/tracemain.html 62, 87

[149] D. Adler, D. Murdoch *et al.*, *rgl: 3D Visualization Using OpenGL*, 2019, r package version 0.100.30. [Online]. Available: https://CRAN.R-project.org/package=rgl 62, 66, 82, 207

[150] J. Jalali, A. Khalili, and H. Steendam, "Antenna Selection and Resource Allocation in Downlink MISO OFDMA Femtocell Networks," in *2020 IEEE 91st Vehicular Technology Conference (VTC2020-Spring)*, May 2020, pp. 1–6. 71

[151] J. Cao, T. Peng, X. Liu, W. Dong, R. Duan, Y. Yuan, W. Wang, and S. Cui, "Resource Allocation for Ultradense Networks With Machine-Learning-Based Interference Graph Construction," *IEEE Internet of Things Journal*, vol. 7, no. 3, pp. 2137–2151, March 2020. 71

[152] Y. Guo, C. Hu, T. Peng, H. Wang, and X. Guo, "Regression-Based Uplink Interference Identification and SINR Prediction for 5G Ultra-Dense Network," in *ICC 2020 - 2020 IEEE International Conference on Communications (ICC)*, June 2020, pp. 1–6. 71

[153] J. S. Milton and J. C. Arnold, *Schaum's Outline of Introduction to Probability & Statistics: Principles & Applications for Engineering & the Computing Sciences*. McGraw-Hill Higher Education, 1994. 91

[154] V. Barnett and T. Lewis, *Outliers in Statistical Data*, ser. Wiley Series in Probability and Statistics. Wiley, 1994. [Online]. Available: https://books.google.pt/books?id=B44QAQAAIAAJ 91

[155] S. Q. Gilani, S. A. Hassan, H. Pervaiz, and S. H. Ahmed, "Performance Analysis of Flexible Duplexing-enabled Heterogeneous Networks Exploiting Multi Slope Path Loss Models," in *2019 International Conference on Computing, Networking and Communications (ICNC)*, Feb 2019, pp. 724–728. 97, 101

[156] J. Berg, "A recursive method for street microcell path loss calculations," in *Proceedings of 6th International Symposium on Personal, Indoor qualityand Mobile Radio Communications*, vol. 1, Sep 1995, pp. 140–143 vol.1. 98, 101

[157] N. Garg, S. Singh, and J. Andrews, "Impact of Dual Slope Path Loss on User Association in HetNets," in *2015 IEEE Globecom Workshops (GC Wkshps)*, Dec 2015, pp. 1–6. 98

[158] A. Turkmani and A. Arowojolu, "Estimation of signal strength characteristics in typical microcell environments for PCN networks," in *Proceedings of 2nd IEEE International Conference on Universal Personal Communications*, vol. 1, Oct 1993, pp. 69–73 vol.1. 98, 102

[159] H. Munir, S. A. Hassan, H. Pervaiz, Q. Ni, and L. Musavian, "User association in 5G heterogeneous networks exploiting multi-slope path loss model," in *2017 2nd Workshop on Recent Trends in Telecommunications Research (RTTR)*, Feb 2017, pp. 1–5. 98, 102

[160] U. Demir, C. U. Bas, and S. Coleri Ergen, "Engine Compartment UWB Channel Model for Intravehicular Wireless Sensor Networks," *IEEE Transactions on Vehicular Technology*, vol. 63, no. 6, pp. 2497–2505, July 2014. 98

[161] C. U. Bas and S. C. Ergen, "Ultra-Wideband channel model for intra-vehicular wireless sensor networks," in *2012 IEEE Wireless Communications and Networking Conference (WCNC)*, April 2012, pp. 42–47. 98

[162] R. Chen and Z. Zhong, "Analysis on V2V connectivity under dual-slope path loss model in urban scenarios," in *2014 XXXIth URSI General Assembly and Scientific Symposium (URSI GASS)*, Aug 2014, pp. 1–4. 98

[163] Lin Cheng, B. E. Henty, Fan Bai, and D. D. Stancil, "Highway and rural propagation channel modeling for vehicle-to-vehicle communications at 5.9 GHz," in *2008 IEEE Antennas and Propagation Society International Symposium*, July 2008, pp. 1–4. 98

[164] I. Rashdan, M. Walter, W. Wang, and G. Cair, "Large Scale Fading Characteristics for Vehicle-to-Cyclist Channel in Urban Environment at 5 GHz," in *2020 14th European Conference on Antennas and Propagation (EuCAP)*, March 2020, pp. 1–5. 98

[165] R. Chen, Z. Sheng, M. Ni, Z. Zhong, and D. G. Michelson, "Channel capacity under measurement-based model for cooperative vehicular ad hoc networks," in *2015 IEEE International Symposium on Antennas and Propagation USNC/URSI National Radio Science Meeting*, July 2015, pp. 302–303. 98

[166] M. G. Doone, S. L. Cotton, D. W. Matolak, C. Oestges, S. F. Heaney, and W. G. Scanlon, "Pedestrian-to-Vehicle Communications in an Urban Environment: Channel Measurements and Modeling," *IEEE Transactions on Antennas and Propagation*, vol. 67, no. 3, pp. 1790–1803, March 2019. 98

[167] P. L. Mehta, T. B. Sørensen, and R. Prasad, "SINR based capacity performance analysis of hovering Ad-Hoc network," in *2016 19th International Symposium on Wireless Personal Multimedia Communications (WPMC)*, Nov 2016, pp. 147–152. 98

[168] M. F. Abughalia, S. M. Tasmeeh Ahsan, and S. Saha, "Comparative Study of Microcell's Performance using Different Models in Different Regions," in *2019 International Conference on Robotics,Electrical and Signal Processing Techniques (ICREST)*, Jan 2019, pp. 517–521. 98, 101

[169] Juyul Lee, Myung-Don Kim, Jinyi Liang, Jae-Joon Park, and Bonghyuk Park, "Frequency range extension of the ITU-R NLOS path loss models applicable for urban

street environments with 28 GHz measurements," in *2016 10th European Conference on Antennas and Propagation (EuCAP)*, April 2016, pp. 1–5. 98

[170] C. B. Andrade and R. P. F. Hoefel, "IEEE 802.11 WLANs: A comparison on indoor coverage models," in *CCECE 2010*, May 2010, pp. 1–6. 98, 101

[171] N. O. Oyie and T. J. O. Afullo, "A Comparative Study of Dual-Slope Path Loss Model in Various Indoor Environments at 14 to 22 GHz," in *2018 Progress in Electromagnetics Research Symposium (PIERS-Toyama)*, Aug 2018, pp. 121–128. 98

[172] S. Sun, T. A. Thomas, T. S. Rappaport, H. Nguyen, I. Z. Kovacs, and I. Rodriguez, "Path Loss, Shadow Fading, and Line-of-Sight Probability Models for 5G Urban Macro-Cellular Scenarios," in *2015 IEEE Globecom Workshops (GC Wkshps)*, Dec 2015, pp. 1–7. 98

[173] S. Sousa, F. J. Velez, and J. M. Peha, "Impact of propagation model on capacity in small-cell networks," in *2017 International Symposium on Performance Evaluation of Computer and Telecommunication Systems (SPECTS)*, July 2017, pp. 1–8. 98, 99, 101, 102

[174] Y. Chang, S. Baek, S. Hur, Y. Mok, and Y. Lee, "A novel dual-slope mm-Wave channel model based on 3D ray-tracing in urban environments," in *2014 IEEE 25th Annual International Symposium on Personal, Indoor, and Mobile Radio Communication (PIMRC)*, Sep 2014, pp. 222–226. 98

[175] K. Kitao, T. Imai, N. Tran, N. Omaki, Y. Okumura, M. Inomata, M. Sasaki, and W. Yamada, "Path loss prediction model for 800 MHz to 37 GHz in NLOS microcell environment," in *2015 IEEE 26th Annual International Symposium on Personal, Indoor, and Mobile Radio Communications (PIMRC)*, Aug 2015, pp. 414–418. 98

[176] Y. F. Solahuddin and R. Mardeni, "Indoor empirical path loss prediction model for 2.4 GHz 802.11n network," in *2011 IEEE International Conference on Control System, Computing and Engineering*, Nov 2011, pp. 12–17. 98, 101

[177] 3GPP, "TR 36.814 Further advancements for E-UTRA physical layer aspects (Release 9)," 3rd Generation Partnership Project, Tech. Rep. V9.2.0, Mar. 2017. [Online]. Available: https://www.3gpp.org/ftp/Specs/archive/36_series/36.814/36814-920.zip 98, 102

[178] E. Skondras, A. Michalas, A. Sgora, and D. D. Vergados, "A downlink scheduler supporting real time services in LTE cellular networks," in *2015 6th International Conference on Information, Intelligence, Systems and Applications (IISA)*, July 2015, pp. 1–6. 99, 100

[179] S. Sousa, F. J. Velez, and J. M. Peha, "Impact of considering the ITU-R two slope propagation model in the system capacity trade-off for LTE-A HetNets with small cells," in *2017 XXXIInd General Assembly and Scientific Symposium of the International Union of Radio Science (URSI GASS)*, Aug 2017, pp. 1–4. 99, 103

[180] E. B. Teixeira, A. R. Ramos, M. S. Lourenço, F. J. Velez, and J. M. Peha, "Capacity/cost trade-off for 5G small cell networks in the UHF and SHF bands," in *2019 22nd International Symposium on Wireless Personal Multimedia Communications (WPMC)*, Nov 2019, pp. 1–6. 99, 108

[181] E. Teixeira, S. Sousa, F. J. Velez, and J. M. Peha, "Impact of the propagation model on the capacity in small-cell networks: comparison between the UHF/SHF and the millimetre wavebands," *Radio Science*, vol. 56, no. 5, p. e2020RS007150, 2021, e2020RS007150 2020RS007150. [Online]. Available: https://agupubs.onlinelibrary.wiley.com/doi/abs/10.1029/2020RS007150 100, 102, 105, 107, 108

[182] X. Zhang and J. G. Andrews, "Downlink cellular network analysis with a dual-slope path loss model," in *2015 IEEE International Conference on Communications (ICC)*, June 2015, pp. 3975–3980. 101

[183] J. Choi, H. Oh, and H. C. Jeon, "Propagation Prediction for LTE Small Cells with Antenna Beam Tilt," in *2014 IEEE 80th Vehicular Technology Conference (VTC2014-Fall)*, Sep 2014, pp. 1–5. 101

[184] A. Merwaday, R. Vannithamby, M. M. Rashid, Yi Zhang, Clark Chen, and Xiaoyun Wu, "On the performance of directional communications in ultra-dense networks," in *2017 IEEE International Conference on Communications Workshops (ICC Workshops)*, May 2017, pp. 522–527. 101

[185] K. Shehzad, N. M. Khan, and J. Ahmed, "Impact of Frequency Reuse and Flexible Cell Association on the Performance of Dense Heterogeneous Cellular Networks Using Dual-Slope Path Loss Model," *IEEE Access*, vol. 7, pp. 166 214–166 234, 2019. 101, 102

[186] A. Karttunen, A. F. Molisch, S. Hur, J. Park, and C. J. Zhang, "Spatially Consistent Street-by-Street Path Loss Model for 28-GHz Channels in Micro Cell Urban Environments," *IEEE Transactions on Wireless Communications*, vol. 16, no. 11, pp. 7538–7550, Nov 2017. 102

[187] 3GPP, "TR 38.900 Study on channel model for frequency spectrum above 6 GHz (Release 15)," 3rd Generation Partnership Project, Tech. Rep. V15.0.0, Jun 2018, technical Specification Group Radio Access Network. [Online]. Available: https://www.3gpp.org/ftp/Specs/archive/38_series/38.900/38900-f00.zip 102

[188] ——, "TR 38.901 Study on channel model for frequencies from 0.5 to 100 GHz (Release 16)," 3rd Generation Partnership Project, Tech. Rep. V16.1.0, Dec 2019, technical Specification Group Radio Access Network. [Online]. Available: https://www.3gpp.org/ftp/Specs/archive/38_series/38.901/38901-g10.zip 102

[189] M. Andrews, "Instability of the proportional fair scheduling algorithm for HDR," *IEEE Transactions on Wireless Communications*, vol. 3, no. 5, pp. 1422–1426, Sep 2004. 102

[190] R. R. Paulo and F. J. Velez, "LTE-SIM-ITU-R-M.2135-1," https://github.com/RRP-IT/LTE-SIM-ITU-R-M.2135-1.git, 2020. 104, 119, 165

[191] 3GPP, "TS 36.213 Physical layer procedures Transport block size table (Release 16)," 3rd Generation Partnership Project, Tech. Rep. V16.2.0, July 2020. [Online]. Available: https://www.3gpp.org/ftp/Specs/archive/36_series/36.213/36213-g20.zip 107

[192] ITU-T, "SERIES G: TRANSMISSION SYSTEMS AND MEDIA, DIGITAL SYSTEMS AND NETWORKS," ITU, Tech. Rep. ITU-T Recommendation G.114, 05 2003. [Online]. Available: https://www.itu.int/rec/T-REC-G.114-200305-I/en 113

[193] ——, "SERIES G: TRANSMISSION SYSTEMS AND MEDIA, DIGITAL SYSTEMS AND NETWORKS," ITU, Tech. Rep. ITU-T Recommendation G.107, 05 2003. [Online]. Available: https://www.itu.int/rec/T-REC-G.107-201506-I/en 113

[194] I. Budhiraja, S. Tyagi, S. Tanwar, N. Kumar, and M. Guizani, "Cross Layer NOMA Interference Mitigation for Femtocell Users in 5G Environment," *IEEE Transactions on Vehicular Technology*, vol. 68, no. 5, pp. 4721–4733, May 2019. 122

[195] B. Khamidehi and M. Sabbaghian, "Resource Allocation for SC-FDMA Femtocell Networks," *IEEE Transactions on Vehicular Technology*, vol. 68, no. 5, pp. 4573–4585, May 2019. 122

[196] Z. Liu, L. Gao, Y. Liu, X. Guan, K. Ma, and Y. Wang, "Efficient QoS Support for Robust Resource Allocation in Blockchain-Based Femtocell Networks," *IEEE Transactions on Industrial Informatics*, vol. 16, no. 11, pp. 7070–7080, Nov 2020. 122

[197] Z. Liu, P. Zhang, K. Y. Chan, K. Ma, and L. Li, "Robust Power Allocation for Femtocell Networks Using Fuzzy Estimation of Dynamic Channel States," *IEEE Access*, vol. 7, pp. 22 872–22 883, 2019. 123

[198] Z. Liu, Y. Yuan, H. Yuan, and X. Guan, "Power Allocation Based on Proportional-Integral Controller in Femtocell Networks With Consideration of Maximum Power Constraint," *IEEE Systems Journal*, vol. 13, no. 1, pp. 88–97, March 2019. 123

[199] J. Ghosh, "A Trade-Off Between Energy Efficiency and Spectral Efficiency in Macro-Femtocell Networks," *IEEE Transactions on Vehicular Technology*, vol. 69, no. 10, pp. 10 914–10 924, Oct 2020. 123

[200] I. Budhiraja, N. Kumar, S. Tyagi, S. Tanwar, and M. Guizani, "An Energy-Efficient Resource Allocation Scheme for SWIPT-NOMA Based Femtocells Users With Imperfect CSI," *IEEE Transactions on Vehicular Technology*, vol. 69, no. 7, pp. 7790–7805, July 2020. 123

[201] W. Chang, W.-Y. Cheng, Z.-T. Meng, and S.-L. Su, "Energy-Efficient Sleep Strategy With Variant Sleep Depths for Open-Access Femtocell Networks," *IEEE Communications Letters*, vol. 23, no. 4, pp. 708–711, April 2019. 124

[202] Y. Liu, L. Hao, Z. Liu, K. Sharif, Y. Wang, and S. K. Das, "Mitigating Interference via Power Control for Two-Tier Femtocell Networks: A Hierarchical Game Approach," *IEEE Transactions on Vehicular Technology*, vol. 68, no. 7, pp. 7194–7198, July 2019. 124

[203] K. Yan, H.-C. Wu, S.-H. Fang, C. Wang, S. Li, and L. Zhang, "Indoor Femtocell Interference Localization," *IEEE Transactions on Wireless Communications*, vol. 19, no. 8, pp. 5176–5187, Aug 2020. 124

[204] C. Liu, P. Huang, L. Xiao, and A. Esfahanian, "Inter-Femtocell Interference Identification and Resource Management," *IEEE Transactions on Mobile Computing*, vol. 19, no. 1, pp. 116–129, Jan 2020. 124

[205] J. Mitola, "Software radios-survey, critical evaluation and future directions," in *[Proceedings] NTC-92: National Telesystems Conference*, May 1992, pp. 13/15–13/23. 124

[206] G. R. project. (2021) GNU Radio. [Online]. Available: https://www.gnuradio.org/ 124

[207] S. E. Zegrar, A. E. Duranay, and H. Arslan, "Precoding Based Cross-Tier Interference Mitigation in Centralized-RAN," *IEEE Wireless Communications Letters*, vol. 10, no. 1, pp. 21–25, Jan 2021. 124

[208] A. Pratap, R. Misra, and S. K. Das, "Maximizing Fairness for Resource Allocation in Heterogeneous 5G Networks," *IEEE Transactions on Mobile Computing*, vol. 20, no. 2, pp. 603–619, Feb 2021. 125

[209] Y. Xu, G. Gui, T. Ohtsuki, H. Gacanin, B. Adebisi, H. Sari, and F. Adachi, "Robust Resource Allocation for Two-Tier HetNets: An Interference-Efficiency Perspective," *IEEE Transactions on Green Communications and Networking*, pp. 1–1, 2021. 125

[210] A. Mukherjee, P. Deb, D. De, and M. S. Obaidat, "WmA-MiFN: A Weighted Majority and Auction Game Based Green Ultra-Dense Micro-Femtocell Network System," *IEEE Systems Journal*, vol. 14, no. 1, pp. 353–362, March 2020. 125

[211] Y. Xu, H. Xie, and R. Q. Hu, "Max-Min Beamforming Design for Heterogeneous Networks With Hardware Impairments," *IEEE Communications Letters*, vol. 25, no. 4, pp. 1328–1332, April 2021. 125

[212] W. Hoiles, S. M. S. Tanzil, and V. Krishnamurthy, "Risk-Averse Caching Policies for YouTube Content in Femtocell Networks using Density Forecasting," *IEEE Transactions on Cloud Computing*, vol. 9, no. 1, pp. 331–346, Jan 2021. 125

[213] M. Lin, N. Bartolini, M. Giallorenzo, and T. F. La Porta, "On Interference Aware Power Adjustment and Scheduling in Femtocell Networks," *IEEE/ACM Transactions on Networking*, vol. 28, no. 2, pp. 736–749, April 2020. 126

[214] I. A. Alablani and M. A. Arafah, "An Adaptive Cell Selection Scheme for 5G Heterogeneous Ultra-Dense Networks," *IEEE Access*, vol. 9, pp. 64 224–64 240, 2021. 126

[215] R. Avanzato and F. Beritelli, "A Smart UAV-Femtocell Data Sensing System for Post-Earthquake Localization of People," *IEEE Access*, vol. 8, pp. 30 262–30 270, 2020. 126

[216] Q. Chen, D. Han, M. Zhang, Z. Ghassemlooy, A. C. Boucouvalas, Z. Zhang, T. Li, and X. Jiang, "Design and Demonstration of a TDD-Based Central-Coordinated Resource-Reserved Multiple Access (CRMA) Scheme for Bidirectional VLC Networking," *IEEE Access*, vol. 9, pp. 7856–7868, 2021. 126

[217] S. Liverman, H. Bialek, A. Natarajan, and A. X. Wang, "VCSEL Array-Based Gigabit Free-Space Optical Femtocell Communication," *Journal of Lightwave Technology*, vol. 38, no. 7, pp. 1659–1667, April 2020. 126

Appendix A

Mathematica© Code to Determine the Average SINR

This Appendix addresses the implementation of the code developed in Wolfram Mathematica©, [118] to determine the average signal-to-interference-plus-noise ratio (SINR) in the 5x5 apartment scenario, where all apartments have home eNodeBs (HeNBs) and reuse pattern 2 is considered. The detailed process do obtain the average SINR is presented in Figure A.1.
The path loss of the interference signal, imposed to the user equipment for each tier of interference is present in Figures A.2, A.3 and A.4. Then the average interference power could be determined for each tier or a combination of the existing tiers Figure A.5, A.6 and A.7.
The path loss of the received signal from the own cell is hampered by the consideration of the Fraunhofer distance, Figures 2.6. As the integral of sum of two or more functions is equal to the sum of their integrals, the path loss calculus is divided into two parts, as follows. A constant part, as shown in Figure A.8, and a variable part, as shown in Figure A.9. After the determination of the path loss, it is possible to determine the average power, as shown in Figure A.10.
With the average received powers from the interference nodes and own cells it is possible to determine the average SINR, as shown in Figures A.11, A.12 and A.13. Results for the average SINR (computed by integrating SINR at given positions) are analyzed in the view chart from Section 2.3.2.

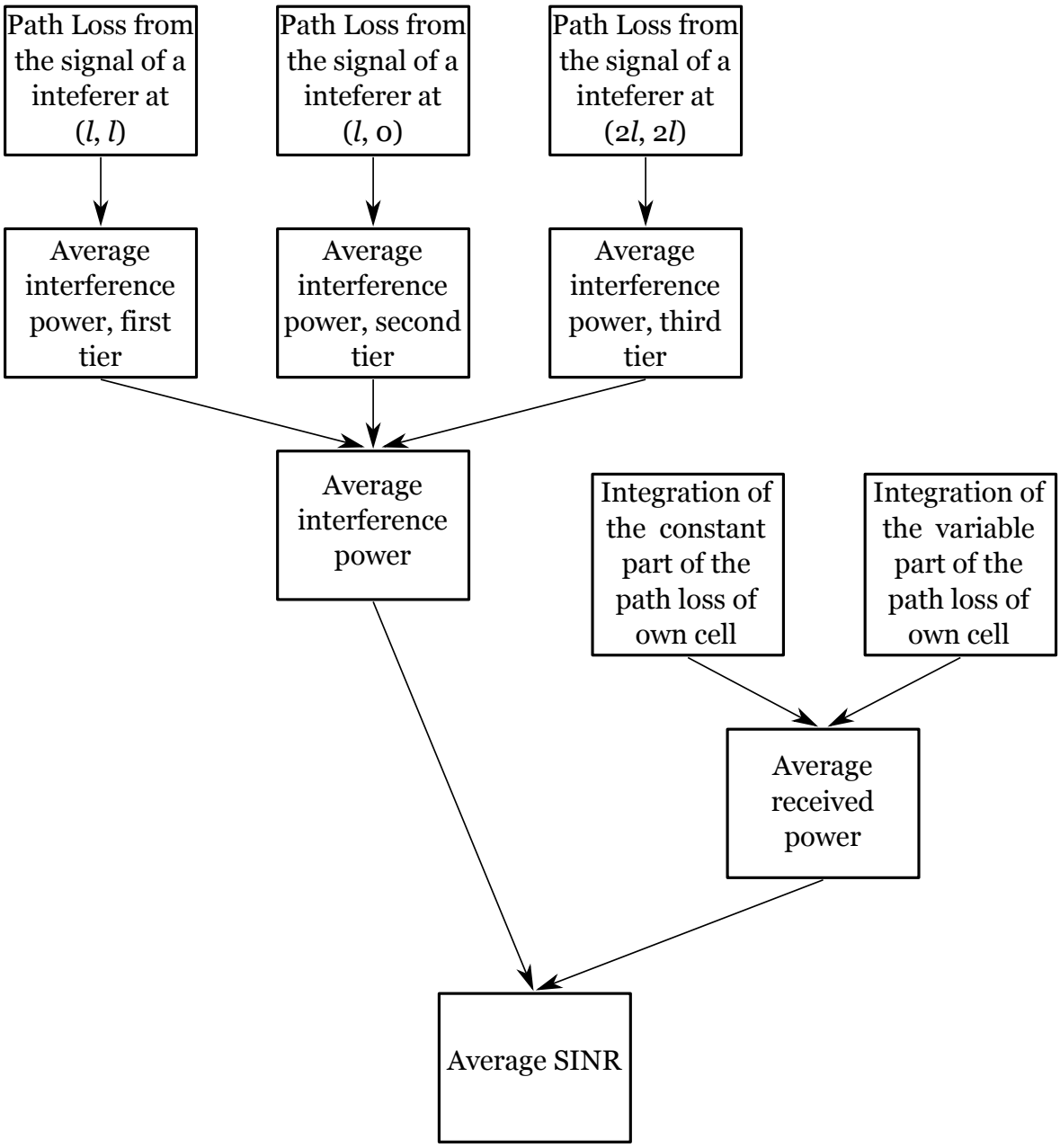

Figure A.1: Flowchart do determine the average SINR.

```
ClearAll["Global`*"]

Femto =
 Integrate[Log[(x - L)^2 + (y - L)^2], {y, -L/2, L/2}, {x, -L/2, L/2}]/Log[10]
```

$$-\frac{L^2\left(24+18\,\pi-20\,\text{ArcTan}\left[\frac{1}{3}\right]-52\,\text{ArcTan}[3]-\text{Log}\left[\frac{150\,094\,635\,296\,999\,121}{62\,500\,000\,000}\right]-8\,\text{Log}\left[L^2\right]\right)}{8\,\text{Log}[10]}$$

```
VarConst =
 Integrate[46.4 + 20 * Log[10, 2/5] + 2 * 10, {y, -L/2, L/2}, {x, -L/2, L/2}]
```

$$58.4412\,L^2$$

```
PLfemto = 20 * 0.5 * (Femto) + VarConst
```

$$58.4412\,L^2-0.542868\,L^2\left(24+18\,\pi-20\,\text{ArcTan}\left[\frac{1}{3}\right]-52\,\text{ArcTan}[3]-\text{Log}\left[\frac{150\,094\,635\,296\,999\,121}{62\,500\,000\,000}\right]-8\,\text{Log}\left[L^2\right]\right)$$

```
PLtier1 = PLfemto
```

$$58.4412\,L^2-0.542868\,L^2\left(24+18\,\pi-20\,\text{ArcTan}\left[\frac{1}{3}\right]-52\,\text{ArcTan}[3]-\text{Log}\left[\frac{150\,094\,635\,296\,999\,121}{62\,500\,000\,000}\right]-8\,\text{Log}\left[L^2\right]\right)$$

Figure A.2: Path Loss from the signal of a interferer at (l, l).

```
ClearAll["Global`*"]

Femto =
 Integrate[Log[(x - 2 * L)^2 + (y)^2], {y, -L/2, L/2}, {x, -L/2, L/2}]/Log[10]
```

$$-\frac{1}{2\,\text{Log}[10]}L^2\left(6+8\,\pi+18\,\text{ArcCot}[3]-50\,\text{ArcCot}[5]+10\,\text{ArcTan}[3]-26\,\text{ArcTan}[5]-5\,\text{Log}[13]+\text{Log}[500]-2\,\text{Log}\left[L^2\right]\right)$$

```
VarConst =
 Integrate[46.4 + 20 * Log[10, 2/5] + 2 * 10, {y, -L/2, L/2}, {x, -L/2, L/2}]
```

$$58.4412\,L^2$$

```
PLfemto = 20 * 0.5 * (Femto) + VarConst
```

$$58.4412\,L^2-2.17147\,L^2\left(6+8\,\pi+18\,\text{ArcCot}[3]-50\,\text{ArcCot}[5]+10\,\text{ArcTan}[3]-26\,\text{ArcTan}[5]-5\,\text{Log}[13]+\text{Log}[500]-2\,\text{Log}\left[L^2\right]\right)$$

```
PLtier1 = PLfemto
```

$$58.4412\,L^2-2.17147\,L^2\left(6+8\,\pi+18\,\text{ArcCot}[3]-50\,\text{ArcCot}[5]+10\,\text{ArcTan}[3]-26\,\text{ArcTan}[5]-5\,\text{Log}[13]+\text{Log}[500]-2\,\text{Log}\left[L^2\right]\right)$$

Figure A.3: Path Loss from the signal of a interferer at $(l, 0)$.

```
ClearAll["Global`*"]
```

```
Femto = Integrate[Log[(x - 2 * L) ^ 2 + (y - 2 * L) ^ 2],
    {y, -L / 2, L / 2}, {x, -L / 2, L / 2}] / Log[10]
```

$$-\frac{1}{2\,\text{Log}[10]}\,L^2\left(6+17\,\pi-26\,\text{ArcTan}\left[\frac{3}{5}\right]-42\,\text{ArcTan}\left[\frac{5}{3}\right]-9\,\text{Log}[3]+\text{Log}[4]-25\,\text{Log}[5]+15\,\text{Log}[17]-2\,\text{Log}\left[L^2\right]\right)$$

```
VarConst =
 Integrate[46.4 + 20 * Log[10, 2 / 5] + 4 * 10, {y, -L / 2, L / 2}, {x, -L / 2, L / 2}]
```

$$78.4412\,L^2$$

```
PLfemto = 20 * 0.5 * (Femto) + VarConst
```

$$78.4412\,L^2-2.17147\,L^2\left(6+17\,\pi-26\,\text{ArcTan}\left[\frac{3}{5}\right]-42\,\text{ArcTan}\left[\frac{5}{3}\right]-9\,\text{Log}[3]+\text{Log}[4]-25\,\text{Log}[5]+15\,\text{Log}[17]-2\,\text{Log}\left[L^2\right]\right)$$

```
PLtier1 = PLfemto
```

$$78.4412\,L^2-2.17147\,L^2\left(6+17\,\pi-26\,\text{ArcTan}\left[\frac{3}{5}\right]-42\,\text{ArcTan}\left[\frac{5}{3}\right]-9\,\text{Log}[3]+\text{Log}[4]-25\,\text{Log}[5]+15\,\text{Log}[17]-2\,\text{Log}\left[L^2\right]\right)$$

Figure A.4: Path Loss from the signal of a interferer at $(2l, 2l)$.

```
ClearAll["Global`*"]
```

```
PLtier1 = 58.441199826559256` L^2 - 0.5428681023790647` L^2
    (24 + 18 π - 20 ArcTan[1/3] - 52 ArcTan[3] - Log[150 094 635 296 999 121/62 500 000 000] - 8 Log[L^2])
```

$$58.4412\,L^2 - 0.542868\,L^2 \left(24 + 18\,\pi - 20\,\text{ArcTan}\left[\frac{1}{3}\right] - 52\,\text{ArcTan}[3] - \text{Log}\left[\frac{150\,094\,635\,296\,999\,121}{62\,500\,000\,000}\right] - 8\,\text{Log}\left[L^2\right]\right)$$

```
Pt = 10^((P - 30)/10)
Gt = 10^(5/10)
Gr = 10^(0/10)
Acell = L^2
Const = Pt * Gt * Gr
```

$$10^{\frac{1}{10}(-30+P)}$$

$$\sqrt{10}$$

$$1$$

$$L^2$$

$$10^{\frac{1}{2}+\frac{1}{10}(-30+P)}$$

```
Pnhtier = Const * 10^(-PLtier1/(10 * Acell))
```

$$10^{\frac{1}{2}+\frac{1}{10}(-30+P)+\frac{-58.4412\,L^2+0.542868\,L^2\left(24+18\,\pi-20\,\text{ArcTan}\left[\frac{1}{3}\right]-52\,\text{ArcTan}[3]-\text{Log}\left[\frac{150\,094\,635\,296\,999\,121}{62\,500\,000\,000}\right]-8\,\text{Log}\left[L^2\right]\right)}{10\,L^2}}$$

```
Pnhtier1 = 4 * Pnhtier
```

$$2^{\frac{5}{2}+\frac{1}{10}(-30+P)+\frac{-58.4412\,L^2+0.542868\,L^2\left(24+18\,\pi-20\,\text{ArcTan}\left[\frac{1}{3}\right]-52\,\text{ArcTan}[3]-\text{Log}\left[\frac{150\,094\,635\,296\,999\,121}{62\,500\,000\,000}\right]-8\,\text{Log}\left[L^2\right]\right)}{10\,L^2}} \times$$
$$5^{\frac{1}{2}+\frac{1}{10}(-30+P)+\frac{-58.4412\,L^2+0.542868\,L^2\left(24+18\,\pi-20\,\text{ArcTan}\left[\frac{1}{3}\right]-52\,\text{ArcTan}[3]-\text{Log}\left[\frac{150\,094\,635\,296\,999\,121}{62\,500\,000\,000}\right]-8\,\text{Log}\left[L^2\right]\right)}{10\,L^2}}$$

Figure A.5: Average interference power, first tier.

```
ClearAll["Global`*"]
```

```
PLtier1 = 58.441199826559256` L^2 -
  2.1714724095162588` L^2 (6 + 8 π + 18 ArcCot[3] - 50 ArcCot[5] +
     10 ArcTan[3] - 26 ArcTan[5] - 5 Log[13] + Log[500] - 2 Log[L^2])
```

$$58.4412\ L^2 - 2.17147\ L^2\ \left(6 + 8\,\pi + 18\ \text{ArcCot}[3] - 50\ \text{ArcCot}[5] + 10\ \text{ArcTan}[3] - 26\ \text{ArcTan}[5] - 5\ \text{Log}[13] + \text{Log}[500] - 2\ \text{Log}\left[L^2\right]\right)$$

```
Pt = 10^((P - 30) / 10)
Gt = 10^(5 / 10)
Gr = 10^(0 / 10)
Acell = L^2
Const = Pt * Gt * Gr
```

$$10^{\frac{1}{10}\,(-30+P)}$$

$$\sqrt{10}$$

$$1$$

$$L^2$$

$$10^{\frac{1}{2}+\frac{1}{10}\,(-30+P)}$$

```
Pnhtier = Const * 10^(-PLtier1 / (10 * Acell))
```

$$10^{\frac{1}{2}+\frac{1}{10}\,(-30+P)+\frac{-58.4412\,L^2+2.17147\,L^2\,\left(6+8\,\pi+18\,\text{ArcCot}[3]-50\,\text{ArcCot}[5]+10\,\text{ArcTan}[3]-26\,\text{ArcTan}[5]-5\,\text{Log}[13]+\text{Log}[500]-2\,\text{Log}[L^2]\right)}{10\,L^2}}$$

```
Pnhtier1 = 4 * Pnhtier
```

$$2^{\frac{5}{2}+\frac{1}{10}\,(-30+P)+\frac{-58.4412\,L^2+2.17147\,L^2\,\left(6+8\,\pi+18\,\text{ArcCot}[3]-50\,\text{ArcCot}[5]+10\,\text{ArcTan}[3]-26\,\text{ArcTan}[5]-5\,\text{Log}[13]+\text{Log}[500]-2\,\text{Log}[L^2]\right)}{10\,L^2}}\times$$
$$5^{\frac{1}{2}+\frac{1}{10}\,(-30+P)+\frac{-58.4412\,L^2+2.17147\,L^2\,\left(6+8\,\pi+18\,\text{ArcCot}[3]-50\,\text{ArcCot}[5]+10\,\text{ArcTan}[3]-26\,\text{ArcTan}[5]-5\,\text{Log}[13]+\text{Log}[500]-2\,\text{Log}[L^2]\right)}{10\,L^2}}$$

Figure A.6: Average interference power, second tier.

```
ClearAll["Global`*"]
```

```
PLtier1 = 78.44119982655926` L^2 -
  2.1714724095162588` L^2 (6 + 17 π - 26 ArcTan[3/5] - 42 ArcTan[5/3] -
     9 Log[3] + Log[4] - 25 Log[5] + 15 Log[17] - 2 Log[L^2])
```

$$78.4412\,L^2 - 2.17147\,L^2\left(6 + 17\,\pi - 26\,\text{ArcTan}\left[\frac{3}{5}\right] - 42\,\text{ArcTan}\left[\frac{5}{3}\right] - 9\,\text{Log}[3] + \text{Log}[4] - 25\,\text{Log}[5] + 15\,\text{Log}[17] - 2\,\text{Log}\left[L^2\right]\right)$$

```
Pt = 10^((P - 30)/10)
Gt = 10^(5/10)
Gr = 10^(0/10)
Acell = L^2
Const = Pt * Gt * Gr
```

$$10^{\frac{1}{10}(-30+P)}$$

$$\sqrt{10}$$

$$1$$

$$L^2$$

$$10^{\frac{1}{2}+\frac{1}{10}(-30+P)}$$

```
Pnhtier = Const * 10^(-PLtier1/(10 * Acell))
```

$$10^{\frac{1}{2}+\frac{1}{10}(-30+P)+\frac{-78.4412\,L^2+2.17147\,L^2\left(6+17\,\pi-26\,\text{ArcTan}\left[\frac{3}{5}\right]-42\,\text{ArcTan}\left[\frac{5}{3}\right]-9\,\text{Log}[3]+\text{Log}[4]-25\,\text{Log}[5]+15\,\text{Log}[17]-2\,\text{Log}\left[L^2\right]\right)}{10\,L^2}}$$

```
Pnhtier1 = 4 * Pnhtier
```

$$2^{\frac{5}{2}+\frac{1}{10}(-30+P)+\frac{-78.4412\,L^2+2.17147\,L^2\left(6+17\,\pi-26\,\text{ArcTan}\left[\frac{3}{5}\right]-42\,\text{ArcTan}\left[\frac{5}{3}\right]-9\,\text{Log}[3]+\text{Log}[4]-25\,\text{Log}[5]+15\,\text{Log}[17]-2\,\text{Log}\left[L^2\right]\right)}{10\,L^2}}\times$$
$$5^{\frac{1}{2}+\frac{1}{10}(-30+P)+\frac{-78.4412\,L^2+2.17147\,L^2\left(6+17\,\pi-26\,\text{ArcTan}\left[\frac{3}{5}\right]-42\,\text{ArcTan}\left[\frac{5}{3}\right]-9\,\text{Log}[3]+\text{Log}[4]-25\,\text{Log}[5]+15\,\text{Log}[17]-2\,\text{Log}\left[L^2\right]\right)}{10\,L^2}}$$

Figure A.7: Average interference power, third tier.

```
In[1]:= Const1 = Integrate[(46.8 + 20 * Log[10, 2/5]) * r, r]
Out[1]= 19.4206 r^2

In[2]:= r = L/2 * (1/Cos[t])
Out[2]= 1/2 L Sec[t]

In[3]:= Rs = Const1
Out[3]= 4.85515 L^2 Sec[t]^2

In[4]:= r = F
Out[4]= F

In[5]:= Ri = Const1
Out[5]= 19.4206 F^2

In[6]:= Rt = Rs - Ri
Out[6]= -19.4206 F^2 + 4.85515 L^2 Sec[t]^2

In[7]:= Ipt = Integrate[Rt, t]
Out[7]= -19.4206 F^2 t + 4.85515 L^2 Tan[t]

In[8]:= t = Pi/4
Out[8]= π/4

In[9]:= Ts = Ipt
Out[9]= -15.2529 F^2 + 4.85515 L^2

In[10]:= t = -Pi/4
Out[10]= -π/4

In[11]:= Ti = Ipt
Out[11]= 15.2529 F^2 - 4.85515 L^2

In[12]:= Ttotal = Ts - Ti
Out[12]= -30.5058 F^2 + 9.7103 L^2

In[13]:= Itotal = 4 * Ttotal
Out[13]= 4 (-30.5058 F^2 + 9.7103 L^2)
```

Figure A.8: Integration of the constant part of the path loss of own cell.

In[1]:= `ClearAll["Global`*"]`

In[2]:= `Ipr = Integrate[r * Log[r], r]`

Out[2]= $-\frac{r^2}{4} + \frac{1}{2} r^2 \text{Log}[r]$

In[3]:= `r = L / 2 * (1 / Cos[t])`

Out[3]= $\frac{1}{2} L \text{Sec}[t]$

In[4]:= `Rs = Ipr`

Out[4]= $-\frac{1}{16} L^2 \text{Sec}[t]^2 + \frac{1}{8} L^2 \text{Log}\left[\frac{1}{2} L \text{Sec}[t]\right] \text{Sec}[t]^2$

In[5]:= `r = F`

Out[5]= F

In[6]:= `Ri = Ipr`

Out[6]= $-\frac{F^2}{4} + \frac{1}{2} F^2 \text{Log}[F]$

In[7]:= `Rt = Rs - Ri`

Out[7]= $\frac{F^2}{4} - \frac{1}{2} F^2 \text{Log}[F] - \frac{1}{16} L^2 \text{Sec}[t]^2 + \frac{1}{8} L^2 \text{Log}\left[\frac{1}{2} L \text{Sec}[t]\right] \text{Sec}[t]^2$

In[8]:= `Ipt = Integrate[Rt, t]`

Out[8]= $\frac{F^2 t}{4} + \frac{L^2 t}{8} - \frac{1}{2} F^2 t \text{Log}[F] - \frac{3}{16} L^2 \text{Tan}[t] + \frac{1}{8} L^2 \text{Log}\left[\frac{1}{2} L \text{Sec}[t]\right] \text{Tan}[t]$

In[9]:= `t = Pi / 4`

Out[9]= $\frac{\pi}{4}$

In[10]:= `Ts = Ipt`

Out[10]= $-\frac{3 L^2}{16} + \frac{F^2 \pi}{16} + \frac{L^2 \pi}{32} - \frac{1}{8} F^2 \pi \text{Log}[F] + \frac{1}{8} L^2 \text{Log}\left[\frac{L}{\sqrt{2}}\right]$

In[11]:= `t = -Pi / 4`

Out[11]= $-\frac{\pi}{4}$

In[12]:= `Ti = Ipt`

Out[12]= $\frac{3 L^2}{16} - \frac{F^2 \pi}{16} - \frac{L^2 \pi}{32} + \frac{1}{8} F^2 \pi \text{Log}[F] - \frac{1}{8} L^2 \text{Log}\left[\frac{L}{\sqrt{2}}\right]$

In[13]:= `Ttotal = Ts - Ti`

Out[13]= $-\frac{3 L^2}{8} + \frac{F^2 \pi}{8} + \frac{L^2 \pi}{16} - \frac{1}{4} F^2 \pi \text{Log}[F] + \frac{1}{4} L^2 \text{Log}\left[\frac{L}{\sqrt{2}}\right]$

In[14]:= `Itotal = 4 * 2 * Ttotal`

Out[14]= $8 \left(-\frac{3 L^2}{8} + \frac{F^2 \pi}{8} + \frac{L^2 \pi}{16} - \frac{1}{4} F^2 \pi \text{Log}[F] + \frac{1}{4} L^2 \text{Log}\left[\frac{L}{\sqrt{2}}\right]\right)$

In[15]:= `FemtoPropria = Itotal / (Log[10])`

Out[15]= $\frac{8 \left(-\frac{3 L^2}{8} + \frac{F^2 \pi}{8} + \frac{L^2 \pi}{16} - \frac{1}{4} F^2 \pi \text{Log}[F] + \frac{1}{4} L^2 \text{Log}\left[\frac{L}{\sqrt{2}}\right]\right)}{\text{Log}[10]}$

Figure A.9: Integration of the variable part of the path loss of own cell.

```
In[1]:= ClearAll["Global`*"]

In[2]:= PLow = 4 (-8.666364207076656` + 9.710299956639812` L^2) +
          64.97045449272646` (0.2519580214951882` - 3 L^2/8 + L^2 π/16 + 1/4 L^2 Log[L/Sqrt[2]])

Out[2]= 4 (-8.66636 + 9.7103 L^2) + 64.9705 (0.251958 - 3 L^2/8 + L^2 π/16 + 1/4 L^2 Log[L/Sqrt[2]])

In[3]:= Pt = 10^((P - 30)/10)
        Gt = 10^(5/10)
        Gr = 10^(0/10)
        Aowcell = L^2 - Pi * 0.533 * 0.533
        Const = Pt * Gt * Gr
        F = 0.533

Out[3]= 10^(1/10 (-30+P))

Out[4]= Sqrt[10]

Out[5]= 1

Out[6]= -0.892492 + L^2

Out[7]= 10^(1/2 + 1/10 (-30+P))

Out[8]= 0.533

In[9]:= Pow = Const * 10^(-PLow/(10 * Aowcell))

Out[9]= 10^(1/2 + 1/10 (-30+P) + (-4 (-8.66636+9.7103 L^2) - 64.9705 (0.251958 - 3 L^2/8 + L^2 π/16 + 1/4 L^2 Log[L/Sqrt[2]]))/(10 (-0.892492+L^2)))
```

Figure A.10: Average received power of the own cell.

In[1]:=
```
ClearAll["Global`*"]
```

In[2]:=
```
noise = 10^(-129.01/10)
```

Out[2]=
$$1.25603\times 10^{-13}$$

In[3]:=
```
Pow = 10^(1/2+1/10 (-30+P)+(-4 (-8.666364207076656`+9.710299956639812` L^2)-64.97045449272646` (0.2519580214951882`-3 L^2/8+L^2 π/16+1/4 L^2 Log[1/Sqrt[2]]))/(10 (-0.8924919153656709`+L^2)))
```

Out[3]=
$$10^{\frac{1}{2}+\frac{1}{10}(-30+P)+\frac{-4\left(-8.66636+9.7103\,L^2\right)-64.9705\left(0.251958-\frac{3L^2}{8}+\frac{L^2\pi}{16}+\frac{1}{4}L^2\,\text{Log}\left[\frac{1}{\sqrt{2}}\right]\right)}{10\left(-0.892492+L^2\right)}}$$

In[4]:=
```
Pnh = 2^(5/2+1/10 (-30+P)+(-58.441199826559256` L^2+0.5428681023790647` L^2 (24+18 π-20 ArcTan[1/3]-52 ArcTan[3]-Log[150094635296999121/62500000000]-8 Log[L^2]))/(10 L^2)) ×
  5^(1/2+1/10 (-30+P)+(-58.441199826559256` L^2+0.5428681023790647` L^2 (24+18 π-20 ArcTan[1/3]-52 ArcTan[3]-Log[150094635296999121/62500000000]-8 Log[L^2]))/(10 L^2))
```

Out[4]=
$$2^{\frac{5}{2}+\frac{1}{10}(-30+P)+\frac{-58.4412\,L^2+0.542868\,L^2\left(24+18\,\pi-20\,\text{ArcTan}\left[\frac{1}{3}\right]-52\,\text{ArcTan}[3]-\text{Log}\left[\frac{150094635296999121}{62500000000}\right]-8\,\text{Log}\left[L^2\right]\right)}{10\,L^2}}\times 5^{\frac{1}{2}+\frac{1}{10}(-30+P)+\frac{-58.4412\,L^2+0.542868\,L^2\left(24+18\,\pi-20\,\text{ArcTan}\left[\frac{1}{3}\right]-52\,\text{ArcTan}[3]-\text{Log}\left[\frac{150094635296999121}{62500000000}\right]-8\,\text{Log}\left[L^2\right]\right)}{10\,L^2}}$$

In[5]:=
```
SINR = Pow/(Pnh + noise)
```

Out[5]=
$$10^{\frac{1}{2}+\frac{1}{10}(-30+P)+\frac{-4\left(-8.66636+9.7103\,L^2\right)-64.9705\left(0.251958-\frac{3L^2}{8}+\frac{L^2\pi}{16}+\frac{1}{4}L^2\,\text{Log}\left[\frac{1}{\sqrt{2}}\right]\right)}{10\left(-0.892492+L^2\right)}}\Big/\left(1.25603\times 10^{-13}+2^{\frac{5}{2}+\frac{1}{10}(-30+P)+\frac{-58.4412\,L^2+0.542868\,L^2\left(24+18\,\pi-20\,\text{ArcTan}\left[\frac{1}{3}\right]-52\,\text{ArcTan}[3]-\text{Log}\left[\frac{150094635296999121}{62500000000}\right]-8\,\text{Log}\left[L^2\right]\right)}{10\,L^2}}\times 5^{\frac{1}{2}+\frac{1}{10}(-30+P)+\frac{-58.4412\,L^2+0.542868\,L^2\left(24+18\,\pi-20\,\text{ArcTan}\left[\frac{1}{3}\right]-52\,\text{ArcTan}[3]-\text{Log}\left[\frac{150094635296999121}{62500000000}\right]-8\,\text{Log}\left[L^2\right]\right)}{10\,L^2}}\right)$$

In[6]:=
```
SINRDB = 10 * Log[10, SINR]
```

Out[6]=
$$\frac{1}{\text{Log}[10]}10\,\text{Log}\left[10^{\frac{1}{2}+\frac{1}{10}(-30+P)+\frac{-4\left(-8.66636+9.7103\,L^2\right)-64.9705\left(0.251958-\frac{3L^2}{8}+\frac{L^2\pi}{16}+\frac{1}{4}L^2\,\text{Log}\left[\frac{1}{\sqrt{2}}\right]\right)}{10\left(-0.892492+L^2\right)}}\Big/\left(1.25603\times 10^{-13}+2^{\frac{5}{2}+\frac{1}{10}(-30+P)+\frac{-58.4412\,L^2+0.542868\,L^2\left(24+18\,\pi-20\,\text{ArcTan}\left[\frac{1}{3}\right]-52\,\text{ArcTan}[3]-\text{Log}\left[\frac{150094635296999121}{62500000000}\right]-8\,\text{Log}\left[L^2\right]\right)}{10\,L^2}}\times 5^{\frac{1}{2}+\frac{1}{10}(-30+P)+\frac{-58.4412\,L^2+0.542868\,L^2\left(24+18\,\pi-20\,\text{ArcTan}\left[\frac{1}{3}\right]-52\,\text{ArcTan}[3]-\text{Log}\left[\frac{150094635296999121}{62500000000}\right]-8\,\text{Log}\left[L^2\right]\right)}{10\,L^2}}\right)\right]$$

```
1/Log[10] 10 Log[10^(1/2+1/10 (-30+P)+(-4 (-8.666364207076656`+9.710299956639812` L^2)-64.97045449272646` (0.2519580214951882`-3 L^2/8+L^2 π/16+1/4 L^2 Log[1/Sqrt[2]]))/(10 (-0.8924919153656709`+L^2)))/
  (1.25603 10^-13 + 2^(5/2+1/10 (-30+P)+(-58.4412 L^2+0.542868 L^2 (24+18 π-20 ArcTan[1/3]-52 ArcTan[3]-Log[150094635296999121/62500000000]-8 Log[L^2]))/(10 L^2)) ×
    5^(1/2+1/10 (-30+P)+(-58.4412 L^2+0.542868 L^2 (24+18 π-20 ArcTan[1/3]-52 ArcTan[3]-Log[150094635296999121/62500000000]-8 Log[L^2]))/(10 L^2)))]
```

$$\frac{1}{\text{Log}[10]}10\,\text{Log}\left[10^{\frac{1}{2}+\frac{1}{10}(-30+P)+\frac{-4\left(-8.66636+9.7103\,L^2\right)-64.9705\left(0.251958-\frac{3L^2}{8}+\frac{L^2\pi}{16}+\frac{1}{4}L^2\,\text{Log}\left[\frac{1}{\sqrt{2}}\right]\right)}{10\left(-0.892492+L^2\right)}}\Big/\left(1.25603\times 10^{-13}+2^{\frac{5}{2}+\frac{1}{10}(-30+P)+\frac{-58.4412\,L^2+0.542868\,L^2\left(24+18\,\pi-20\,\text{ArcTan}\left[\frac{1}{3}\right]-52\,\text{ArcTan}[3]-\text{Log}\left[\frac{150094635296999121}{62500000000}\right]-8\,\text{Log}\left[L^2\right]\right)}{10\,L^2}}\times 5^{\frac{1}{2}+\frac{1}{10}(-30+P)+\frac{-58.4412\,L^2+0.542868\,L^2\left(24+18\,\pi-20\,\text{ArcTan}\left[\frac{1}{3}\right]-52\,\text{ArcTan}[3]-\text{Log}\left[\frac{150094635296999121}{62500000000}\right]-8\,\text{Log}\left[L^2\right]\right)}{10\,L^2}}\right)\right]$$

(a) First part

```
col[v_] := Hue[Rescale[v, {4, 50}]]

Plot3D[SINRDB, {P, -20, 35}, {L, 5, 35}, ColorFunction → col,
 ColorFunctionScaling → False, ViewPoint → {-Pi, Pi, Pi},
 AxesLabel → {"Transmitter Power [dBm]", "Apt. Side [m]", "Avg. SINR [dB]"},
 BaseStyle → { FontColor → Orange, FontSize → 16,
   FontFamily → "Times New Roman"}, ImageSize → Large ]
```

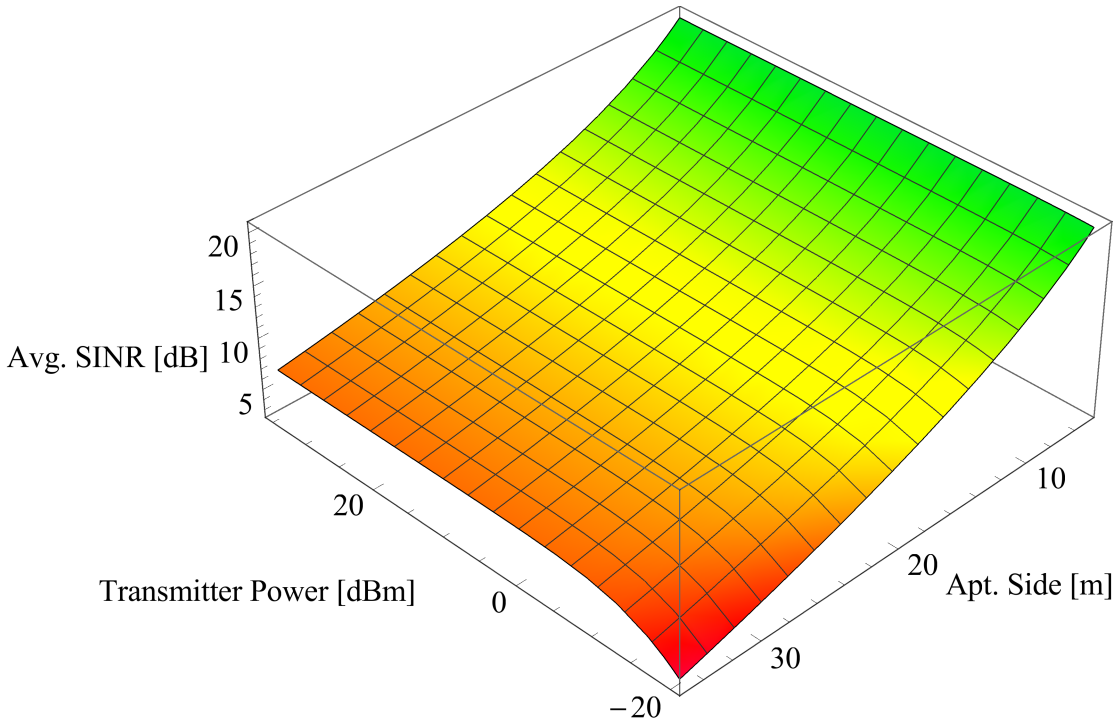

(b) Second part

Figure A.11: Computation of the Average SINR for the first tier of interference following the approach followed in Section 2.3.2.

```
ClearAll["Global`*"]
noise = 10^(-129.01/10)
```

$$1.25603 \times 10^{-13}$$

```
Pow = 10^(1/2 + 1/10 (-30 + P) + (-4 (-8.666364207076656` + 9.710299956639812` L^2) - 64.97045449272646` (0.2519580214951882` - 3 L^2/8 + L^2 π/16 + 1/4 L^2 Log[1/Sqrt[2]]))/(10 (-0.89249191536567 09` + L^2)))
```

$$10^{\frac{1}{2}+\frac{1}{10}(-30+P)+\frac{-4\left(-8.66636+9.7103\,L^2\right)-64.9705\left(0.251958-\frac{3L^2}{8}+\frac{L^2\pi}{16}+\frac{1}{4}L^2\,\text{Log}\left[\frac{1}{\sqrt{2}}\right]\right)}{10\left(-0.892492+L^2\right)}}$$

```
Pnh =
 2^(5/2 + 1/10 (-30 + P) + (-58.441199826559256` L^2 + 2.1714724095162588` L^2 (6 + 8 π + 18 ArcCot[3] - 50 ArcCot[5] + 10 ArcTan[3] - 26 ArcTan[5] - 5 Log[13] + Log[500] - 2 Log[L^2]))/(10 L^2)) ×
  5^(1/2 + 1/10 (-30 + P) + (-58.441199826559256` L^2 + 2.1714724095162588` L^2 (6 + 8 π + 18 ArcCot[3] - 50 ArcCot[5] + 10 ArcTan[3] - 26 ArcTan[5] - 5 Log[13] + Log[500] - 2 Log[L^2]))/(10 L^2))
```

$$2^{\frac{5}{2}+\frac{1}{10}(-30+P)+\frac{-58.4412\,L^2+2.17147\,L^2\left(6+8\,\pi+18\,\text{ArcCot}[3]-50\,\text{ArcCot}[5]+10\,\text{ArcTan}[3]-26\,\text{ArcTan}[5]-5\,\text{Log}[13]+\text{Log}[500]-2\,\text{Log}[L^2]\right)}{10\,L^2}}\times$$
$$5^{\frac{1}{2}+\frac{1}{10}(-30+P)+\frac{-58.4412\,L^2+2.17147\,L^2\left(6+8\,\pi+18\,\text{ArcCot}[3]-50\,\text{ArcCot}[5]+10\,\text{ArcTan}[3]-26\,\text{ArcTan}[5]-5\,\text{Log}[13]+\text{Log}[500]-2\,\text{Log}[L^2]\right)}{10\,L^2}}$$

```
SINR = Pow / (Pnh + noise)
```

$$10^{\frac{1}{2}+\frac{1}{10}(-30+P)+\frac{-4\left(-8.66636+9.7103\,L^2\right)-64.9705\left(0.251958-\frac{3L^2}{8}+\frac{L^2\pi}{16}+\frac{1}{4}L^2\,\text{Log}\left[\frac{1}{\sqrt{2}}\right]\right)}{10\left(-0.892492+L^2\right)}} \Big/ \left(1.25603\times10^{-13}+\right.$$
$$2^{\frac{5}{2}+\frac{1}{10}(-30+P)+\frac{-58.4412\,L^2+2.17147\,L^2\left(6+8\,\pi+18\,\text{ArcCot}[3]-50\,\text{ArcCot}[5]+10\,\text{ArcTan}[3]-26\,\text{ArcTan}[5]-5\,\text{Log}[13]+\text{Log}[500]-2\,\text{Log}[L^2]\right)}{10\,L^2}}\times$$
$$\left.5^{\frac{1}{2}+\frac{1}{10}(-30+P)+\frac{-58.4412\,L^2+2.17147\,L^2\left(6+8\,\pi+18\,\text{ArcCot}[3]-50\,\text{ArcCot}[5]+10\,\text{ArcTan}[3]-26\,\text{ArcTan}[5]-5\,\text{Log}[13]+\text{Log}[500]-2\,\text{Log}[L^2]\right)}{10\,L^2}}\right)$$

```
10^(1/2 + 1/10 (-30 + P) + (-4 (-8.666364207076656` + 9.710299956639812` L^2) - 64.97045449272646` (0.2519580214951882` - 3 L^2/8 + L^2 π/16 + 1/4 L^2 Log[1/Sqrt[2]]))/(10 (-05.8924919153656709` + L^2))) /
 (1.2560299636948753` *^-13 +
  2^(5/2 + 1/10 (-30 + P) + (-58.441199826559256` L^2 + 2.1714724095162588` L^2 (6 + 8 π + 18 ArcCot[3] - 50 ArcCot[5] + 10 ArcTan[3] - 26 ArcTan[5] - 5 Log[13] + Log[500] - 2 Log[L^2]))/(10 L^2)) ×
  5^(1/2 + 1/10 (-30 + P) + (-58.441199826559256` L^2 + 2.1714724095162588` L^2 (6 + 8 π + 18 ArcCot[3] - 50 ArcCot[5] + 10 ArcTan[3] - 26 ArcTan[5] - 5 Log[13] + Log[500] - 2 Log[L^2]))/(10 L^2))
 )
```

```
SINRDB = 10 * Log[10, SINR]
```

$$\frac{1}{\text{Log}[10]}\,10\,\text{Log}\left[10^{\frac{1}{2}+\frac{1}{10}(-30+P)+\frac{-4\left(-8.66636+9.7103\,L^2\right)-64.9705\left(0.251958-\frac{3L^2}{8}+\frac{L^2\pi}{16}+\frac{1}{4}L^2\,\text{Log}\left[\frac{1}{\sqrt{2}}\right]\right)}{10\left(-0.892492+L^2\right)}} \Big/ \left(1.25603\times10^{-13}+\right.\right.$$
$$2^{\frac{5}{2}+\frac{1}{10}(-30+P)+\frac{-58.4412\,L^2+2.17147\,L^2\left(6+8\,\pi+18\,\text{ArcCot}[3]-50\,\text{ArcCot}[5]+10\,\text{ArcTan}[3]-26\,\text{ArcTan}[5]-5\,\text{Log}[13]+\text{Log}[500]-2\,\text{Log}[L^2]\right)}{10\,L^2}}\times$$
$$\left.\left.5^{\frac{1}{2}+\frac{1}{10}(-30+P)+\frac{-58.4412\,L^2+2.17147\,L^2\left(6+8\,\pi+18\,\text{ArcCot}[3]-50\,\text{ArcCot}[5]+10\,\text{ArcTan}[3]-26\,\text{ArcTan}[5]-5\,\text{Log}[13]+\text{Log}[500]-2\,\text{Log}[L^2]\right)}{10\,L^2}}\right)\right]$$

```
col[v_] := Hue[Rescale[v, {4, 50}]]
```

(a) First part

```
Plot3D[SINRDB, {P, -20, 35}, {L, 5, 35}, ColorFunction → col,
 ColorFunctionScaling → False, ViewPoint → {-Pi, Pi, Pi},
 AxesLabel → {"Transmitter Power [dBm]", "Apt. Side [m]", "Avg. SINR [dB]" },
 BaseStyle → { FontColor → Orange, FontSize → 16,
   FontFamily → "Times New Roman"}, ImageSize → Large ]
```

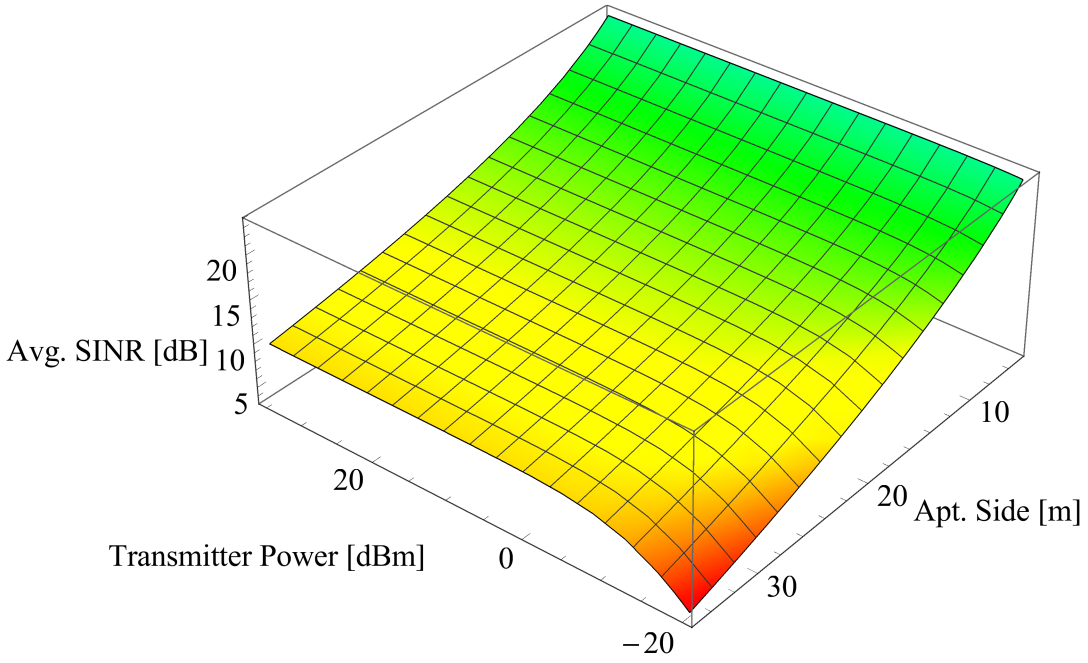

(b) Second part

Figure A.12: Computation of the Average SINR for the second tier of interference following the approach followed in Section 2.3.2.

In[1]:=
```
ClearAll["Global`*"]
```

In[2]:=
```
noise = 10^(-129.01/10)
```

Out[2]=
$$1.25603\times 10^{-13}$$

In[3]:=
```
Pow = 10^(1/2+1/10 (-30+P)+(-4 (-8.666364207076656`+9.710299956639812` L^2)-64.97045449272646` (0.2519580214951882`-3/8 L^2+L^2 π/16+1/4 L^2 Log[1/Sqrt[2]]))/(10 (-0.8924919153656709`+L^2)))
```

Out[3]=
$$10^{\frac{1}{2}+\frac{1}{10}(-30+P)+\frac{-4\left(-8.66636+9.7103\,L^2\right)-64.9705\left(0.251958-\frac{3L^2}{8}+\frac{L^2\pi}{16}+\frac{1}{4}L^2\,\text{Log}\left[\frac{1}{\sqrt{2}}\right]\right)}{10\left(-0.892492+L^2\right)}}$$

In[4]:=
```
Pnh = 2^(5/2+1/10 (-30+P)+(-78.44119982655926` L^2+2.1714724095162588` L^2 (6+17 π-26 ArcTan[3/5]-42 ArcTan[5/3]-9 Log[3]+Log[4]-25 Log[5]+15 Log[17]-2 Log[L^2]))/(10 L^2)) ×
  5^(1/2+1/10 (-30+P)+(-78.44119982655926` L^2+2.1714724095162588` L^2 (6+17 π-26 ArcTan[3/5]-42 ArcTan[5/3]-9 Log[3]+Log[4]-25 Log[5]+15 Log[17]-2 Log[L^2]))/(10 L^2))
```

Out[4]=
$$2^{\frac{5}{2}+\frac{1}{10}(-30+P)+\frac{-78.4412\,L^2+2.17147\,L^2\left(6+17\,\pi-26\,\text{ArcTan}\left[\frac{3}{5}\right]-42\,\text{ArcTan}\left[\frac{5}{3}\right]-9\,\text{Log}[3]+\text{Log}[4]-25\,\text{Log}[5]+15\,\text{Log}[17]-2\,\text{Log}\left[L^2\right]\right)}{10\,L^2}}\times 5^{\frac{1}{2}+\frac{1}{10}(-30+P)+\frac{-78.4412\,L^2+2.17147\,L^2\left(6+17\,\pi-26\,\text{ArcTan}\left[\frac{3}{5}\right]-42\,\text{ArcTan}\left[\frac{5}{3}\right]-9\,\text{Log}[3]+\text{Log}[4]-25\,\text{Log}[5]+15\,\text{Log}[17]-2\,\text{Log}\left[L^2\right]\right)}{10\,L^2}}$$

In[5]:=
```
SINR = Pow/(Pnh + noise)
```

Out[5]=
$$10^{\frac{1}{2}+\frac{1}{10}(-30+P)+\frac{-4\left(-8.66636+9.7103\,L^2\right)-64.9705\left(0.251958-\frac{3L^2}{8}+\frac{L^2\pi}{16}+\frac{1}{4}L^2\,\text{Log}\left[\frac{1}{\sqrt{2}}\right]\right)}{10\left(-0.892492+L^2\right)}}\Bigg/\left(1.25603\times 10^{-13}+2^{\frac{5}{2}+\frac{1}{10}(-30+P)+\frac{-78.4412\,L^2+2.17147\,L^2\left(6+17\,\pi-26\,\text{ArcTan}\left[\frac{3}{5}\right]-42\,\text{ArcTan}\left[\frac{5}{3}\right]-9\,\text{Log}[3]+\text{Log}[4]-25\,\text{Log}[5]+15\,\text{Log}[17]-2\,\text{Log}\left[L^2\right]\right)}{10\,L^2}}\times 5^{\frac{1}{2}+\frac{1}{10}(-30+P)+\frac{-78.4412\,L^2+2.17147\,L^2\left(6+17\,\pi-26\,\text{ArcTan}\left[\frac{3}{5}\right]-42\,\text{ArcTan}\left[\frac{5}{3}\right]-9\,\text{Log}[3]+\text{Log}[4]-25\,\text{Log}[5]+15\,\text{Log}[17]-2\,\text{Log}\left[L^2\right]\right)}{10\,L^2}}\right)$$

In[6]:=
```
SINRDB = 10 * Log[10, SINR]
```

Out[6]=
$$\frac{1}{\text{Log}[10]}10\,\text{Log}\Bigg[10^{\frac{1}{2}+\frac{1}{10}(-30+P)+\frac{-4\left(-8.66636+9.7103\,L^2\right)-64.9705\left(0.251958-\frac{3L^2}{8}+\frac{L^2\pi}{16}+\frac{1}{4}L^2\,\text{Log}\left[\frac{1}{\sqrt{2}}\right]\right)}{10\left(-0.892492+L^2\right)}}\Bigg/\left(1.25603\times 10^{-13}+2^{\frac{5}{2}+\frac{1}{10}(-30+P)+\frac{-78.4412\,L^2+2.17147\,L^2\left(6+17\,\pi-26\,\text{ArcTan}\left[\frac{3}{5}\right]-42\,\text{ArcTan}\left[\frac{5}{3}\right]-9\,\text{Log}[3]+\text{Log}[4]-25\,\text{Log}[5]+15\,\text{Log}[17]-2\,\text{Log}\left[L^2\right]\right)}{10\,L^2}}\times 5^{\frac{1}{2}+\frac{1}{10}(-30+P)+\frac{-78.4412\,L^2+2.17147\,L^2\left(6+17\,\pi-26\,\text{ArcTan}\left[\frac{3}{5}\right]-42\,\text{ArcTan}\left[\frac{5}{3}\right]-9\,\text{Log}[3]+\text{Log}[4]-25\,\text{Log}[5]+15\,\text{Log}[17]-2\,\text{Log}\left[L^2\right]\right)}{10\,L^2}}\right)\Bigg]$$

(a) First part

```
Plot3D[SINRDB, {P, -20, 35}, {L, 5, 35}, ColorFunction → col,
 ColorFunctionScaling → False, ViewPoint → {-Pi, Pi, Pi},
 AxesLabel → {"Transmitter Power [dBm]", "Apt. Side [m]", "Avg. SINR [dB]" },
 BaseStyle → { FontColor → Orange, FontSize → 16,
   FontFamily → "Times New Roman"}, ImageSize → Large ]
```

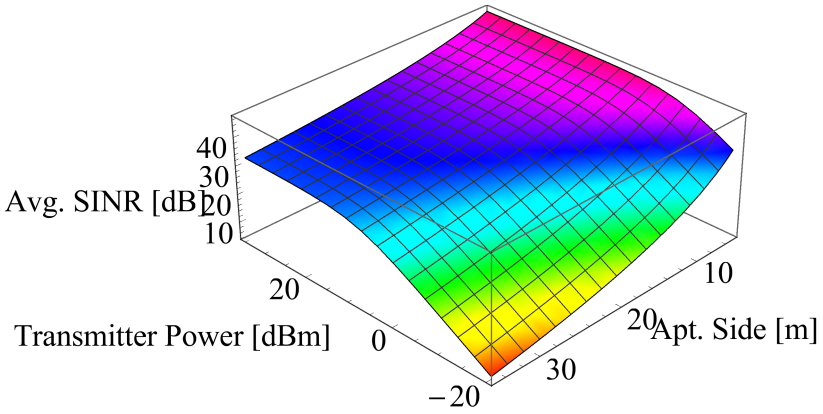

(b) Second part

Figure A.13: Computation of the Average SINR for the third tier of interference following the approach followed in Section 2.3.2.

Appendix B

Developed and Implemented Code in LTE-Sim to Obtain the EESM

This Appendix addresses the implementation of code in LTE-Sim to obtain the exponential effective SINR mapping (EESM). Firstly is presented the implemented scenario and the updates to LTE-Sim. Secondly is presented a scenario that turned possible to simulate any number of deployed home eNodeBs (HeNBs) in a 3GPP 5x5 grid geometry.
The code is presented in the files named “test-sinr-femto.h” is fully available in [129], [190]. The first file, with name “test-sinr-femto.h”, presents the correction on the code to obtain the EESM, channel quality indicator (CQI), modulation and coding scheme (MCS), and transport block size (TBS). The considered path loss model is WINNER II [113]. As in the original code the apartment side could be any value. In this scenario, apartment sides of 5 m, 10 m or 20 m are considered. The boundaries of the building need to defined in the simulation scenario to avoid a “segmentation fault (core dumped) error”. This definition is made according to the apartment side. The code was updated, by considering the WINNER II path loss model. In order to speed up the results analysis, some output information was avoided by commenting the code.
The second file, with name “test-sinr-femto.h”, presents the implementation of the code to simulate any reuse pattern, as well as to define the exact location of the HeNBs. With the code available in [129], [190], it is possible to obtain the EESM, CQI, MCS, and TBS for deployment scenarios with: 2 HeNBs, 4 HeNBs, four different deployments with 5 HeNBs, 6 HeNBs and 9 HeNBs. Frequency reuse has to be select according to the deployment of the HeNBs. Papers [94], [100], [102] present results with the provided code.

```
 1 /* -*- Mode:C++; c-file-style:"gnu"; indent-tabs-mode:nil; -*- */
 2 /*
 3  * Copyright (c) 2010,2011,2012,2013 TELEMATICS LAB, Politecnico di Bari
 4  *
 5  * This file is part of LTE-Sim
 6  *
 7  * LTE-Sim is free software; you can redistribute it and/or modify
 8  * it under the terms of the GNU General Public License version 3 as
 9  * published by the Free Software Foundation;
10  *
11  * LTE-Sim is distributed in the hope that it will be useful,
12  * but WITHOUT ANY WARRANTY; without even the implied warranty of
13  * MERCHANTABILITY or FITNESS FOR A PARTICULAR PURPOSE.  See the
14  * GNU General Public License for more details.
15  *
16  * You should have received a copy of the GNU General Public License
17  * along with LTE-Sim; if not, see <http://www.gnu.org/licenses/>.
18  *
19  * Author: Francesco Capozzi <f.capozzi@poliba.it>
20  *
21  * Updated by: Rui R.Paulo   <rrp@lx.it.pt>>
22  *
23  */
24
25 #include "../channel/LteChannel.h"
26 #include "../phy/enb-lte-phy.h"
27 #include "../phy/ue-lte-phy.h"
28 #include "../core/spectrum/bandwidth-manager.h"
29 #include "../networkTopology/Cell.h"
30 #include "../protocolStack/packet/packet-burst.h"
31 #include "../protocolStack/packet/Packet.h"
32 #include "../core/eventScheduler/simulator.h"
33 #include "../flows/application/InfiniteBuffer.h"
34 #include "../flows/application/VoIP.h"
35 #include "../flows/application/CBR.h"
36 #include "../flows/application/TraceBased.h"
37 #include "../device/IPClassifier/ClassifierParameters.h"
38 #include "../flows/QoS/QoSParameters.h"
39 #include "../flows/QoS/QoSForEXP.h"
40 #include "../flows/QoS/QoSForFLS.h"
41 #include "../flows/QoS/QoSForM_LWDF.h"
42 #include "../componentManagers/FrameManager.h"
43 #include "../utility/seed.h"
44 #include "../utility/RandomVariable.h"
45 #include "../utility/UsersDistribution.h"
46 #include "../utility/IndoorScenarios.h"
47 //#include "../channel/propagation-model/channel-realization-helper.h"  //
   RRP:  Only the WINNER II is considered
48 #include "../channel/propagation-model/winner-downlink-channel-
   realization.h"
49 #include "../load-parameters.h"
50 #include "../device/HeNodeB.h"
51 #include <iostream>
```

```
 52 #include <queue>
 53 #include <fstream>
 54 #include <stdlib.h>
 55 #include <cstring>
 56 #include <math.h>
 57
 58 static void TestSinrFemto (int riuso, double activityFactor)
 59 {
 60
 61     srand (time(NULL));
 62
 63     int nbBuildings = 1;
 64     double duration = 0.2;
 65     double bandwidth = 20./riuso;
 66
 67     // CREATE COMPONENT MANAGER
 68     Simulator *simulator = Simulator::Init();
 69     FrameManager *frameManager = FrameManager::Init();
 70     NetworkManager* nm = NetworkManager::Init();
 71     FlowsManager* flowsManager = FlowsManager::Init ();
 72
 73     // CREATE FEMTOCELLS with HeNB
 74     int idFemto = 101;
 75     int idBuilding = 1101;
 76     int buildType = 0; // TYPE_3GPP_5x5_grid
 77     int nbFloors = 1;
 78     int apartmentSide = 20; // RRP: Also change bellow
 79     int femtoCellsInBuilding = 25;
 80     int nbFemtoCells = nbBuildings * femtoCellsInBuilding;
 81
 82     for (int i = 0; i < nbBuildings; i++)
 83     {
 84         double rnd = (double) rand()/RAND_MAX;
 85         if (rnd <= activityFactor)
 86         {
 87             double buildingCenter_X = 0;
 88             double buildingCenter_Y = 0;
 89
 90             nm->CreateBuildingForFemtocells(idBuilding, buildType,
    apartmentSide, nbFloors, buildingCenter_X, buildingCenter_Y, idFemto,
    femtoCellsInBuilding);
 91
 92             /* // RRP: We do not need this information
 93            std::cout << "Building " << idBuilding
 94                      <<" position " << buildingCenter_X
 95                      << " " << buildingCenter_Y
 96                      << " with " << femtoCellsInBuilding << " femtocells"
    << std::endl;
 97              */
 98
 99     // Consult https://github.com/RRP-IT/LTE-SIM-ITU-R-M.2135-1.git and
    ttps://github.com/RRP-IT/LTE-Sim-RP.git
100     }
```

```
101
102     int idUE = 3001;
103
104     // RRP: Update to avoid the Segmentation fault (core dumped) error. In
    2019 this problem was not yet solved.
105
106     // RRP: For 20 m apartment side
107     // RRP: Comment and uncommnet to use other side apartment sides
108     for (double x = -49.95; x < 49.95; x=x+0.999)
109     {
110         for (double y = -49.95; y < 49.95; y=y+0.999)
111         {
112             /*
113     // For 10 m apartment side
114     for (double x = -24.975; x < 24.975; x=x+0.999)
115     {
116         for (double y = -24.975; y < 24.975; y=y+0.999)
117         {
118              */
119             /*
120     // For 5 m apartment side
121     for (double x = -12.4875; x < 12.4875; x=x+0.4995)
122     {
123         for (double y = -12.4875; y < 12.4875; y=y+0.4995)
124         {
125              */
126             double posX = x;
127             double posY = y;
128             double speed = 3;
129             double speedDirection = (double)(rand() %360) * ((2*3.14)/
    360);
130
131             UserEquipment* ue = new UserEquipment (idUE,
132                     posX, posY, speed, speedDirection,
133                     nm->GetFemtoCellContainer ()->at (0),
134                     nm->GetHomeENodeBContainer ()->at (0),
135                     1,
136                     Mobility::CONSTANT_POSITION);
137
138             // Consult https://github.com/RRP-IT/LTE-SIM-ITU-R-M.
    2135-1.git and ttps://github.com/RRP-IT/LTE-Sim-RP.git
139
140             // // RRP: In this scenario WINNER II is considered.
141             target->RegisterUserEquipment (ue);
142             WinnerDownlinkChannelRealization* c_dl = new
    WinnerDownlinkChannelRealization (target, ue);
143             target->GetPhy ()->GetDlChannel ()->GetPropagationLossModel
    ()->AddChannelRealization (c_dl);
144             WinnerDownlinkChannelRealization* c_ul = new
    WinnerDownlinkChannelRealization (ue, target);
145             target->GetPhy ()->GetUlChannel ()->GetPropagationLossModel
    ()->AddChannelRealization (c_ul);
146
```

```
147             nm->GetUserEquipmentContainer ()->push_back (ue);
148 
149             /* // RRP: We do not need this information
150           std::cout << "UE " << idUE << " position " << posX << " " << 
    posY
151                     << " cell " <<  ue->GetCell ()->GetIdCell ()
152                     << " henb " << ue->GetTargetNode ()->GetIDNetworkNode () 
    << std::endl;
153              */
154 
155             ue->GetPhy ()->GetDlChannel ()->AddDevice (ue);
156             idUE++;
157 
158         }
159     }
160 
161     simulator->SetStop(duration);
162     simulator->Run ();
163 }
164 
```

```
 1 /* -*- Mode:C++; c-file-style:"gnu"; indent-tabs-mode:nil; -*- */
 2 /*
 3  * Copyright (c) 2010,2011,2012,2013 TELEMATICS LAB, Politecnico di Bari
 4  *
 5  * This file is part of LTE-Sim
 6  *
 7  * LTE-Sim is free software; you can redistribute it and/or modify
 8  * it under the terms of the GNU General Public License version 3 as
 9  * published by the Free Software Foundation;
10  *
11  * LTE-Sim is distributed in the hope that it will be useful,
12  * but WITHOUT ANY WARRANTY; without even the implied warranty of
13  * MERCHANTABILITY or FITNESS FOR A PARTICULAR PURPOSE.  See the
14  * GNU General Public License for more details.
15  *
16  * You should have received a copy of the GNU General Public License
17  * along with LTE-Sim; if not, see <http://www.gnu.org/licenses/>.
18  *
19  * Author: Francesco Capozzi <f.capozzi@poliba.it>
20  *
21  * Updated by: Rui R.Paulo   <rrp@lx.it.pt>>
22  *
23  */
24
25 #include "../channel/LteChannel.h"
26 #include "../phy/enb-lte-phy.h"
27 #include "../phy/ue-lte-phy.h"
28 #include "../core/spectrum/bandwidth-manager.h"
29 #include "../networkTopology/Cell.h"
30 #include "../protocolStack/packet/packet-burst.h"
31 #include "../protocolStack/packet/Packet.h"
32 #include "../core/eventScheduler/simulator.h"
33 #include "../flows/application/InfiniteBuffer.h"
34 #include "../flows/application/VoIP.h"
35 #include "../flows/application/CBR.h"
36 #include "../flows/application/TraceBased.h"
37 #include "../device/IPClassifier/ClassifierParameters.h"
38 #include "../flows/QoS/QoSParameters.h"
39 #include "../flows/QoS/QoSForEXP.h"
40 #include "../flows/QoS/QoSForFLS.h"
41 #include "../flows/QoS/QoSForM_LWDF.h"
42 #include "../componentManagers/FrameManager.h"
43 #include "../utility/seed.h"
44 #include "../utility/RandomVariable.h"
45 #include "../utility/UsersDistribution.h"
46 #include "../utility/IndoorScenarios.h"
47 //#include "../channel/propagation-model/channel-realization-helper.h"  //
   RRP:  Only the WINNER II is considered
48 #include "../channel/propagation-model/winner-downlink-channel-
   realization.h"
49 #include "../load-parameters.h"
50 #include "../device/HeNodeB.h"
51 #include <iostream>
```

```
 52 #include <queue>
 53 #include <fstream>
 54 #include <stdlib.h>
 55 #include <cstring>
 56 #include <math.h>
 57
 58 static void TestSinrFemto (int riuso, double activityFactor)
 59 {
 60
 61     srand (time(NULL));
 62
 63     int nbBuildings = 1;
 64     double duration = 0.2;
 65     double bandwidth = 20./riuso;
 66
 67     // CREATE COMPONENT MANAGER
 68     Simulator *simulator = Simulator::Init();
 69     FrameManager *frameManager = FrameManager::Init();
 70     NetworkManager* nm = NetworkManager::Init();
 71     FlowsManager* flowsManager = FlowsManager::Init ();
 72
 73     // CREATE FEMTOCELLS with HeNB
 74     int idFemto = 101;
 75     int idBuilding = 1101;
 76     int buildType = 0; // TYPE_3GPP_5x5_grid
 77     int nbFloors = 1;
 78     int apartmentSide = 20; // RRP: Also change bellow
 79     int femtoCellsInBuilding = 25;
 80     int nbFemtoCells = nbBuildings * femtoCellsInBuilding;
 81
 82     for (int i = 0; i < nbBuildings; i++)
 83     {
 84         double rnd = (double) rand()/RAND_MAX;
 85         if (rnd <= activityFactor)
 86         {
 87             double buildingCenter_X = 0;
 88             double buildingCenter_Y = 0;
 89
 90             nm->CreateBuildingForFemtocells(idBuilding, buildType,
    apartmentSide, nbFloors, buildingCenter_X, buildingCenter_Y, idFemto,
    femtoCellsInBuilding);
 91
 92             std::cout << "Building " << idBuilding
 93                     <<" position " << buildingCenter_X
 94                     << " " << buildingCenter_Y
 95                     << " with " << femtoCellsInBuilding << " femtocells"
    << std::endl;
 96
 97             //create HeNB
 98             for (int j = 0; j < femtoCellsInBuilding; j++)
 99             {
100                 //RRP: Select a deployment scene or create a new one.
101                 //if ( j==7 || j==12) // 2 HeNB E
```

```
102                 if (j==6 || j==8 || j==16 || j==18) // 4 HeNB
103                 //if (j==0 || j==4 || j==12 || j==20 || j==24) // 5 HeNB
104                 //if (j==1 || j==9 || j==12 || j==15 || j==23) // 5 HeNB B
105                 //if (j==2 || j==10 || j==12 || j==14 || j==22) // 5 HeNB
    C e D
106                 //if (j==0 || j==4 || j==12 || j==20 || j==24) // 5 HeNB E
107                 //if (j==0 || j==2 || j==4 || j==10 || j==12 || j==14 ||
    j==20 || j==22 || j==24) // 9 HeNB
108                 //if (j==5 || j==7 || j==9 || j==15 || j==17 || j==19) //
    6 HeNB F
109                 {
110
111                     // Consult https://github.com/RRP-IT/LTE-SIM-ITU-R-M.
    2135-1.git and https://github.com/RRP-IT/LTE-Sim-RP.git
112
113                     if (riuso == 1)
114                     {
115                         enb->GetPhy ()->SetBandwidthManager (new
    BandwidthManager (bandwidth, bandwidth, 0, 0));
116                     }
117
118                     // RRP: To get the correct order of bandwidth
    distribution  doi={10.1109/VTCSpring.2018.8417715}
119                     else if (riuso == 2)
120                     {
121                         //if (j==12) //5 HeN
122                         if (j==6 || j==18) // 4 HeNB
123                         //if (j==0 || j==12 || j==24) //5 HeNB
124                         //if (j==1 || j==12 || j==23) //5 HeNB B
125                         //if (j==2 || j==12 || j==22) //5 HeNB C
126                         //if (j==7 ||j==12) //5 HeNB D E
127                         //if (j==0 || j==4 || j==12 || j==20 || j==24) //9
    HeNB
128                         //if (j==5 || j==9 || j==17) //6 HeNB
129                         {
130                             enb->GetPhy ()->SetBandwidthManager (new
    BandwidthManager (bandwidth, bandwidth, 50*(j%2), 50*(j%2)));
131                         }
132                         else
133                         {
134                             enb->GetPhy ()->SetBandwidthManager (new
    BandwidthManager (bandwidth, bandwidth, 50*((j+1)%2), 50*((j+1)%2)));
135                         }
136                     }
137                     else if (riuso == 4)
138                     // Consult https://github.com/RRP-IT/LTE-SIM-ITU-R-M.
    2135-1.git and https://github.com/RRP-IT/LTE-Sim-RP.git
139                 }
140             }
141         }
142         idBuilding++;
143     }
144
```

```
145     int idUE = 3001;
146
147     //  RRP: Update to avoid the Segmentation fault (core dumped) error.
    In 2019 this problem was not yet solved.
148     //  RRP: For 20 m apartment side
149     //  RRP: Comment and uncommnet to use other side apartment sides
150     for (double x = -49.95; x < 49.95; x=x+0.999)
151     {
152         for (double y = -49.95; y < 49.999; y=y+0.95)
153         {
154 /*
155     // For 10 m apartment side
156     for (double x = -24.975; x < 24.975; x=x+0.999)
157     {
158         for (double y = -24.975; y < 24.975; y=y+0.999)
159         {
160     // For 5 m apartment side
161     for (double x = -12.4875; x < 12.4875; x=x+0.4995)
162     {
163         for (double y = -12.4875; y < 12.4875; y=y+0.4995)
164         {
165 */
166
167             // Consult https://github.com/RRP-IT/LTE-SIM-ITU-R-M.
    2135-1.git and https://github.com/RRP-IT/LTE-Sim-RP.git
168
169             // RRP In this scenario WINNER II is considered.
170             target->RegisterUserEquipment (ue);
171             WinnerDownlinkChannelRealization* c_dl = new
    WinnerDownlinkChannelRealization (target, ue);
172             target->GetPhy ()->GetDlChannel ()->GetPropagationLossModel
    ()->AddChannelRealization (c_dl);
173             WinnerDownlinkChannelRealization* c_ul = new
    WinnerDownlinkChannelRealization (ue, target);
174             target->GetPhy ()->GetUlChannel ()->GetPropagationLossModel
    ()->AddChannelRealization (c_ul);
175
176             // Consult https://github.com/RRP-IT/LTE-SIM-ITU-R-M.
    2135-1.git and https://github.com/RRP-IT/LTE-Sim-RP.git
177         }
178     }
179
180     simulator->SetStop(duration);
181     simulator->Run ();
182 }
183
```

Appendix C

EESM Results for Reuse Pattern One

This Appendix explores exponential effective SINR mapping (EESM) results for reuse pattern one. Figure C.1 up to Figure C.3 present results for the 25 home eNodeBs (HeNBs) deployment. Results for 4 HeNBs are presented from Figure C.6 up to Figure C.4. For 5 HeNBs from Figure C.9 to Figure C.7. Finally results for 6 HeNBs deployment are presented from Figure C.12 to Figure C.10c. This Appendix considers the parameters considered in Chapter 2.

C.1 Twenty-five HeNB

Figure C.1 presents results when 25 active HeNBs, reuse pattern one and apartment side length equal to 20 m are considered. Figure C.1a presents EESM results for transmitter

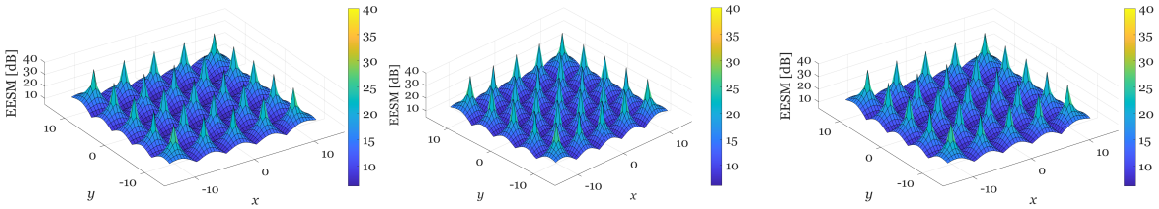

(a) 0 dBm (b) 10 dBm (c) 20 dBm

Figure C.1: ESSM in a 5x5 geometry, 25 HeNB, reuse pattern one, apartment side length 5 m, transmitter power 0 dBm, 10 dBm and 20 dBm.

power of 0 dBm, while Figure C.1b and Figure C.1c present results for transmitter powers of 10 dBm and 20 dBm, respectively. In the three cases, the variation of the transmitter power did not show a major impact on the EESM results. The maximum EESM value (40 dBm) is only obtained in the center of the apartment.

When the apartment side length is 10 m, as shown in Figure C.2, results are identical to the previous ones. For all the transmitter powers, i.e., 0 dBm, as shown in Figure C.2a, 10 dBm, as shown in Figure C.2b and 20 dBm, as shown in Figure C.2c, there is not any noticeable variation on the obtained EESM results. The maximum EESM is obtained only in the center of the apartments again.

When the apartment side length is 20 m, as shown in Figure C.3, and for the same values of transmitter power is possible to observe the same behavior as for the previous values of the side length, as shown in Figure C.1 and Figure C.2. Since the distance between the nodes is longer, the co-channel interference is lower, and the area where the EESM achieves its maximum value of 40 dB is larger. For frequency reuse one, it is also possible to confirm

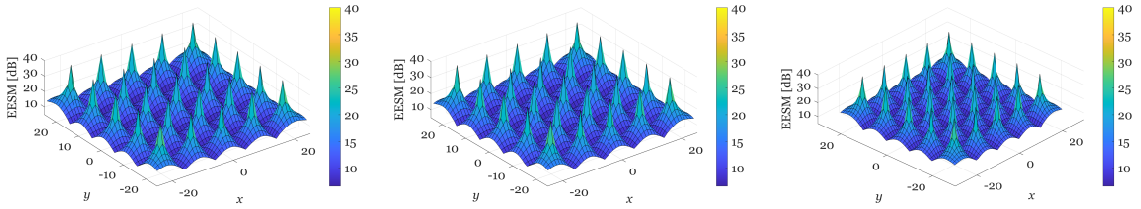

(a) 0 dBm (b) 10 dBm (c) 20 dBm

Figure C.2: ESSM in a 5x5 geometry, 25 HeNB, reuse pattern one, apartment side length 10 m, transmitter power 0 dBm, 10 dBm and 20 dBm.

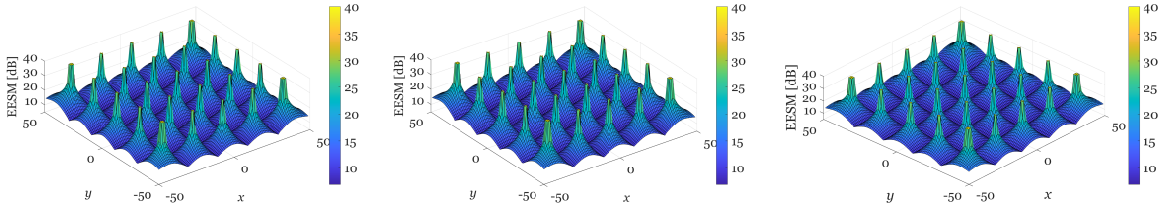

(a) 0 dBm (b) 10 dBm (c) 20 dBm

Figure C.3: ESSM in a 5x5 geometry, 25 HeNB, reuse pattern one, apartment side length 20 m, transmitter power 0 dBm, 10 dBm and 20 dBm.

the lessons learned from the theoretical study in Section 2.3.4. For the same apartment side length, the variation on the transmitter power does not affect the values of the EESM.

C.2 Four HeNB

Results for the EESM are presented in Figures C.4 and C.5 and C.6 for a 3GPP 5x5 grid geometry with 4 HeNBs on it. Figure C.4 presents results for an apartment side length of 20 m. With 4 HNBs only and an apartment side length of 20 m, in Figure C.4a, it is possible

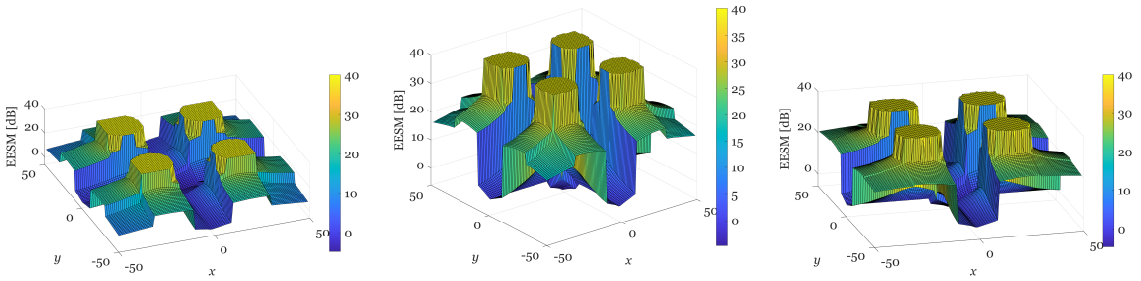

(a) 0 dBm (b) 10 dBm (c) 20 dBm

Figure C.4: ESSM in a 5x5 geometry, 4 HeNB, reuse pattern one, apartment side length 20 m, transmitter power 0 dBm, 10 dBm and 20 dBm.

to observe the effect of the attenuation imposed by walls in the apartments at the corners of the building (example for a transmitter power of 0 dBm). In Figure C.4a, the effect of walls is noticeable in the apartment that are in the corners of the topology but its influence decreases when the transmitter power increases to 10 dBm, as shown in Figure C.4b, and

20 dBm, as shown in Figure C.4c. The area where the ESSM achieves the maximum (of 40 dBm) increases when the transmitter power increases, as shown in Figure C.4c (example for a transmitter power of 20 dBm). In the neighbor apartments, the EESM increase is specially significant at the apartments on the edges of the building, specially for apartments at the corners. Finally, it is worthwhile to note that, due to the co-channel interference, the central area of the building floor keeps to be a problematic area.
Figure C.5 presents results for an apartment side length of 10 m. With this apartment side

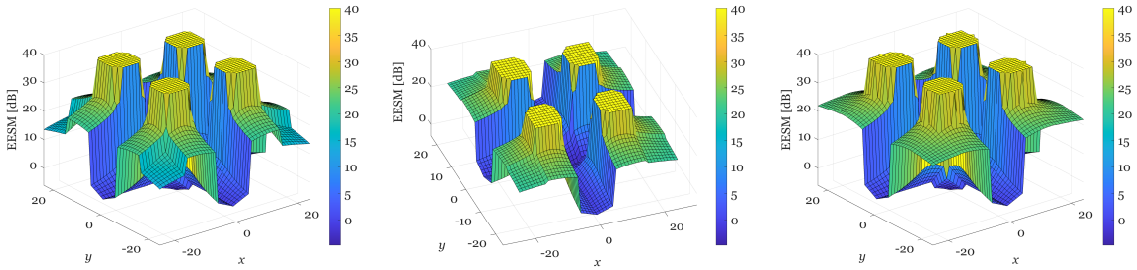

(a) 0 dBm (b) 10 dBm (c) 20 dBm

Figure C.5: ESSM in a 5x5 geometry, 4 HeNB, reuse pattern one, apartment side length 10 m, transmitter power 0 dBm, 10 dBm and 20 dBm.

length, it is possible to observe that the EESM increases in the areas where the it took the lowest values (before). This behavior occurs in the zones that exclude the central zone of the building. In Figure C.4a at apartments at the corners of the building the EESM was lower than 10 dBm, in Figure C.5a at the same apartments the EESM higher than 15 dBm. Them same increase in EESM occurs for side lengths of 20 and 10 m, as shown in Figure C.4b and Figure C.5b, respectively. By analyzing Figure C.5c, where the maximum transmitter power is considered, one observes that the effect of the walls attenuation is mitigated, and higher values are obtained for the EESM.
Figure C.6 presents the surface for the variation of the EESM over the floor area for apartment side lengths of 5 m.

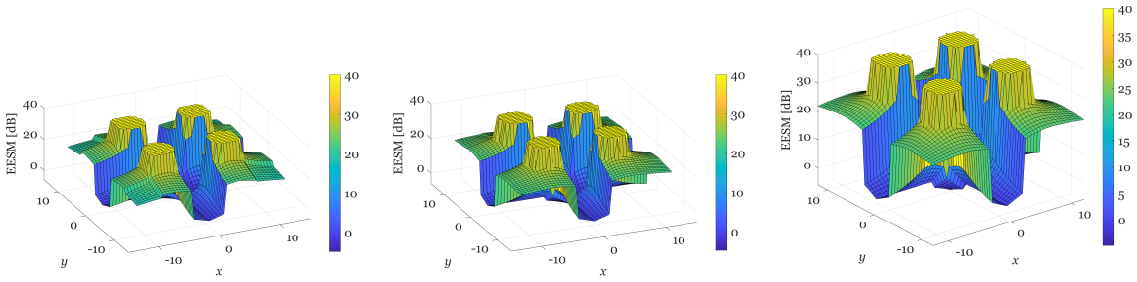

(a) 0 dBm (b) 10 dBm (c) 20 dBm

Figure C.6: ESSM in a 5x5 geometry, 4 HeNB, reuse pattern one, apartment side length 5 m, transmitter power 0 dBm, 10 dBm and 20 dBm.

In the neighbor apartments, when the transmitter power increases, the EESM increase is specially significant at the apartments on the edges of the building, specially for apartments at the corners.

For a transmitter power of 0 dBm, the wall attenuation causes a decrease in the EESM value, as shown in Figure C.6a. Again, this behavior is less evident for a transmitter power of 10 dBm, as shown in Figure C.6b, and disappears for a transmitter power of 20 dBm, as shown in Figure C.6c.

In the topology with 4 HeNBs, and the studied combinations of apartment side lengths and transmitter powers, the central area of the building floor is always a problematic area in terms of SINR. In this area, the lowest EESM values corresponds to 5.76% of the total area of the building floor (the same value that was obtained for reuse pattern 2, as discussed in Section 2.5.1.2). With frequency reuse one and for 4 HeNBs, co-channel interference imposes a high degradation on the ESSM. The highest values are obtained inside or near the apartments that contain the four HeNBs.

C.3 Five HeNB

Figure C.7 presents results for an apartment side length of 20 m.

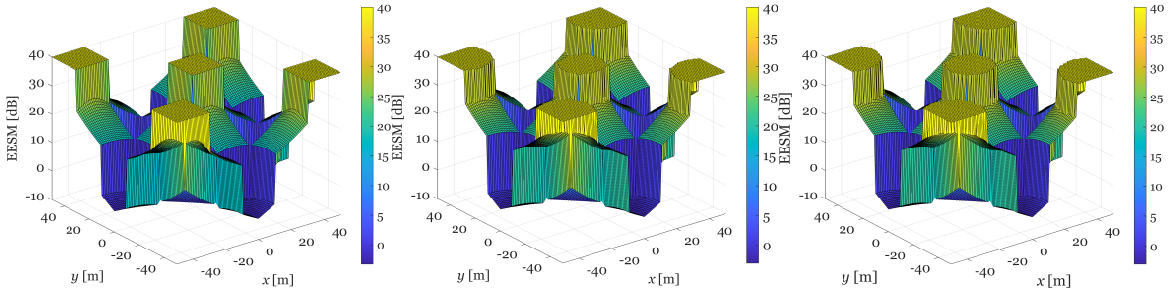

(a) 0 dBm (b) 10 dBm (c) 20 dBm

Figure C.7: ESSM in a 5x5 geometry, 5 HeNB, reuse pattern one, apartment side length 20 m, transmitter power 0 dBm, 10 dBm and 20 dBm.

As shown in Figure C.7a, it is possible to observe that, when transmitter power is 0 dBm, the maximum EEESM (40 dBm) is only achieved inside the five apartments where the HeNBs were deployed. When the transmitter power is increased to 10 dBm or 20 dBm, it is possible to observe a slight increase in the area of the zones where the EESM is the maximum within the considered five apartments, as shown in Figure C.7b and Figure C.7c, respectively.

For an apartment side length of 10 m, results are shown in Figure C.8. As shown in Figure C.8a, with the increase in apartment side length, near the corners of the building the areas of the zones where the EESM is the maximum increase. In the central apartment, the maximum EESM is confined to the own apartment. When the transmitter power increases to 10 dBm and 20 dBm, as shown in Figure C.8b and Figure C.8c, respectively, there is a slight increase in the areas with an EESM equal to 40 dBm.

Figure C.9 presents results for an apartment side length of 5 m. The variation on the transmitter power has a small or even a null impact in the results of EESM, as shown in Figures C.9a, C.9b and C.9c. The area where the EESM is 40 dBm is the same for the three values of the transmitter power.

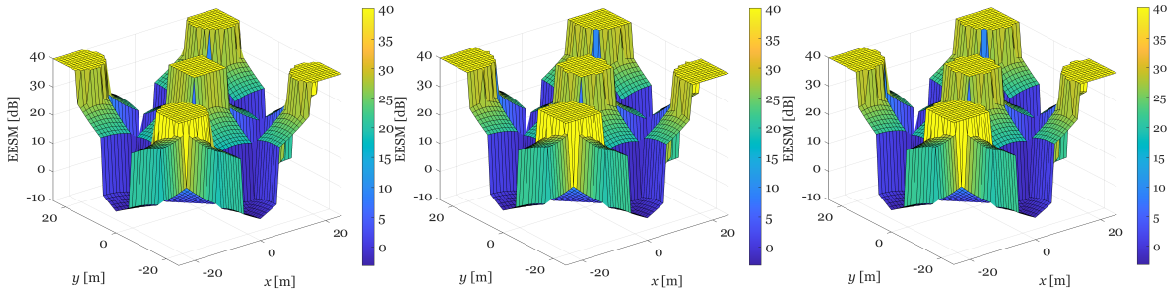

(a) 0 dBm (b) 10 dBm (c) 20 dBm

Figure C.8: ESSM in a 5x5 geometry, 5 HeNB, reuse pattern one, apartment side length 10 m, transmitter power 0 dBm, 10 dBm and 20 dBm.

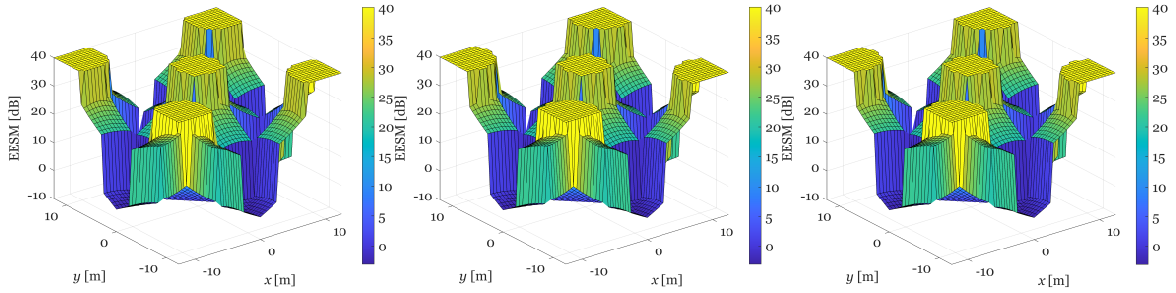

(a) 0 dBm (b) 10 dBm (c) 20 dBm

Figure C.9: ESSM in a 5x5 geometry, 5 HeNB, reuse pattern one, apartment side length 5 m, transmitter power 0 dBm, 10 dBm and 20 dBm.

Compared to the 4 HeNBs scenario, with a reuse pattern one, the introduction of one HeNB to eliminate the central area (of the apartment floor topology) with lower EESM values was successfully achieved. However, in areas near the middle of the building sidewalls, the EESM drops to values lower than or closer to 0 dB (the areas identified with dark blue fill in the Figures). These amount of area is around 7.2% of the total area of the building. Contrary to the case with frequency reuse two from Section 2.5.1.3, co-channel interference imposed by the co-channel HeNBs nullifies the increase in EESM (when the transmitter power increases).

C.4 Six HeNB

Results for the EESM for deployment of 6 HeNBs for apartment side lengths of 20 m are shown in Figure C.10. Figures C.10a, C.10b and C.10b, show that HeNBs can not provide higher values of EESM for apartments contiguous to the building walls placed at x = -50 and x = 50 m. However, when the transmitter power increases, the EESM increase is especially significant at these apartments (contiguous to the building walls placed at x = -50 and x = 50 m). When the transmitter power increase from 0 dBm to 10 dBm, the areas where the EESM is 40 dBm slightly increases.

The impact of reducing the apartment side length from 20 m to 10 m are shown in Figure C.11. The underlying variation on the transmitter power has a small or even a null impact, as shown in Figures C.11a, C.11b and C.11c.

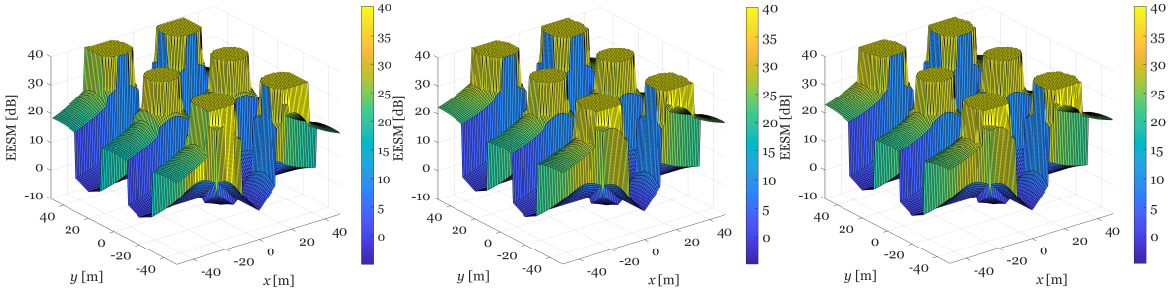

(a) 0 dBm (b) 10 dBm (c) 20 dBm

Figure C.10: ESSM in a 5x5 geometry, 6 HeNB, reuse pattern one, apartment side length 20 m, transmitter power 0 dBm, 10 dBm and 20 dBm.

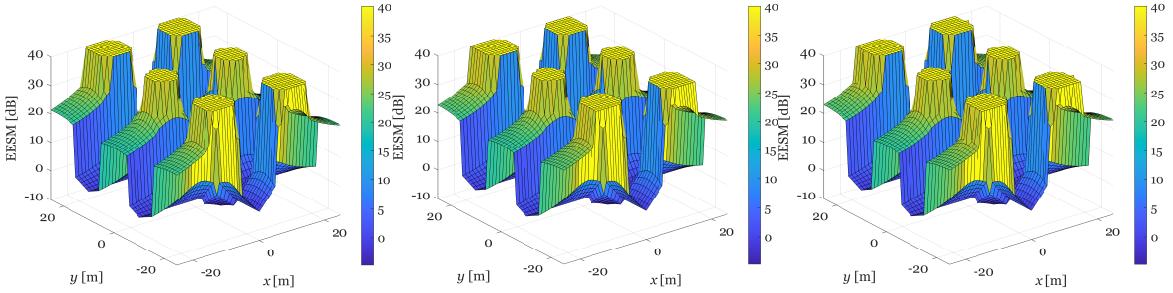

(a) 0 dBm (b) 10 dBm (c) 20 dBm

Figure C.11: ESSM in a 5x5 geometry, 6 HeNB, reuse pattern one, apartment side length 10 m, transmitter power 0 dBm, 10 dBm and 20 dBm.

Results for shorter apartment side lengths of 5 m are shown in Figure C.12. In these cases, a

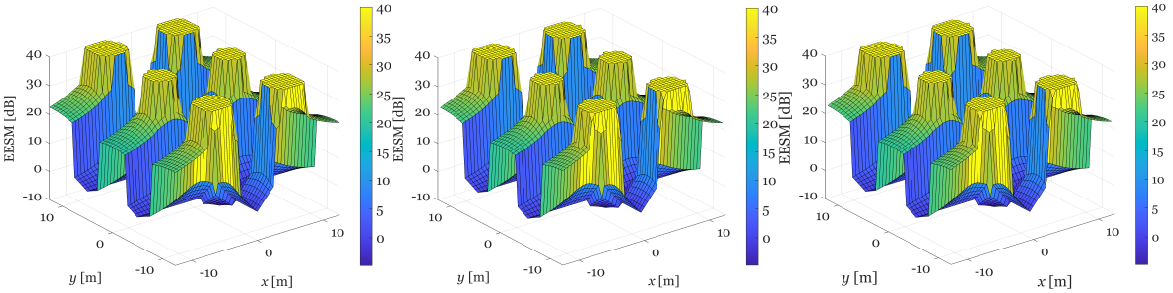

(a) 0 dBm (b) 10 dBm (c) 20 dBm

Figure C.12: ESSM in a 5x5 geometry, 6 HeNB, reuse pattern one, apartment side length 5 m, transmitter power 0 dBm, 10 dBm and 20 dBm.

variation on the transmitter power also did not show any impact on values of EESM.
For all apartments side lengths, the areas where the ESSM drops to the lowest values (near 1 dB, in blue) continue to be around 10.4% of the floor area (as also occurred with frequency reuse pattern two). Co-channel interference imposed by the co-channel HeNBs mitigate the effect of varying the transmitter power. For a reuse pattern one, the co-channel interference (instead of the attenuation) is the most limiting factor for the EESM. Compared with the previous building topologies, with 4 HeNBs or 5 HeNBs, the area with the lowest values for the ESSM increases.

Appendix D

LTE-Sim Upgrade for extended 25 HeNB Scenario

This Appendix addresses the overall updates performed in LTE-Sim code. First update is the development of a scenario with 25 home eNodeBs (HeNBs) with reuse one at the macrocell layer and reuse two in femtocell layer. Then the implementation of the Mersenne Twister pseudorandom generator. 3GPP defines in [79] the possibility to consider the variation of the transmitter power of HeNBs. The code presented below presents that option. The presented updates were considered to obtain the results in Chapter 3, as well as to obtain results for other scenarios.

```
  1/* -*- Mode:C++; c-file-style:"gnu"; indent-tabs-mode:nil; -*- */
  2 /*
  3 * Copyright (c) 2010,2011,2012,2013 TELEMATICS LAB, Politecnico di Bari
  4 *
  5 * This file is part of LTE-Sim
  6 *
  7 * LTE-Sim is free software; you can redistribute it and/or modify
  8 * it under the terms of the GNU General Public License version 3 as
  9 * published by the Free Software Foundation;
 10 *
 11 * LTE-Sim is distributed in the hope that it will be useful,
 12 * but WITHOUT ANY WARRANTY; without even the implied warranty of
 13 * MERCHANTABILITY or FITNESS FOR A PARTICULAR PURPOSE.  See the
 14 * GNU General Public License for more details.
 15 *
 16 * You should have received a copy of the GNU General Public License
 17 * along with LTE-Sim; if not, see <http://www.gnu.org/licenses/>.
 18 *
 19 * Author: Giuseppe Piro <g.piro@poliba.it>
 20 */
 21
 22
 23 /*
 24 * LTE-Sim is the main program of the LTE-Sim simulator.
 25 * To run simulations you can
 26 * (i) select one of example scenarios developed in Scenario/ ("./LTE-Sim
    -h" for details)
 27 * (ii) create a new scenario and add its reference into the main program.
 28 *
 29 *  To create a new scenario, see documentation in DOC/ folder.
 30 *
 31 *  For any questions, please contact the author at
 32 *  g.piro@poliba.it
 33 */
 34 * Updated by: Rui R.Paulo   <rrp@lx.it.pt>>
 35#include "TEST/test.h"
 36#include "scenarios/simple.h"
 37 #include "scenarios/single-cell-without-interference.h"
 38#include "scenarios/single-cell-with-interference.h"
 39#include "scenarios/building.h"
 40#include "scenarios/single-cell-with-femto-with-riuso.h" // RRP: Update to
    include scenario
 41#include "scenarios/single-cell-with-femto.h"
 42#include "scenarios/multi-cell.h"
 43#include "scenarios/single-cell-with-streets.h"
 44#include "scenarios/multi-cell-sinrplot.h"
 45#include "TEST/scalability-test-macro-with-femto.h"
 46#include "TEST/test-sinr-femto.h"
 47#include "TEST/test-throughput-macro-with-femto.h"
 48#include "TEST/test-sinr-urban.h"
 49#include "TEST/test-throughput-urban.h"
 50#include "TEST/test-throughput-building.h"
 51#include "TEST/test-uplink-fme.h"
```

```
 52#include "TEST/test-uplink-channel-quality.h"
 53#include "utility/help.h"
 54#include <iostream>
 55#include <queue>
 56#include <fstream>
 57#include <stdlib.h>
 58#include <cstring>
 59
 60 int
 61main (int argc, char *argv[])
 62 {
 63
 64  if (argc > 1)
 65    {
 66
 67      /* Help */
 68      if (!strcmp(argv[1], "-h") || !strcmp(argv[1], "-H") || !
   strcmp(argv[1],
 69               "--help") || !strcmp(argv[1], "--Help"))
 70        {
 71          Help ();
 72          return 0;
 73        }
 74
 75      /* run tests */
 76      if(strcmp(argv[1], "test")==0)
 77        {
 78          /* To enable a test, please modify the file LTE-Sim/src/TESTS/
   test.h */
 79          Test ();
 80        }
 81
 82      /* Run simple scenario */
 83      if (strcmp(argv[1], "Simple")==0)
 84        {
 85          Simple ();
 86        }
 87
 88      /* Run more complex scenarios */
 89      // Consult https://github.com/RRP-IT/LTE-SIM-ITU-R-M.2135-1.git and
   https://github.com/RRP-IT/LTE-Sim-RP.git
 90
 91       if (strcmp(argv[1], "SoBuil")==0)
 92                {
 93              double radius = atof(argv[2]);
 94              int nbBuilding = atoi(argv[3]);
 95              int buildingType = atoi(argv[4]);
 96              double activityRatio = atof(argv[5]);
 97              int nbUE = atoi(argv[6]);
 98              int nbFemtoUE = atoi(argv[7]);
 99              int nbVoIP = atoi(argv[8]);
100              int nbVideo = atoi(argv[9]);
101              int nbBE = atoi(argv[10]);
```

```
102              int nbCBR = atoi(argv[11]);
103              int sched_type = atoi(argv[12]);
104              int frame_struct = atoi(argv[13]);
105              int speed = atoi(argv[14]);
106              int accessPolicy = atoi(argv[15]);
107              double maxDelay = atof(argv[16]);
108              int video_bit_rate = atoi(argv[17]);
109              int Power = atoi(argv[18]);
110             double LWall =atof(argv[19]);
111              int seed;
112              if (argc==21) seed = atoi(argv[20]);
113              else seed = -1;
114              SoBuilding (radius, nbBuilding, buildingType, activityRatio,
    nbUE, nbFemtoUE, nbVoIP, nbVideo, nbBE, nbCBR, sched_type, frame_struct,
    speed, accessPolicy, maxDelay, video_bit_rate, Power, LWall, seed);
115        }
116        if (strcmp(argv[1], "SingleCellWithFemtoWithRiuso")==0)
117        {
118          double radius = atof(argv[2]);
119                      int nbBuilding = atoi(argv[3]);
120                  int buildingType = atoi(argv[4]);
121                  double activityRatio = atof(argv[5]);
122                  int nbUE = atoi(argv[6]);
123                  int nbFemtoUE = atoi(argv[7]);
124                  int nbVoIP = atoi(argv[8]);
125                  int nbVideo = atoi(argv[9]);
126                  int nbBE = atoi(argv[10]);
127                  int nbCBR = atoi(argv[11]);
128                  int sched_type = atoi(argv[12]);
129                  int frame_struct = atoi(argv[13]);
130                  int speed = atoi(argv[14]);
131                  int accessPolicy = atoi(argv[15]);
132                  double maxDelay = atof(argv[16]);
133                  int video_bit_rate = atoi(argv[17]);
134                  double Power = atof(argv[18]);
135                  double LWall =atof(argv[19]);
136                  int seed;
137                  if (argc==21) seed = atoi(argv[20]);
138                  else seed = -1;
139                SingleCellWithFemtoWithRiuso(radius, nbBuilding,
    buildingType, activityRatio, nbUE, nbFemtoUE, nbVoIP, nbVideo, nbBE,
    nbCBR, sched_type, frame_struct, speed, accessPolicy, maxDelay,
    video_bit_rate, Power, LWall, seed);
140        }
141
142        // Consult https://github.com/RRP-IT/LTE-SIM-ITU-R-M.2135-1.git
    and https://github.com/RRP-IT/LTE-Sim-RP.git
143
144      /* other dedicated simulations */
145
146        // Consult https://github.com/RRP-IT/LTE-SIM-ITU-R-M.2135-1.git
    and https://github.com/RRP-IT/LTE-Sim-RP.git
147
```

```
148    }
149 }
150
```

```
 1 /* -*- Mode:C++; c-file-style:"gnu"; indent-tabs-mode:nil; -*- */
 2 /*
 3  * Copyright (c) 2010,2011,2012,2013 TELEMATICS LAB, Politecnico di Bari
 4  *
 5  * This file is part of LTE-Sim
 6  *
 7  * LTE-Sim is free software; you can redistribute it and/or modify
 8  * it under the terms of the GNU General Public License version 3 as
 9  * published by the Free Software Foundation;
10  *
11  * LTE-Sim is distributed in the hope that it will be useful,
12  * but WITHOUT ANY WARRANTY; without even the implied warranty of
13  * MERCHANTABILITY or FITNESS FOR A PARTICULAR PURPOSE.  See the
14  * GNU General Public License for more details.
15  *
16  * You should have received a copy of the GNU General Public License
17  * along with LTE-Sim; if not, see <http://www.gnu.org/licenses/>.
18  *
19  * Author: Francesco Capozzi <f.capozzi@poliba.it>
20  *
21  * Updated by: Rui R.Paulo   <rrp@lx.it.pt>>
22  *
23  */
24
25 #ifndef INDOORSCENARIOS_H_
26 #define INDOORSCENARIOS_H_
27
28 #include <vector>
29 #include <iostream>
30 #include <cmath> // RRP:  Libraries to run the pseudorandom number
   generator (PRNG)
31 #include <random> // RRP:  Libraries to run the PRNG
32 #include <chrono> // RRP:  Libraries to the clock
33 #include "../networkTopology/Building.h"
34 #include "../componentManagers/NetworkManager.h"
35
36 //using namespace std;
37
38 static vector<CartesianCoordinates*>*
39 GetUniformBuildingDistribution (int idCell, int nbBuilding)
40 {
41   NetworkManager * networkManager = NetworkManager::Init();
42   vector<CartesianCoordinates*> *vectorOfCoordinates = new
   vector<CartesianCoordinates*>;
43
44   Cell *cell = networkManager->GetCellByID(idCell);
45
46   double radii = (cell->GetRadius()*1000)*0.8;
47
48   CartesianCoordinates *cellCoordinates = cell->GetCellCenterPosition();
49   double r; double angle;
50
51   for (int i = 0; i < nbBuilding; i++)
```

```
52    {
53      // RRP:  implementation of the Mersenne Twister PRNG
54     unsigned seed =
  std::chrono::system_clock::now().time_since_epoch().count();
55     std::mt19937 rng_mt(seed);
56     std::uniform_real_distribution<double> dist_double(0.0, 1.0);
57     std::uniform_real_distribution<double> theta_double(0.0, 360.0);
58
59     double r=dist_double(rng_mt);
60     double th=theta_double(rng_mt);
61
62     double theta = 2*M_PI*th/360;
63     double r1 = sqrt(r);
64     double radius = radii*r1;
65     double x = radius*cos(theta);
66     double y = radius*sin(theta);
67
68      CartesianCoordinates *newCoordinates = new
  CartesianCoordinates( cellCoordinates->GetCoordinateX () + x,
69
  cellCoordinates->GetCoordinateY () + y);
70
71      vectorOfCoordinates->push_back(newCoordinates);
72    }
73
74  return vectorOfCoordinates;
75 }
76
77 static double*
78 GetFemtoCellOffsetInBuilding (Building::BuildingType type, int idCell,
  double side)
79 {
80    // Consult https://github.com/RRP-IT/LTE-SIM-ITU-R-M.2135-1.git and
  https://github.com/RRP-IT/LTE-Sim-RP.git
81 }
82
83 #endif /* INDOORSCENARIOS_H_ */
84
```

```
 1 /* -*- Mode:C++; c-file-style:"gnu"; indent-tabs-mode:nil; -*- */
 2 /*
 3  * Copyright (c) 2010,2011,2012,2013 TELEMATICS LAB, Politecnico di Bari
 4  *
 5  * This file is part of LTE-Sim
 6  *
 7  * LTE-Sim is free software; you can redistribute it and/or modify
 8  * it under the terms of the GNU General Public License version 3 as
 9  * published by the Free Software Foundation;
10  *
11  * LTE-Sim is distributed in the hope that it will be useful,
12  * but WITHOUT ANY WARRANTY; without even the implied warranty of
13  * MERCHANTABILITY or FITNESS FOR A PARTICULAR PURPOSE.  See the
14  * GNU General Public License for more details.
15  *
16  * You should have received a copy of the GNU General Public License
17  * along with LTE-Sim; if not, see <http://www.gnu.org/licenses/>.
18  *
19  * Author: Giuseppe Piro <g.piro@poliba.it>
20   *
21  * Updated by: Rui R.Paulo   <rrp@lx.it.pt>>
22  *
23  */
24
25 #ifndef USERSDISTRIBTION_H_
26 #define USERSDISTRIBTION_H_
27
28 #include "../core/cartesianCoodrdinates/CartesianCoordinates.h"
29 #include "CellPosition.h"
30 #include "../componentManagers/NetworkManager.h"
31
32 #include <vector>
33 #include <iostream>
34 #include <cmath> // RRP:  Libraries to run the pseudorandom number
   generator (PRNG)
35 #include <random> // RRP:  Libraries to run the PRNG
36 #include <chrono> // RRP:  Libraries to the clock
37
38 // Consult https://github.com/RRP-IT/LTE-SIM-ITU-R-M.2135-1.git and
   https://github.com/RRP-IT/LTE-Sim-RP.git
39
40 static vector<CartesianCoordinates*>*
41 GetUniformUsersDistribution (int idCell, int nbUE)
42 {
43   NetworkManager * networkManager = NetworkManager::Init();
44   vector<CartesianCoordinates*> *vectorOfCoordinates = new
   vector<CartesianCoordinates*>;
45
46   Cell *cell = networkManager->GetCellByID(idCell);
47
48   double radii = (cell->GetRadius()*1000)*0.8;
49
50   CartesianCoordinates *cellCoordinates = cell->GetCellCenterPosition();
```

```
 51   double r; double angle;
 52
 53   for (int i = 0; i < nbUE; i++)
 54     {
 55       // RRP:  implementation of the Mersenne Twister PRNG
 56          unsigned seed =
   std::chrono::system_clock::now().time_since_epoch().count();
 57          std::mt19937 rng_mt(seed);
 58          std::uniform_real_distribution<double> dist_double(0.0, 1.0);
 59          std::uniform_real_distribution<double> theta_double(0.0, 360.0);
 60
 61          double radius=dist_double(rng_mt);
 62          double th=theta_double(rng_mt);
 63
 64          double angle = 2*M_PI*th/360;
 65          double r1 = sqrt(radius);
 66          double r = radii*r1;
 67
 68          CartesianCoordinates *newCoordinates =
   GetCartesianCoordinatesFromPolar (r, angle);
 69
 70       //Compute absoluteCoordinates
 71       newCoordinates->SetCoordinateX (cellCoordinates->GetCoordinateX () +
   newCoordinates->GetCoordinateX ());
 72       newCoordinates->SetCoordinateY (cellCoordinates->GetCoordinateY () +
   newCoordinates->GetCoordinateY ());
 73
 74       vectorOfCoordinates->push_back(newCoordinates);
 75     }
 76
 77   return vectorOfCoordinates;
 78 }
 79
 80 static vector<CartesianCoordinates*>*
 81 GetUniformUsersDistributionInFemtoCell (int idCell, int nbUE)
 82 {
 83   NetworkManager * networkManager = NetworkManager::Init();
 84   vector<CartesianCoordinates*> *vectorOfCoordinates = new
   vector<CartesianCoordinates*>;
 85
 86   Femtocell *cell = networkManager->GetFemtoCellByID(idCell);
 87
 88   double sidehome = cell->GetSide(); // RRP: Apartment side lenght
 89
 90   CartesianCoordinates *cellCoordinates = cell->GetCellCenterPosition();
 91   double r; double angle;
 92
 93   for (int i = 0; i < nbUE; i++)
 94     {
 95          // RRP:  implementation of the Mersenne Twister PRNG
 96          unsigned seed =
   std::chrono::system_clock::now().time_since_epoch().count();
 97          std::mt19937 rng_mt(seed);
```

```
 98          std::uniform_real_distribution<double> distx_double(0.0, 1);
 99          std::uniform_real_distribution<double> disty_double(0.0, 1);
100
101         // RRP: Generate users only inside of the own apartment
102          double xa=distx_double(rng_mt);
103          double ya=disty_double(rng_mt);
104          double x = sidehome*xa-(sidehome/2);
105          double y = sidehome*ya-(sidehome/2);
106
107         CartesianCoordinates *newCoordinates = new CartesianCoordinates
    ();
108          newCoordinates->SetCoordinates(x,y);
109       //Compute absoluteCoordinates
110       newCoordinates->SetCoordinateX (cellCoordinates->GetCoordinateX () +
    newCoordinates->GetCoordinateX ());
111       newCoordinates->SetCoordinateY (cellCoordinates->GetCoordinateY () +
    newCoordinates->GetCoordinateY ());
112
113       vectorOfCoordinates->push_back(newCoordinates);
114     }
115
116   return vectorOfCoordinates;
117 }
118
119 #endif /* USERSDISTRIBTION_H_ */
120
```

```
 1 /* -*- Mode:C++; c-file-style:"gnu"; indent-tabs-mode:nil; -*- */
 2 /*
 3  * Copyright (c) 2010,2011,2012,2013 TELEMATICS LAB, Politecnico di Bari
 4  *
 5  * This file is part of LTE-Sim
 6  *
 7  * LTE-Sim is free software; you can redistribute it and/or modify
 8  * it under the terms of the GNU General Public License version 3 as
 9  * published by the Free Software Foundation;
10  *
11  * LTE-Sim is distributed in the hope that it will be useful,
12  * but WITHOUT ANY WARRANTY; without even the implied warranty of
13  * MERCHANTABILITY or FITNESS FOR A PARTICULAR PURPOSE.  See the
14  * GNU General Public License for more details.
15  *
16  * You should have received a copy of the GNU General Public License
17  * along with LTE-Sim; if not, see <http://www.gnu.org/licenses/>.
18  *
19  * Author: Francesco Capozzi <f.capozzi@poliba.it>
20   *
21  * Updated by: Rui R.Paulo   <rrp@lx.it.pt>>
22  *
23  */
24
25 #include "henb-lte-phy.h"
26
27 HenbLtePhy::HenbLtePhy()
28 {
29   // RRP: Transmitter power of the HeNB is set in the scenario
30   //SetTxPower(20); //dBm
31 }
32
33 HenbLtePhy::~HenbLtePhy()
34 {}
35
```

Appendix E

LTE-Sim Upgrade to extended 4 HeNB and 8 Uses Scenario

This Appendix addresses the overall updates performed in LTE-Sim code to perform simulations in a scenario with 4 home eNodeBs (HeNBs) and eight users per HeNB. The code for this scenario is presented considering the uniform distribution of users in the femtocell area. The presented code has been used to obtain the results in Chapter 4.

```
 1 /* -*- Mode:C++; c-file-style:"gnu"; indent-tabs-mode:nil; -*- */
 2 /*
 3  * Copyright (c) 2010,2011,2012,2013 TELEMATICS LAB, Politecnico di Bari
 4  *
 5  * This file is part of LTE-Sim
 6  *
 7  * LTE-Sim is free software; you can redistribute it and/or modify
 8  * it under the terms of the GNU General Public License version 3 as
 9  * published by the Free Software Foundation;
10  *
11  * LTE-Sim is distributed in the hope that it will be useful,
12  * but WITHOUT ANY WARRANTY; without even the implied warranty of
13  * MERCHANTABILITY or FITNESS FOR A PARTICULAR PURPOSE.  See the
14  * GNU General Public License for more details.
15  *
16  * You should have received a copy of the GNU General Public License
17  * along with LTE-Sim; if not, see <http://www.gnu.org/licenses/>.
18  *
19  * Author: Francesco Capozzi <f.capozzi@poliba.it>
20  *
21  * Updated by: Rui R.Paulo   <rrp@lx.it.pt>>
22  *
23  */
24
25 #include "../channel/LteChannel.h"
26 #include "../phy/enb-lte-phy.h"
27 #include "../phy/ue-lte-phy.h"
28 #include "../core/spectrum/bandwidth-manager.h"
29 #include "../networkTopology/Cell.h"
30 #include "../protocolStack/packet/packet-burst.h"
31 #include "../protocolStack/packet/Packet.h"
32 #include "../core/eventScheduler/simulator.h"
33 #include "../flows/application/InfiniteBuffer.h"
34 #include "../flows/application/VoIP.h"
35 #include "../flows/application/CBR.h"
36 #include "../flows/application/TraceBased.h"
37 #include "../device/IPClassifier/ClassifierParameters.h"
38 #include "../flows/QoS/QoSParameters.h"
39 #include "../flows/QoS/QoSForEXP.h"
40 #include "../flows/QoS/QoSForFLS.h"
41 #include "../flows/QoS/QoSForM_LWDF.h"
42 #include "../componentManagers/FrameManager.h"
43 #include "../utility/seed.h"
44 #include "../utility/RandomVariable.h"
45 #include "../utility/UsersDistribution.h"
46 #include "../utility/IndoorScenarios.h"
47 #include "../channel/propagation-model/macrocell-urban-area-channel-
   realization.h"
48 //#include "../channel/propagation-model/femtocell-urban-area-channel-
   realization.h"
49 #include "../channel/propagation-model/winner-downlink-channel-
   realization.h"
50 #include "../load-parameters.h"
```

```
 51 #include "../device/HeNodeB.h"
 52 #include <iostream>
 53 #include <queue>
 54 #include <fstream>
 55 #include <stdlib.h>
 56 #include <cstring>
 57
 58 #include <vector>
 59 #include <iostream>
 60 #include <iterator>
 61
 62 static void SingleCellWithFemtoWithRiuso (double radius, int nbBuildings,
    int buildingType, double activityRatio,
 63                         int nbUE, int nbFemtoUE,
 64                         int nbVoIP, int nbVideo, int nbBE, int nbCBR,
 65                         int sched_type,
 66                         int frame_struct,
 67                         int speed, int accessPolicy,
 68                         double maxDelay, int videoBitRate,
 69                         double Power,
 70                         double LWall,
 71                         int seed)
 72 {
 73   int nbCell = 1;
 74
 75   // define simulation times
 76   double duration = 30;
 77   double flow_duration = 20;
 78
 79   // RRP: eNB operates with reuse 1
 80   int cluster_enb=1;
 81   int bandwidth_enb=20;
 82
 83   // RRP: HeNBs operate with reuse 2
 84   int cluster_henb=2;
 85   int bandwidth_henb=10;
 86
 87   // CREATE COMPONENT MANAGER
 88   Simulator *simulator = Simulator::Init();
 89   FrameManager *frameManager = FrameManager::Init();
 90   NetworkManager* nm = NetworkManager::Init();
 91
 92   // Consult https://github.com/RRP-IT/LTE-SIM-ITU-R-M.  2135-1.git and
    https://github.com/RRP-IT/LTE-Sim-RP.git
 93
 94   ////////////////////
 95   //create femto-cells
 96   //
 97    int femtoCellsInBuilding = 1;
 98    if ( buildingType == 0 )
 99      {
100          femtoCellsInBuilding = 25;
101
```

```
102       }
103       else if ( buildingType == 4 ) // RRP: A 5x5 building with 4 H2NBs
104       {
105           femtoCellsInBuilding = 4;
106       }
107       else
108       {
109           femtoCellsInBuilding = 40;
110       }
111   int nbFemtoCells = nbBuildings * femtoCellsInBuilding;
112   int firstFemtoinBuildingID = nbCell;
113   int apartmentSide = LWall; // RRP: Apartments side length are given in
    the parameters of the scenario
114   int nbFloors = 1;
115   //users are distributed uniformly into a cell
116   vector<CartesianCoordinates*> *building_positions =
    GetUniformBuildingDistribution (0, nbBuildings);
117
118   // Consult https://github.com/RRP-IT/LTE-SIM-ITU-R-M.  2135-1.git and
    https://github.com/RRP-IT/LTE-Sim-RP.git
119
120   // RRP: It is needed to differentiate the frequency for the eNB and the
    HeNBs
121   // Then it in needed to concatenate them
122   // RRP: eNB
123   std::vector <BandwidthManager*> spectrums = RunFrequencyReuseTechniques
    (nbCell, cluster_enb, bandwidth_enb);
124   // RRP: HeNB
125   std::vector <BandwidthManager*> zx = RunFrequencyReuseTechniques
    (femtoCellsInBuilding, cluster_henb, bandwidth_henb);
126    //Concatenate eNB ans HeNBs
127    spectrums.insert(spectrums.end(), zx.begin(),  zx.end() );
128
129    // Consult https://github.com/RRP-IT/LTE-SIM-ITU-R-M.  2135-1.git and
    https://github.com/RRP-IT/LTE-Sim-RP.git
130
131   //create Home eNBs
132   std::vector <Femtocell*> *femtocells = nm->GetFemtoCellContainer();
133
134   for (int i = nbCell; i < nbCell + nbFemtoCells; i++)
135   {
136       double HeNBdrop = (double) rand()/ (double) RAND_MAX;
137
138       if ( HeNBdrop <= activityRatio )
139       {
140           HeNodeB* enb = new HeNodeB (i, femtocells->at (i-nbCell));
141           enb->GetPhy ()->SetDlChannel (dlChannels->at (i));
142           enb->GetPhy ()->SetUlChannel (ulChannels->at (i));
143           enb->SetDLScheduler (downlink_scheduler_type);
144
145           // RRP:  HeNBs transmitter power are given in the parameters of
    the scenario
146           enb->GetPhy ()->SetTxPower(Power);
```

```
147
148           enb->GetPhy ()->SetBandwidthManager (spectrums.at (i));
149
150           // Consult https://github.com/RRP-IT/LTE-SIM-ITU-R-M.
   2135-1.git and https://github.com/RRP-IT/LTE-Sim-RP.git
151       }
152   }
153
154   int totalNbUE = nbCell*nbUE + nbFemtoCells*nbFemtoUE;
155   int totalNbCell = nbCell + nbFemtoCells;
156
157   //Define Application Container
158   VoIP VoIPApplication[ nbVoIP*totalNbUE ];
159   TraceBased VideoApplication[ nbVideo*totalNbUE ];
160   InfiniteBuffer BEApplication[ nbBE*totalNbUE ];
161   CBR CBRApplication[ nbCBR*totalNbUE ];
162   int voipApplication = 0;
163   int videoApplication = 0;
164   int cbrApplication = 0;
165   int beApplication = 0;
166   int destinationPort = 101;
167   int applicationID = 0;
168
169   //Create GW
170   Gateway *gw = new Gateway ();
171   nm->GetGatewayContainer ()->push_back (gw);
172
173   // Users in MACRO CELL
174   //nbUE is the number of users that are into each cell at the beginning
   of the simulation
175   int idUE = totalNbCell;
176   for (int j = 0; j < nbCell; j++)
177     {
178
179       //users are distributed uniformly into a cell
180       vector<CartesianCoordinates*> *positions =
   GetUniformUsersDistribution (j, nbUE);
181
182       //Create UEs
183       for (int i = 0; i < nbUE; i++)
184         {
185
186           // Consult https://github.com/RRP-IT/LTE-SIM-ITU-R-M.2135-1.git
   and https://github.com/RRP-IT/LTE-Sim-RP.git
187
188   // Users in FEMTO CELLS
189   //nbUE is the number of users that are into each cell at the beginning
   of the simulation
190   //idUE = nbCell*nbUE;
191   std::vector <HeNodeB*> *HeNBs = nm->GetHomeENodeBContainer();
192   //for (int j = 0; j < nbFemtoCells; j++)
193   for (int j = 0; j < HeNBs->size(); j++)
194     {
```

```
195       int idCell = j + nbCell;
196
197       std::vector<double> vectorOfCoordinates;
198
199      vector<CartesianCoordinates*> *positions =
   GetUniformUsersDistributionInFemtoCell (idCell, nbFemtoUE, buildingType);
200
201       //Create UEs
202       for (int i = 0; i < nbFemtoUE; i++)
203         {
204           //ue's random position
205           double posX = positions->at (i)->GetCoordinateX ();
206           double posY = positions->at (i)->GetCoordinateY ();
207           double speedDirection = (double)(rand() %360) * ((2*3.14)/360);;
208
209           UserEquipment* ue = new UserEquipment (idUE,
210                                                  posX, posY, speed,
   speedDirection,
211                                                  femtocells->at (j),
212                                                  HeNBs->at (j),
213                                                  0, //HO deactivated! //
   RRP: Users shall not leave the own apartment
214
   Mobility::CONSTANT_POSITION);
215
216           std::cout << "Created UE in femto-cell - id " << idUE << "
   position " << posX << " " << posY
217                     << ", cell " <<  ue->GetCell ()->GetIdCell ()
218                     << ", target enb " << ue->GetTargetNode ()-
   >GetIDNetworkNode () << std::endl;
219
220           ue->GetPhy ()->SetDlChannel (HeNBs->at (j)->GetPhy ()-
   >GetDlChannel ());
221           ue->GetPhy ()->SetUlChannel (HeNBs->at (j)->GetPhy ()-
   >GetUlChannel ());
222
223           ue->SetIndoorFlag(true);
224
225           if (accessPolicy == 1)
226
227           // Consult https://github.com/RRP-IT/LTE-SIM-ITU-R-M.2135-1.git
   and https://github.com/RRP-IT/LTE-Sim-RP.git
228
229           // register ue to the enb
230           HeNBs->at (j)->RegisterUserEquipment (ue);
231           // define the channel realization
232           FemtoCellUrbanAreaChannelRealization* c_dl = new
   FemtoCellUrbanAreaChannelRealization (HeNBs->at (j), ue);
233           HeNBs->at (j)->GetPhy ()->GetDlChannel ()-
   >GetPropagationLossModel ()->AddChannelRealization (c_dl);
234           FemtoCellUrbanAreaChannelRealization* c_ul = new
   FemtoCellUrbanAreaChannelRealization (ue, HeNBs->at (j));
235           HeNBs->at (j)->GetPhy ()->GetUlChannel ()-
```

```
   >GetPropagationLossModel ()->AddChannelRealization (c_ul);
236
237           idUE++;
238         }
239     }
240
241   // Consult https://github.com/RRP-IT/LTE-SIM-ITU-R-M.  2135-1.git and
   https://github.com/RRP-IT/LTE-Sim-RP.git
242             }
243         }
244   simulator->SetStop(duration);
245   simulator->Run ();
246 }
247
```

```
 1 /* -*- Mode:C++; c-file-style:"gnu"; indent-tabs-mode:nil; -*- */
 2 /*
 3  * Copyright (c) 2010,2011,2012,2013 TELEMATICS LAB, Politecnico di Bari
 4  *
 5  * This file is part of LTE-Sim
 6  *
 7  * LTE-Sim is free software; you can redistribute it and/or modify
 8  * it under the terms of the GNU General Public License version 3 as
 9  * published by the Free Software Foundation;
10  *
11  * LTE-Sim is distributed in the hope that it will be useful,
12  * but WITHOUT ANY WARRANTY; without even the implied warranty of
13  * MERCHANTABILITY or FITNESS FOR A PARTICULAR PURPOSE.  See the
14  * GNU General Public License for more details.
15  *
16  * You should have received a copy of the GNU General Public License
17  * along with LTE-Sim; if not, see <http://www.gnu.org/licenses/>.
18  *
19  * Author: Francesco Capozzi <f.capozzi@poliba.it>
20  *
21  * Updated by: Rui R.Paulo   <rrp@lx.it.pt>>
22  *
23  */
24
25 #ifndef INDOORSCENARIOS_H_
26 #define INDOORSCENARIOS_H_
27
28 //#include "../core/cartesianCoodrdinates/CartesianCoordinates.h"
29 //#include "../componentManagers/NetworkManager.h"
30
31 #include <vector>
32 #include <iostream>
33 #include "../networkTopology/Building.h"
34 #include "../componentManagers/NetworkManager.h"
35
36   // Consult https://github.com/RRP-IT/LTE-SIM-ITU-R-M.  2135-1.git and
   https://github.com/RRP-IT/LTE-Sim-RP.git
37
38   // RRP: For scenario with 4 HeNBs
39
40   else if ( type == Building::TYPE_3GPP_5x5_grid_4 )
41   {
42       int x_offset [25] = { -1, 1, -1, 1};
43       int y_offset [25] = {  1, 1, -1,-1};
44
45       offset = new double[2];
46       offset[0] = (x_offset [idCell] * side);
47       offset[1] = (y_offset [idCell] * side);
48
49   }
50   else
51   {
52       std::cout << "ERROR: Wrong Building Type. Exiting...." << std::endl;
```

```
53       exit(1);
54   }
55
56   return offset;
57 }
58
59 static int cellsIndex_5x5grid [2][25] =
60 {
61   {
62     0, 1, 2, 3, 4, 0, 1, 2, 3, 4, 0, 1, 2, 3, 4, 0, 1, 2, 3, 4, 0, 1, 2, 3,
   4,
63   },
64   {
65     0, 0, 0, 0, 0, 1, 1, 1, 1, 1, 2, 2, 2, 2, 2, 3, 3, 3, 3, 3, 4, 4, 4, 4,
   4,
66   },
67 };
68
69 // Consult https://github.com/RRP-IT/LTE-SIM-ITU-R-M.  2135-1.git and
   https://github.com/RRP-IT/LTE-Sim-RP.git
70
71 }
72
73 #endif /* INDOORSCENARIOS_H_ */
74
```

```
 1 /* -*- Mode:C++; c-file-style:"gnu"; indent-tabs-mode:nil; -*- */
 2 /*
 3  * Copyright (c) 2010,2011,2012,2013 TELEMATICS LAB, Politecnico di Bari
 4  *
 5  * This file is part of LTE-Sim
 6  *
 7  * LTE-Sim is free software; you can redistribute it and/or modify
 8  * it under the terms of the GNU General Public License version 3 as
 9  * published by the Free Software Foundation;
10  *
11  * LTE-Sim is distributed in the hope that it will be useful,
12  * but WITHOUT ANY WARRANTY; without even the implied warranty of
13  * MERCHANTABILITY or FITNESS FOR A PARTICULAR PURPOSE.  See the
14  * GNU General Public License for more details.
15  *
16  * You should have received a copy of the GNU General Public License
17  * along with LTE-Sim; if not, see <http://www.gnu.org/licenses/>.
18  *
19  * Author: Giuseppe Piro <g.piro@poliba.it>
20  *
21  * Updated by: Rui R.Paulo   <rrp@lx.it.pt>>
22  *
23  */
24
25 #ifndef USERSDISTRIBTION_H_
26 #define USERSDISTRIBTION_H_
27
28 #include "../core/cartesianCoodrdinates/CartesianCoordinates.h"
29 #include "CellPosition.h"
30 #include "../componentManagers/NetworkManager.h"
31
32 #include <vector>
33 #include <iostream>
34 #include <cmath> // RRP:  Libraries to run the pseudorandom number
   generator (PRNG)
35 #include <random> // RRP:  Libraries to run the PRNG
36 #include <chrono> // RRP:  Libraries to the clock
37
38 static CartesianCoordinates*
39
40 // Consult https://github.com/RRP-IT/LTE-SIM-ITU-R-M.2135-1.git and
   https://github.com/RRP-IT/LTE-Sim-RP.git
41
42 static vector<CartesianCoordinates*>*
43 GetUniformUsersDistribution (int idCell, int nbUE)
44 {
45   NetworkManager * networkManager = NetworkManager::Init();
46   vector<CartesianCoordinates*> *vectorOfCoordinates = new
   vector<CartesianCoordinates*>;
47
48   Cell *cell = networkManager->GetCellByID(idCell);
49
50   double radii = (cell->GetRadius()*1000)*0.8;
```

```
51
52   CartesianCoordinates *cellCoordinates = cell->GetCellCenterPosition();
53   double r; double angle;
54
55   for (int i = 0; i < nbUE; i++)
56     {
57           // RRP:  implementation of the Mersenne Twister PRNG
58           unsigned seed =
   std::chrono::system_clock::now().time_since_epoch().count();
59           std::mt19937 rng_mt(seed);
60           std::uniform_real_distribution<double> dist_double(0.0, 1.0);
61           std::uniform_real_distribution<double> theta_double(0.0, 360.0);
62
63           double radius=dist_double(rng_mt);
64           double th=theta_double(rng_mt);
65
66           double angle = 2*M_PI*th/360;
67           double r1 = sqrt(radius);
68           double r = radii*r1;
69
70       CartesianCoordinates *newCoordinates =
   GetCartesianCoordinatesFromPolar (r, angle);
71
72       //Compute absoluteCoordinates
73       newCoordinates->SetCoordinateX (cellCoordinates->GetCoordinateX () +
   newCoordinates->GetCoordinateX ());
74       newCoordinates->SetCoordinateY (cellCoordinates->GetCoordinateY () +
   newCoordinates->GetCoordinateY ());
75
76       vectorOfCoordinates->push_back(newCoordinates);
77     }
78
79   return vectorOfCoordinates;
80 }
81
82 static vector<CartesianCoordinates*>*
83 GetUniformUsersDistributionInFemtoCell (int idCell, int nbUE, int
   buildingType)
84 {
85   NetworkManager * networkManager = NetworkManager::Init();
86   vector<CartesianCoordinates*> *vectorOfCoordinates = new
   vector<CartesianCoordinates*>;
87
88   Femtocell *cell = networkManager->GetFemtoCellByID(idCell);
89
90   double sidehome = cell->GetSide();
91
92   CartesianCoordinates *cellCoordinates = cell->GetCellCenterPosition();
93   double r; double angle;
94
95   for (int i = 0; i < nbUE; i++)
96     {
97
```

```
 98 if ( buildingType == 4)
 99 {
100              // RRP:  implementation of the Mersenne Twister PRNG
101              unsigned seed =
    std::chrono::system_clock::now().time_since_epoch().count();
102              std::mt19937 rng_mt(seed);
103              std::uniform_real_distribution<double> distx_double(0.0, 1);
104              std::uniform_real_distribution<double> disty_double(0.0, 1);
105
106              double xa=distx_double(rng_mt);
107              double ya=disty_double(rng_mt);
108
109             double x;
110             double y;
111              if ( idCell == 1 )
112              {
113                   // RRP:  Users coordinates on HeNB number 1
114                   x= 2.5*sidehome*xa-(3*sidehome/2);
115                   y= 2.5*sidehome*ya-(sidehome);
116              }
117              else if (idCell == 2)
118              {
119                 // RRP:  Users coordinates on HeNB number 2
120                 x = 2.5*sidehome*xa-(sidehome);
121                 y = 2.5*sidehome*ya-(sidehome);
122
123              }
124             else if (idCell == 3)
125             {
126                 // RRP:  Users coordinates on HeNB number 3
127                 x = 2.5*sidehome*xa-(3*sidehome/2);
128                 y = 2.5*sidehome*ya-(3*sidehome/2);
129
130             }
131             else
132             {
133                 // RRP:  Users coordinates on HeNB number 4
134                 x = 2.5*sidehome*xa-(sidehome);
135                 y = 2.5*sidehome*ya-(3*sidehome/2);
136
137             }
138
139              CartesianCoordinates *newCoordinates = new
    CartesianCoordinates ();
140              newCoordinates->SetCoordinates(x,y);
141           //Compute absoluteCoordinates
142           newCoordinates->SetCoordinateX (cellCoordinates->GetCoordinateX
    () + newCoordinates->GetCoordinateX ());
143           newCoordinates->SetCoordinateY (cellCoordinates->GetCoordinateY
    () + newCoordinates->GetCoordinateY ());
144
145           vectorOfCoordinates->push_back(newCoordinates);
146 }
```

```
147 else
148 {
149     unsigned seed =
    std::chrono::system_clock::now().time_since_epoch().count();
150              std::mt19937 rng_mt(seed);
151              std::uniform_real_distribution<double> distx_double(0.0, 1);
152              std::uniform_real_distribution<double> disty_double(0.0, 1);
153
154              double xa=distx_double(rng_mt);
155              double ya=disty_double(rng_mt);
156
157              double x = 2*sidehome*xa-(sidehome/2);
158              double y = 2*sidehome*ya-(sidehome/2);
159
160             CartesianCoordinates *newCoordinates = new
    CartesianCoordinates ();
161               newCoordinates->SetCoordinates(x,y);
162           //Compute absoluteCoordinates
163           newCoordinates->SetCoordinateX (cellCoordinates->GetCoordinateX
    () + newCoordinates->GetCoordinateX ());
164           newCoordinates->SetCoordinateY (cellCoordinates->GetCoordinateY
    () + newCoordinates->GetCoordinateY ());
165
166           vectorOfCoordinates->push_back(newCoordinates);
167 }
168
169     }
170   return vectorOfCoordinates;
171 }
172
173 #endif /* USERSDISTRIBTION_H_ */
174
```

Appendix F

Average Delay in Scenarios with 4, 5, and 6 HeNBs

This Appendix presents results for the average delay for topologies with 4, 5, and 6 home eNodeBs (HeNBs). Results for the average delay in the scenario with 4 HeNBs and eight users corresponding to the analysis presented in Section 4.2, and are presented from Figure F.1a up to Figure F.1c.
Results presented in Figure F.2a up to Figure F.2c correspond to the analysis in Section 4.3. These results are obtained by considering the 2% target for PLR suggested by 3GPP, for deployments with 4, 5, and 6 HeNBs. We produced fitting surfaces by using a polynomial surface with a confidence interval of 95%, by following the approach from [149].
Figure F.1 presents results for the scenario with 4 HeNBs, frequency reuse pattern two, and by assuming that each HeNB serves eight user equipments (UEs). Details can be found in Table 4.1. The proportional fair (PF), frame level scheduler (FLS), and exponential rule (EX-

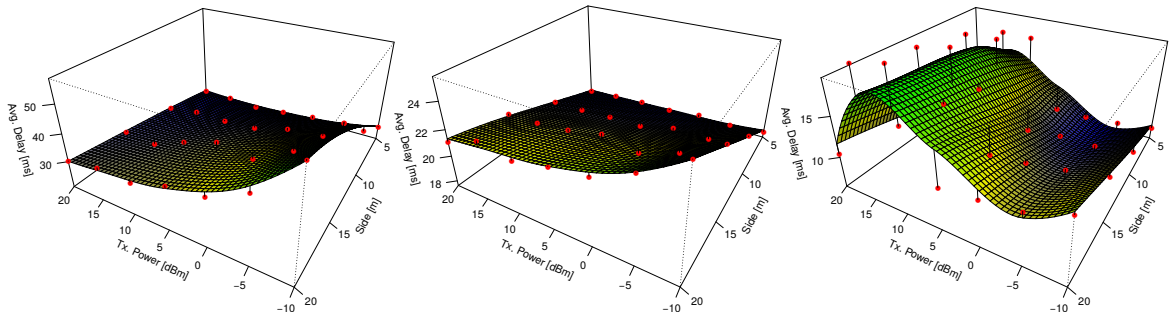

(a) Proportional fair (b) Frame level scheduler (c) Exponential rule

Figure F.1: Variation of the average delay of video flows with 4 HeNBs scenario, with different schedulers, for different values of the transmitter power and apartment side length.

PRule) schedulers have been considered in this analysis. Transmitter power varies between -10 dBm and 20 dBm. Figure F.1a presents results for PF. The minimum delay was obtained for transmitter power of 20 dBm and an apartment side length of 5 m. Delay increases with the increase in the apartment length and the decrease in the transmitter power. The maximum value obtained was $\approx$ 57 ms. Figure F.1b presents results for FLS. The average delay presents the same behavior for These two schedulers (PF and FLS). Although FLS presents better results, the maximum obtained average delay is $\approx$ 25 ms.
With the EXPRule Figure F.1c, the minimum average delay also occurs for the shortest apartment side length but for values of transmitter power lower than 0 dBm. The highest values have also been obtained for the longest apartment side lengths but for transmitter powers between 10 dBm and 15 dBm. The maximum average delay obtained has been $\approx$ 21 ms.
Figure F.2 presents results for the scenarios with 4, 5, and 6 HeNBs, for a PLR target for video of PLR<2%.

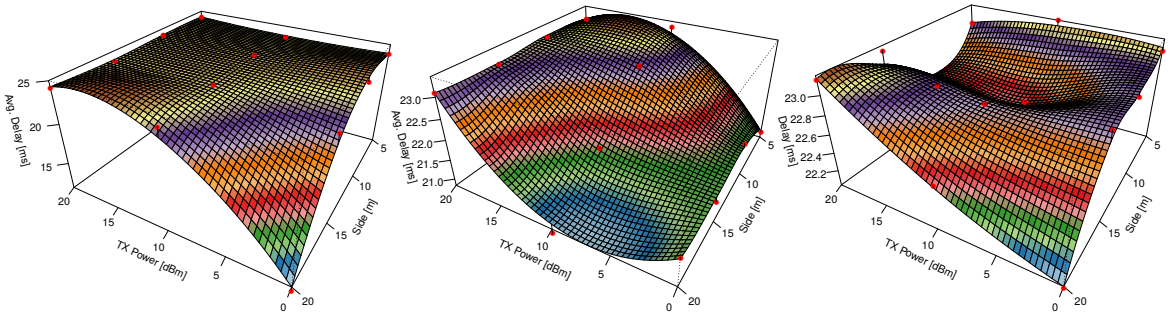

(a) 4 HeNBs (b) 5 HeNBs (c) 6 HeNBs

Figure F.2: Maximum average delay for target PLR of 2%, for video with 4, 5 and 6 HeNBs and the FLS scheduler.

The considered scheduler is the FLS. The simulation parameters are presented in Table 4.2. Transmitter power varies between 0 dBm and 20 dBm. For the scenario with 4 HeNBs, the maximum and minimum average delay have been obtained for an apartment side length of 20 m, as shown in Figure F.2a. The minimum and the maximum average delay were obtained considering a transmitter power of 0 dBm. The maximum delay of $\approx$ 25 ms occurs between 10 dBm and 20 dBm.

With 5 HeNBs, the minimum average delay was also obtained for an apartment side length of 20 m, a shown in Figure F.2b. The maximum delay has been obtained for an apartment side length of 5 m and a transmitter power between 10 dBm and 20 dBm (its value is $\approx$ 23.4 ms).

For the scenario that considers 6 HeNBs, the maximum and minimum average delay have also been obtained for the apartment side length of 20 m, as shown in Figure F.2c. The minimum delay occurred for a transmitter power of 0 dBm while its maximum is achieved for a transmitter power of 20 dBm (this maximum value is $\approx$ 23.2 ms).

In none of the scenarios presented in Figure F.1 or Figure F.2 the average delay for video exceeded the maximum 3GPP limit of 150 ms [97].